

Catalytic hydroprocessing of biomass derived compounds to renewable biofuels and chemicals using polyoxometalate catalysts



Universität Hamburg

DER FORSCHUNG | DER LEHRE | DER BILDUNG

Dissertation with the aim of achieving a doctoral degree (Dr.rer.nat.)

Institute of technical and macromolecular chemistry,

Faculty of Mathematics, Informatics and Natural Sciences,

University of Hamburg

Submitted by

Magdy Sherbi

Hamburg, 2023

DAAD



This work was conducted between April 2019 and March 2023 at the Institute of Chemical Reaction Engineering, Friedrich-Alexander-University, Erlangen, Germany and the Institute of Technical and Macromolecular Chemistry, University of Hamburg, Hamburg, Germany under the supervision of Prof. Dr. Ing. Jakob Albert.

Reviewer 1: Prof. Dr. Ing. Jakob Albert
Reviewer 2: Prof. Dr. Marcus Rose

Date of Disputation: 01.12.2023

Examiner 1: Prof. Dr. Ing. Jakob Albert
Examiner 2: Prof. Dr. Axel Jacobi von Wangelin
Examiner 3: Prof. Dr. Ing. Martin Kaltschmitt

List of publication

1- **M.Sherbi**, M. Stuckart, and J. Albert. "Selective catalytic hydrogenation of biomass derived furans to secondary alcohols using Pt/polyoxometalate catalysts under mild reaction conditions." *Biofuels, Bioproducts and Biorefining* ,2021, 15 (5), 1431-1446, DOI: 10.1002/bbb.2248

2- **M.Sherbi** , J. Albert ."Modeling and optimization of bio-2-hexanol production from biomass derived dimethylfuran using Pt/K3PW12O40 by response surface methodology." *Computers & Chemical Engineering* ,2021,155, 107546. DOI: 10.1016/j.compchemeng.2021.107546

3- **Sherbi, M.**, Wesner, A., Wisniewski, V. K., Bukowski, A., Velichkova, H., Fiedler, B., & Albert, J. (2021). Superior CNT-supported bimetallic RuCu catalyst for the highly selective hydrogenolysis of glycerol to 1, 2-propanediol. *Catalysis Science & Technology*, 2021,11, 6649-6653, DOI: 10.1039/D1CY01518D

Table of contents

List of publication	i
List of abbreviations	iv
Zusammenfassung	vii
Abstract	ix
Introductory part of the dissertation	1
Chapter 1. Introduction	1
1.1. Motivation.....	1
1.2. Objective: Biomass valorization through catalytic hydroprocessing.....	2
1.3. Outline of the dissertation.....	4
1.4. Strategy of the research.....	5
Chapter 2. Theoretical background	6
2.1. Biomass valorization through catalytic hydroprocessing.....	6
2.2. Polyoxometalates.....	12
2.3. Hydrogenation of biomass derived furans.....	20
2.4. Reductive catalytic fractionation for lignin valorization.....	25
2.5. Hydrogenolysis of glycerol.....	34
2.6. One-factor-at-a-time approach & Response surface methodology.....	40
Cumulative part of the dissertation	41
Part I: Hydroprocessing of biomass derived furans	41
Chapter 3. Selective catalytic hydrogenation of biomass derived furans to secondary alcohols using Pt/polyoxometalate catalysts under mild reaction conditions	42
Chapter 4. Modeling and optimization of bio-2-hexanol production from biomass derived dimethylfuran using Pt/K₃[PW₁₂O₄₀] by response surface methodology	59
Part II: Hydroprocessing of biomass derived glycerol	73
Chapter 5. Superior CNT-supported bimetallic RuCu catalyst for the highly selective hydrogenolysis of glycerol to 1,2-propanediol	74
Unpublished part of the dissertation	80
Part III: Hydroprocessing of lignin	80
Chapter 6. Reductive catalytic fractionation for lignin valorization into aromatic monomers under mild reaction conditions	81
6.1. Introduction.....	81
6.2. Experimental.....	82
6.3. Results and discussion.....	87

6.4. Conclusion.....	95
Part IV: Influence of polyoxometalates (POMs) in hydrogenation of furans, glycerol hydrogenolysis, and lignin valorization via reductive catalytic fractionation	96
Chapter 7. Assessing the influence of polyoxometalates in hydrogenation of furans, glycerol hydrogenolysis, and lignin valorization via reductive catalytic fractionation	97
7.1. Introduction	97
7.2. Experimental	98
7.3. Results and discussion.....	99
7.4. Conclusion.....	109
Chapter 8. Comprehensive discussion	110
8.1. Hydrogenation of furans.....	110
8.2. Hydrogenolysis of glycerol	113
8.3. Reductive catalytic fractionation for lignin valorization.....	113
Chapter 9. Bibliography	115
Chapter 10. Appendix.....	128
10.1. List of hazardous substances used according to GHS	128
10.2. List of figures.....	131
10.3. List of tables	133
10.4. Online ESI of 1st publication (chapter 3).....	134
10.5. Online ESI of 2nd publication (chapter 4).....	141
10.6. Online ESI of 3rd publication (chapter 5)	156
10.7. Supplementary information of chapter 6.....	166
Acknowledgements	169
Declaration on oath	170
Curriculum Vitae.....	171

List of abbreviations

1,2 PD	1,2-Propandiol
1,3 PD	1,3-Propandiol
3-HPA	3-Hydroxypropanal
A	Temperature
AIC	Akaike information criterion
ANOVA	Analysis of variance
ASTM	American society for testing and materials
B	Pressure
BET	Brunauer-Emmett-Teller
BIC	Bayesian information criterion
C	Substrate/catalyst ratio
CCD	Central composite design
CHNS	Carbon, hydrogen, nitrogen, and sulfur elemental analysis
CI	Confidence interval
CNT	Carbon nanotube
CO	Carbon monoxide
CO ₂	Carbon dioxide
D ₂ O	Deuterium oxide
DFT	Density functional theory
DMDHF	2,5-Dimethyldihydrofuran
DMF	2,5 Dimethylfuran
DMTHF	2,5-Dimethyltetrahydrofuran
DoE	Design of experiments
DP	Degree of polymerization
EDX	Energy-dispersive X-ray spectroscopy
EG	Ethylene glycol
ESI	Electronic supplementary information
EtOH	Ethanol
FDLA	δ-Furfurylidenelevulinic acid
FFR	Furfural
FID	Flame ionization detector
FTIR	Fourier transform infrared
GC	Gas chromatography
GC-MS	Gas chromatography-mass spectrometry
GHS	Globally harmonized system of classification and labelling of chemicals
GL	Glycerol
GP	2-Methoxy-4-propyl-phenol or 4-n-Propyl guaiacol
GP _a	3-(4-Hydroxy-3-methoxyphenyl) propionic acid
GP _a Me	3-(4-Hydroxy-3-methoxyphenyl)-propanoic acid methyl ester
GPC	Gel permeation chromatography
GP _e	2-Methoxy-4-(1-propenyl)-phenol
GP _e aMe	3-(4-Hydroxy-3-methoxyphenyl)-2-propenoic acid methyl ester

GPOH	3-(4-Hydroxy-3-methoxyphenyl)-1-propanol or 4-n-Propanol guaiacol
GTBE	Glycerol tertiary butyl ether
H ₂ -TPR	H ₂ -Temperature-programmed reduction
HA	Hydroxyacetone
HD	2,5-Hexanedione
HDO	Hydrodeoxygenation
HMF	Hydroxymethylfurfural
HP	4-Propylphenol
HPa	Hydroxy-benzenepropanoic acid
HPaMe	Hydroxy-benzenepropanoic acid methyl ester
HPe	4-(1-Propenyl) phenol
HPeMe	3-(4-Hydroxyphenyl)-2-propenoic acid methyl ester
HPLC	High-performance liquid chromatography
HPMo	Phosphomolybdic acid (H ₃ PMo ₁₂ O ₄₀)
HPOH	3-(4-Hydroxyphenyl)-1-propanol
HPW	Phosphotungstic acid (H ₃ PW ₁₂ O ₄₀)
HSiW	Silicotungstic acid (H ₄ SiW ₁₂ O ₄₀)
HX	n-Hexane
HXL	2-Hexanol
HXN	2-Hexanone
ICP-OES	Inductively coupled plasma optical emission spectroscopy
i-Pr	iso-Propanol
LPCtoN	Liquid-phase cellulose-to-naphtha
MCF	Microcrystalline cellulose fibers
MeOH	Methanol
MF	2-Methylfuran
MIBK	Methyl isobutyl ketone
MP	2-Methylpentane
MTHF	2- Methyltetrahydrofuran
MWCNT	Multi-walled carbon nanotube
n-BuOH	n-Butanol
NCF	Nano cellulose fibers
NH ₃ -TPD	NH ₃ -Temperature programmed desorption
NiSat	NiO/SiO ₂ -Al ₂ O ₃
NMR	Nuclear magnetic resonance
NREL	National renewable energy laboratory
OFAT	One-factor-at-a-time
P	Pressure
PA	Propanoic acid
PDs	Propanediols
PI	Prediction interval
POMs	Polyoxometalates
PTFE	Polytetrafluoroethylene
PXRD	Powder X-ray diffraction measurements

RCF	Reductive catalytic fractionation
RSM	Response surface methodology
S	Selectivity
S/C	Substrate/catalyst ratio
SEM-EDX	Scanning electron microscopy with energy dispersive X-ray spectroscopy
SI	Supplementary information
SP	2,6-Methoxy-4-propyl phenol or 4-n-Propyl syringol
SPa	3-(4-Hydroxy-3,5-dimethoxyphenyl) propanoic acid
SPaMe	3-(4-Hydroxy-3,5-dimethoxyphenyl) propanoic acid methyl ester
SPe	2,6-Dimethoxy-4-(prop-1-en-1-yl) phenol
SPeMe	3-(4-Hydroxy-3,5-dimethoxyphenyl) propenoic acid methyl ester
SPOH	4-(3-Hydroxypropyl)-2,6-dimethoxyphenol or 4-n-Propanol syringol
T	Temperature
t	Reaction time
TCD	Thermal conductivity detector
TEM-EDX	Transmission electron microscopy energy-dispersive X-ray spectroscopy
TGA	Thermogravimetric analysis
THF	Tetrahydrofuran
UV spectrometry	Ultraviolet spectrometry
WD-type	Wells–Dawson POM structure
X	Conversion
XRD	X-Ray diffraction
Y	Yield
γ -H	Propyl-substituted phenols (SP/GP)
γ -OH	Propanol-substituted phenols (SPOH/GPOH)

Zusammenfassung

Die katalytische Hydrierung ist eine wichtige Reaktionskategorie bei der Umwandlung von Biomasse-Molekülen in eine breite Palette von Brennstoffen und Chemikalien. Dazu gehören die Hydrierung von Furanen aus Zellulose und Hemizellulose zu Alkoholen, die Hydrogenolyse von Glycerin aus Ölen zu 1,2-Propandiol und die reduktive katalytische Fraktionierung von Lignin zu phenolischen Monomeren.

Im Zusammenhang mit der Furanhydrierung wurden vielversprechende bifunktionelle Katalysatorsysteme mit Platin und Polyoxometallaten (POMs) erfolgreich für die selektive katalytische Hydrierung von 2,5-Dimethylfuran (DMF) zu 2-Hexanol unter milden Reaktionsbedingungen eingesetzt. Unter den verschiedenen untersuchten Platinvorläufern wurde $\text{Pt}(\text{acac})_2$ als das effektivste für die Ringöffnung von DMF identifiziert. Darüber hinaus erwies sich der Keggin-Typ POM ($\text{K}_3[\text{PW}_{12}\text{O}_{40}]$) als effizientester saurer Träger für die Herstellung von 2-Hexanol bei 80 °C und 10 bar H_2 -Druck mit n-Decan als Trägerflüssigkeit. Es wurde festgestellt, dass Modifikationen im Syntheseprozess des $\text{Pt}/\text{K}_3[\text{PW}_{12}\text{O}_{40}]$ -Katalysatorsystems die katalytische Leistung verbessern können. So konnte eine höhere Ausbeute an 2-Hexanol (72,5 %) im Vergleich zu einem kommerziellen Pt/C -Katalysator mit gleicher Pt-Beladung (49 %) erzielt werden. Weiterhin wurden Furan und 2-Methylfuran unter den gleichen Reaktionsbedingungen selektiv zu 1-Butanol (59,7% Ausbeute) und 1/2-Pentanol (44,3 % Ausbeute) hydriert. Charakterisierungen mit N_2 -Physisorption, NH_3 - Temperaturprogrammierte Desorption, CO -Chemisorption und TEM zeigten, dass die höhere Gesamtsäurestellendichte von $\text{K}_3[\text{PW}_{12}\text{O}_{40}]$ die $\text{C}=\text{O}$ -Hydrierung verbessert und den geschwindigkeitsbestimmenden Schritt der 2-Hexanon-Hydrierung zu 2-Hexanol überwindet.

Weitere Untersuchungen wurden mit der Response-Surface-Methode (RSM) durchgeführt, um den Einfluss verschiedener Prozessparameter wie Temperatur (T), Druck (P) und Substrat-Katalysator-Verhältnis (S/C) auf die selektive Hydrierung von DMF als Modellverbindung für Furane zu untersuchen. Ziel war die Maximierung der Ausbeute des Alkoholprodukts (2-Hexanol) unter Verwendung des bifunktionellen Katalysatorsystems Platin auf einem Keggin-Polyoxometallat durch die Wahl optimaler Bedingungen dieser Parameter. Um die optimalen Betriebsbedingungen für eine maximale Ausbeute des Alkoholprodukts in der Hydrierungsreaktion zu bestimmen, wurden vier Vorhersagemodelle entwickelt, die in der Lage sind, die Ausbeute jedes Produkts zu schätzen. Die Leistung der Modelle wurde sowohl statistisch als auch experimentell bewertet und zeigte eine ausgezeichnete Übereinstimmung zwischen den Vorhersagen und den experimentellen Daten. Anschließend wurde eine numerische Optimierung durchgeführt, um die optimalen Bedingungen für eine maximale Ausbeute des Alkoholprodukts zu ermitteln. Mit Hilfe der RSM konnten wir eine Ausbeute von 78% 2-Hexanol unter Verwendung eines $\text{Pt}/\text{K}_3[\text{PW}_{12}\text{O}_{40}]$ Katalysators bei Bedingungen von 83°C, einem (S/C) Verhältnis von 88 (Mol (DMF)/Mol (Pt)) und einem H_2 -druck von 5-15 bar bei vollständiger Umsetzung von DMF erzielen.

Die Untersuchungen zur Hydrogenolyse von Glycerin zeigten, dass Ru/C aufgrund seiner Fähigkeit, C-O- und C-C-Bindungen zu spalten, die höchste katalytische Aktivität unter

den getesteten Katalysatoren aufwies. Zusätzlich verbesserte die Zugabe von POMs zum Reaktionssystem die Selektivität gegenüber 1,2-Propandiol (1,2 PD), wobei $H_3[PMo_{12}O_{40}]$ mit einer Selektivität von ca. 70 % am effektivsten war. TEM-EDX und FTIR Analysen zeigten, dass sich die POMs auf dem verbrauchten Katalysator angesammelt hatten, was zu Oberflächenmodifikationen von Ru und schließlich zu einer Erhöhung der Selektivität gegenüber 1,2 PD führte, während die Methanbildung abnahm. Die Untersuchungen untersuchten auch die Oberflächenmodifikation von Ru-basierten Katalysatoren mit anderen Übergangsmetallen wie Fe und Cu und stellten fest, dass solche Modifikationen die Selektivität gegenüber 1,2 PD signifikant verbesserten. Die Verwendung des Ru_1Cu_2/CNT Katalysators führte zu einer beeindruckenden 1,2 PD Selektivität von 93,4%. Die Studie deutet darauf hin, dass der Einbau von Cu in Ru-Nanopartikel die Reduzierbarkeit erhöhen und die Oberfläche des Katalysators modifizieren kann, was zu einer Bevorzugung der C-O-Bindungsspaltung durch Cu gegenüber der C-C-Bindungsspaltung durch kleine Ru-Nanopartikel führt.

Die Untersuchungen zur reduktiven katalytischen Fraktionierung (RCF) haben das Potenzial der Verwendung von industriellem Strohdigestat als Substrat für die Produktion phenolischer Monomere aufgezeigt. Die Ergebnisse der Zusammensetzungsanalyse zeigten, dass der Ligningehalt des Digestats mit dem von Buchenholz vergleichbar oder sogar höher ist. Darüber hinaus wurde festgestellt, dass das Digestat signifikante Mengen an phenolischen Estern (Ferulat und p-Cumarat) enthielt. Die durchgeführten Untersuchungen haben gezeigt, dass die Wahl des Katalysatorträgers einen großen Einfluss auf die Ausbeute der produzierten Monomere hat, wobei der Katalysator auf Kohlenstoffträger im Vergleich zu dem auf Aluminiumträger eine höhere Monomerausbeute ergab. Dieser Unterschied in der Monomerausbeute kann auf die höhere Säureaktivität von Aluminium zurückgeführt werden, die Kondensationsreaktionen begünstigt. Darüber hinaus zeigte die Studie, dass die Metallspezies des Katalysators eine entscheidende Rolle bei der Bestimmung der Selektivität für bestimmte Produkte spielt. Zum Beispiel bevorzugte der Ru-Katalysator die Produktion von Propyl-substituierte Phenole (γ -H), während der $NiO/SiO_2-Al_2O_3$ (NiSat) eine Selektivität für Propanol-substituierte Phenole (γ -OH) zeigte. Die Studien untersuchten auch den Einfluss von POMs als Additive in Kombination mit kommerziellen Katalysatoren während des RCF. Die Ergebnisse zeigten, dass die Zugabe von POMs zu einer Verschiebung der Produktselektivität führte, die sich in einer Abnahme der Gesamtmonomerausbeute und des γ -OH: γ -H-Verhältnisses äußerte. Die Gültigkeit der Ergebnisse wurde durch Gelpermeationschromatographie (GPC)-Analysen bestätigt, die zeigten, dass $H_3PMo_{12}O_{40}$ als Additiv den höchsten Peak ergab, der den Dimeren bei der Repolymerisation entsprach. Anschließend wurde der Einfluss verschiedener Parameter wie alkalische Behandlung, Vorspülung, Reaktionszeit und H_2 -Druck auf die RCF von industriellen Gärrückständen untersucht. Es wurde festgestellt, dass eine Vorspülung und eine längere Reaktionszeit vorteilhaft sind, um eine höhere Monomerausbeute zu erzielen. Außerdem kann eine selektive Produktion von Propanol-substituierte Phenole durch höhere H_2 -Drücke und kürzere Reaktionszeiten erreicht werden.

Abstract

Catalytic hydroprocessing is an essential reaction category in the transformation of biomass molecules into a wide array of fuels and chemicals. The objective of this work was to valorize various types of biomass classes into chemicals and fuels using selective hydroprocessing techniques, including hydrogenation of furans derived from cellulose and hemicellulose into alcohols, hydrogenolysis of glycerol derived from oils into 1,2-propanediol (1,2 PD), and reductive catalytic fractionation (RCF) of lignin into phenolic monomers.

In the context of furan hydrogenation, promising bifunctional catalyst systems containing platinum and polyoxometalates (POMs) have been successfully utilized for the selective catalytic hydrogenation of 2,5-dimethylfuran (DMF) to 2-hexanol under mild reaction conditions. Among the different platinum precursors studied, $\text{Pt}(\text{acac})_2$ has been identified as the most effective for the ring opening of DMF. Furthermore, the Keggin-type POM $\text{K}_3[\text{PW}_{12}\text{O}_{40}]$ has been found to be the most efficient acidic support for the production of 2-hexanol at 80 °C and 10 bar H_2 pressure, with n-decane serving as the carrier liquid. It was revealed that modifications in the synthetic procedure of the $\text{Pt}/\text{K}_3[\text{PW}_{12}\text{O}_{40}]$ catalytic system can enhance its catalytic performance. Thus, a higher yield of 2-hexanol (72.5%) was achieved compared to that (49%) obtained using a commercial Pt/C catalyst with the same Pt loading. Additionally, furan and 2-methylfuran were selectively hydrogenated to 1-butanol (59.7% yield) and 1/2-pentanol (44.3% yield), respectively, under the same reaction conditions. Catalyst characterization using N_2 -physisorption, NH_3 Temperature programmed desorption, CO chemisorption, and TEM, revealed that the higher total acid site density of the $\text{K}_3[\text{PW}_{12}\text{O}_{40}]$ enhances C=O hydrogenation and overcomes the rate-limiting step of 2-hexanone hydrogenation to 2-hexanol.

Further investigations were conducted using response surface methodology (RSM) to study the impact of various process parameters, including temperature (T), pressure (P), and substrate-to-catalyst ratio (S/C), on the selective hydrogenation of DMF, which served as a model compound for bio-derived furans. The aim was to maximize the yield of the alcoholic product (2-hexanol) using the bifunctional catalyst system platinum supported on a Keggin-POM by choosing the optimum conditions of those parameters. To determine the optimal operating conditions for achieving maximum yield of the alcoholic product in the hydrogenation reaction, four predictive models capable of estimating the yield of each product were constructed. The performance of the models was then evaluated both statistically and experimentally, demonstrating an excellent agreement between the predictions and experimental data. Numerical optimization was subsequently performed to identify the optimal conditions for maximum yield of the alcoholic product. Employing RSM, we were able to achieve a 78% yield of 2-hexanol at complete DMF conversion using a $\text{Pt}/\text{K}_3[\text{PW}_{12}\text{O}_{40}]$ catalyst under reaction conditions of 83 °C, S/C ratio of 88 (mol (DMF)/mol(Pt)), and 5-15 bar hydrogen pressure.

Regarding glycerol hydrogenolysis, it was observed that among the tested catalysts, Ru/C exhibited the highest catalytic activity due to its capability of C-O and C-C bonds cleavage. Additionally, the incorporation of POMs into the reaction system enhanced the selectivity towards 1,2-propanediol (1,2 PD), with $\text{H}_3\text{PMo}_{12}\text{O}_{40}$ being the most effective, resulting in

an approximately 70% selectivity towards 1,2 PD. TEM-EDX and FTIR analysis revealed that POMs accumulated on the spent catalyst, leading to surface modifications of Ru, ultimately leading to an increase in selectivity towards 1,2 PD while decreasing methane formation. The investigations also examined the surface modification of Ru-based catalysts with other transition metals, including Fe and Cu, and found that such modification significantly enhanced selectivity towards 1,2 PD. Notably, the utilization of the Ru₁Cu₂/CNT catalyst resulted in an impressive 1,2 PD selectivity of 93.4%. The study proposes that the inclusion of Cu to Ru nanoparticles can enhance reducibility and modify the catalyst's surface, inducing a preference for C-O bond cleavage promoted by Cu rather than C-C bond cleavage catalyzed by small Ru nanoparticles.

The investigations on reductive catalytic fractionation (RCF) highlighted the potential of utilizing straw industrial digestate as a substrate for the production of phenolic monomers. The results of compositional analysis indicated that the lignin content in the digestate was comparable to or higher than that in beech wood. Moreover, the digestate was found to contain significant amounts of phenolic esters (ferulate and p-coumarate), which are characteristic of herbaceous biomass, unlike beech wood. The investigations conducted revealed that the choice of catalyst support greatly impacts the yield of produced monomers, with the catalysts supported on carbon yielding higher amounts of monomers compared to those supported on alumina. This difference in monomer yield may be attributed to the higher acidity of alumina, which promotes condensation reactions. Furthermore, the study revealed that the metal site of the catalyst plays a crucial role in determining the selectivity towards specific products. For instance, the Ru-based catalyst showed a preference for the production of propyl-substituted phenols (γ -H), while NiO/SiO₂-Al₂O₃(NiSat) exhibited selectivity towards propanol-substituted phenols (γ -OH).

The studies further explored the effect of POMs as additives in combination with commercial catalysts during RCF. Results showed that the incorporation of POMs led to a shift in product selectivity, resulting in a decrease of the total monomer yield and the γ -OH: γ -H ratio. The validity of the findings was confirmed through gel permeation chromatography (GPC), which revealed that H₃[PMo₁₂O₄₀] as an additive yielded the highest peak corresponding to dimers formed through repolymerization. After that, the effect of several parameters, such as alkaline treatment, pre-washing, reaction time, and H₂ pressure, on RCF of industrial straw digestate was examined. It was revealed that prewashing and increasing the reaction time are beneficial for achieving a higher yield of monomers. Moreover, selective production of propanol-substituted phenols can be achieved by employing higher H₂ pressure and lower reaction times.

Introductory part of the dissertation

Chapter 1. Introduction

1.1. Motivation

Since the advent of the industrial revolution in the mid-nineteenth century until the present day, the energy and chemical sectors have primarily relied on fossil carbon resources, such as natural gas, coal, and crude oil. This heavy reliance on fossil fuels has contributed to the emission of over 82% of greenhouse gases into the atmosphere [1]. Furthermore, it has become evident that fossil fuel reserves are finite and will eventually be depleted. Figure 1.1 indicates that the estimated global crude oil reserves currently stand at 169 billion tons. At the current rate of consumption, these reserves will only last for additional 36 years, until the end of 2058. Similarly, natural gas reserves are estimated to be $181 \times 10^{12} \text{ m}^3$, which can last only for another 58 years as predicted [2]. These issues have prompted scientific research to investigate the feasibility of sustainable and clean energy alternatives. In this regard, biomass, comprising of diverse organic compounds such as carbohydrates, lignin, fats, and oils, has emerged as a viable substitute for fossil fuels. As depicted in Figure 1.1, estimates of the global reserves of renewable biomass as a raw material are comparable to those of crude oil reserves, standing at approximately 170 billion tons. Notably, unlike crude oil, the reserves of biomass are renewable, and replenished annually through the process of photosynthesis.

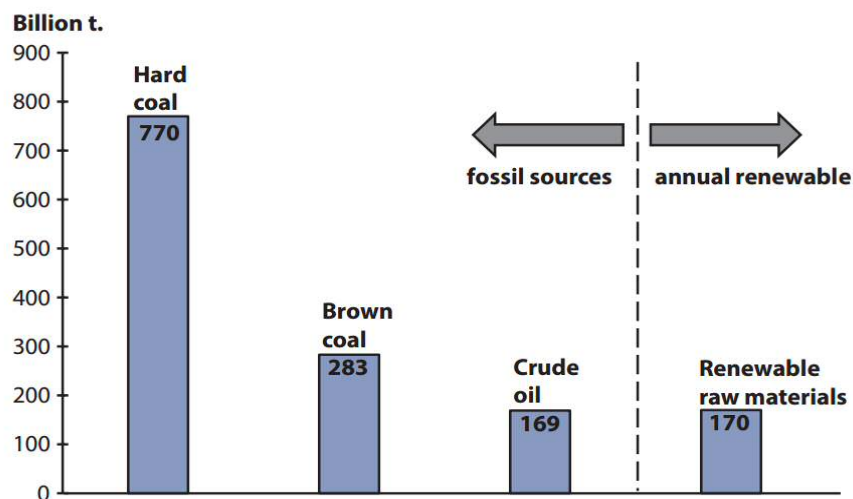


Figure 1.1 Reserves for C raw materials [2].

Biomass, beyond serving as a renewable source of carbon for energy and chemical production, possesses the capacity to mitigate greenhouse gas emissions in the atmosphere. Biomass is formed originally from CO_2 , water and sunlight through photosynthesis, and it can be seen from Figure 1.2 that carbon dioxide released into the atmosphere during biomass-based energy and chemical production can be recaptured and converted again to biomass via photosynthesis. Consequently, this cycle of energy and chemical production from biomass is considered to be carbon neutral. In contrast, the utilization of fossil fuels as resources leads to

a carbon positive outcome, whereby the carbon dioxide released from fossil fuels remains and accumulates in the atmosphere, exacerbating the greenhouse effect and contributing to climate change. Therefore, the development of biomass upgrading technologies for the production of renewable biochemicals and fuels has emerged as a significant research objective. Several biomass valorization processes have been explored in literature, such as dehydration, esterification, transesterification, hydrolysis, isomerization, etherification, reforming, aldol condensation, oxidation, hydrogenation, and hydrogenolysis. Among these upgrading techniques, hydroprocessing stands out as a key method for converting different types of biomasses into valuable chemicals and fuels.

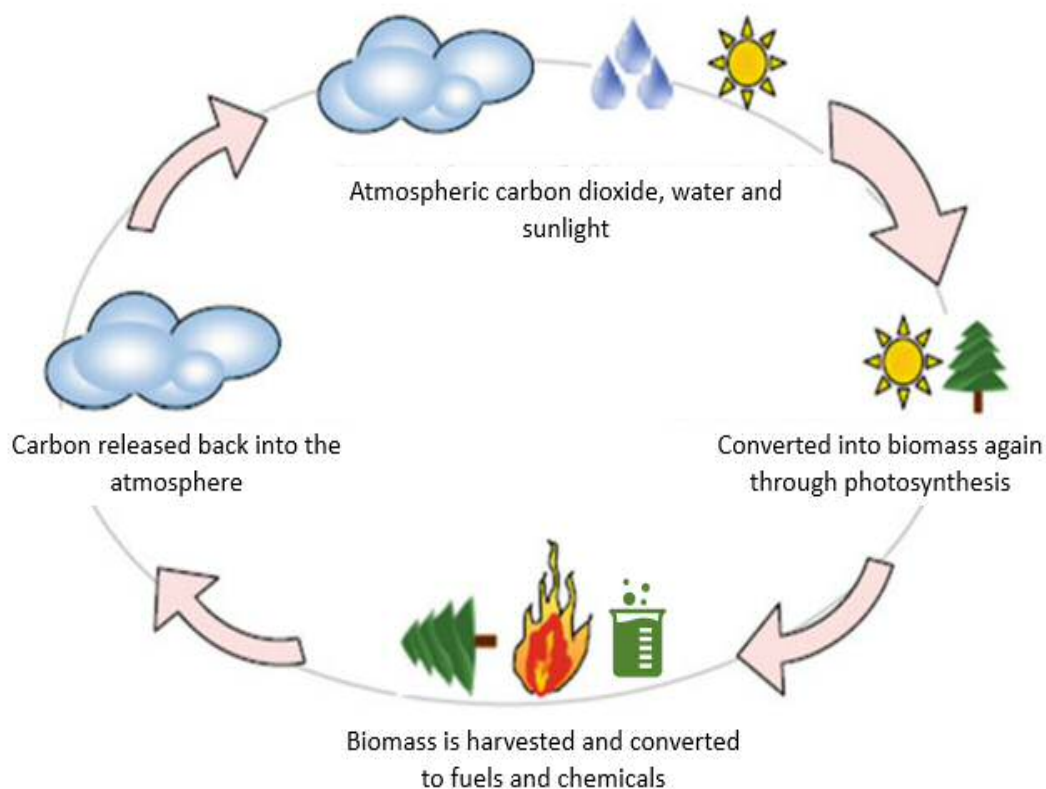


Figure 1.2 Biomass as a renewable and clean resource for fuel and chemical production, modified from [3].

1.2. Objective: Biomass valorization through catalytic hydroprocessing

Catalytic hydroprocessing is a key reaction class in the valorization of biomass molecules into a variety of fuels and chemicals. Over the last two decades, a large amount of experimental and computational research related to hydroprocessing of biomass has been carried out with the aim of introducing innovative methodologies, developing new processes and improving the understanding of the underlying reaction mechanisms. The primary aim of this work was to valorize different classes of biomass into chemicals and fuels by selective hydroprocessing. The study of three different reaction systems, shown in Figure 1.3, is the focus of the present work.

The initial objective was to identify a viable approach for achieving selective alcohol production from biomass-derived feedstocks, rather than relying on fossil-derived sources. Furans: furan, 2-methylfuran (MF), and 2,5-dimethylfuran (DMF) are attractive biomass

derived molecules that can serve in achieving this target. Furans can be produced with more than 90 % selectivity at complete conversion from furfural (FFR) and hydroxymethylfurfural (HMF) derived from cellulose and hemicellulose [4]. Therefore, the selective ring opening of furans through hydrogenation reaction in order to produce alcohols as shown in Figure 1.3 was firstly targeted. Another class of biomass is fats/oils or triglycerides. They are mainly used for the production of biodiesel through transesterification with methanol. A major byproduct of biodiesel production during transesterification is glycerol (GL), which corresponds to 10 wt.% of the biodiesel produced. In order to achieve the sustainability of biodiesel production, it is necessary to upgrade this huge amount of GL into valuable products. Accordingly, the second objective of the present work was to valorize GL, as a derivative of biomass, into 1,2 propanediol (1,2 PD) through hydrogenolysis. The third objective of this work was to produce aromatics from a renewable source, such as lignin obtained from biomass, rather than relying on finite fossil resources. Reductive catalytic fractionation (RCF) represents a promising technology for achieving this goal. Consequently, RCF was applied on some rich-in-lignin-feedstocks such as beech wood, rye straw and industrial straw digestate in order to maximize the aromatic monomer yields produced from biomass.

One intriguing class of catalysts that exhibit excellent physicochemical properties, tunable Brønsted/Lewis-acidity and redox properties are polyoxometalates (POMs). For achieving each of the above-mentioned objectives, the application of POMs was also investigated either by using metal incorporated POMs, using POMs as catalyst support or even by using POMs as an additive to the reaction medium.

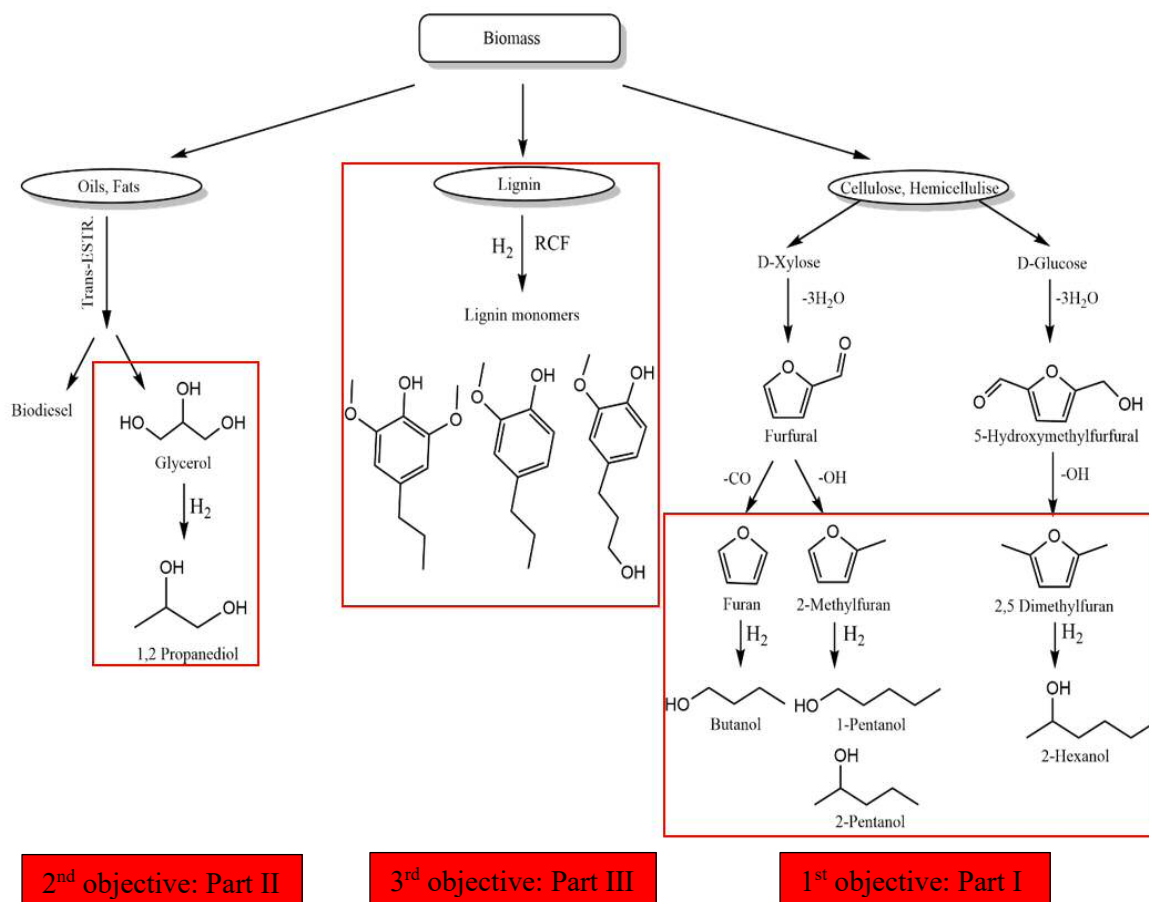


Figure 1.3 Scope of the thesis: in which three different reaction systems were investigated for biomass valorization into chemicals and fuels through selective hydroprocessing.

1.3. Outline of the dissertation

The dissertation, “Catalytic hydroprocessing of biomass derived compounds to renewable biofuels and chemicals using polyoxometalate catalysts” aims at valorizing the biomass molecules into higher value-added products using different hydroprocessing techniques. It is organized in 10 chapters and generally contains: introductory part which includes chapter 1 & 2, cumulative part of the dissertation which includes 3 publications, and unpublished part of the dissertation.

Chapter 1 of this dissertation provides an introduction to the significance of upgrading biomass in order to substitute fossil resources and outlines the objectives of the current work. Chapter 2 provides a theoretical background on biomass, including its composition and properties. The chapter also discusses the use of hydrogen in different biomass upgrading routes and reports several applications of POMs as efficient catalysts or co-catalysts in different biomass hydroprocessing reactions. In addition, the chapter provides background information on the three hydroprocessing reaction systems under investigation.

The experimental work of the dissertation can be divided into four parts:

Part I: Hydroprocessing of biomass derived furans

This part encompasses chapters 3 & 4 and focuses on the selective production of alcohols from bioderived furans through hydrogenation. DMF was chosen as a model substrate in order to find a selective catalyst system towards ring opening and alcohol formation. After that, the best catalytic system found was extended to two additional furan compounds. Chapter 4 entails a response surface methodology investigation employing DMF as a model substrate, aiming to determine the optimum reaction conditions that yield the highest alcohol output.

Part II: Hydroprocessing of biomass derived glycerol

This part includes chapter 5 which focuses on the selective production of 1,2 PD from GL through hydrogenolysis and reports the effect of surface modification of Ru based catalyst with other transition metals such as Fe or Cu on the selectivity towards 1,2 PD.

Part III: Hydroprocessing of lignin

This part belongs to the unpublished section of the dissertation and comprises chapter 6 which focuses on the production of aromatic monomers from lignin through RCF under mild reaction conditions. Industrial digestates were discussed in this chapter as a potential lignin-first-substrate for RCF under hydrogen atmosphere. The effect of different operating reaction conditions on the selective production of propanol-substituted phenols (SPOH/GPOH) was investigated as well.

Part IV: Influence of POMs in hydrogenation of furans, glycerol hydrogenolysis, and lignin valorization via reductive catalytic fractionation

This part belongs to the unpublished section of the dissertation and includes chapter 7. This chapter provides an elucidation for the effect of applying POM catalysts in the three biomass hydroprocessing reactions discussed in parts I, II and III.

Chapter 8-10 are comprehensive discussion, bibliography, and appendix, respectively.

1.4. Strategy of the research

Regarding the three above-mentioned approaches of biomass upgrading through hydroprocessing (hydroprocessing of biomass derived furans, hydroprocessing of biomass derived glycerol, and hydroprocessing of lignin), a systematic research strategy was employed when performing the investigations.

The initial step was to choose a suitable model substrate as a reactant for the first set of experiments. For instance, DMF in the hydroprocessing of furans and beech wood for the hydroprocessing of lignin. Once the model substrate was chosen, a comprehensive literature review was conducted to identify potential reaction pathways that may occur during the hydroprocessing reaction. This enabled the identification of a range of potential products that may be formed, which was then validated through analytical techniques such as gas chromatography (GC) and high-performance liquid chromatography (HPLC). A calibration was then performed on those analytical equipment to accurately quantify the yield of each product, allowing for a detailed evaluation of the reaction under investigation.

Subsequently, the experimental investigations commenced by assessing the catalytic activity of various metal active sites within the catalyst. The aim was to determine the most suitable metal site in terms of both activity and selectivity towards the desired product. In order to optimize the performance of the catalytic system, POMs were applied to the reaction under investigation. The application of POMs took various forms, including the use of metal-substituted POMs, (chapter 3 & 7), and POMs as a support for the chosen metal site (chapter 3 & 4), or even as an additive in the reaction medium (chapter 7).

Following the selection and optimization of the catalytic system, a number of characterization techniques including: Transmission electron microscope (TEM), Inductively coupled plasma optical emission spectroscopy (ICP-OES), Fourier Transform Infrared Spectroscopy (FTIR), CO-chemisorption, N₂-physisorption, X-ray diffraction (XRD), Temperature programmed desorption of ammonia (NH₃-TPD) and H₂-Temperature programmed reduction (H₂-TPR) were employed to gain insight into the underlying reasons for the observed higher performance of this catalytic system in the specified reaction.

Upon that, the investigations were extended to include other substrates to assess the potential of applying the hydroprocessing reaction to alternative substrates. For instance, in the case of DMF hydrogenation, investigations were extended to include furan and MF. In case of RCF, the investigations were extended to include straw, and straw digestates. Moreover, if the composition of substrate is too complex, the effect of its pre-treatment was also examined (chapter 6). Sometimes, the effect of changing the solvent on the selectivity towards the desired product was studied as well (chapter 3). Additionally, time resolved investigations were performed to gain insights into the kinetics of each hydroprocessing reaction.

The investigations ended up with studying and optimizing the system by changing the crucial reaction conditions such as hydrogen pressure, hydroprocessing temperature, reaction time, and catalyst to substrate ratio using either the one-factor-at-a-time (OFAT) method or the response surface methodology (RSM). In chapter 4, RSM, that involves statistical design of experiments (DoE) where all variables are varied together over a set of experimental runs, was applied on the hydrogenation reaction of DMF. On the other hand, the OFAT method, in which the effect of each variable on a process is studied while holding the others constant, was applied on RCF reaction.

Chapter 2. Theoretical background

This chapter represents the theoretical background of the dissertation. It starts with an introductory discussion of biomass, its classification, and a brief discussion about the relevant processes for biomass upgrading with a focus on hydroprocessing as a key technology for biomass upgrading. Following this, background information is given about each of the upgrading hydroprocessing reactions under investigation i.e., hydrogenation of furans, hydrogenolysis of glycerol and RCF for lignin valorization. Each hydroprocessing reaction is comprehensively reviewed in terms of the derivation of the biomass substrate and the diverse strategies employed for its valorization. The industrial significance of the desired products, the conventional pathways utilized for producing them, and the attendant limitations of these conventional approaches are also described. Furthermore, the reaction network, other potential by products and mechanisms underpinning each reaction are elucidated. Moreover, an in-depth analysis of the typical reaction conditions and catalysts employed, alongside other pertinent aspects, is presented. In order to find new application of POMs in hydroprocessing reactions of biomass, POMs are applied to each reaction under investigation either in the form of metal substituted POMs, as catalyst supports, or as additives to the reaction medium. Thus, a theoretical background on POMs as efficient catalytic systems and their applications is provided. Finally, the chapter ends with a comparison between the two distinct methodologies employed for studying the effects of varying the reaction conditions in the systems, namely OFAT approach and RSM.

2.1. Biomass valorization through catalytic hydroprocessing

2.1.1. Biomass

Biomass represents one of the most abundant resources with immense potential for sustainable and renewable energy and chemical production, and is the only renewable organic resource on our planet. It comprises all materials of organic origin containing carbon. This definition extends beyond plants and their derivatives to include animal sources as well [5]. On an annual basis, around 170 billion tons of biomass are produced, yet merely 3.5% of this vast resource is harnessed by humans. In terms of quantity and as presented in Figure 2.1, cellulose is the most available biomass raw material and accounts for over a third of its quantity, closely followed by lignin and hemicellulose. Although oils and fats represent only less than 5 % of the biomass quantity, they remain of tremendous interest due to their significant involvement in the production of biodiesel [2].

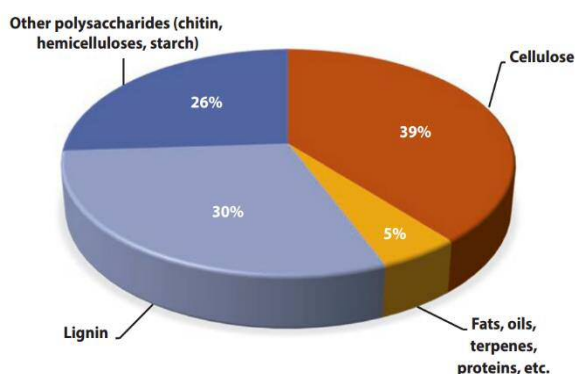


Figure 2.1 Main ingredients of biomass (in wt.%) [2].

Cellulose

Cellulose is the most common polysaccharide and represents the main constituent of biomass. It is a homopolymer of D-glucose units linked to each other via β -1,4-glycosidic bonds (Figure 2.2). It has the formula $(C_6H_{10}O_5)_n$ and a mean molecular weight of $100,000 \text{ g mol}^{-1}$ [6]. The origin of the cellulose source defines its degree of polymerization (DP), for example DP of cellulose is between 300-1700 for pulpwood and 800-10,000 for cotton [7]. Cellulose is insoluble in water and most common organic solvents, and this is due to the intra and intermolecular hydrogen bonds resulted from high number of hydroxyl groups and β -1,4-glycosidic bonds linkage [8]. Cellulose is composed not only of crystalline domains but also of amorphous domains. It has several forms, and the crystal features define which form exists. Natural cellulose is denoted as cellulose I, which is a mixture of cellulose I $_{\alpha}$ (triclinic) and I $_{\beta}$ (monoclinic). Cellulose II is formed through alkali treatment of cellulose I. Cellulose III $_{I}$ and III $_{II}$ are obtained via liquid ammonia treatment of cellulose I and Cellulose II, respectively. Heating celluloses III $_{I}$ and III $_{II}$ produces celluloses IV $_{I}$ and IV $_{II}$, respectively [9]. Some examples of cellulose-derived platform chemicals are levulinic acid, ethylene glycol, 5-hydroxymethylfurfural, furfuryl alcohol, and γ -valerolactone [9]. Cellulose and its derivatives have several industrial applications in food, pharmaceutical, emulsifier, paper and textile industries [5, 6].

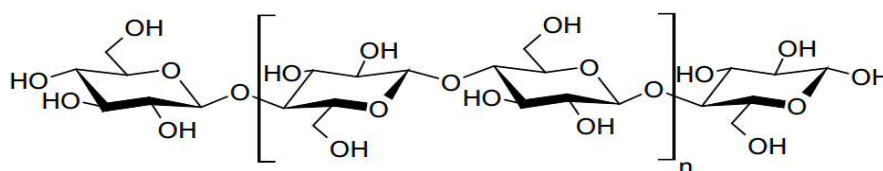


Figure 2.2 Structural section of cellulose [10].

Hemicellulose

Hemicellulose is an amorphous heteropolymer with a very diverse composition. It composes mainly of several pentoses (xylose and arabinose) and hexoses (galactose, glucose and mannose) with xylose being the most abundant building block [9], as presented in Figure 2.3. Unlike cellulose, hemicellulose typical chain is branched and shorter than the cellulose chain, which inhibits the formation of crystals and make hemicellulose easier to be hydrolyzed compared to cellulose [11]. In lignocellulosic biomass, the hemicellulose fraction is partially bound to lignin fraction through its side chains. Additionally, cellulose strands are intertwined with hemicellulose. Therefore, if the recovery of glucose from cellulose is targeted with high selectivity from lignocellulosic biomass, it is preferred to remove hemicellulose fraction during pretreatment. Through dilute acid hydrolysis of hemicellulose fraction, xylose monomers are produced with high selectivity, which can be further processed either by fermentation to produce ethanol or dehydration to produce furfural [9, 10].

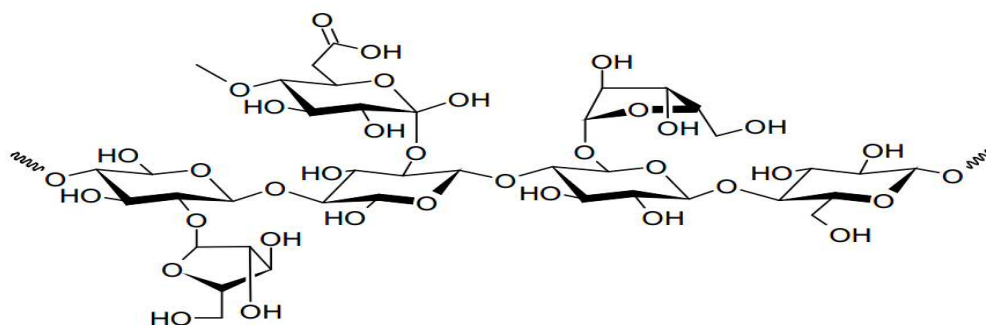


Figure 2.3 Structural section of hemicellulose [10].

Lignin

Lignin is the second most abundant biopolymer on the planet, after cellulose, and considered to be the largest natural source of aromatics [12]. It is a heavily branched (co-)polymer composed of methoxylated phenylpropane building blocks (monolignols) such as: *p*-coumaryl, coniferyl and sinapyl alcohols. These monolignols constitute the lignin structure either in hardwood, softwood, or herbaceous crops, and are described in Figure 2.4 (a). In addition to the above mentioned building blocks, other phenolic compounds such as hydroxycinnamates (*p*-coumarate, ferulate), Figure 2.4 (b), might be incorporated in lignin structure [13].

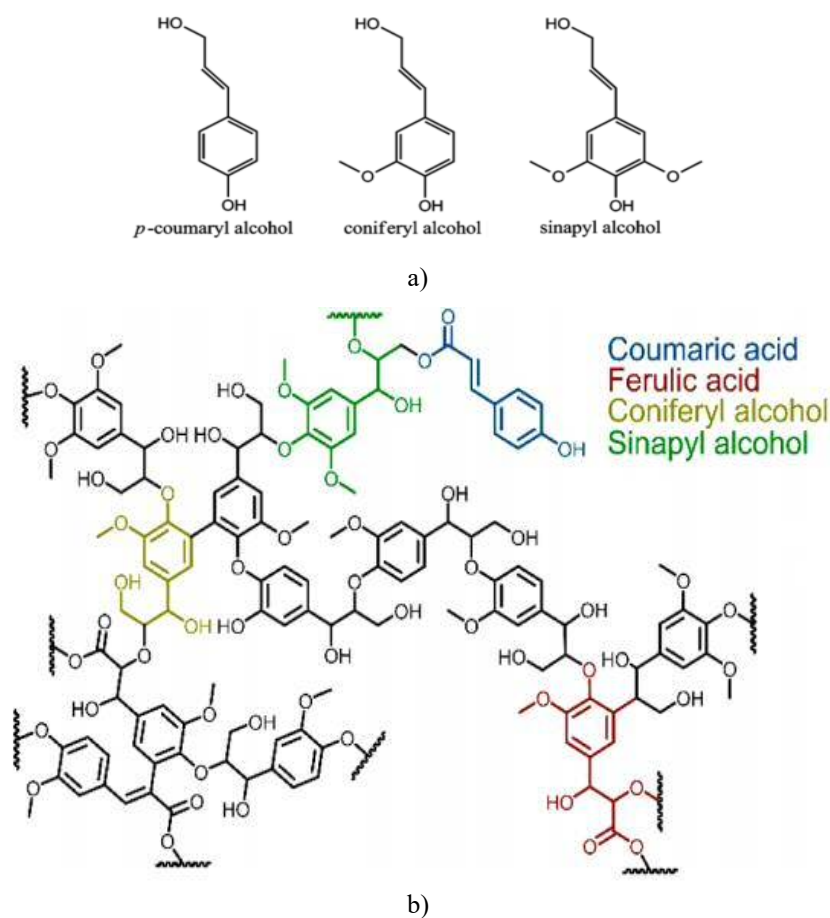


Figure 2.4 a) The methoxylated phenylpropane building blocks of lignin b) Coumaric acid and ferulic acid incorporated in lignin structure of herbaceous biomass [14].

Lignin is a hydrophobic amorphous polymer and has extreme resistance towards degradation [9, 15]. It is responsible for the structural rigidity and the hydrophobic transportation system of water and solutes in plants [16]. In lignin, the monolignols have three different numbers (0,1,2) of methoxy groups attached to the phenol ring, which result in three lignin units (H (hydroxyphenyl), G (guaiacyl), and S (syringyl), respectively). The ratio between the units differs depending on the origin of lignin. Softwood lignin contains a percentage of 90-95 % of G units, whereas it is only limited to 25-50 % in hardwood lignin and the majority are S units (50-75 %). In grass lignin, G units represent (35-80 %), S units (20-55 %) and H units (5-35 %) [12, 17]. Unlike most of the natural polymers, there are many linkages between phenylpropanoid units that exist in lignin. The interconnection involves ether bonds (C–O–C) or “non-condensed bonds”, such as β -O-4', α -O-4, 4-O-5'; and carbon–carbon bonds (C–C)

or “condensed bonds” like β - β' , β -1', β -5' and 5-5' (see Figure 2.5) [12]. Generally, β -O-4 ether bond is the most abundant linkage with 50 % in softwoods and 60-85 % in hardwood. The existence of other linkages in the lignin structure is largely dependent on the plant families. For example, hardwood lignin contains less 5-5 and β -5 linkages than softwood lignin. This is attributed to the high abundance of S units in hardwood, which results in the additional presence of methoxy groups in the aromatic ring that prevent C-C formation [18, 19]. Lignin can either be burnt in order to provide energy for the biorefinery or valorized through several techniques to phenolic resins and aromatics [9, 10].

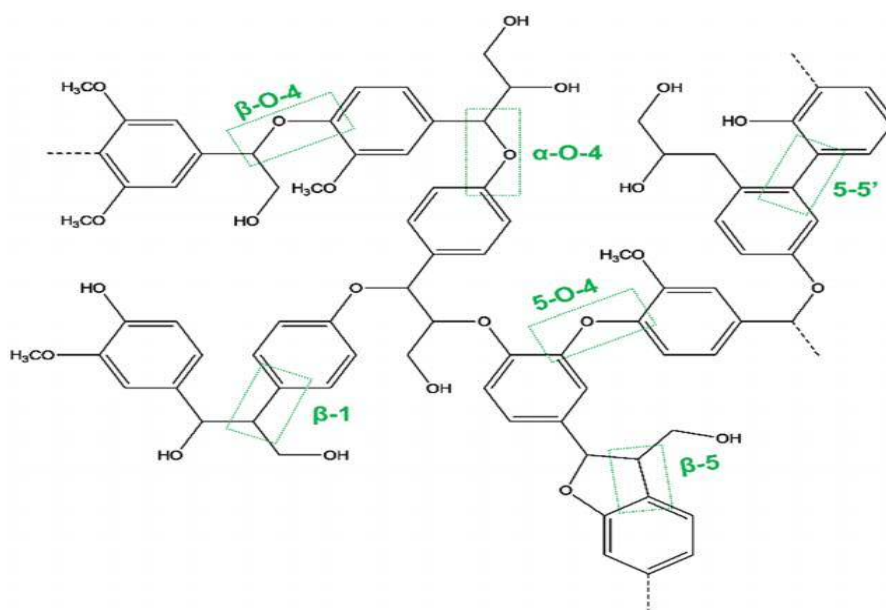


Figure 2.5 Hypothetical molecular structure of lignin [12].

Fats and oils

Natural fats are a group of lipids consisting of triglycerides, three long-chain fatty acids attached to a glycerol backbone, as shown in Figure 2.6. The chain is usually unbranched and contains from 4 to 26 carbon atoms. If the fats exist in the liquid phase at room temperature, they are referred to as oils [6, 20]. Sources of fatty oils are diverse and include various vegetable oils, waste oils as well as algal sources [10]. For example, pressing the seeds of rape or sunflower crops produces vegetable oil, which has several industrial applications in coatings, cosmetics, lubrication, and biodiesel production [5, 21, 22].

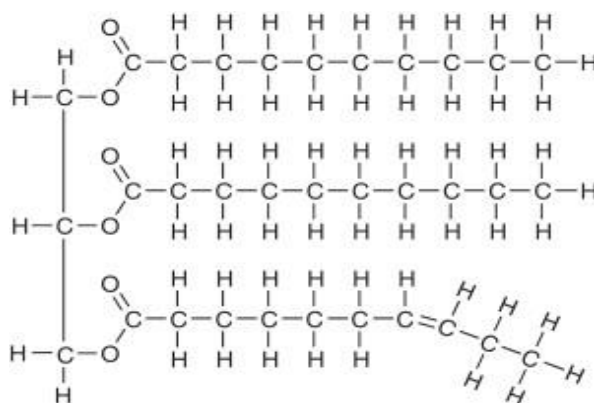


Figure 2.6 Molecular structure of triglycerides.

2.1.2. Hydrogen and its role in biomass valorization

Hydrogen is considered to be one of the most promising energy carriers in the future. In addition to the conventional ways of hydrogen production, (e.g., steam reforming in which methane reacts with water to produce hydrogen and carbon monoxide), it can be produced renewably through water electrolysis using surplus electricity gained from renewable wind and solar energies [2, 23, 24]. The utility of this hydrogen spans across multiple domains, with one of the most discussed options being its reconversion back into electricity. However, low round trip efficiencies render this option unattractive [23]. In lieu of this, employing renewable hydrogen as a (co-)feedstock for chemical industries, refineries, and biorefineries seems to hold significant promise.

Within chemical and industrial applications, a distinction arises between processing crude oil and natural biomass feedstocks due to their differing chemical compositions. Crude oil is primarily composed of simple hydrocarbon chains containing only carbon and hydrogen, with minimal oxygen content. In contrast, biomass as a renewable resource is considerably more complex, containing higher quantities of oxygen in addition to carbon and hydrogen (see Figure 2.7). Sometimes, biomass contains considerable amounts of other elements such as nitrogen, phosphorus, and sulfur. The majority of chemicals utilized in our daily lives comprise carbon, hydrogen, oxygen, or nitrogen. Present-day chemistry, which relies on crude oil as a feedstock, necessitates the introduction of these elements through oxidative-type chemistry. In contrast, the chemistry of the future, which relies on biomass as a feedstock, will necessitate the removal of oxygen or the implementation of the reductive chemistry [2].

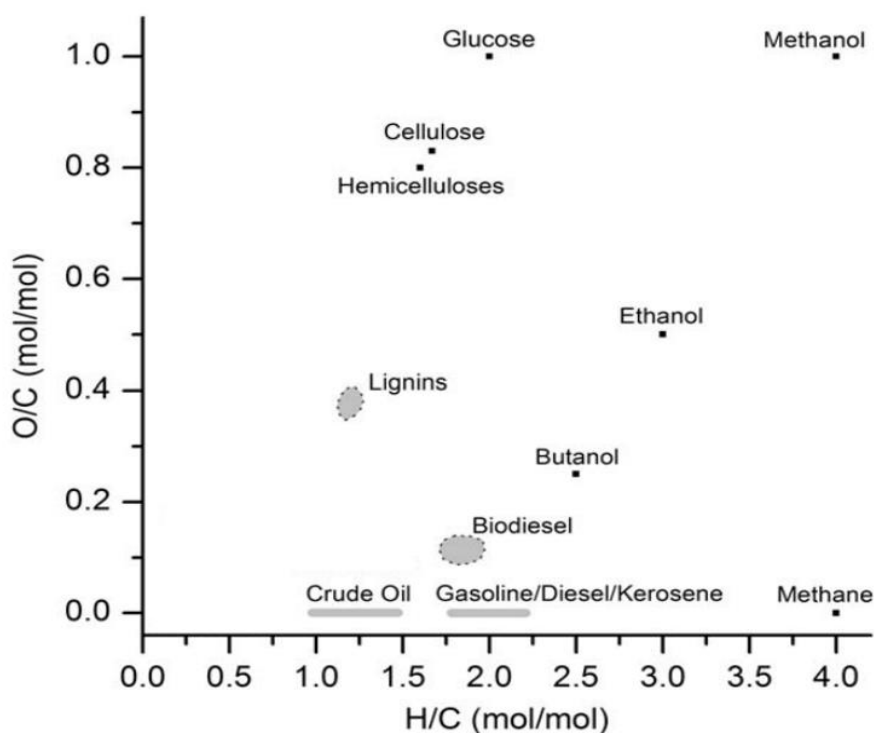


Figure 2.7 Oxygen and hydrogen content of biomass components compared to fossil resources and other traditional chemicals, modified from [25].

Figure 2.7 illustrates why the reductive chemistry will be the chemistry of the future. A cursory observation of the figure shows that the primary components of biomass contain higher amounts of oxygen and lower amounts of hydrogen than the majority of the potential target end products. While decarboxylation and decarbonylation reaction pathways can be employed to reduce the O/C ratio in biomass, they are insufficient for achieving this objective. Hydrodeoxygenation (HDO) represents the only viable pathway that can be utilized in conjunction with these methods to further remove oxygen. To increase the H/C ratio, hydrogen must be added directly, either through hydrogenation and hydrogenolysis pathways or indirectly after the dehydration pathway [26].

Irrespective of the choice of gasification [26], thermochemical or hydrolytic [27] upgrading pathway for biomass valorization, hydrogen represents an essential (co-)feedstock for this process in order to increase H/C ratio [28, 29]. Upgrading of biomass through gasification produces syngas with a H₂/CO ratio of 1, but the process of producing methanol from this syn-gas and the Fischer-Tropsch process need twice this amount of hydrogen. Therefore, the addition of external hydrogen is required in both cases. Methanation even requires higher H₂/CO ratio which is equal to 3 [23]. Thermochemical upgrading processes of biomass produce pyrolysis oil with poor chemical stability, consequently further hydrotreatment with hydrogen to reduce oxygen content and increase the H/C ratio is mandatory [30]. Most upgrading techniques for sugars into furan derivatives, hydrolytic pathway, require hydrogen in several steps such as hydrogenation and hydrogenolysis in order to increase H/C ratio [31]. Additionally, hydrogen is mainly required in the valorization of lignin fraction into aromatic hydrocarbons. Table 2.1 outlines various processes in which hydrogen is utilized to valorize biomass and biomass derived compounds into chemical intermediates and end products.

Table 2.1 Examples for biomass valorization processes that use hydrogen as a (co-)feedstock.

	Process	Ref.
1	Hydrolytic hydrogenation of cellulose and hemicellulose to sorbitol and xylitol	[27]
2	Hydroconversion of furfural and 5-hydroxymethylfurfural	[32]
3	Hydrogenation and hydrodeoxygenation of furans into alkanes and diesel fuel	[33, 34]
4	Hydrogenation of levulinic acid to g-valerolactone	[35]
5	Hydrogenation of 2,5 dimethylfuran into 2-hexanone	[36]
6	Reductive catalytic fractionation for lignin valorization	[37]
7	Catalytic hydrogenolysis and subsequent HDO of lignin	[27]
8	Methanol production from biomass derived syn-gas	[26]
9	Fischer-Tropsch process using biomass derived syn-gas	[26]
10	Methane production from biomass derived syn-gas	[26]
11	Catalytic hydrotreatment of fast pyrolysis oils	[38]
12	Hydroconversion of vegetable oils into biofuels	[39]
13	Hydrogenolysis of glycerol to propanediols	[40]

In summary, hydroprocessing represents a critical element of biomass valorization, due to the low H/C ratio in biomass compared to traditional chemicals and fuels. Fortunately, the hydrogen required for these hydroprocessing techniques can be obtained renewably via water electrolysis. The present work focuses on three hydroprocesses, described in Figure 1.3, for valorizing biomass and biomass derived compounds. These processes include hydrogenation of furans, RCF for lignin valorization, and hydrogenolysis of glycerol. Sections (2.3-2.5) provide details on each of these processes. However, before discussing these topics, section 2.2 offers a theoretical background on POMs and their applications in biomass valorization via hydroprocessing.

2.2. Polyoxometalates

Polyoxometalates (POMs) are a distinctive class of anionic metal oxide clusters that have a wide range of applications including medicine, fuel cells, material science, analytical chemistry, corrosion protection and catalysis [41-44]. They own tailored physicochemical properties, such as high solubility in various solvents, chemical and thermal stability, modifiable Brønsted/Lewis-acidity and redox properties [45]. POMs have several applications in the field of homogenous and heterogenous catalysis, and can be applied as acidic homogenous catalyst, metal-POM composites, acidic support for noble or transition metals, and as additives that can control the activity or selectivity towards the desired products. In the present work they will be applied for the hydroprocessing reactions under investigation, and thus, pertinent fundamentals of POMs will be explicated herein.

2.2.1. Molecular structure and classification of POMs

In general, POMs are typical inorganic polyatomic species composed of several $(\text{MO}_x)_n$ units, where M is a light transition metal such as vanadium (V), molybdenum (Mo), niobium (Nb), tungsten (W), or tantalum (Ta), in their highest oxidation state and x ranges from (4-7) [46, 47]. Usually, POMs are formed by protonation of an oxometalate ion under suitable temperature and pH value with polycondensation of the $[\text{MO}_4]^{2-}$ units. If the condensation reaction happens between two identical units, an isopolyanion will be formed. On the other hand, if the condensation of several oxoanions takes place around a central heteroatom Z, heteropolyanions will be formed [5, 48]. POMs can be classified into two main categories. The first group are isopolyoxometalates with the form $[\text{M}_x\text{O}_y]^{n-}$, where M is a transition metal such as Mo, W, or V. The second group are heteropolyoxometalates with the form $[\text{Z}_z\text{M}_x\text{O}_y]^{n-}$ where $z < x$ [5, 45]. POMs are categorized into those two groups depending on the absence or the presence of the central heteroatom (Z) in the POM skeleton. In contrast to isopolyoxometalates, which do not have any heteroatom in their structure, the heteropolyoxometalates have one or more metallic or non-metallic heteroatoms such as B, Si, Ge, P, or As incorporated into their structure [49, 50].

As no isopolyoxometalates were applied in the present work, heteropolyoxometalates will be only discussed further. The most popular heteropolyanions are the Keggin- $[\text{ZM}_{12}\text{O}_{40}]^n$, Wells-Dawson- $[\text{Z}_2\text{M}_{18}\text{O}_{62}]^n$ and the Anderson-type $[\text{ZM}_6\text{O}_{24}]^n$ [51, 52]. The three structures of those heteropolyanions are presented in Figure 2.8. In the Keggin and Wells-Dawson POMs (Figure 2.8 a, b), the tetrahedral coordinated heteroatoms (Z) are surrounded by metal oxide units spherically, while in the Anderson type (Figure 2.8 c) the metal oxide units shape a ring around the central heteroanion [5]

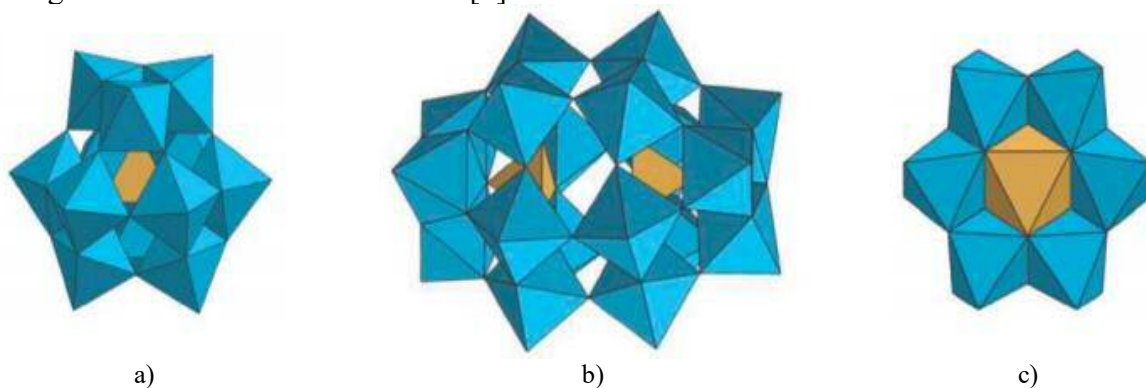


Figure 2.8 Structure of hetero-POMs a) Keggin structure b) Wells-Dawson structure c) Anderson structure, brown clusters represent heteroanions in POMs structure, adapted from [53].

Figure 2.9 presents an example for the different rotational isomers of a Keggin structure $[ZM_{12}O_{40}]^n$ POM. The α -isomer, the most stable structure, consists of a central tetrahedral coordinated ZO_4 encapsulated by 12 edge- and corner-sharing MO_6 octahedra units. Those 12 MO_6 units form four groups of M_3O_{13} . The central heteroanion ZO_4 is attached to each of those four M_3O_{13} groups through its four oxygen atoms [54]. If one M_3O_{13} group is rotated by 60° , the β -isomer, which is energetically less favorable than the α -isomer, will be formed. Further rotation of other M_3O_{13} groups result in unstable γ , δ , and ϵ -isomers [55, 56]. Similar to Keggin type, the Wells-dawson type has several rotational isomers.

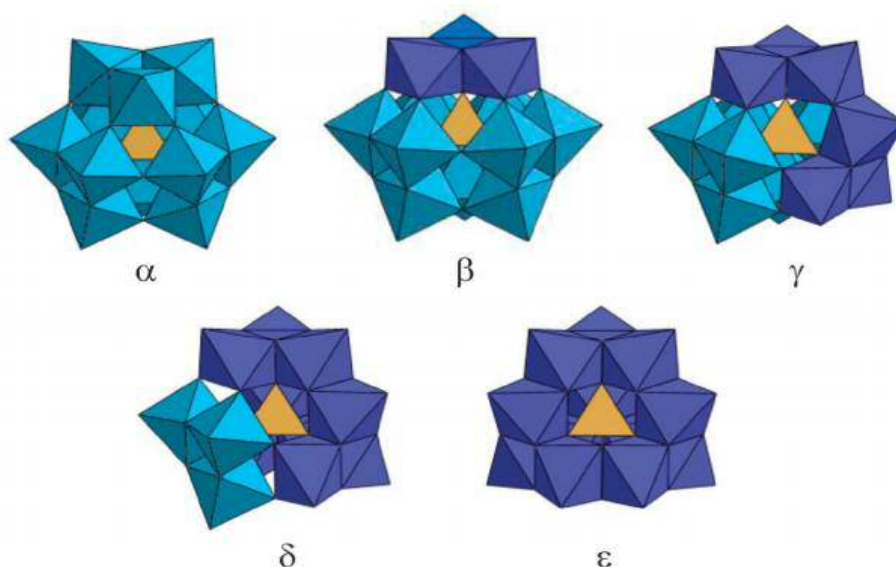


Figure 2.9 Graphical illustration of the five rotational isomers of the Keggin structure, adapted from [41, 53].

The polyoxometalate clusters are usually anionic and their negative charge are balanced by protons that form heteropolyacids or by inorganic counter-cations (e.g., Na^+ , Ag^+ , K^+ , Cs^+ , NH_4^+) that form acid salts [54]. The properties of POMs such as solubility, acidity and redox potential can be adjusted by incorporating those counter cations or by changing element components to form metal-POM composites [57, 58]. As shown in Figure 2.10, the removal of one or more M centers from the polyanion leaves free positions for incorporation of catalytic active metals or their complexes in the POM skeleton and results in metal-POM composites [4, 59].

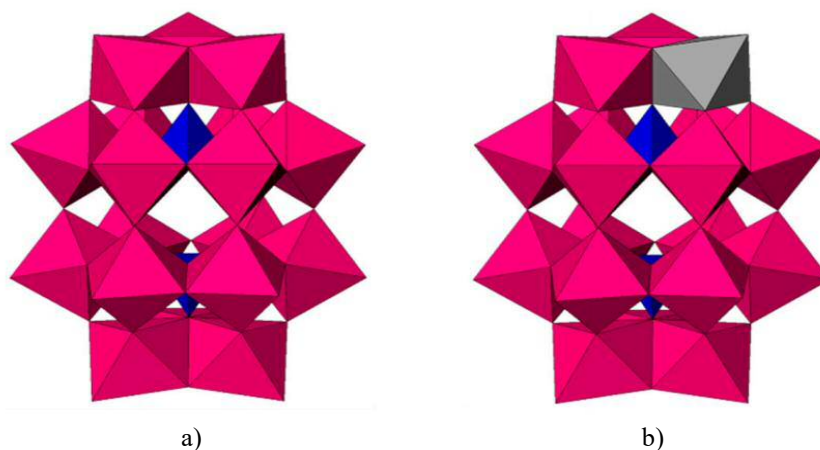


Figure 2.10 a) Wells–Dawson structure POMs b) Metal incorporated in Wells–Dawson structure POMs, blue clusters represent heteroanions (ZO_4), grey cluster represent Ru, Pt or Pd cluster [59].

In this work the above mentioned Keggin-type POMs and Well-Dawson-type POMs in forms of heteropolyacids, heteropolyacid salts, metal-POMs composites, or metal supported POMs were applied to the reactions under investigations.

2.2.2. POMs applications in hydroprocessing reactions

POMs have already demonstrated their applicability in both heterogeneous and homogeneous catalysis of acid-catalyzed reactions and oxidation reactions [44, 60-64]. Their applicability in reduction transformations and hydroprocessing is currently being actively explored and has already been demonstrated for photoreduction of CO₂ [44, 65], selective catalytic reduction of NO with ammonia [66], and other hydroprocessing reactions presented in Table 2.2. In some instances, heteropolyacids or their corresponding salts have been employed as sole reductive catalysts under H₂ atmosphere (Table 2.2 entry 1-4). Another efficient approach for POM applications in hydroprocessing reactions involves the substitution of metals within the POM skeleton, as demonstrated (Table 2.2 entry 5,6). Additionally, POMs can serve as supports for metal sites, thereby generating bifunctional catalysts within the reaction medium, as presented in Table 2.2 entry 7-10. Furthermore, various studies have utilized physical mixtures of POMs and other metal-supported catalysts for hydroprocessing reactions (Table 2.2 entry 10,11). In all those studies, the addition of POMs proved to enhance either the activity of the catalyst or the selectivity towards some specific products.

Table 2.2 POMs applications in hydroprocessing reactions.

Entry	Catalyst	Process	Ref.
1	K ₅ PV ₂ Mo ₁₀ O ₄₀ , K ₄ SiW ₁₂ O ₄₀	Deoxygenation and hydrogenation of aromatic ketones and aldehydes	[67]
2	Co _{1.5} [PMo ₁₂ O ₄₀], Ni _{1.5} [PMo ₁₂ O ₄₀], H ₃ [PMo ₁₂ O ₄₀]/TiO ₂ , H ₃ [PMo ₁₂ O ₄₀]/Al ₂ O ₃	Hydrodesulfurization of thiophene	[68]
3	H _{3+n} [PMo _{12-n} V _n O ₄₀] (n=0–2) and their Cs ⁺ salts	Vapor phase hydrogenation of propanoic acid	[69]
4	H _{3+n} [PMo _{12-n} V _n O ₄₀] (n=0–2) and their Cs ⁺ salts	Gas-phase hydrogenation of hexanoic acid	[70]
5	K ₅ PPdW ₁₁ O ₃₉ /C, K ₅ PPdW ₁₁ O ₃₉ /Al ₂ O ₃	Catalytic hydrogenation of aromatic compounds and ketones	[71]
6	PdMPA/SiO ₂ *	Reductive amination of carbonyl compounds	[72]
7	Pt/C _{S2.5} H _{0.5} PW ₁₂ O ₄₀	Hydrodeoxygenation of 3-pentanone to n-pentane	[73]
8	Pd/ C _{S2.5} H _{0.5} PW ₁₂ O ₄₀	One pot conversion of acetone to methyl isobutyl ketone through condensation followed by dehydration and selective hydrogenation	[74]
9	Pd–H ₃ PW ₁₂ O ₄₀ /SiO ₂ **	One-pot conversion of citronellal to menthol via acid-catalyzed cyclization followed by Pd catalyzed hydrogenation	[75]
10	Pt/C _{S2.5} H _{0.5} PW ₁₂ O ₄₀ , Pt/Al ₂ O ₃ + C _{S2.5} H _{0.5} PW ₁₂ O ₄₀	Catalytic hydroisomerization of n-butane into iso-butane	[76]
11	Pt complex +H ₅ PV ₂ Mo ₁₀ O ₄₀	Reductive coupling of aryl aldehydes	[77]

* Palladium exchanged molybdophosphoric acid catalyst.

** Catalyst prepared by impregnation of 20% H₃PW₁₂O₄₀/SiO₂ with Pd-precursor followed by reduction of Pd(II) to Pd(0).

There is limited research involving POMs in valorization of biomass and biomass-derived compounds through reductive transformation and hydroprocessing compared to valorization through oxidation. Nonetheless, a number of instances of such applications have been documented in the literature and are summarized in Tables (2.3-2.5). The majority of studies found in the literature for applying POMs in valorizing biomass via hydroprocessing have predominantly utilized POMs as either a support or an acid site in conjunction with noble or transition metal sites (Table 2.4) or by combining them with another catalyst as a physical mixture in the reaction medium (Table 2.5). However, a comparatively lesser number of investigations, as presented in Table 2.3, have been conducted utilizing heteropolyacids, their corresponding salts, or metal-substituted POMs as sole reductive catalysts for the valorization of biomass via hydroprocessing.

In Tables (2.3-2.5), POMs are applied for valorization of several biomass compounds including straw bulb, cellulose, biomass derived furfural, HMF, lignin oil, lignin monomers, and glycerol into valuable chemicals through hydroprocessing reactions, including hydrogenation, hydrogenolysis, hydrolytic hydrogenation, hydrodeoxygenation, and one pot conversion processes that involve at least one hydroconversion step necessary for valorization. A quick glance on the tables demonstrates how POMs can affect the catalyst or metal site activity, resulting in significant changes in the final conversion (X %) of the process. Furthermore, POMs can significantly alter the selectivity (S %) towards a desired product.

Entries (32-54) in Table 2.4 represent a good example that clearly illustrates how POMs can be utilized to modify the activity of the catalyst and alter the selectivity towards a specific product during glycerol hydrogenolysis. For instance, Pt-Li₂H₂SiW₁₂O₄₀/ZrO₂, Table 2.4 (entry 35), is responsible for high selectivity up to (53.6 %) towards 1,3-propanediol. On the other hand, Pt-H₄SiW₁₂O₄₀/ZrO₂, Table 2.4 (entry 40) showed less affinity towards 1,3-propanediol and higher selectivity up to (80 %) towards n-propanol. Additionally, Ru/Cs_{2.5}H_{0.5}PW₁₂O₄₀, Table 2.4 (entry 53) resulted in higher selectivity up to (73.6 %) towards 1,2-propanediol. Other examples for hydrolytic hydrogenation of cellulose and hydrodeoxygenation of δ -furfurylidenelevulinic acid (FDLA) are given in Table 2.5 (entries 4-6) and (entries 15-18), respectively. Another general observation that can be made from comparing various entries in Table 2.3 and Tables 2.4-2.5 is that the application of POMs as an acid function in conjunction with a metal function, or in a physical mixture with another catalyst in the reaction medium yields superior results in hydroprocessing compared to using POMs alone or employing metal POM composites as reductive catalysts.

The tables presented (2.3-2.5) comprehensively summarize the diverse applications of POMs in biomass valorization through hydroprocessing reported in literature and show how tunable POMs are. Changing counter cation, metal substitution in POMs skeleton, impregnating of POMs with another metal on a commercial support, using POMs as a support, and adding them in a physical mixture to the reaction medium, all these alternatives provide different characteristics in the reaction medium, which in turn allows for different applications and provide a way for controlling the selectivity towards the desired products during the reaction.

After presenting a theoretical background about POMs and their applications in biomass valorization via hydroprocessing, the following sections 2.3, 2.4, 2.5 present background information about the three hydroprocessing reactions under investigation.

Table 2.3 Application of heteropolyacids, their salts and metal-POMs composites in biomass valorization via hydroprocessing.

Entry	Catalyst	Substrate	Reaction	Conversion (%)	Desired product	Selectivity (%)	Ref.
1	H ₃ PMo ₁₂ O ₄₀ /AC	Cellulose	Hydrolytic hydrogenation /hydrogenolysis	87	Ethylene glycol	4	[78]
2	H ₄ SiW ₁₂ O ₄₀ /AC	Cellulose	Hydrolytic hydrogenation /hydrogenolysis	79	Ethylene glycol	4	[78]
3	H ₃ PW ₁₂ O ₄₀ /AC	Cellulose	Hydrolytic hydrogenation /hydrogenolysis	92	Ethylene glycol	6	[78]
4	H ₄ SiW ₁₂ O ₄₀ /ZrO ₂	Furfural	Transfer hydrogenation /alcoholysis	7.3	Alkyl levulinate	4.7	[79]
5	H ₃ PMo ₁₂ O ₄₀ /TiO ₂	Anisole (lignin model)	Hydrodeoxygenation and alkylation	82	Hydrodeoxygenated products	72	[80]
6	Cs _{2.5} H _{0.5} PW ₁₂ O ₄₀	Anisole (lignin model)	Hydrodeoxygenation	19	Cyclohexane	12	[81]
7	H ₃ PMo ₁₂ O ₄₀ /TiO ₂	4-Propylguaiacol	Hydrodeoxygenation and alkylation	100	Propylbenzene	41	[80]
8	H ₃ PW ₁₂ O ₄₀	Guaiacol	Hydrodeoxygenation	30.8	Cyclohexane	34.2	[82]
9	Cs _{2.5} H _{0.5} PW ₁₂ O ₄₀	Biomass derived methyl isobutyl ketone (MIBK)	Hydrogenation	3	2-methylpentane (MP)	22	[83]
10	Cs ₁ H ₃ SiW ₁₂ O ₄₀ /Al ₂ O ₃	Glycerol	Hydrogenolysis	13.2	n-Propanol	35.4	[84]
11	Cs ₂ H ₂ SiW ₁₂ O ₄₀ /Al ₂ O ₃	Glycerol	Hydrogenolysis	4.8	n-Propanol	21.9	[84]
12	Cs ₃ H ₁ SiW ₁₂ O ₄₀ /Al ₂ O ₃	Glycerol	Hydrogenolysis	2.6	n-Propanol	31.5	[84]
13	Cs ₄ SiW ₁₂ O ₄₀ /Al ₂ O ₃	Glycerol	Hydrogenolysis	1.1	n-Propanol	40.4	[84]
14	H ₄ SiW ₁₂ O ₄₀ /Al ₂ O ₃	Glycerol	Hydrogenolysis	14.5	n-Propanol	30.5	[85]
15	H ₄ SiW ₁₂ O ₄₀ /ZrO ₂	Glycerol	Hydrogenolysis	10.6	n-Propanol	5.1	[86]
16	α-K ₆ P ₂ W ₁₈ O ₆₂	Glycerol	Hydrogenolysis	1	1,2-Propanediol	8	[59]
17	α ₂ -K _X P ₂ RuW ₁₇ O ₆₁	Glycerol	Hydrogenolysis	26	1,2-Propanediol	42	[59]
18	α ₂ -K _X P ₂ PdW ₁₇ O ₆₁	Glycerol	Hydrogenolysis	1	1,2-Propanediol	60	[59]
19	α ₂ -K _X P ₂ PtW ₁₇ O ₆₁	Glycerol	Hydrogenolysis	3	1,2-Propanediol	63	[59]

Table 2.4 Application of bifunctional catalysts composed of metal site and acid POMs site in biomass valorization via hydroprocessing.

Entry	Catalyst	Substrate	Reaction	X (%)	Desired product	S (%)	Ref.
1	Ru/Cs ₂ HPW ₁₂ O ₄₀	Cellobiose	Hydrolytic hydrogenation	100	Sorbitol	90	[87]
2	Ru/Cs ₃ PW ₁₂ O ₄₀	Cellobiose	Hydrolytic hydrogenation	100	Sorbitol	85	[87]
3	Ru/Cs ₃ PW ₁₂ O ₄₀	Ball-milled cellulose	Hydrolytic hydrogenation	-	Sorbitol	43	[87]
4	Ru/H ₃ PMo ₁₂ O ₄₀ -AC	Cellulose	Acid hydrolysis/hydrogenation/ hydrogenolysis	88	Ethylene glycol	8	[78]
5	Ru/H ₄ SiW ₁₂ O ₄₀ -AC	Cellulose	Acid hydrolysis/hydrogenation/ hydrogenolysis	97	Ethylene glycol	13	[78]
6	Ru/H ₃ PW ₁₂ O ₄₀ -AC	Cellulose	Acid hydrolysis/hydrogenation/ hydrogenolysis	98	Ethylene glycol	25	[78]
7	Ru/H ₃ PW ₁₂ O ₄₀ -HSAG	Cellulose	Acid hydrolysis/hydrogenation/ hydrogenolysis	99	Ethylene glycol	16	[78]
8	Ru-H ₄ SiW ₁₂ O ₄₀ /AC	Fructose	Hydrolytic hydrogenation / hydrogenolysis	93	1,2-Propanediol	48	[88]
9	Ru-H ₃ PW ₁₂ O ₄₀ /AC	Fructose	Hydrolytic hydrogenation / hydrogenolysis	92	1,2-Propanediol	37	[88]
10	Pd-Cs _{2.5} H _{0.5} PW ₁₂ O ₄₀ /K- 10 clay	Hydroxymethylfurfural (HMF)	Selective hydrogenation/ hydrogenolysis	98	2,5-Dimethylfuran	81	[89]
11	Au-H ₄ SiW ₁₂ O ₄₀ /ZrO ₂	Furfural	Transfer hydrogenation/alcoholysis	100	Alkyl levulinate	80.2	[79]
12	Au-H ₃ PW ₁₂ O ₄₀ /ZrO ₂	Furfural	Transfer hydrogenation/alcoholysis	100	Alkyl levulinate	55	[79]
13	Au-H ₃ PMo ₁₂ O ₄₀ /ZrO ₂	Furfural	Transfer hydrogenation/alcoholysis	100	Alkyl levulinate	29.7	[79]
14	Pt-H ₄ SiW ₁₂ O ₄₀ /ZrO ₂	Furfural	Transfer hydrogenation/alcoholysis	100	Alkyl levulinate	55.7	[79]
15	Pd-H ₄ SiW ₁₂ O ₄₀ /ZrO ₂	Furfural	Transfer hydrogenation/alcoholysis	100	Alkyl levulinate	56.7	[79]
16	Ru-H ₄ SiW ₁₂ O ₄₀ /ZrO ₂	Furfural	Transfer hydrogenation/alcoholysis	100	Alkyl levulinate	48.9	[79]
17	Pt/Cs _{2.5} H _{0.5} PW ₁₂ O ₄₀	Anisole (lignin model)	Hydrodeoxygenation	87	Cyclohexane	89	[81]
18	Ru/Cs _{2.5} H _{0.5} PW ₁₂ O ₄₀	Anisole (lignin model)	Hydrodeoxygenation	64	Cyclohexane	86	[81]
19	Cu/Cs _{2.5} H _{0.5} PW ₁₂ O ₄₀	Anisole (lignin model)	Hydrodeoxygenation	7	Cyclohexane	63	[81]
20	Ni/Cs _{2.5} H _{0.5} PW ₁₂ O ₄₀	Anisole (lignin model)	Hydrodeoxygenation	10	Cyclohexane	22	[81]
21	Ru/H ₃ PW ₁₂ O ₄₀ -C	Phenolic monomers	Hydrodeoxygenation	Up to 99.9	Hydrodeoxygenated products	Up to 99.9	[82]
22	Pd/H ₃ PW ₁₂ O ₄₀ -C	Guaiacol	Hydrodeoxygenation	99.9	Cyclohexane	62.7	[82]
23	Pt/H ₃ PW ₁₂ O ₄₀ -C	Guaiacol	Hydrodeoxygenation	99.9	Cyclohexane	92.1	[82]
24	Ru/H ₃ PW ₁₂ O ₄₀ -C	Guaiacol	Hydrodeoxygenation	99.9	Cyclohexane	98.6	[82]

Table 2.4 Application of bifunctional catalysts composed of metal site and acid POMs site in biomass valorization via hydroprocessing “Continued”.

25	Ru/H ₃ PW ₁₂ O ₄₀ -C	Lignin oil	Hydrodeoxygenation	100	Upgraded hydrocarbons	78.9	[82]
26	Pt/Cs _{2.5} H _{0.5} PW ₁₂ O ₄₀	MIBK	Hydrogenation	99	MP	100	[90]
27	Pd/Cs _{2.5} H _{0.5} PW ₁₂ O ₄₀	MIBK	Hydrogenation	7	MP	34	[90]
28	Ru/Cs _{2.5} H _{0.5} PW ₁₂ O ₄₀	MIBK	Hydrogenation	5	MP	100	[90]
29	Cu/Cs _{2.5} H _{0.5} PW ₁₂ O ₄₀	MIBK	Hydrogenation	<1	MP	100	[90]
30	Pt/Cs _{2.5} H _{0.5} PW ₁₂ O ₄₀	Biomass-derived diisobutyl ketone	Hydrogenation	100	2,6-Dimethylheptane	97	[90]
31	Pt/Cs _{2.5} H _{0.5} PW ₁₂ O ₄₀	Aliphatic ketones	Hydrogenation	Up to 100	Alkanes	Up to 100	[83]
32	Pt-H ₄ SiW ₁₂ O ₄₀ /ZrO ₂	Glycerol	Hydrogenolysis	24.1	1,3-Propanediol	48.1	[91]
33	Pt-H ₃ PW ₁₂ O ₄₀ /ZrO ₂	Glycerol	Hydrogenolysis	25.5	1,3-Propanediol	32.9	[91]
34	Pt-H ₃ PMo ₁₂ O ₄₀ /ZrO ₂	Glycerol	Hydrogenolysis	27.1	1,3-Propanediol	7.8	[91]
35	Pt-Li ₂ H ₂ SiW ₁₂ O ₄₀ /ZrO ₂	Glycerol	Hydrogenolysis	43.5	1,3-Propanediol	53.6	[92]
36	Pt-K ₂ H ₂ SiW ₁₂ O ₄₀ /ZrO ₂	Glycerol	Hydrogenolysis	24	1,3-Propanediol	36.8	[92]
37	Pt-Rb ₂ H ₂ SiW ₁₂ O ₄₀ /ZrO ₂	Glycerol	Hydrogenolysis	16.6	1,3-Propanediol	31.6	[92]
38	Pt-Cs ₂ H ₂ SiW ₁₂ O ₄₀ /ZrO ₂	Glycerol	Hydrogenolysis	41.2	1,3-Propanediol	40.2	[92]
39	Pt-H ₃ PMo ₁₂ O ₄₀ /ZrO ₂	Glycerol	Hydrogenolysis	72.3	n-Propanol	54.1	[86]
40	Pt-H ₄ SiW ₁₂ O ₄₀ /ZrO ₂	Glycerol	Hydrogenolysis	99.7	n-Propanol	80	[86]
41	Pd-H ₄ SiW ₁₂ O ₄₀ /ZrO ₂	Glycerol	Hydrogenolysis	25.3	n-Propanol	27.4	[86]
42	Cu-H ₄ SiW ₁₂ O ₄₀ /ZrO ₂	Glycerol	Hydrogenolysis	15.2	n-Propanol	11.3	[86]
43	Ni-H ₄ SiW ₁₂ O ₄₀ /ZrO ₂	Glycerol	Hydrogenolysis	24.7	n-Propanol	16.1	[86]
44	Ni/H ₄ SiW ₁₂ O ₄₀ /Al ₂ O ₃	Glycerol	Hydrogenolysis	39.2	n-Propanol	54.7	[85]
45	Pd/H ₄ SiW ₁₂ O ₄₀ /Al ₂ O ₃	Glycerol	Hydrogenolysis	34.1	n-Propanol	51.4	[85]
46	Pt/H ₄ SiW ₁₂ O ₄₀ /Al ₂ O ₃	Glycerol	Hydrogenolysis	45.3	n-Propanol	59.2	[85]
47	Cu/H ₄ SiW ₁₂ O ₄₀ /Al ₂ O ₃	Glycerol	Hydrogenolysis	18	n-Propanol	31	[85]
48	Ni-H ₄ SiW ₁₂ O ₄₀ /Al ₂ O ₃	Glycerol	Hydrogenolysis	28.6	1,2-Propanediol	15.8	[84]
49	Ni-Cs ₁ H ₃ SiW ₁₂ O ₄₀ /Al ₂ O ₃	Glycerol	Hydrogenolysis	21	1,2-Propanediol	18.6	[84]
50	Ni-Cs ₂ H ₂ SiW ₁₂ O ₄₀ /Al ₂ O ₃	Glycerol	Hydrogenolysis	21.3	1,2-Propanediol	30.6	[84]
51	Ni-Cs ₃ H ₁ SiW ₁₂ O ₄₀ /Al ₂ O ₃	Glycerol	Hydrogenolysis	22.6	1,2-Propanediol	58.2	[84]
52	Ni-Cs ₄ SiW ₁₂ O ₄₀ /Al ₂ O ₃	Glycerol	Hydrogenolysis	23.1	1,2-Propanediol	51.4	[84]
53	Ru/Cs _{2.5} H _{0.5} PW ₁₂ O ₄₀	Glycerol	Hydrogenolysis	23	1,2-Propanediol	73.6	[93]
54	Rh/Cs _{2.5} H _{0.5} PW ₁₂ O ₄₀	Glycerol	Hydrogenolysis	6.3	1,2-Propanediol	65.4	[93]

Table 2.5 Application of adding POMs to the reaction medium combined with other metal catalysts in biomass valorization via hydroprocessing.

Entry	Catalyst	Substrate	Reaction	X (%)	Desired product	S(%)	Ref.
1	Ru/C+ H ₄ SiW ₁₂ O ₄₀	Delignified CIMV wheat straw pulp	Hydrolysis/hydrogenation/dehydration	100	Isosorbide	63	[94]
2	Ru/C + H ₄ SiW ₁₂ O ₄₀	Ball milled Avicel PH-101 cellulose	Hydrolysis/hydrogenation/dehydration	100	Isosorbide	61	[94]
3	Ru/C+ H ₄ SiW ₁₂ O ₄₀	Ball-milled Cellulose	Acid hydrolysis/hydrogenation	100	Hexitols	100	[95]
4	Ru/C+ Cs _{3.5} H _{0.5} SiW ₁₂ O ₄₀	Cellulose	Hydrolytic hydrogenation	100	Hexitols	90	[96]
5	Ru/C+ Cs _{2.5} H _{0.5} PW ₁₂ O ₄₀	Cellulose	Hydrolytic hydrogenation	100	Hexitols	65	[96]
6	Ru/C+ H ₃ PW ₁₂ O ₄₀	Cellulose	Hydrolytic hydrogenation	81	Hexitols	51	[96]
7	Ru/C+ H ₄ SiW ₁₂ O ₄₀	Cellulose	Hydrolysis/hydrogenation	98.8	C4–C6 sugar alcohols	80.6	[97]
8	Ru/C+ H ₃ PW ₁₂ O ₄₀	Cellulose	Hydrolysis/hydrogenation	93.8	C4–C6 sugar alcohols	66.4	[97]
9	Ru/C+ H ₄ SiW ₁₂ O ₄₀	Cellulose	Hydrolysis/dehydration /hydrogenation	90	n-Hexane	41.6	[98]
10	RANEY® Ni+ H ₄ SiW ₁₂ O ₄₀	Cellulose	Hydrolysis/hydrogenolysis	-	Ethylene glycol	32	[99]
11	RANEY® Ni+ H ₃ PW ₁₂ O ₄₀	Cellulose	Hydrolysis/hydrogenolysis	-	Ethylene glycol	49	[99]
12	Au/ZrO ₂ +H ₄ SiW ₁₂ O ₄₀ /ZrO ₂	Furfural	Transfer hydrogenation/alcoholysis	100	Alkyl levulinate	47.6	[79]
13	Pt/C + Cs _{2.5} H _{0.5} PW ₁₂ O ₄₀	Anisole (lignin monomer)	Hydrodeoxygenation	100	Cyclohexane	90	[81]
14	Pt/C + Cs _{2.5} H _{0.5} PW ₁₂ O ₄₀	MIBK	Hydrogenation	99	MP	100	[83]
15	Rh/C + H ₃ PW ₁₂ O ₄₀	δ-furfurylidenelevulinic acid (FDLA)	Hydrodeoxygenation	90	n-Decane	70	[100]
16	Rh/C + H ₄ SiW ₁₂ O ₄₀	FDLA	Hydrodeoxygenation	89	n-Decane	69	[100]
17	Pd/C + H ₃ PW ₁₂ O ₄₀	FDLA	Hydrodeoxygenation	93	n-Decane	89	[100]
18	Pd/C + H ₄ SiW ₁₂ O ₄₀	FDLA	Hydrodeoxygenation	86	n-Decane	67	[100]
19	Pt/Al ₂ O ₃ + H ₃ PW ₁₂ O ₄₀	Glycerol	Hydrogenolysis	19	1,3-Propanediol	38	[101]
20	Pt/Al ₂ O ₃ + H ₄ SiW ₁₂ O ₄₀	Glycerol	Hydrogenolysis	48	1,3-Propanediol	28	[101]
21	Pt/SiO ₂ + H ₃ PW ₁₂ O ₄₀	Glycerol	Hydrogenolysis	57	1,3-Propanediol	24	[101]
22	Pt/SiO ₂ + H ₄ SiW ₁₂ O ₄₀	Glycerol	Hydrogenolysis	24	1,3-Propanediol	22	[101]
23	Ru/C + H ₃ PW ₁₂ O ₄₀ /ZrO ₂	Glycerol	Hydrogenolysis	44	1,2-Propanediol	64.3	[102]
24	Ru/C + Cs ₂ HPW ₁₂ O ₄₀	Glycerol	Hydrogenolysis	21	1,2-Propanediol	60.2	[102]
25	Ru/C+ Cs ₂ HPW ₁₂ O ₄₀ /ZrO ₂	Glycerol	Hydrogenolysis	25	1,2-Propanediol	67	[102]

2.3. Hydrogenation of biomass derived furans

Lignocellulosic biomass, which is the most prevalent type of biomass, offers a promising alternative for the production of renewable fuels and chemicals. As discussed in section 2.3.1, cellulose and hemicellulose can be selectively converted to simple furans, including furan, MF, and DMF [4]. Finding a way for selective production of alcohols from those renewable bio-derived furans can further mitigate the environmental impact of the production of these chemicals, as it will reduce the reliance on fossil resources, leading to decreased greenhouse gas emissions.

2.3.1. Production of furans from lignocellulosic biomass

The acid hydrolysis pretreatment of lignocellulosic biomass has been demonstrated to effectively convert cellulose and hemicellulose into C6 (glucose) and C5 (xylose) sugars, respectively [103]. These sugars can be further transformed into FFR and HMF through acid-catalyzed dehydration reactions as illustrated in Figure 2.11. Numerous reviews [32, 104-106] have been published summarizing the production of FFR and HMF from lignocellulosic biomass. FFR and HMF can be produced from xylose and glucose with very high selectivities (>90 %) and conversions [36, 106]. The selective production of furan, MF, and DMF from FFR and HMF has been extensively studied, and previous research has shown that they can be produced in high yields and selectivities [32]. For instance, decarbonylation of FFR using Pd/C catalyst at 250 °C resulted in 100 % conversion of FFR and a very high selectivity (up to 98 %) towards furan [107]. Hydrogenolysis of the side C-O bond in FFR using Raney Ni catalyst at the same temperature, resulted in 89 % selectivity towards MF at complete conversion [108]. At a temperature of 80 °C, Pd/C showed superior activity for HMF hydrogenolysis into 2,5 DMF with a selectivity of 100 % at complete conversion [109]. The high selectivity in the production of furan, MF, and DMF provides a promising avenue for the subsequent processing and valorization of these compounds into other industrially relevant chemicals.

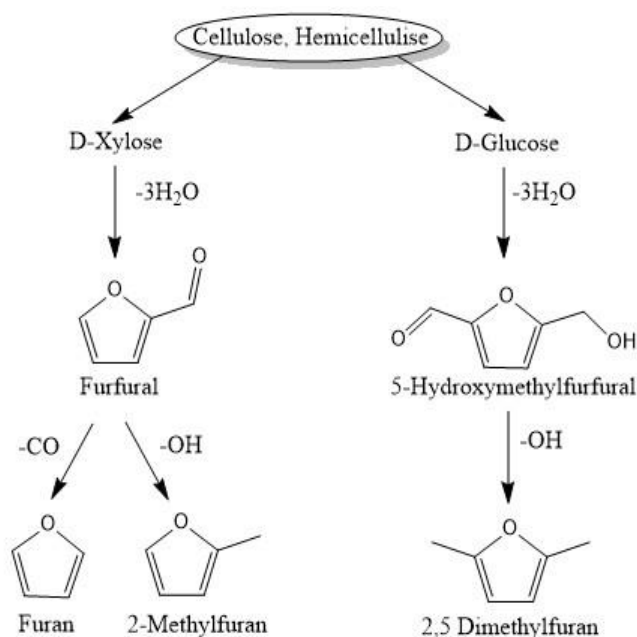


Figure 2.11 Furan, MF, and DMF production from cellulose and hemicellulose.

2.3.2. Valorization of furans

Despite the promising potential of some furans, such as DMF, in fuel applications, there are still technical barriers that hinder their widespread usage. Among these barriers, oxidation stability issues and the formation of soot precursors with high molecular weight have been reported as significant challenges by Djokic et al. [110]. DMF has been found to form peroxides, which leads to gum deposits during storage [111, 112]. Furthermore, Lange et al. have demonstrated that furans, in general, can degrade the oxidation stability of gasoline fuels by forming deposits that can be problematic for engine operation [105]. McCormick et al. reported that 20 % DMF gasoline blend failed the standard ASTM D525 oxidation stability test, highlighting the stability issues associated with DMF in fuel applications [113]. These concerns pose a significant challenge to the use of DMF in the fuel sector and underline the need to explore alternative routes for converting it into other chemicals.

Different catalytic technologies such as aromatization, hydroxyalkylation/alkylation followed by hydrodeoxygenation and hydrogenation can be used for furan transformations into other products. Aromatization and cycloaddition could be used to produce p-xylene, and other valuable aromatic hydrocarbons from furans [114, 115]. Hydroxyalkylation/alkylation of MF with acetone and butanal using solid acid catalysts followed by HDO is another application for renewable diesel production from furans [116]. Hydrogenation of furans represents also another route and can produce ring saturated products such as 2- methyltetrahydrofuran (MTHF) [117] and 2,5-dimethyltetrahydrofuran (DMTHF) [118], or ring opened products such as ketones [36], alcohols [4], and alkanes [119].

The selective production of alcohols from bio-derived furans offers significant benefits, as alcohols are versatile chemicals with a wide range of industrial uses and applications. N-butanol, in particular, has a broad range of industrial applications. It is commonly used as a solvent in the production of paints, coatings, inks, and resins, as well as a pharmaceutical extracting agent for the manufacture of antibiotics, hormones, and vitamins. Furthermore, it can serve as a paint thinner and as a component of hydraulic and brake fluids, industrial cleaners, and paint removers. N-butanol is also an important intermediate for the production of butyl acrylate, a key component in the manufacture of acrylic resins. In addition to these applications, n-butanol is being investigated as a potential biofuel, which could replace diesel and gasoline fuels [120, 121]. It is commonly used as a solvent and as an intermediate in the manufacture of other chemicals in the pharmaceutical and cosmetic industries. It is also used as a flavoring ingredient in food and beverage products. Moreover, different proportions of 2-pentanol are blended with diesel fuel to reduce particulate emissions in diesel engines [121, 122]. It is also considered as a very important solvent in the manufacturing of petroleum additives, urea-formaldehyde plastics processing, organic chemical manufacturing and raw material for pharmaceutical preparations [120]. 1-Pentanol is considered to be an important intermediate in numerous chemical industrial applications, including but not limited to its use as a corrosion inhibitor, flotation aid, lubricating oil additive, herbicide, and antioxidant. 2-hexanol is used in the perfume [123] and tobacco [124] industries. Moreover, hexanol is broadly used as lubricant and coating additive, and recently, there are other investigations for its usage as a fuel additive [125-127].

Furthermore, selective production of open-ring products such as alcohols from furans has an additional research advantage. It can contribute to a better understanding of the ring-opening

reaction of furans, which is critical for maximizing the production of gasoline range aliphatic hydrocarbons [128] and diesel fuels from more complex furans through reductive catalytic ring-opening reactions [34, 129, 130].

2.3.3. Alcohol production

There are several ways for alcohols like n-butanol, pentanols and 2-hexanol production. This includes hydration of alkenes [131] using acid catalysts and hydrogenation of aldehydes and ketones [132, 133], resulting in the formation of the corresponding alcohols. Most of these conventional ways depend mainly on fossils as a primary feedstock. Therefore, finding a sustainable way for producing alcohols selectively from a renewable source such as biomass-derived furans, instead of relying on fossil fuels, represents a promising step towards creating a more sustainable and eco-friendly future.

As presented in Figure 2.12, n-butanol can be produced from furan via reductive ring opening using 3 moles of hydrogen. In a similar way, pentanols and 2-hexanol can be produced from MF, and DMF, respectively [4]. According to Aliaga et al. [134], more cracking products were observed in gas phase hydrogenation of those furans with decreasing the number of methyl groups attached to the furan ring. Therefore, gas phase hydrogenation of furan produced a high amount of propylene, relative to what was observed for MF and DMF hydrogenation. This can be illustrated by the steric and electronic hindrance effects of extra methyl groups in MF and DMF. Kang et al. observed that the increased activity of DMF in gas-phase hydrogenation compared to MF was due to the extra methyl group substituent present in DMF [119]. Therefore, DMF was chosen as a model substrate in different hydrogenation reaction investigations [36, 118, 119, 135].

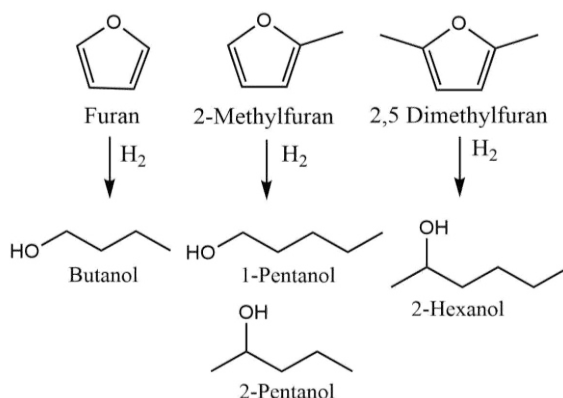


Figure 2.12 Alcohol production from furans.

2.3.4. Hydrogenation mechanism of 2,5 DMF over Pt/C

Pt occupied a prominent position among other metal catalysts, due to its remarkable ability to catalyze the reaction at temperatures lower than 200 °C [139]. In their investigation [36] of the hydrogenation mechanism of DMF on Pt/C catalyst under mild reaction conditions, Louie et al. proposed that ring saturation leading to the formation of DMTHF and ring opening producing ring opened products occur via parallel pathways rather than in a series as shown in Figure 2.13. Contrary, other studies suggest that hydrogenation of the furan ring occurs first to form the tetrahydrofuran derivative followed by subsequent ring opening of the tetrahydrofuran derivative, as the C-O bond in DMTHF has a weaker bond strength than in

DMF by approximately 28 KJ/mol [34, 135, 136]. However, a study reported by Aliaga et al. [134], showed that the interaction between the furan ring and the metal surface of the catalyst weakens the C-O bond in the furan ring and allows for its cleavage directly in an unsaturated species instead of ring saturated tetrahydrofuran. The DMF adsorbs parallel to the surface of Pt via interaction with the π orbitals of the aromatic ring, whereas DMTHF adsorbs upright via the O atom. Further DFT calculations [137], reveal that the orbitals of DMF involved in the adsorption on the surface depend on the noble metal site of the catalyst. DMF binds parallel to the metal surface in two different forms of binding, either through a single, π C=C bond, which is more favorable over Pd, Ru, and Rh, or through two σ bonds with the two carbon atoms of the C=C bond, which is more favored over Pt.

Ring saturation starts with the syn-addition of hydrogen across the C=C bond of DMF adsorbed parallel to the surface of the catalyst to form a dihydro intermediate that contributes to the production of DMTHF species (cis and trans isomers). Dimethyldihydrofuran (DMDHF) is only detected when the catalyst used is selective to ring saturation and produces high yields of DMTHF. This suggests that further hydrogenation of this intermediate is very rapid. According to DFT calculations by Wang et al., it is unlikely that such an intermediate is involved in reductive ring opening [138]. The C-O bond cleavage occurs as a result of aromatic furan ring opening on Pt surface that forms an enol intermediate. The formation of 2-hexanone (HXN) and 2-hexanol (HXL) takes place in parallel through this intermediate. If the enol intermediate is converted to its thermodynamically favored keto tautomer, HXN will be formed and if the enol undergoes hydrogenation before tautomerization to the keto form, HXL will be formed as a primary product. HXN production from this intermediate is more favorable than HXL formation, as the Gibbs free energy difference between the enol and the keto form is -33 kJ/mol at 353 °K [36]. HXL can be produced as a secondary product as well through secondary hydrogenation of HXN. In case that an acidic support exists in the reaction medium, n-hexane is produced through the dehydration reaction of HXL to produce 1-hexene, which is further hydrogenated on the metal site of the catalyst to n-hexane. A more detailed reaction scheme outlining all the potential products that can be formed under hydrogenation reaction conditions is given in chapter 3.

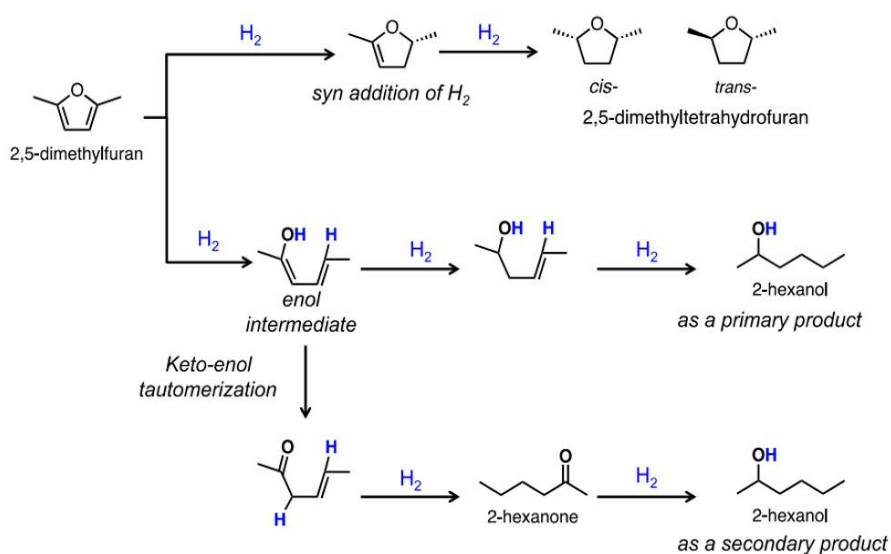


Figure 2.13 Proposed reaction network for the hydrogenation of DMF into ring saturated and ring opened products [36].

2.3.5. Catalysts, operating conditions, and solvent effects in DMF hydrogenation

The catalytic hydrogenation of the furan ring was first investigated by Padoa and Ponti in 1906. In 1908, Bourguignon examined the hydrogenation of furan over a nickel catalyst at 170° C producing only (8%) butan-1-ol [139]. Subsequent studies have revealed that the formation of ring-opened products occurs preferentially in the vapor phase, and for this reason, this reaction has been extensively studied in the literature in the vapor phase using various catalysts, including: Ba/Cu/Cr , Cu/Cr/Ni/Zn/Fe, Cu-Ru/C, Pt, Pt-Al, Os, Ru, Ir, Raney Ni ,Pd, Pd-Al ,Cu, Mo, Fe-Cu, Co-Cu, Cu-Al , Ni-Zn at temperatures (200-350 °C) [139-142]. Pt occupied a prominent position among other metal catalysts, due to its remarkable ability to catalyze the reaction at temperatures lower than 200 °C. Regarding the liquid phase hydrogenation, which is less investigated in the literature, Adkins et al. performed the reaction in liquid phase using a copper chromite catalyst under conditions of 202 bar H₂ and 250°C, and reported a yield of 30% and 33% for 1- pentanol and 2-pentanol, respectively. The reaction was extended to furan, which gave 70% yield of n-butanol and to DMF which gave mainly HXL [143] . Recent studies have reported the use of milder reaction conditions for the hydrogenation of furan compounds, where a Ru/C catalyst was employed in a catalytic transfer hydrogenation at 80°C and 20 bar N₂ pressure to achieve a 19 % yield of HXL [118]. Additionally, high selectivity (92%) towards HXN was obtained at 80°C and 4.2 bar H₂ using a Pt/C catalyst [36]. These results highlight that performing the reaction in the liquid phase under mild reaction conditions with the aim of achieving high selectivity towards the ring-opening products, especially alcohols, can be achieved by the right choice of catalyst.

In addition to catalyst selection, the choice of solvent or carrier liquid plays a critical role in hydrogenation reactions, as it affects the efficient transport of H₂ from the gas phase to the surface of the catalyst through the liquid phase. According to Figure 2.14, alkanes have the highest hydrogen solubility among the solvents, which in turn allows to overcome mass transfer limitations during hydrogenation. Alkanes also meet other requirements, being liquid at room temperature, very efficient at absorbing the heat released and stable up to 100 °C in a reducing atmosphere.

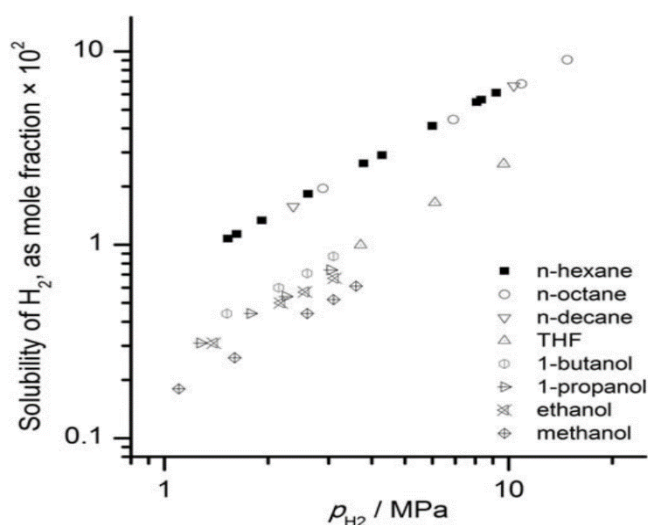


Figure 2.14 Solubility of hydrogen in some organic solvents [23, 144, 145].

2.4. Reductive catalytic fractionation for lignin valorization

Lignin, a highly abundant biopolymer that accounts for approximately one-third of all lignocellulosic biomass, holds great potential as a renewable feedstock for the production of aromatic compounds, thus offering an attractive alternative to the utilization of limited edible fossil resources. Despite the potential of lignin as a valuable source of renewable chemicals, the isolation processes used in pulp and paper industries often cause structural modifications that limit its utility in value-added chemical production, thus reducing its worth to simply being used for heat generation. Consequently, the central focus among scientific researchers is to develop cost-effective and environmentally sustainable lignin-first biorefinery strategies for the effective valorization of lignin into phenolic chemicals.

2.4.1. Lignin classification

The structural composition of lignin derived from lignocellulosic biomass can be broadly categorized into three main types: hardwood lignin, softwood lignin, and herbaceous lignin [146]. The relative proportions of the three monolignols, p-coumaryl alcohol/H, coniferylalcohol/G, and sinapylalcohol/S, present in the biomass can vary significantly across these three types. Softwood lignin is primarily composed of G units (>95%), whereas hardwood lignin consists of both G and S units. In contrast, lignin derived from herbaceous plants contains all three H, G, and S units [147, 148]. The β -O-4 ether bonds are the most abundant lignin linkages and have a relatively low bond dissociation energy. Bouxin et al. have shown that the catalytic depolymerization of various lignins produced different yields and selectivity of alkylphenols, depending on the abundance of β -O-4 linkages [149].

The pulp industry is the primary source of technical lignins, with Kraft pulping being the dominant process. Technical lignins can be categorized into two main types based on the fractionation approach utilized. One type is extracted lignin (soda, Kraft, sulfite lignin/lignosulfonate, organosolv lignin, ionic liquid lignin, and deep eutectic solvent-extracted lignin). The other type is hydrolytic lignin, which is left behind after removing carbohydrates via hydrolysis. During most of fractionation approaches utilized, the harsh conditions lead to structural changes in the lignin, such as undesired condensation reactions and a reduction in the abundance of β -O-4 linkages, resulting in the formation of technical lignin [148, 149].

2.4.2. Conventional methods for lignin valorization

Pyrolysis

The thermal degradation of lignocellulosic biomass via pyrolysis results in the formation of gaseous (biogas), liquid (bio-oil), and solid residue (biochar) products. The inherent complexity of the pyrolysis process is due to the heterogeneous nature of the feedstock and the high temperatures (350–800°C) required for effective conversion, which poses challenges in controlling the distribution and types of products obtained. In addition, the high energy requirements of pyrolysis, which necessitates temperatures higher than those needed for solvolysis, makes it economically unfavorable [150]. Moreover, direct pyrolysis of raw biomass generates both lignin-derived phenols and sugar-derived products, but with low selectivity, presenting significant hurdles for downstream separation and recovery of the desired products [151].

Solvolysis

Lignin solvolysis has garnered considerable attention in recent years for the production of value-added chemicals and analytical purposes. However, the efficient depolymerization of lignin via acidolysis or base-catalyzed depolymerization is still challenging due to the instability of intermediates and the need to maximize phenolic monomer yields. Under both acidic and basic conditions, condensed C-C or C-O bonds are formed via nucleophiles [152]. In an effort to circumvent lignin condensation, non-catalytic solvolysis in the presence of formic acid has also been investigated [153]. However, catalytic oxidative and reductive pathways have emerged as preferred alternatives to catalytic and non-catalytic solvolysis for lignin depolymerization.

Catalytic oxidative depolymerization

In recent years, transition metal ions, including Fe (III), Mn (II), (III), Co (II), and Zr (IV), have been recognized for their ability to increase oxygen reactivity and to promote the breakdown of β -O-4 and pinacol C-C linkages in technical lignin [154, 155]. Furthermore, the application of heterogeneous metal oxide catalysts, such as CuO, MnO₂, TiO₂, and ZnO, has demonstrated comparable efficiency to that of homogeneous metal ion catalysts, with the added benefit of simplified catalyst recovery [155]. In addition, alternative catalysts, such as POM [156, 157] and biomimetic catalysts (metallo-salen, metalloporphyrins) [155], have shown effective cleavage of β -O-4 linkages in lignin. The oxidative pathway has been found to require milder conditions compared to reductive approaches, with a reaction temperature of around 100°C, resulting in a reduced energy cost [158]. Additionally, the oxidative pathway offers the production of valuable aromatic monomers containing active functional groups, such as aldehydes, which offer various functionalization opportunities [159]. However, limiting over-oxidation of the lignin, such as ring opening, remains a challenging task, especially when using hydrogen peroxide as the oxidant [160]. Furthermore, a severe drawback of the oxidative pathway is the radical repolymerization of lignin fragments [161].

Catalytic reductive depolymerization

Various Ni, Ru, Pt, and Pd-based catalysts have been utilized for reductive catalytic depolymerization of technical lignin aiming at achieving high monomer yields. In pure water, Zhang et al. achieved only 6.8 wt.% yield of monomers at 10 bar H₂ pressure from organosolv birch lignin. As solubilizing lignin is an essential step, subsequent research being conducted in organic solvents such as methanol (MeOH), ethanol (EtOH), iso-propanol (i-Pr), n-butanol (n-BuOH), or organic/H₂O cosolvents [162]. Wang et al. revealed that H₂ plays a prominent role in achieving high monomer yields, as they achieved 3.9 wt.% and 14.3 wt. % yield of monomers with N₂ and H₂ applied, respectively [163]. Over sulfided NiMo/ γ -Al₂O₃ and under identical conditions, the catalytic conversion of organosolv beech lignin only produced 4.3 wt.% yield of monomers, while direct conversion of beech wood achieved 18.1 wt.% yield of monomers [164]. This yield difference observed suggested that catalytic depolymerization of technical lignin is more challenging, as the condensed structure of technical lignin significantly restrains monomer yields. The following section introduces the emerging lignin-first strategy, which can overcome the limitations of conventional approaches.

2.4.3. Reductive catalytic fractionation (lignin first strategy)

Lignocellulosic biomass fractionation techniques have undergone a paradigm shift with the advent of lignin-first-fractionation processes, which prioritize lignin valorization and seek to prevent lignin condensation. In 2015, Sels and Abu-Omar proposed a novel approach to lignin fractionation, termed "reductive catalytic fractionation" (RCF) based on the principles of a lignin-first biorefinery [165, 166]. This approach involves dissolving lignin from raw biomass and depolymerizing it into phenolic monomers, dimers, and oligomers in a reductive atmosphere using appropriate catalysts, while preserving the solid carbohydrate pulp for subsequent valorization.

Typically, RCF is conducted in batch reactors, where untreated biomass is mixed with a redox-active catalyst such as supported Pd, Ru, or Ni under temperature (180-250 °C) in a polar protic solvent containing a hydrogen donor such as hydrogen gas or alcoholic solvents (MeOH, EtOH, i-Pr, etc.) at pressures ranging from 30 to 60 bar [167]. Sometimes, a cocatalyst such as a Brønsted [14, 168, 169] or Lewis acid [170, 171] is utilized.

2.4.3.1. Mechanism & typical products of RCF

Several pathways and mechanisms have been proposed for RCF of lignocellulosic biomass. Regardless of the specific approach, the core steps of the RCF process involve solvolysis, hydrogenolysis of ether bonds (Figure 2.15), removal of benzylic OH-groups (OH_α), and potential removal of OH_γ -groups. Lignin solvolysis is the process of lignin extraction from the plant cell walls, which results in the production of a mixture of oxoaromatic fragments. These fragments are subsequently reduced on the surface of the redox-active catalyst. In particular, the aryl ether bonds (primarily β -O-4, with 4-O-5 and α -O-4) undergo cleavage via hydrogenolysis, while reactive C=C double bonds are either partially or fully hydrogenated to produce stable monomers and oligomers. The end product of this process is a stabilized mixture comprising oxygenated aromatic monomers and oligomers, which is recovered as a lignin oil [167].

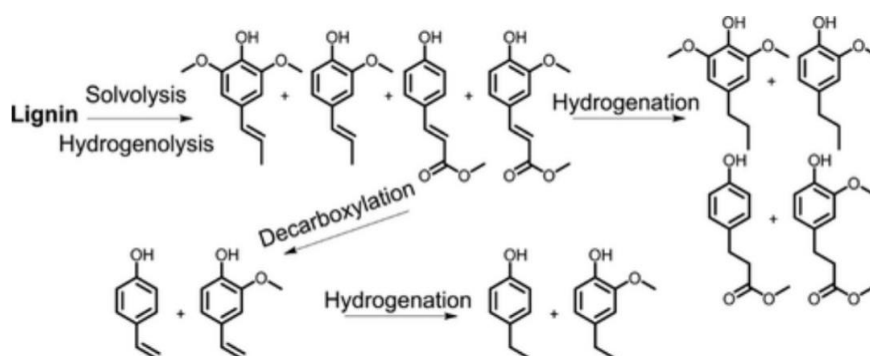


Figure 2.15 Mechanisms for reductive catalytic fractionation of lignocellulosic biomass [14].

During the RCF of lignocellulosic biomass, a range of phenolic monomers, presented in Figure 2.16, are produced. This includes propenyl-substituted phenols such as (GPe and SPe), propyl-substituted phenols (4-n-propyl guaiacol (GP) and 4-n-propyl syringol (SP)), and direct hydrogenation products i.e., propanol-substituted phenols (4-n-propanol guaiacol (GPOH) and 4-n-propanol syringol (SPOH)), which might be more attractive for the chemical industry because they offer various functionalization opportunities. Additionally,

saturated and etherified products (GPOR and SPOR) have also been observed. The distribution of phenolic monomers during RCF has been found to be highly dependent on the gas atmosphere (H_2 or N_2) and the amount of H_2 pressure applied, as discovered by Sels and colleagues [155]. In the absence of hydrogen, the dominant pathway for the hydrogenolysis of monolignols produces GPe and SPe, as illustrated in Figure 2.16. However, when a lower pressure of H_2 (5 bar) is applied, subsequent hydrogenation of unsaturated $C_\alpha-C_\beta$ bonds takes place and produces GP and SP. At elevated pressures beyond 10 bar, the direct hydrogenation of monolignols (coniferyl alcohol/sinapyl alcohol) to GPOH and SPOH predominates, which can be attributed to distinctive hydrogen-dependent properties of hydrogenolysis and hydrogenation reactions [172]. Studies have also indicated that during the initial stages of lignin extraction and depolymerization, where primary monolignols such as p-coumaryl, coniferyl, and sinapyl alcohol are formed as reactive intermediates, the unsaturated side-chain $C=C$ bonds might undergo radical repolymerization, resulting in the formation of higher molecular weight oligomers. This process runs counter to the lignin-first biorefinery approach aimed at producing value-added phenolic monomers [173, 174]. Therefore, selective hydrogenation of side-chain $C=C$ bonds in those reactive intermediates is essential for maximizing phenolic monomer yields.

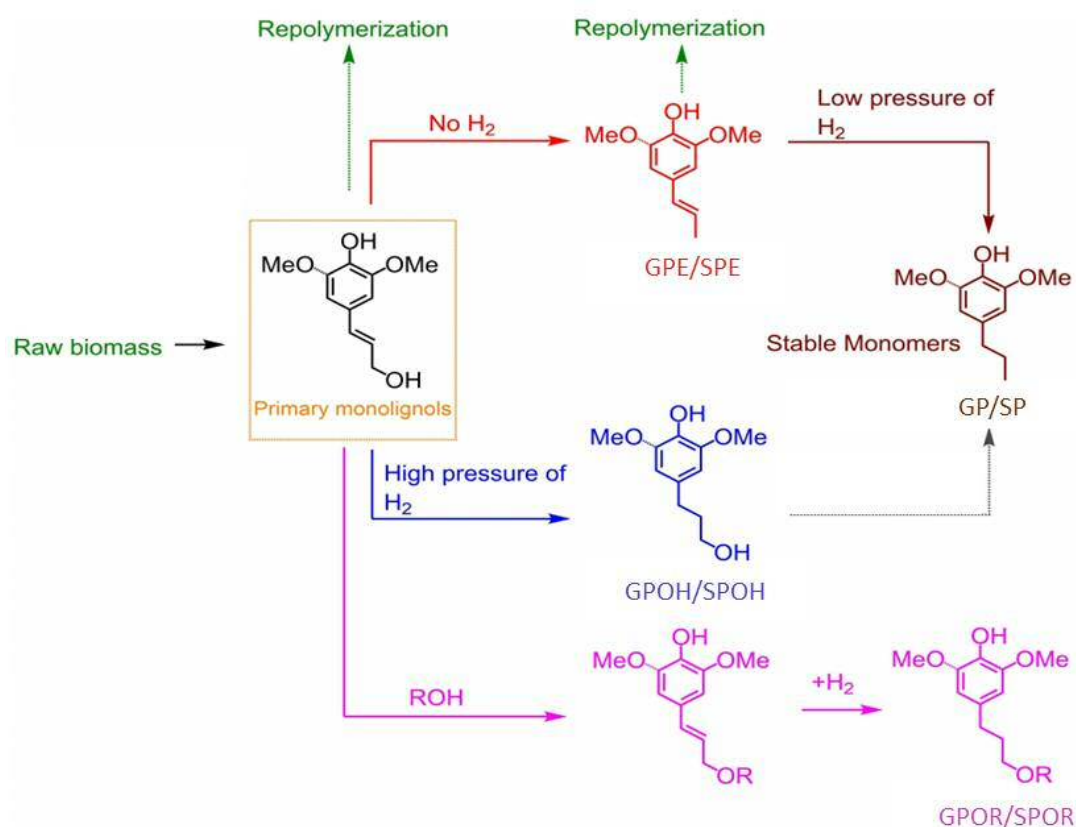


Figure 2.16 Reaction pathways and the typical products of RCF [155].

During RCF of herbaceous biomass, other products derived from phenolic acids such as 3-(4-hydroxyphenyl)-2-propenoic acid methyl ester (HPeMe), 3-(4-hydroxy-3-methoxyphenyl)-2-propenoic acid methyl ester (GPeMe), 4-hydroxy-benzenepropanoic acid methyl ester (HPaMe), and 3-(4-hydroxy-3-methoxyphenyl)-propanoic acid methyl ester (GPaMe) might be also present.

2.4.3.2. Operating conditions, catalysts, source of feedstocks, and solvent effects in RCF

Operating conditions

The influence of hydrogen pressure in controlling the selectivity towards different products in RCF process was previously addressed in the aforementioned section (2.4.4). Rinaldi et al. examined the effect of reaction temperature using the same catalysts, solvent mixture, and biomass feedstock [175]. Elevated temperatures were found to enhance overall delignification yields, and to produce low molar mass fragments. Additionally, hydroxyl groups located in the sidechains of monolignols were preferentially cleaved via hydrodeoxygenation, resulting in decreasing the oxygen content in the produced oils.

The particle size of the biomass is also a critical factor affecting product yield in RCF. Román-Leshkov et al. [176], developed mesoscale reaction-diffusion models for lignin-first fractionation. The models predict that solvolytic lignin extraction is governed by mass transfer at the mesoscale. The diffusion of lignin fragments competes with mass transfer resistance, which dominates when the biomass particle size exceeds 2 mm. Thus, for catalyst evaluation tests, it is recommended to perform experiments using biomass particles smaller than 2 mm.

Catalyst

Heterogeneous catalysis has been predominantly studied for RCF. However, there have been recent reports of homogenous catalysts such as Ru/Ir complexes and $B(C_6F_5)_3$ that achieved relatively low yields of phenolic monomers, typically below 10 wt.% [155]. If heterogeneous catalysts are employed, a significant challenge arises in the form of catalyst recycling, as the residual pulp remains mixed with the catalyst. Several innovative approaches have been developed to address this issue. These include using a magnetic catalyst [177], membrane filtration [178], or embedding the metal function in a cage [173] for catalyst separation. Another approach involves converting all process residues, thereby allowing the catalyst for reuse [179].

The utilization of high-pressure hydrogenation and hydrogenolysis of wood using heterogeneous catalysis can be traced back to the 1940s when it was initially employed to elucidate the lignin structure [180]. Since then, various catalysts such as Ni, Pd, Rh, and Ru have been evaluated for their effectiveness in the hydrogenolysis of spruce wood under mild reaction conditions (195 °C, 35 bar H_2). The highest yield of GPOH (16%) was obtained using Pd/C as the catalyst, whereas the highest monomeric yield (34%) was achieved with Rh/C [148, 181]. In a separate study involving birch treatment, four catalysts (Ru/C, Pd/C, Rh/C, and Pt/C) were compared, and the monomer yields were found to be dependent on the catalyst and additives used in the reaction medium. The highest total yield of monomers (34%) was obtained using Pt/C catalyst, which was further enhanced to 38% upon the addition of acid (H_3PO_4). The inclusion of dioxane as an additive resulted in a further increase in yield to 46 %, demonstrating the potential of additives in improving product yield [169].

Lately, significant research efforts have focused on the production of high yields of phenolic products from lignin during RCF using different heterogeneous catalysts. Sels and co-

workers observed that Ru/C and Pd/C catalysts produced similar total yields (around 50 wt.%) of monomers, but with different distributions. Ru/C exhibited 75% selectivity towards GP/SP due to efficient hydrogenolysis of C γ -OH, whereas Pd/C favored the formation of GPOH and SPOH with 91% selectivity [182]. The synergistic effect of Pd/C and ZnCl₂ on β -O-4 linkages cleavage was explored by Parsell et al., who observed a remarkable 54 wt.% yield of phenolic products, with nearly 100% selectivity towards GP and SP [166]. Xu et al. used a Ni/C catalyst in a methanol-water co-solvent to convert beech to natural phenolic alcohols, yielding around 51% total yield [183]. The role of the Ni/Al₂O₃ catalyst in the solubilization, depolymerization, and stabilization of lignin from birch in methanol was also investigated by Sels et al. in 2017 [173], where recuperation and reuse of the Ni/Al₂O₃ pellets were facilitated using a catalyst basket. These findings provided valuable insights into the mechanism of β -O-4 linkage cleavage and suggested the potential of using different catalysts to selectively produce specific phenolic monomers.

The impact of acidic and alkaline additives on delignification and yield of phenolic monomers in Pd/C-catalyzed reductive processing of poplar wood in methanol was investigated. It was observed that both acidic and basic additives could enhance the delignification to GPOH/SPOH as main monomeric products. The distinct difference is that H₃PO₄ results in a higher yield of phenolic monomers in oil compared with neutral conditions, but NaOH leads to a significant loss of cellulose and promotes the repolymerization thus produced lower yield [168]. Román-Leshkov et al. conducted a study on the RCF of corn stover using Ru/C and Ni/C catalysts with H₃PO₄ as a cocatalyst in methanol [14]. The acid co-catalyst proved to be effective in increasing lignin solvolysis and enhancing the cleavage of ester bonds of coumarate and ferulate structure in corn stover. However, the acid also promoted hemicellulose and cellulose dissolution. The impact of other various acid co-catalysts, such as HCl, H₂SO₄, Al(OTf)₃, and CH₃COOH, on the RCF of oak wood sawdust was investigated in another publication [184]. The use of Al(OTf)₃ and HCl as co-catalysts with Pd/C resulted in the production of 46 wt.% and 44 wt.% lignin monomers, respectively. As discussed in this section, the addition of acid co catalyst or acidic additive might provide a potential for enhancing delignification of some lignocellulosic biomass feedstocks and increasing monomer yield.

Source of lignocellulosic feedstock

Controlling the reaction conditions such as temperature, pressure, and treatment time, as well as the polarity of solvents, can generally enhance both the delignification degree and yield of lignin products. However, the lignin yield is also strongly dependent on the source of lignocellulosic feedstock. Various types of feedstocks have been investigated for RCF, including hardwoods (e.g., birch, poplar, and beech), softwoods (e.g., pine and spruce), and herbaceous crops (e.g., miscanthus and corn stover). In the 1940s, the earliest study on RCF of wood involving hydrogenation and hydrogenolysis was reported. Later, (1993-2011), other lignocellulosic feedstocks, including rice husks, birch, and pine, were tested [169, 185, 186]. The main products reported were SP and GP, with monomer yields ranging from 22-46 wt.%. Abu Omar et al. [187]. conducted a study in 2015 to investigate the impact of biomass type on the production of monomers. The study revealed that birch resulted in higher monomer yields (32 wt.%) compared to poplar (26 wt.%) and eucalyptus (28 wt.%). Sels et al. [165] performed reductive catalytic experiments to investigate the effect of different lignocellulosic

biomasses, such as birch, poplar, miscanthus, and spruce/pine mixtures, on the yield of monomers. The study revealed a positive correlation between the S-units in lignin, which correlate with the β -ether content in lignin, and the total monomer yield produced. The findings of Samec et al. [148] supported this trend, demonstrating a decreasing order of monomer yield in woody substrates, including birch, poplar, spruce, and pine, under RCF conditions. The total monomer yield produced from RCF typically follows the order of hardwoods > herbaceous crops > softwoods [148]. The increased monomer yield with hardwoods as feedstock is attributed to their higher S to G ratio, resulting in fewer C-C bonds and higher β -O-4 ether bonds content. The majority of published research on RCF has centered on the use of wood as a feedstock. There are only a limited number of studies exploring agricultural residues, such as corn or wheat straw as potential feedstock for RCF. Furthermore, to our knowledge, no studies have been conducted on the RCF of biologically treated biomasses, including digestates.

Solvent

Xu et al. investigated the reductive catalytic fractionation of lignin using different alcohols, namely MeOH, EtOH, and i-Pr, and reported varying yields of phenolic monomers. The highest yield of 50 wt.% was obtained in MeOH, followed by 48 wt.% in EtOH and 27 wt.% in i-Pr [188]. The authors also found that alcohols could provide active hydrogen species. In a recent study, Ouyang et al. reported a 49% yield of phenolic monomers with 82% selectivity towards SP in a methanol/water mixture (1:2 v/v) [189]. They reported that the selectivity towards GPe/SPe and GP/SP could be adjusted by varying the ratio of MeOH and water in addition to reaction temperature. Zhang et al. [190] performed reductive catalytic depolymerization of birch using a Ni-W₂C/C catalyst. The use of methanol and ethylene glycol solvents instead of water resulted in increased yields of monophenols. In another study, the effect of solvent was investigated in the catalytic depolymerization of cork over Rh/C catalyst. It was found that the highest bio-oil yield of 43 wt.% was achieved using a 2-methyl tetrahydrofuran/water solvent mixture [191].

Renders and colleagues investigated the impact of alcohol/water mixtures on the RCF of poplar wood and observed a synergistic effect of the solvent system. The delignification was found to increase with solvent polarity, but excessive polarity led to the solubilization of carbohydrate pulp. The group discovered that a lower water concentration enhanced lignin removal from the biomass, while preserving most of the carbohydrates. However, a higher water concentration (70%) favored the solubilization of hemicellulose and lignin, resulting in high purity cellulosic residues [192, 193].

2.4.3.3. RCF as an advantage for biorefinery and petrorefinery

In the pursuit of complete utilization of lignocellulosic biomass, previous studies have addressed the fate of hemicellulose and cellulose during RCF [14, 165, 166, 194]. As indicated in the previous section the retention of cellulose and hemicellulose varied depending on the solvent utilized. A study was performed investigating the synergistic effects of alcohol/H₂O mixtures on RCF of poplar using MeOH/H₂O and EtOH/H₂O co-solvents with varying volume ratios [192]. The retention of cellulose was observed to be consistent regardless of the MeOH/H₂O and EtOH/H₂O ratios, while the proportion of hemicellulose in the pulp was modulated by altering the percentage of water. Greater percentages of H₂O led

to decreased retention of hemicellulose, and complete removal was observed in pure water due to cleavage of the ester and ether linkages between lignin and hemicellulose. The dissimilar retention behavior of cellulose and hemicellulose observed in RCF can be attributed to the greater resistance offered by the semi-crystalline structure of cellulose, which impedes its solubility characteristics [155, 192]. Hence, with changing solvent systems RCF can provide two valorization biorefinery strategies presented in Figure 2.17, either to produce phenolic monomers and holocellulose pulp for further valorization or to produce phenolic monomers, polyols and sugars in addition to pure cellulose pulp for further valorization into bio-ethanol, microcrystalline cellulose fibers (MCF), and nano cellulose fibers (NCF).

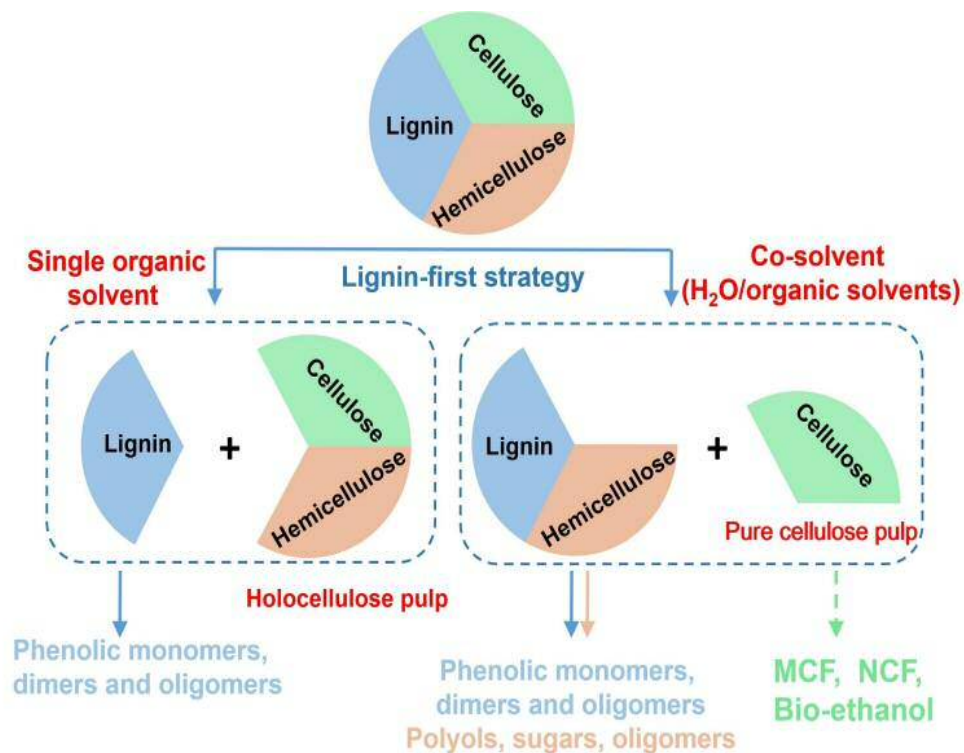


Figure 2.17 Two "lignin first" biorefinery strategies, depending on solvent choice [155].

Sels et al. [195, 196] presented another two step strategy which presents an advantage for petrorefinery, as it integrates RCF-based biorefinery process into existing petrorefinery schemes. Firstly, using methanol as a solvent and Ni/Al₂O₃ catalyst, birch wood was depolymerized by RCF, resulting in nearly 50 % yield of phenolic monomers and a solid carbohydrate pulp with a high retention of C5 and C6 sugars (83% and 93%, respectively). In the second step, the solid carbohydrate pulp obtained can be converted into alkanes (light naphtha) using liquid-phase cellulose-to-naphtha (LPCtoN) technology which uses an acidic reactive aqueous phase and a redox catalyst (Ru/C + H₄SiW₁₂O₄₀). A two-phase (water/fossil naphtha) catalytic slurry process followed by isomerization was employed to produce bio-enriched gasoline from the (hemi)cellulose pulp, as illustrated in Figure 2.18.

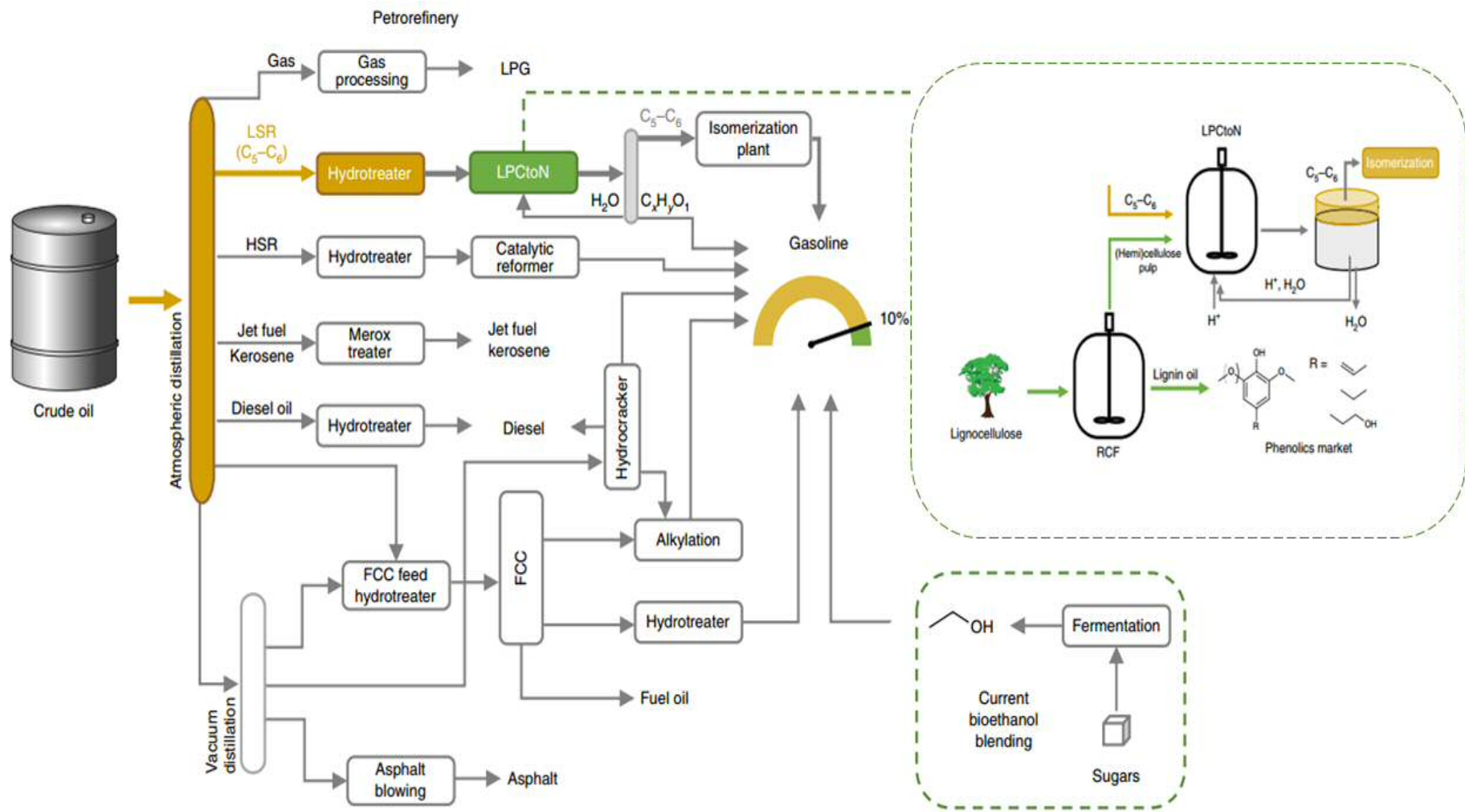


Figure 2.18 Schematic representation for integrating RCF-based biorefinery process and (LPCtoN) technology into existing petrorefinery, adapted from [195].

2.5. Hydrogenolysis of glycerol

The remarkable yearly expansion of biodiesel manufacturing has led to a significant overabundance of glycerol (GL), as it is a main by-product, which corresponds to 10 wt.% of biodiesel production [5]. In 2018, a total production of 4.2 million tons of GL was estimated, with a strong expectation of continued growth in the coming decades. This enlarging production of GL has had a profound impact on its market value, leading to a substantial decrease in price. For instance, in Europe, the cost of GL plummeted from 4000 \$/ton to below 500 \$/ton in just a decade between 2000 and 2010 [197]. The significant increase in GL production coupled with its decreasing market value, along with its enormous potential for valorization into many value-added products makes it one of the most promising feedstocks for the future. Moreover, the valorization of glycerol presents an opportunity to reduce the production costs of biodiesel and establish sustainability in the biodiesel manufacturing process.

2.5.1. Glycerol manufacturing process

As presented in Figure 2.19, GL is produced predominantly as a byproduct in biodiesel industry, wherein the triglycerides (oils) undergo transesterification with an alcohol, such as methanol, yielding fatty esters (biodiesel) and glycerol as a co-product. Both heterogeneous and homogenous catalysts can be utilized in this process. Homogeneous reactions usually involve the use of sodium hydroxide or sodium methylate as the catalyst, which are dissolved in the reaction medium. Following the reaction, a settler is employed to separate the glycerol from the remaining flow, which is then subjected to further processing to purify the biodiesel from the aqueous mixture. The recycled aqueous mixture, along with any unreacted methanol, is returned to the reactor [198].

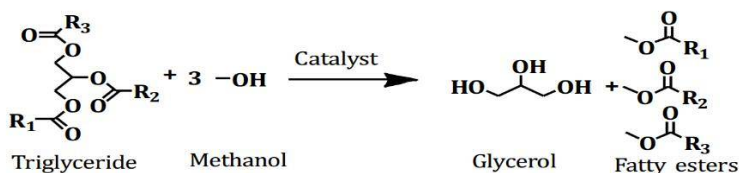


Figure 2.19 Transesterification reaction for biodiesel and glycerol production, adapted from [199].

2.5.2. Glycerol valorization

Various catalytic technologies such as oxidation, dehydration, etherification, esterification, acetylation, carboxylation, chlorination and hydrogenolysis [200, 201], can be employed to convert GL into value-added products. Some important glycerol-derived products with diverse industrial applications in sectors such as pharmaceuticals, plastics, agriculture, and fuels include hydrogen, lactic acid, propionic acid, succinic acid, 1,3-propanediol (1,3 PD), 1,2-propanediol (1,2 PD), epichlorohydrin, ethanol (EtOH), n-butanol, i-butanol, poly-3-hydroxybutyrate, 1,2-isopropylidene glycerol acetate (a biodiesel additive), and glycerol tertiary butyl ether (GTBE). Figure 2.20 illustrates a scheme for glycerol valorization into some of these valuable products through different catalytic technologies [200].

The conversion of GL into 1,2 PD is regarded as one of the most significant glycerol valorization techniques, since 1,2 PD is a highly valuable commodity chemical with diverse industrial applications. It is utilized as biodegradable functional fluid and as antifreeze agent, which can potentially replace ethylene glycol in anti-freeze systems and aircraft de-icers. Additionally, It is widely utilized as a monomer for the production of thermoset composites,

and it can also be employed for the synthesis of other important chemicals, such as esters, dipropylene glycol, tripropylene glycol, and polyether polyols [202]. Furthermore, it has substantial applications in food, pharmaceuticals, cosmetics, detergents and tobacco industries [5, 23, 40, 203, 204].

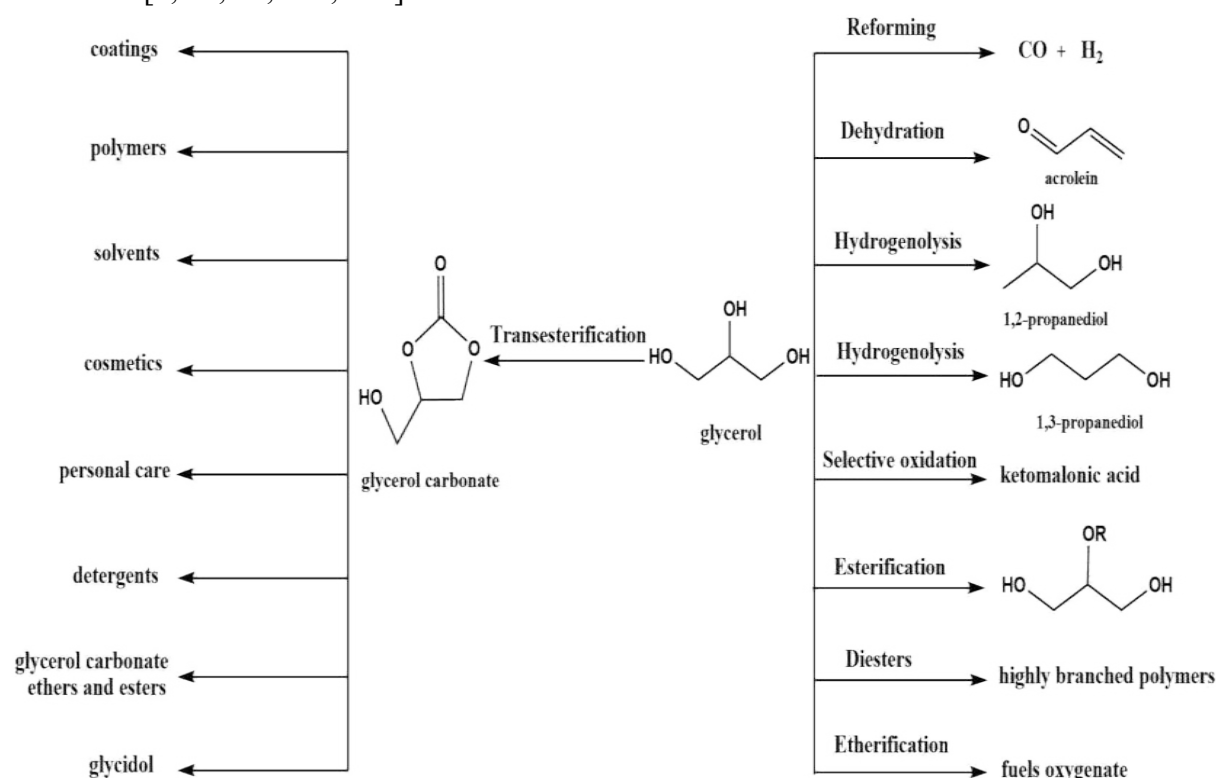


Figure 2.20 Glycerol valorization through different reactions into value-added products, adapted from [200].

2.5.3. 1,2 propanediol production

Figure 2.21 illustrates the conventional production process of 1,2 PD through the hydrolysis of fossil-derived propylene oxide with water at specific reaction conditions, namely, a temperature of 125°C, a pressure of 20 bar, and a water to propylene oxide ratio of 15:1. However, the undesired side reaction of sequential propylene oxide addition to 1,2 PD occurs during the production process, resulting in the formation of dipropylene glycol and tripropylene glycol. To increase the selectivity towards 1,2 PD, the water to propylene oxide ratio can be increased. Nonetheless, such an increase in the ratio results in elevated recycling flow rates, which in turn substantially increases the energy costs [202].

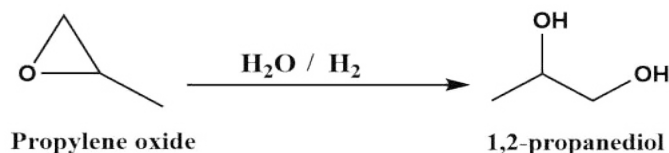


Figure 2.21 Hydrogenolysis of propylene oxide to form 1,2 PD [202].

As previously discussed, the utilization of bioderived glycerol as a promising feedstock for the sustainable production of 1,2 PD through hydrogenolysis has gained considerable attention due to the increasing growth of biodiesel production [205]. The process has been also commercialized (USP grade) and contains two stages, presented in Figure 2.22, that take

place in the presence of hydrogen atmosphere and metal catalyst. In the first stage, glycerol undergoes dehydration to produce acetol as an intermediate, which is then hydrogenated in the second stage to yield 1,2 PD [5].

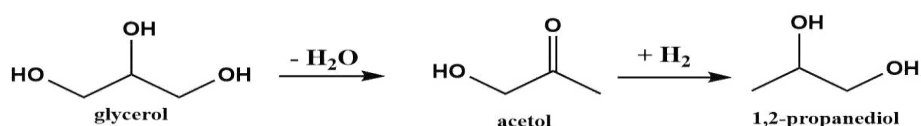


Figure 2.22 Two stage commercial 1,2 PD production from glycerol [202].

2.5.4. Mechanisms for glycerol hydrogenolysis into propanediols

The literature provides a plethora of proposed mechanisms for glycerol hydrogenolysis, with the predominant controlling mechanism being contingent mainly upon the catalyst's inherent characteristics, including acidity, basicity, and metal catalytic properties. In general, three reaction mechanisms, namely dehydration- hydrogenation mechanism, glyceraldehyde-based mechanism, and hydride-attack mechanism, have been widely accepted and are depicted in (Figure 2.23 - Figure 2.25).

i) Dehydration- hydrogenation mechanism:

In the presence of an acidic catalyst, such as amberlyst or zeolites, the aforementioned dehydration-hydrogenation mechanism is favored, resulting in enhanced glycerol conversion and selectivity towards 1,2 PD [206, 207]. The acid catalyst facilitates the dehydration of GL to form an intermediate, which subsequently undergoes hydrogenation on the metal site of the catalyst, as shown in Figure 2.23. If the proton attacks the -OH linked to the terminal C of GL, hydroxyacetone (HA) will be produced as an intermediate. In the event that dehydration of the middle hydroxyl group of GL takes place, 3-hydroxypropanal (3-HPA) is generated as an intermediate. Subsequent hydrogenation of HA and 3-HPA results in producing 1,2 PD and 1,3 PD, respectively [23, 208]. Due to the thermal stability of HA in comparison with 3-HPA, the formation of 1,2 PD is more favorable than 1,3 PD [209]. Furthermore, when this mechanism is dominant, a major product is n-propanol (n-Pr), which is formed by the subsequent hydrogenation of acrolein generated through acid-catalyzed dehydration of GL.

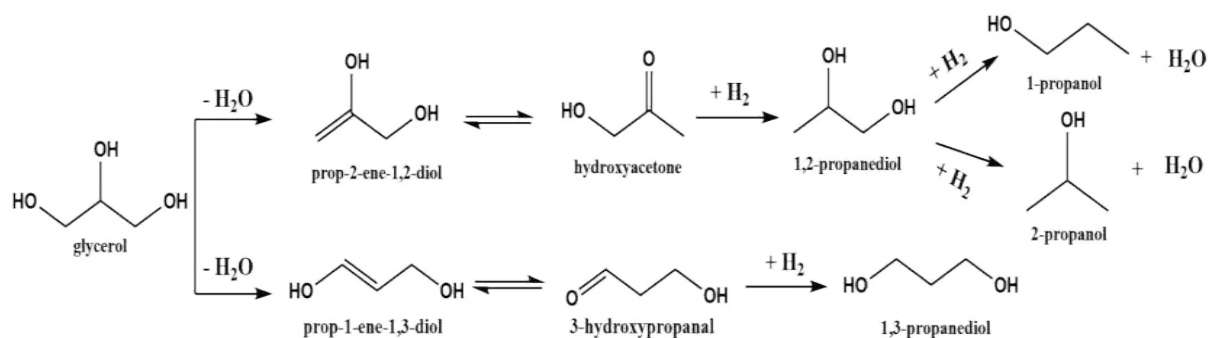


Figure 2.23 Dehydration- hydrogenation mechanism [208].

ii) Glyceraldehyde-based mechanism

Under neutral or alkaline conditions, the glyceraldehyde-based mechanism, also known as the dehydrogenation-dehydration-hydrogenation mechanism (Figure 2.24), typically dominates

[208]. Montasier et al. [210] proposed that in the initial step, GL undergoes dehydrogenation on the metal site of the catalyst to form glyceraldehyde as an intermediate. In the presence of a base, the subsequent dehydration of glyceraldehyde to form 2-hydroxyacrylaldehyde is accelerated. Sequential hydrogenation of 2-hydroxyacrylaldehyde on metal site of the catalyst produces HA and 1,2 PD [208, 210]. Under those alkaline conditions, C-C bond cleavage leading to the formation of ethylene glycol (EG) and C1 byproducts cannot be neglected [211]. Moreover, glyceraldehyde may undergo decarbonylation via the metal site or retroaldolization on basic sites, followed by hydrogenation on the metal site, to generate EG as a side reaction.

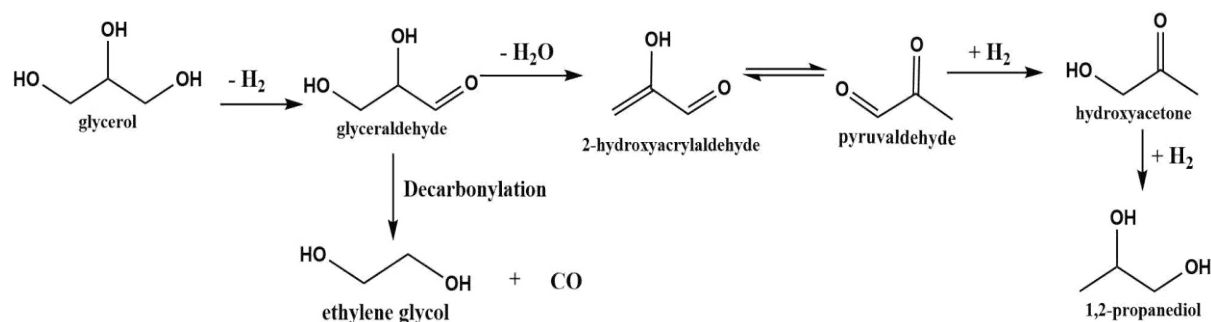


Figure 2.24 Glyceraldehyde-based mechanism [208].

iii) Hydride-attack mechanism

The hydride-attack mechanism is observed when Ir–ReO_x/SiO₂ catalysts are applied to the GL hydrogenolysis reaction system. Tomishige et al. [212] proposed that GL is adsorbed at the interface between Ir and ReO_x to form either 2,3-dihydroxypropoxide (Figure 2.25-a) or 1,3-dihydroxyisopropoxide (Figure 2.25-b). Concurrently, the Ir metal promotes the formation of hydrides that cleave C-O bonds by attacking the 2nd-position of 2,3-dihydroxypropoxide to produce 1,3 PD and the 3rd-position of 2,3-dihydroxypropoxide to form 1,2 PD. A noteworthy characteristic of this mechanism is the lower selectivity of 1,2 PD relative to 1,3 PD in the reaction system, which can be explained by the higher stability of 6-membered ring transition state (Figure 2.25-a) compared to the unstable 7-membered ring transition state (Figure 2.25-b) [208, 212-214].

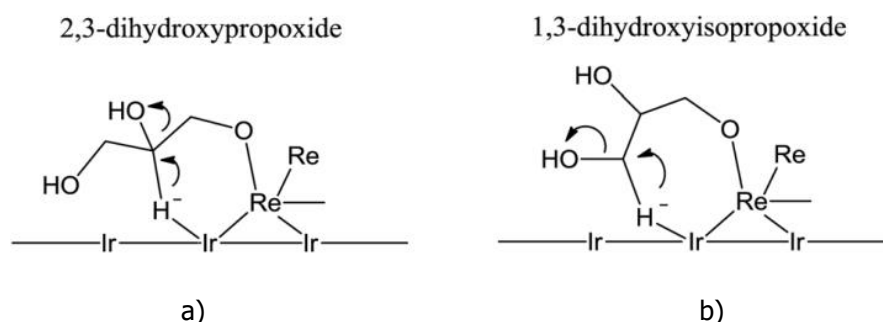


Figure 2.25 Hydride-attack mechanism a) from glycerol to form 1,3 PD b) from glycerol to form 1,2 PD [214].

2.5.5. Reaction network for hydrogenolysis of glycerol

The hydrogenolysis of glycerol exhibits various reaction pathways that depend on the catalyst, solvent, and reaction conditions of temperature and H₂ pressure. Figure 2.26

provides an overview of the typical reaction pathways and main products observed during the reaction. Initially, GL is dehydrated via an acid-based reaction to form an intermediate. If the dehydrated intermediate is prop-2-ene-1,2-diol, HA is formed. HA contributes to the production of 1,2 PD via further catalytic hydrogenation [208]. Subsequent hydrogenolysis of 1,2 PD leads to the formation of n-Pr and i-Pr. Further reaction steps of dehydration and hydrogenation of propanols produce propene and propane. On the other hand, if the dehydrated intermediate formed is prop-1-ene-1,3-diol, this ends with the formation of 1,3 PD from 3HPA. Although 3HPA has not been detected in previous studies, quantum mechanical calculations have suggested its formation and its instant transformation either to 1,3 PD through hydrogenation or to acrolein through dehydration [215]. The oxidation of acrolein in aqueous solution leads to the production of propanoic acid (PA), while its decomposition produces CO and short linear alkanes, including ethane and propane [59].

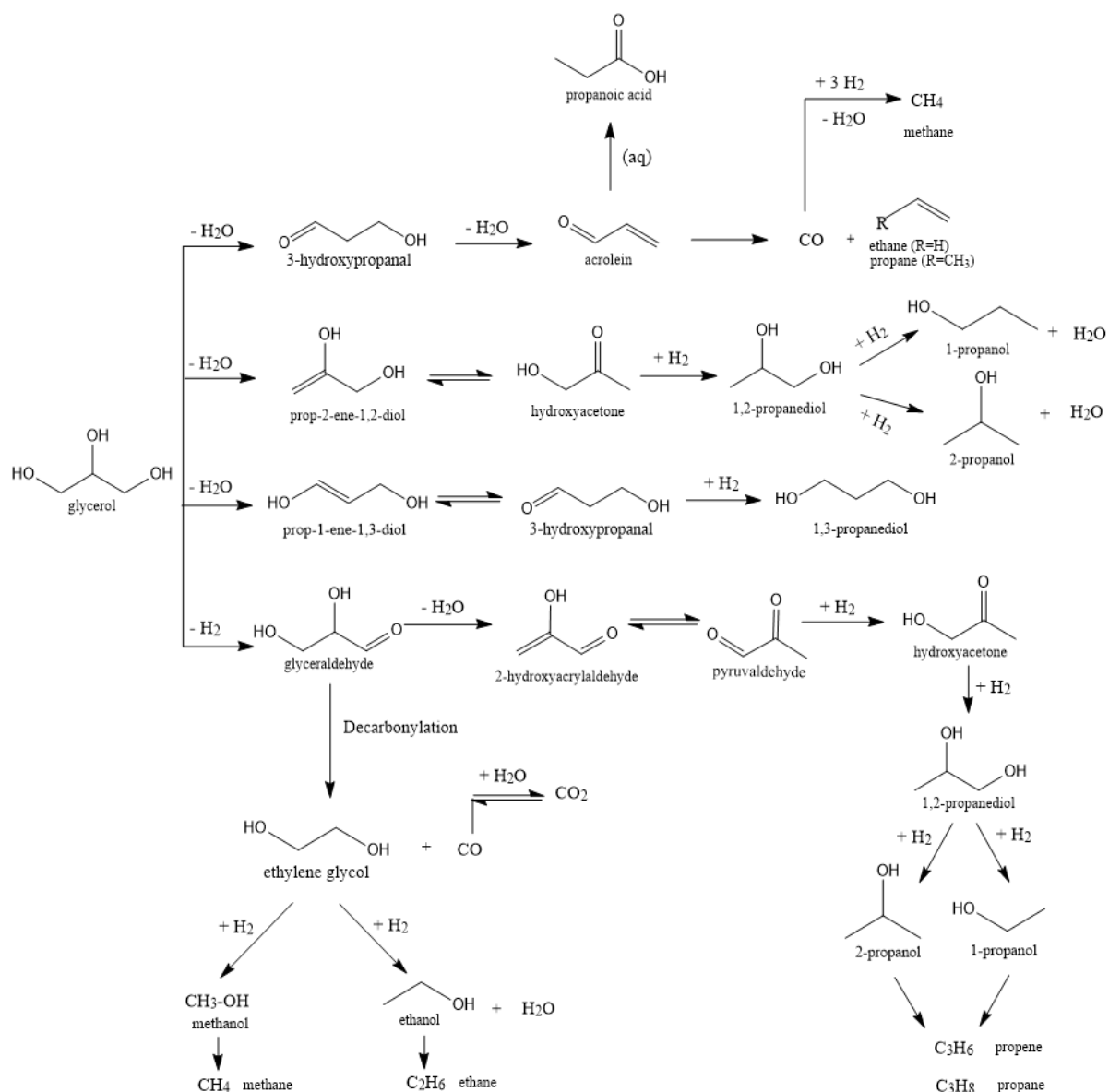


Figure 2.26 Reaction scheme of glycerol hydrogenolysis [59, 208, 210, 215, 216].

1,2 PD can be formed through another reaction pathway, dehydrogenation-dehydration-hydrogenation, which starts with the dehydrogenation of glycerol into glyceraldehyde

followed by dehydration of the glyceraldehyde to 2-hydroxyacrylaldehyde which can be hydrogenated sequentially and produces HA and 1,2 PD [210]. Decarbonylation of glyceraldehyde can be responsible for EG and CO formation. MeOH and EtOH can be formed via subsequent hydrogenolysis of ethylene glycol. Further hydrogenation of CO and hydrogenolysis of methanol causes the formation of methane. Ethane can be formed from ethanol in the same way. And finally, CO can be converted to CO₂ through aqueous phase reforming mechanism [217].

2.5.6. Catalyst: the main factor that controls the selectivity

Most studies of GL hydrogenolysis focus on catalyst development, as it plays a vital role in determining the reaction mechanism, which controls the selectivity towards a particular product in the reaction system, as discussed in the previous section. Both noble-metal catalysts (Ru, Pt, Rh Pd, Ag and Ir) and transition-metal catalysts (Ni, Cu and Co) have been successfully employed for hydrogenolysis of glycerol [208]. Detailed information about the behavior of these different catalysts in glycerol hydrogenolysis, and their influence on conversion (X) and product selectivity (S) can be obtained from existing literature [208, 218, 219].

Generally, Ru-based catalysts proved to be very active due to their superior ability to cleave C-C and C-O bonds. Conversely, Cu based catalysts showed a higher selectivity towards 1,2 PD but at a lower conversion. Pt and Ir based catalysts have a higher potential for the selective production of 1,3 PD from glycerol [208, 212-214, 219]. As shown in Table 2.6, the conversion and 1,2 PD selectivity are not only affected by the metal site but also by the catalyst support, modifiers, and acidic or basic additives. For instance, the addition of an acid (e.g. Amberlyst 15 or zeolites) to Ru/C, Table 2.6 entries (4,5), led to an increase in glycerol conversion and 1,2 PD selectivity [206, 207]. Similarly, the addition of lithium or sodium base (i.e. LiOH, NaOH, Li₂CO₃ or Na₂CO₃), Table 2.6 entries (6-10), significantly increased the conversion of GL and 1,2 PD selectivity [220]. Furthermore, the surface modification of Ru with another metal such as Fe resulted in an increase in selectivity towards 1,2 PD formation, as presented in Table 2.6 entries (11-13) [221].

Table 2.6 Some examples for catalysts utilized in glycerol hydrogenolysis.

Entry	Catalyst	X (%)	product	S (%)	Ref.
1	Rh/C	0.3	1,2 PD	58.6	[206]
2	Pd/C	0.7	1,2 PD	93.1	[206]
3	Pt/C	1.1	1,2 PD	87.6	[206]
4	Ru/C	6.3	1,2 PD	17.9	[206]
5	Ru/C + Amberlyst	15	1,2 PD	53.4	[206]
6	Ru/TiO ₂	66.3	1,2 PD	47.7	[220]
7	Ru/TiO ₂ + LiOH	89.6	1,2 PD	86.8	[220]
8	Ru/TiO ₂ + NaOH	83.4	1,2 PD	83.5	[220]
9	Ru/TiO ₂ + Li ₂ CO ₃	80.1	1,2 PD	82.3	[220]
10	Ru/TiO ₂ + Na ₂ CO ₃	78	1,2 PD	83.6	[220]
11	Ru/CNT	64.5	1,2 PD	22.1	[221]
12	Ru ₄ Fe ₁ /CNT	64.1	1,2 PD	37.4	[221]
13	Ru ₃ Fe ₁ /CNT	56.4	1,2 PD	46.3	[221]
14	Ru ₂ Fe ₁ /CNT	59.5	1,2 PD	52.7	[221]

2.6. One-factor-at-a-time approach & Response surface methodology

As highlighted in sections 2.2-2.4, variations in reaction variables, such as temperature, H₂ pressure, reaction time, and catalyst to substrate ratio, in hydroprocessing reactions have a significant influence on the reaction kinetics, the activity of the catalyst, and the selectivity towards specific products. Therefore, investigating the effect of these parameters in any hydroprocessing reaction system is crucial. There are two strategies for performing such investigations: i) One-factor-at-a-time approach (OFAT) and ii) Response surface methodology (RSM) [222].

OFAT is a way to identify optimal operating conditions that maximize the yield of a specific product, in which the influence of each variable on a process is studied individually while keeping all other variables constant. On the other hand, RSM involves the use of statistical design of experiment (DoE) to simultaneously vary multiple variables across a set of experimental runs. This approach is superior in achieving the same objective of finding optimal operating conditions, particularly when there are potential interactions between the variables being investigated.

RSM is a collection of mathematical and statistical methods used for empirical model building, analysis, and optimization of a process. This approach provides a more efficient way to investigate the effect of different variables on a specific response, because [223]:

- i) It is a more economic method that saves time and money as it requires less experiments.
- ii) The interaction between the different variables can be estimated using it.
- iii) It makes the optimization more efficient, as it allows us to search for optimal solution over the entire variable space.

The implementation of RSM typically involves the selection of an appropriate design such as full factorial design, Box-Behnken design, or central composite design (CCD). Following the design selection, a recommended set of experimental runs by the chosen design is performed in the laboratory. The next step involves constructing a statistical model that establishes a relationship between the various variables and the response. The model-building process can be carried out manually or automatically using forward or backward selection methods. The selection criterion used may include P-value, Bayesian information criterion (BIC), Akaike information criterion (AIC) or R² adjusted criterion. The constructed models are then statistically validated using analysis of variance (ANOVA) and experimentally validated using additional experiments. Finally, a graphical and numerical optimization can be employed to identify the optimal reaction conditions that maximize the desired product or minimize the undesired ones [223, 224]. RSM has been successfully applied in many different scientific fields such as technical chemistry, petroleum refining, biomass valorization, CO₂ capture, chemical engineering, materials engineering, and environmental protections [224-228].

Both methods were applied in the present work with the aim of maximizing the yield of the desired products. OFAT is applied on reductive catalytic fractionation of lignin (chapter 6) to study the effect of changing H₂ pressure and reaction time on maximizing SPOH/GPOH monomers yield. RSM is applied on the hydrogenation of DMF (chapter 4) to study the effect of changing temperature, H₂ pressure and catalyst to substrate ratio on maximizing HXL yield.

Cumulative part of the dissertation

Part I: Hydroprocessing of biomass derived furans

Part I of this dissertation is dedicated to the exploration of the catalytic hydroprocessing of biomass-derived furans to alcohols under mild reaction conditions. This part* encompasses two chapters, namely, chapter 3 and chapter 4. In chapter 3, the focus is on the investigation of the bifunctional Pt/polyoxometalate catalyst's ability to act as a selective catalyst for ring opening of furan compounds, for the production of butanol, pentanols, and 2-hexanol from biomass-derived furan, 2-methylfuran, and 2,5 dimethylfuran, respectively. Chapter 4 presents a response surface methodology study using 2,5 dimethylfuran as a model substrate. The objective of this chapter is to determine the optimal reaction conditions that would result in maximum alcohol yield.

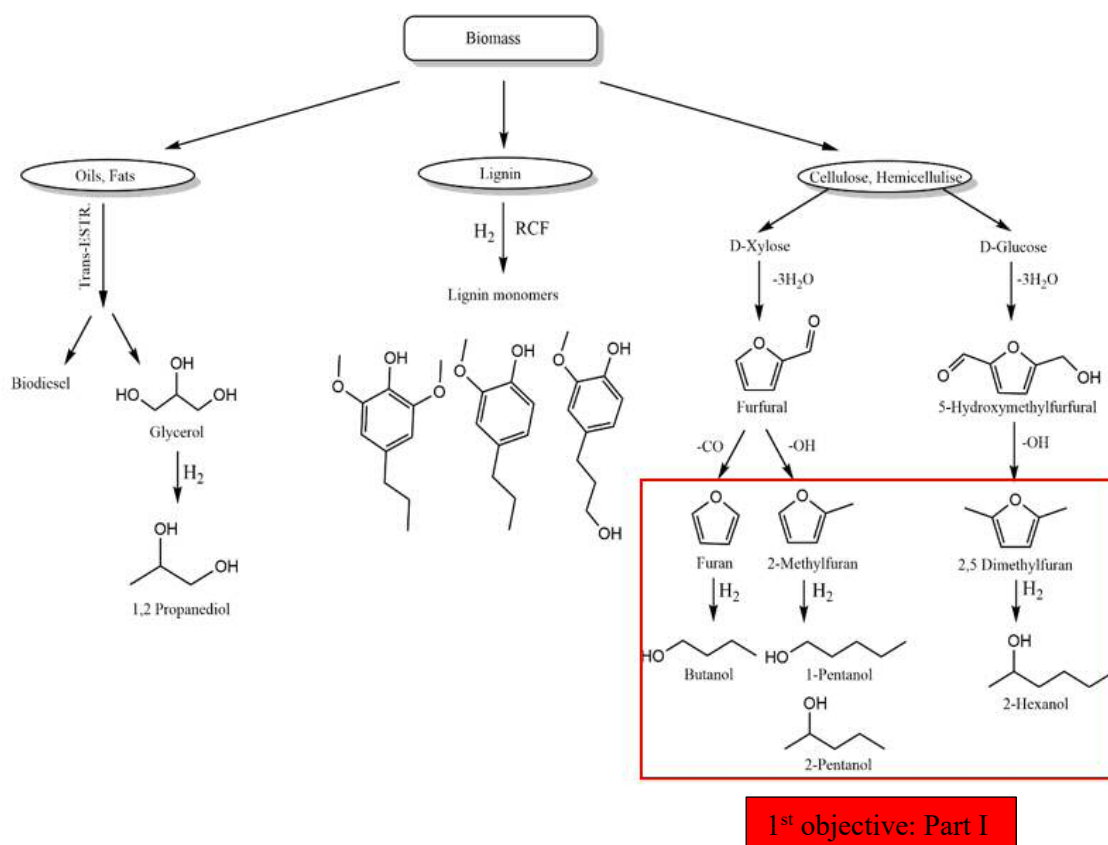


Figure 1.3 Scope of the thesis: 1st objective (hydroprocessing of biomass derived furans).

* This part includes two publications, wherein the synthesis of non-commercial catalysts employed in the investigations was undertaken and written by Dr. Maria Stuckart (Friedrich-Alexander-Universität Erlangen-Nürnberg).

Chapter 3. Selective catalytic hydrogenation of biomass derived furans to secondary alcohols using Pt/polyoxometalate catalysts under mild reaction conditions

This chapter is based on publication [4]. In the following chapter several commercial and synthesized catalysts were tested to identify a suitable catalyst with enhanced activity towards selective ring opening of furanic compounds under mild hydrogenation reaction conditions. 2,5-dimethylfuran was chosen as a model substrate for the hydrogenation reaction under 80 °C and 10 bar H₂. According to the first set of screening experiments, Pt turned out to be the most selective active metal site towards the ring opening of 2,5-dimethylfuran. Subsequent investigations on the liquid carrier utilized during the reaction revealed that the use of n-decane enhances the production of 2-hexanol. Conversely, the use of n-hexadecane enhances maximizing 2-hexanone. The bifunctional Pt/polyoxometalate catalysts were also identified as selective catalysts for furan ring opening. Pt/Keggin-type POM K₃[PW₁₂O₄₀] showed high selectivity for 2-hexanol formation at 80 °C and 10 bar H₂ pressure using n-decane as a carrier liquid. Pt/Wells–Dawson-type POM K₆[α P₂W₁₈ O₆₂] was found to be selective for 2-hexanone formation under identical reaction conditions. Optimization of bi-functional Keggin-type POM catalyst synthesis was conducted to obtain a higher 2-hexanol yield. This was followed by an extension of the study to two other furan compounds, namely furan and 2-methylfuran, in order to selectively produce the corresponding alcohols, 1-butanol and 1/2-pentanol, respectively. Moreover, multiple catalyst characterization techniques were carried out to explain the superior performance of the bi-functional catalyst system Pt/K₃[PW₁₂O₄₀] towards the ring opening of the furans and the high selectivity towards alcohol formation, as compared to the commercial Pt/C catalyst. Further supporting information can be found in Appendix 10.4.

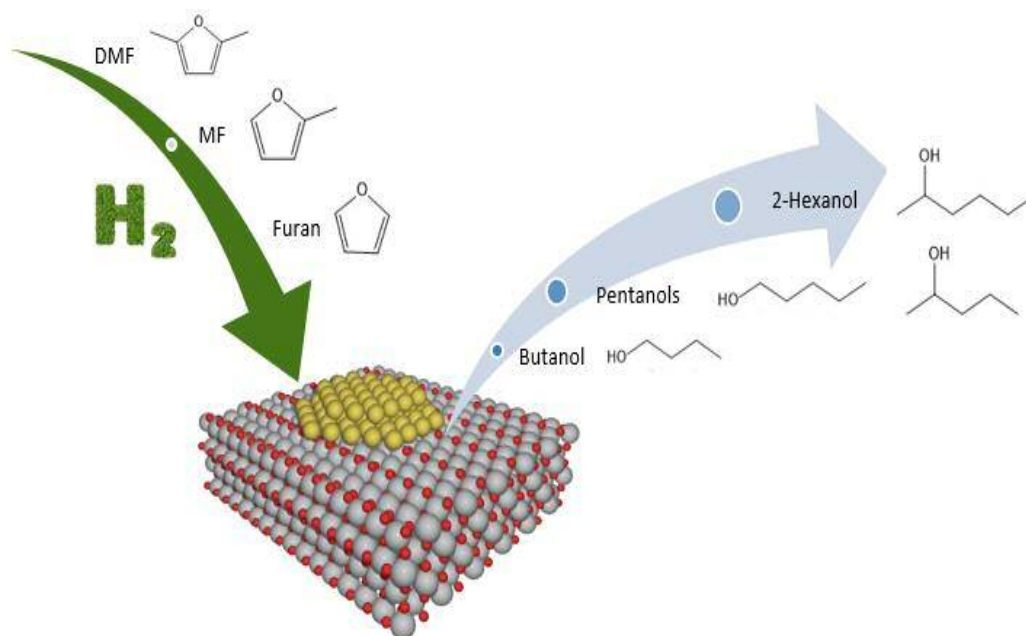



Figure 3.1 Selective catalytic hydrogenation of 2,5-dimethylfuran (DMF), 2-methylfuran (MF) and furan to the corresponding alcohols 2-hexanol, 1/2-pentanol and 1-butanol, respectively, using Pt/K₃[PW₁₂O₄₀] catalyst under mild reaction conditions.

Selective catalytic hydrogenation of biomass derived furans to secondary alcohols using Pt/polyoxometalate catalysts under mild reaction conditions

Magdy Sherbi, Institute for Technical and Macromolecular Chemistry, University of Hamburg, Hamburg, Germany

Maria Stuckart, Institute for Chemical Reaction Engineering, Friedrich-Alexander-Universität Erlangen-Nürnberg, Erlangen, Germany

Jakob Albert , Institute for Technical and Macromolecular Chemistry, University of Hamburg, Hamburg, Germany

Received December 17 2020; Revised March 01 2021; Accepted May 06 2021;

View online June 3, 2021 at Wiley Online Library (wileyonlinelibrary.com);

DOI: 10.1002/bbb.2248; *Biofuels*, *Bioprod. Bioref.* 15:1431–1446 (2021)



Abstract: Promising bifunctional catalyst systems composed of platinum and polyoxometalates (POMs) were applied successfully for the selective catalytic hydrogenation of 2,5-dimethylfuran (DMF) to 2-hexanol under mild conditions. Pt(acac)₂ was found to be the most active Pt precursor for the ring opening of DMF, and the Keggin-type POM K₃[PW₁₂O₄₀] was identified as the most promoting acidic support for 2-hexanol formation at 80 °C and 10 bar H₂ pressure using *n*-decane as a carrier liquid. It was revealed that modifications in the synthetic procedure of the Pt/K₃[PW₁₂O₄₀] catalytic system allowed its catalytic performance to be enhanced. Thus, a higher yield of 2-hexanol (72.5%) was achieved compared to that (49%) obtained using a commercial Pt/C catalyst with the same Pt loading. The Wells–Dawson-type POM containing catalyst Pt/K₆[α-P₂W₁₈O₆₂] was found to be selective for 2-hexanone formation (56.4% yield) under identical reaction conditions. Furthermore, furan and 2-methylfuran were also selectively hydrogenated to 1-butanol (59.7% yield) and 1/2-pentanol (44.3% yield), respectively, under the applied reaction conditions. Moreover, using analytical tools like N₂-physisorption, NH₃-TPD, inductively coupled plasma optical emission spectroscopy (ICP-OES), CO chemisorption, and transmission electron microscopy (TEM), revealed that the higher total acid site density of the K₃[PW₁₂O₄₀] enhances C=O hydrogenation and overcomes the rate-limiting step of 2-hexanone hydrogenation to 2-hexanol. This demonstrates the high performance of the bi-functional catalyst system Pt/K₃[PW₁₂O₄₀] towards ring opening of various furans and the very high selectivity towards alcohol formation. This approach opens new interesting valorization pathways for several furanic compounds with respect to

sustainable alcohol formation. © 2021 The Authors. *Biofuels, Bioproducts and Biorefining* published by Society of Industrial Chemistry and John Wiley & Sons Ltd.

Supporting information may be found in the online version of this article.

Key words: 2,5-dimethylfuran; selective catalytic hydrogenation; polyoxometalates; ring opening; alcohol formation; 2-hexanol

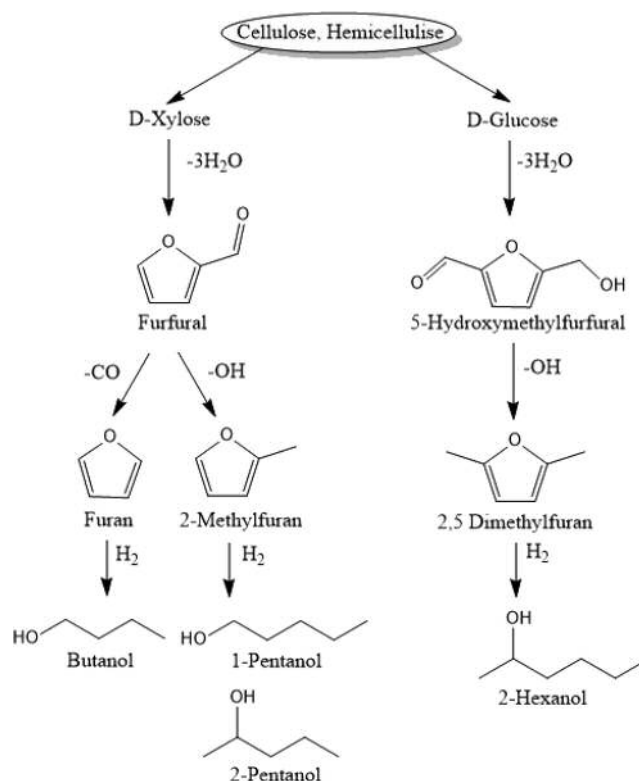
Introduction

Accessible oil reserves have been diminishing for decades.^{1,2} Fossil-fuel burning produces more than 82% of the total greenhouse gas emissions.^{3,4} Consequently, finding a sustainable and renewable alternative to oil is essential to maintain the supply of fuels and chemicals.^{5,6}

Biomass as an alternative source of fuels and chemicals is receiving increasing attention.⁷ Lignocellulose, the most abundant class of biomass, is exemplified by switchgrass, miscanthus, agricultural residues, municipal wastes, and waste from wood processing. Lignocellulosic biomass contains three main fractions: cellulose, hemicellulose, and lignin.² Cellulose and hemicellulose represent the carbohydrate fraction (70–75%) and are attractive starting materials to produce renewable fuels and chemicals.^{8,9} Current pathways to transform lignocellulosic biomass are classified into two approaches: (i) thermochemical conversion and (ii) hydrolysis. Thermochemical processes require higher temperatures (750–1000 K). Hydrolysis (350–400 K) is therefore preferred for energy purposes. During acid hydrolysis, cellulose and hemicellulose are converted to C6 (glucose) and C5 (xylose) sugars, respectively.¹⁰ Transformation of these sugars by dehydration to furfural (FFR) and hydroxymethylfurfural (HMF) requires an increase in the C/O ratio. Many reviews have been published summarizing the production of FFR and HMF.^{11–13} Generally, they are produced through dehydration of xylose and glucose in the presence of acidic catalysts as shown in Scheme 1. These furanic species can be produced from sugars with very high yields and selectivities (>90%),^{14,15} which paves the way for further processing to industrially relevant chemicals.¹⁶ Selective production of furans, that is furan, 2-methylfuran (MF), and 2,5-dimethylfuran (DMF) from FFR and HMF is well documented and the previous products can be received in high yields and selectivities.⁸ For example, furan is produced in 98% selectivity at complete conversion by decarbonylation of FFR using 5 wt% Pd/C at 250 °C.¹⁷ 2-Methylfuran is produced through hydrogenolysis of the side C-O bond from FFR with 89% selectivity at

100% conversion using Raney Ni at 250 °C.¹⁸ At 80 °C, HMF hydrogenolysis using Pd/C results in 100% selectivity of DMF at complete conversion.¹⁹

Finding a way to produce alcohols selectively from those renewable bio-derived furans rather than from fossils is considered to be beneficial in building a sustainable world that is completely independent of fossil resources. Alcohols are very important chemicals, which have numerous industrial applications. 1-Butanol is used as a carrier liquid for the extraction of essential oils, paints, coatings, natural resins, gums, synthetic resins, dyes, alkaloids, and camphor. It is also used as an extracting agent in the manufacture of antibiotics, hormones, and vitamins, as a paint thinner, as a component of hydraulic and brake fluids, and in the



Scheme 1. Pathway for catalytic conversion of sugars to secondary alcohols.

manufacturing of industrial cleaners and paint removers. Butanol is considered as a potential biofuel (butanol fuel), which may replace diesel and gasoline fuels.^{20,21} 2-Pentanol is used as a solvent and as an intermediate in the manufacture of other chemicals in pharmaceuticals and cosmetics. It is also used in the food industry as a flavoring agent. Different pentanol proportions are blended with diesel fuel to reduce particulate emissions in diesel engines.^{21,22} It is also considered as a very important carrier liquid in the manufacturing of petroleum additives, urea-formaldehyde plastics processing, organic chemical manufacturing, and raw material for pharmaceutical preparations.²⁰ 2-Hexanol (2-HXL) is used in the perfume²³ and tobacco²⁴ industries. Moreover, it can be mixed with other alcohols produced from biomass and used directly in a compression ignition engine.²⁵ The C-C self-coupling and hydrodeoxygenation of 2-HXL produces C₉–C₂₄ hydrocarbons suitable for jet fuel applications and diesel substitutes.²⁶ 2-Hexanol can also be used as a co-feed with other C₂ to C₁₁ alcohols for the production of jet and other heavy fuels.²⁷

The first investigation of the catalytic hydrogenation of furan was carried out by Padoa and Ponti in 1906, and in 1908 Bourguignon examined the hydrogenation of furan over a nickel catalyst at 170 °C, producing only (8%) 1-butanol.²⁸ Key factors for realizing selective hydrogenation of furans are catalyst properties like Brønsted acidity, metal dispersion, number of active sites, and system parameters like carrier liquid, hydrogen partial pressure, reaction temperature as well as reaction phase. For example, various furan derivatives are hydrogenated to the corresponding tetrahydrofurans in liquid phase over an Adams platinum or palladium catalyst. However, in the vapor phase, palladium retains its property of saturating the furan ring, whereas over platinum the furan ring is always opened.²⁸ Further investigation showed that the ring opened products are formed favorably in the vapor phase, and therefore this reaction was extensively studied in the literature using different heterogeneous catalysts including Ba/Cu/Cr, Cu/Cr/Ni/Zn/Fe, Cu-Ru/C, Pt, Pt-Al, Os, Ru, Ir, Raney Ni, Pd, Pd-Al, Cu, Mo, Fe-Cu, Co-Cu, Cu-Al, Ni-Zn at temperatures of 200–350 °C in the vapor phase.^{28–31} Pt showed an exceptional behaviour as it could perform the reaction at lower temperatures than 200 °C. Further investigations on the adsorption of furans on Pt surfaces^{32,33} and different supports used for Pt-based catalysts in the vapor phase can be seen elsewhere.^{34–36} Regarding the liquid phase hydrogenation, which has been investigated less in the literature, Adkins *et al.* used a copper chromite catalyst at 202 bar H₂ and 250 °C resulting in 30% yield of 1-pentanol and 33% yield of 2-pentanol, respectively. The reaction was

extended to furan, which gave a 70% yield of *n*-butanol and to DMF, which gave mainly 2-hexanol.³⁷ Recently, milder reaction conditions were published using a Ru/C catalyst at 80 °C, 20 bar H₂ pressure in catalytic transfer hydrogenation to produce 19% 2-hexanol.¹⁶ Moreover, 92% selectivity towards 2-hexanone at 80 °C and 4.2 bar H₂ was reported using a Pt/C catalyst.¹⁵ It is obvious from the above discussion that performing the reaction in the liquid phase using mild reaction conditions to achieve high selectivity towards ring opening products can only be done with the right choice of the catalyst.

Polyoxometalates (POMs) are typical inorganic polyatomic discrete anionic species composed of several {MO_x} units (M = Mo^{VI}, W^{VI} and/or V^V), which are arranged around one or several {XO_y} groups (X = P^V, Si^{IV}). The most common examples are the Keggin-([XM₁₂O₄₀]ⁿ⁻) and the Wells–Dawson (WD)-type ([X₂M₁₈O₆₂]ⁿ⁻) POMs.³⁸ Removal of one or more M centers leaves free positions for incorporation of catalytic active metals or their complexes in the POM skeleton. Polyoxometalates are usually obtained as solid hydrated acids or salts due to the interaction of POM anions with protons or cations (e.g., Na⁺, K⁺, Cs⁺, NH₄⁺), respectively. The discrete ionic structure in the solid state and remarkable acidic and redox properties differentiate POMs from other commonly metal-oxo compounds used in catalysis like zeolites, which have infinitely extended framework structure.^{39–41}

Polyoxometalates have already shown their applicability in heterogeneous as well as in homogeneous catalysis (e.g., acid-catalyzed reactions and oxidation).⁴² Their potential as catalysts for reduction reactions is currently actively explored^{40,43} and was already demonstrated for the hydrogenolysis of glycerol,^{44–47} hydrodeoxygenation and hydrogenation of ketones,^{48,49} hydrogenation of aromatics,⁴³ reductive deoxygenation and hydrogenation of carbonyl compounds,⁵⁰ and the vapor-phase hydrogenation of propanoic acid.⁵¹

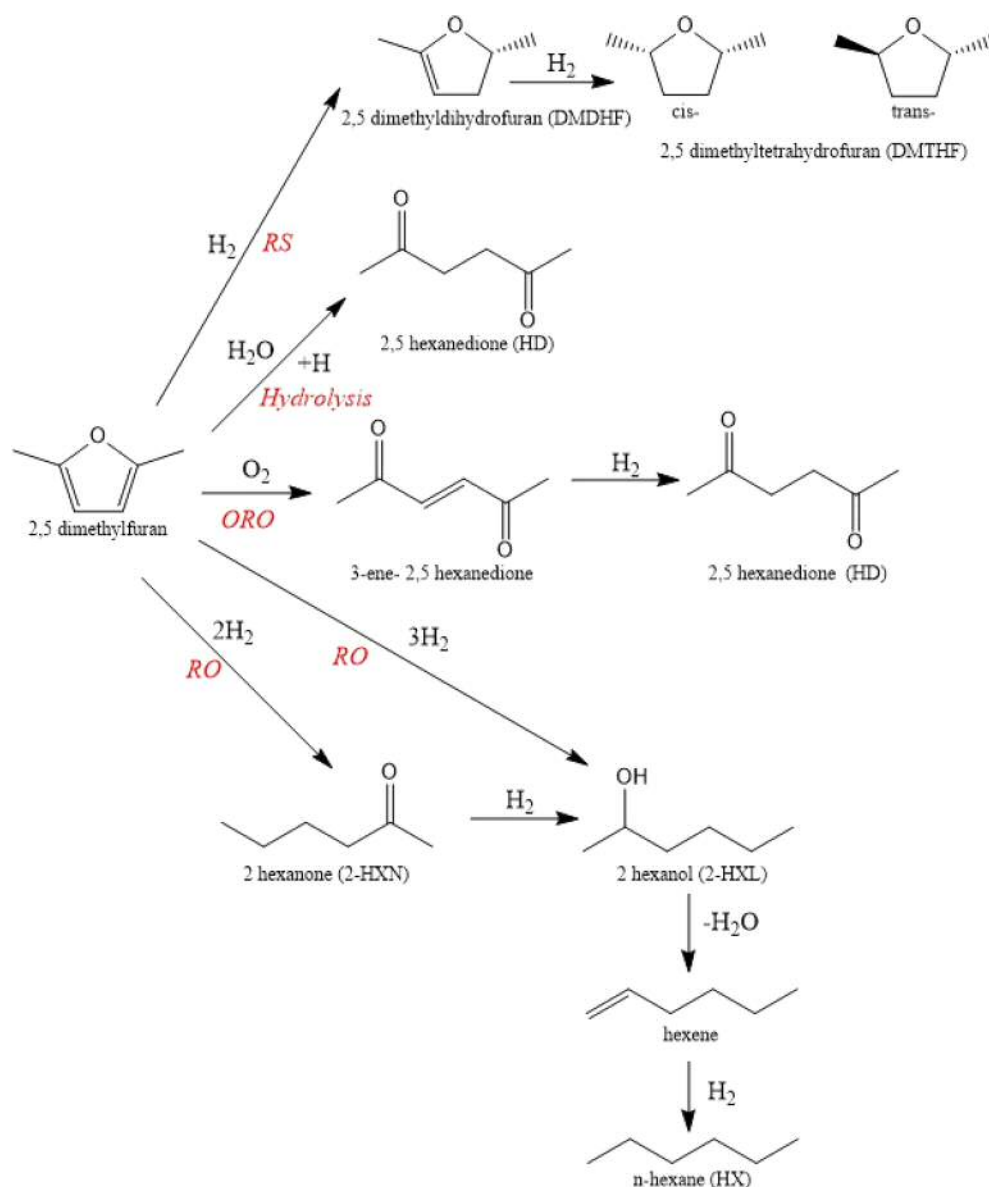
In this contribution, we show an interesting bifunctional catalyst system composed of platinum supported on a Keggin-type polyoxometalate for the selective production of ring opening products, especially alcohols, from bio-derived furans and renewable hydrogen under mild reaction conditions. This shows a route to produce alcohols from renewable sources like lignocellulosic biomass rather than fossils. However, the general motivation for this work was to study selective furan ring opening reactions, which are very important in many aspects with respect to biomass valorization. We started our investigations with DMF as a model compound for finding the most promising catalyst system for selective ring opening of furans.

Results and discussion

Reaction network for hydrogenation of DMF

Different reaction pathways are known for the hydrogenation of DMF, depending on the choice of catalyst, carrier liquid, reaction temperature as well as hydrogen pressure. Typically, efficient hydrogenation catalysts allow for mild reaction conditions with temperatures below 100 °C and 10 bar of hydrogen pressure using a high boiling organic carrier liquid. This allows a direct combination with electrolysis hydrogen as a source for green hydrogen. Generally, the main products

observed are 2,5-dimethyltetrahydrofuran (DMTHF) via two-step ring-saturation (RS) hydrogenation with 2,5-dimethyldihydrofuran (DMDHF) as an intermediate, 2,5-hexanedione (HD) via either direct hydrolysis of DMF in aqueous solution or oxidative ring opening (ORO) to 3-ene-2,5 hexanedione followed by hydrogenation to HD, 2-hexanone (2-HXN) via ring opening (RO) using 2 mol hydrogen or 2-hexanol (2-HXL) via RO using 3 mol of hydrogen. 2-Hexanol is of major interest here because of its importance in fuel applications.^{25–27,52} Scheme 2 gives an overview of the typical products observed during DMF hydrogenation. 2-Hexanol can undergo consecutive



Scheme 2. Reaction network for hydrogenation of 2,5-dimethylfuran.^{15,49,53,54}

dehydration to 1-hexene, which, in turn, can be hydrogenated to *n*-hexane.

Ring saturation starts with the syn-addition of hydrogen across the C=C bond of DMF adsorbed on the surface of the catalyst to form a dihydro intermediate that contributes to the production of tetrahydrofuran species (*cis* and *trans* isomers). 2,5-Dimethyldihydrofuran is only noticed when the catalyst used is selective to ring saturation and produces high yields of DMTHF. 2,5-Hexanedione production is typically limited to 1% and is suggested to be produced either by oxidative ring opening of DMF, followed by hydrogenation to HD⁵³ due to the existence of very small amounts of air that contain O₂ during the reaction after purging, or by hydrolysis as suggested by Li *et al.*⁵⁴ due to limited amounts of H₂O from moisture in the atmosphere. The C-O bond cleavage occurs as a result of an aromatic furan ring opening, which produces ring-opened intermediates that are responsible for the production of both 2-HXL and 2-HXN in parallel. 2-Hexanol is also produced as a secondary product through hydrogenation of 2-HXN. Experimental evidence that ring-opened products are not produced from hydrogenated furans but are produced directly from DMF can be found elsewhere.^{15,33,55} Furthermore, theoretical DFT studies proved that ring opening becomes a simple matter upon the hydrogenation of the α -carbon of furan.^{56,57} *N*-Hexane (HX) is produced through the dehydration reaction of HXL to produce 1-hexene, which is further hydrogenated on the metal site of the catalyst to *n*-hexane.

Influence of the active metal

In the first set of experiments, we wanted to find the most suitable metal for the selective production of 2-HXL from DMF. Based on previous studies, we focused on carbon as a support material^{15,16} and *n*-decane as an inert hydrocarbon carrier liquid. We used mild reaction conditions of 80 °C and 10 bar hydrogen pressure to be able to use hydrogen directly from an electrolyzer without any pre-treatment. Equal amounts of noble metal (2 mg) were used in each experiment to allow a direct comparison of the different

catalysts. Mass balances for all experiments using the applied analytical methods were 95 % or higher. Table 1 presents the catalyst's metal site screening study showing that only Pt/C is selective for the desired furan ring opening reaction under the reaction conditions that were applied, achieving a 2-HXL yield of 50% (entry 1) after 3 h reaction time at full DMF conversion. On the other hand, Ru/C (Y = 84%) and Pd/C (Y = 47%) are very selective to hydrogenate DMF to the ring-closed product, DMTHF (entries 2 and 3). Re does not seem to be active for ring saturation or ring opening under the applied reaction conditions (entry 4). We can see a significant influence of Pd from the results in entry 3, leading to 47% DMF conversion, whereas pure Re (entry 4) did not show any DMF conversion at all. It has also been published elsewhere that Pd is selective to DMTHF formation using similar conditions.¹⁵ The Ru selectivity towards DMTHF was also confirmed by Gilkey *et al.*¹⁶ The Pt selectivity to ring opening is related to the adsorption configuration of DMF on the surface of the metal site in the catalyst. Generally, furans including furan, MF and DMF were found to bind parallel to noble metal surfaces. The preferred configuration for adsorption on most metals is π_{cc} . However, on Pt, the preferred adsorption configuration is σ_{cc} .⁵⁸ This difference in adsorption configuration explains why Pt is selective to the desired ring-opening reaction. Based on these results, we chose Pt as an active metal for further investigation.

Influence of the carrier liquid

To further increase the amount of 2-HXL using the most selective 5 wt% Pt/C catalyst for ring opening, we investigated the influence of the carrier liquid on the hydrogenation of DMF. The carrier liquid has to fulfill four requirements: (i) it should be liquid at room temperature for recycling purposes (e.g., pumping); (ii) it should absorb the released heat in a very efficient manner without evaporating under reaction conditions; (iii) it should dissolve the maximum amount of hydrogen to overcome mass transport limitations, and (iv) it should be stable under a reductive atmosphere up to 100 °C.

Table 1. 2,5-Dimethylfuran conversion and product yields for different active metals supported on carbon.

Entry	Catalyst	Conv. (%)	Yield (%)					Carbon balance (%)
			2-HXL	2-HXN	DMTHF	DMDHF	HX	
1	5% Pt/C	100	49.7	30.6	14.3	0	0.7	95.4
2	5% Ru/C	100	5.3	2.9	83.7	5.6	0.5	98.0
3	5% Re+Pd/C	47.0	0	0	45.8	0	0	98.8
4	5% Re/C	0	0	0	0	0	0	100

Reaction conditions: 0.001 mol DMF, 10.0 mL *n*-decane as a solvent, 5% metal/C (0.04 g) – 2 mg metal, 80 °C, 10 bar H₂, 770 rpm, 3 h.

Henry's constants for hydrogen depend on the chemical nature of the carrier liquid used in the following order: $H_{\text{diols}} > H_{\text{alcohols}} > H_{\text{esters}} > H_{\text{aldehydes}} > H_{\text{ethers}} > H_{\text{alkanes}}$.⁵⁹ Alkanes therefore have the lowest Henry's constants, meaning they have the highest hydrogen solubility. Alkanes with medium carbon chain length (C8-C16) fulfill all of the requirements mentioned above and were subsequently tested for DMF hydrogenation. However, the diffusion coefficient of hydrogen in alkanes decreases with increasing chain length due to the inverse relationship between the diffusion coefficient of the gas and the viscosity of the liquid. We varied the carbon chain length of our carrier liquid from octane to hexadecane to find the best performing carrier liquid. Table 2 presents the product yields in different alkanes used as liquid carriers. As presented in entries (1–3), increasing the alkane chain from *n*-octane to *n*-decane reduced the yield of undesired DMTHF from 19.6 to 14.3 mol% and increased the yield of the desired 2-HXL from 42.3% to 49.7%. This is attributed to the increasing hydrogen solubility in the alkane solvent with increasing carbon chain length. However, using very high molecular weight alkanes like *n*-hexadecane (entry 4) led to lower DMF conversion (79%) within the applied reaction time of 3 h coupled with a lower HXL yield of only 6%. This can be explained in terms of the reduced hydrogen diffusion of hydrogen in hexadecane due to its higher viscosity. Furthermore, the selectivity towards the ring-opened intermediate HXN was drastically increased to 77.3%. *n*-Decane was therefore chosen as most promising carrier liquid in order to minimize side product formation (lowest DMTHF yield at full DMF conversion) and to maximize ketone (2-HXN) to alcohol (2-HXL) transformation at the same time.

Screening various POM structures for their catalytic activity

The purpose of this study was to increase the alcohol yield further by using suitable POM catalysts for selective DMF hydrogenation to 2-HXL under mild reaction conditions

using *n*-decane as a carrier liquid. We therefore tested different Pt-substituted POMs in their initial form and after reduction in a hydrogen atmosphere (see Table S1 in Appendix S1 in the supplementary material for details) for their ability to act as heterogeneous catalysts for DMF hydrogenation in our slurry system. However, no significant DMF conversion could be achieved under the applied reaction conditions. Consequently, we turned to use Pt-free POMs in combination with a Pt-precursor to generate a bi-functional catalyst, which might have a significant selective DMF hydrogenation effect. Pt(acac)₂ was chosen as a promising Pt precursor due to its ability to form Pt/POM materials with high Pt dispersion.⁴⁹ To allow for a better comparison and to prove the beneficial effect of the POM structures in combination with Pt(acac)₂, we exclusively used K salts of all POM structures tested together with a constant amount of Pt (2 mg) using Pt(acac)₂. Interestingly, none of the tested pre-reduced Pt precursors (Pt(acac)₂, H₂PtCl₆ and H₂Pt(OH)₆) without the addition of POMs showed any catalytic activity for DMF hydrogenation under the applied reaction conditions (see Table S2 in Appendix S1). Furthermore, Table 3 shows that only the pre-reduced compounds obtained after combination of Pt(acac)₂ with strongly acidic potassium salts of Keggin- or WD-type POMs (entries 1 and 2) achieved significant DMF conversion (up to 95%) and ring opening to 2-HXL (up to 47%). However, the most active Pt/K₃[PW₁₂O₄₀] (entry 1) also gave a large amount (24% yield) of DMTHF via ring-saturation hydrogenation. Moreover, both active species showed high amounts of the intermediate ketone (2-HXN) on the way to 2-HXL, suggesting that the second hydrogenation step from 2-HXN to 2-HXL might be rate-determining. Pt/K₆[α-P₂W₁₈O₆₂] (entry 2) showed a high selectivity to 2-HXN formation (56%), so a combination of this catalyst and *n*-hexadecane as carrier liquid might be useful in the selective production of ketones. We also observed that the amount of *n*-hexane produced is higher in both cases in comparison with using carbon as a support (see Table 1, entry 1). This might be related to the higher Brønsted acidity of the POMs, which enhances

Table 2. 2,5-Dimethylfuran conversion and product yields for different carrier liquids.

Entry	Carrier liquid	Conv. (%)	Yield (%)					Carbon balance (%)
			2-HXL	2-HXN	DMTHF	DMDHF	HX	
1	<i>n</i> -octane	99.5	42.3	33.3	19.6	0.6	0.7	97.0
2	<i>n</i> -nonane	98.8	47.9	26.9	18.0	0.5	0.9	95.4
3	<i>n</i> -decane	100	49.7	30.6	14.3	0	0.7	95.4
4	<i>n</i> -hexadecane	78.9	6.3	61.1	6.9	0	0.4	95.7

Reaction conditions: 0.001 mol DMF, 10.0 mL alkane as a solvent, 5% Pt/C (0.04 g) – 2 mg metal, 80 °C, 10 bar H₂, 770 rpm, 3 h.

Table 3. 2,5-Dimethylfuran conversion and product yields for different Pt/POM combinations.

Entry	Catalyst ^a	Conv. (%)	Yield (%)					Carbon balance (%)
			2-HXL	2-HXN	DMTHF	HD	HX	
1	Pt/K ₃ [PW ₁₂ O ₄₀]	94.3	46.5	20.1	23.7	0	4.7	100
2	Pt/K ₆ [α-P ₂ W ₁₈ O ₆₂]	95.2	17	56.4	14.0	0.6	3.6	96.5
3	Pt/K ₁₄ [NaP ₅ W ₃₀ O ₁₁₀]	9.3	0.9	3.3	1.2	1.1	0.3	97.4
4	Pt/K ₆ [HSiW ₉ V ₃ O ₄₀]	5.0	0.7	0.3	0.9	1.1	2.4	100
5	Pt/K ₈ [HP ₂ W ₁₅ V ₃ O ₆₂]	5.2	0	0.4	0.5	1.3	0.3	97.5
6	Pt/K ₅ [V ₃ W ₃ O ₁₉]	4.2	0	0.3	0.5	1.4	0.2	98.4
7	Pt/K ₇ [α-PW ₁₁ O ₃₉]	1.8	0	0.3	0.4	1.5	0	100
8	K ₃ [PW ₁₂ O ₄₀]	0	0	0	0	0	0	100

^aPt (acac)₂ was used as platinum precursor for all experiments. Reaction conditions: 0.001 mol DMF, 10.0 mL decane as a solvent, 5% metal/cat – 2 mg Pt, 80 °C, 10 bar H₂, 770 rpm, 3 h.

Table 4. 2,5-Dimethylfuran conversion and product yields of different Pt/Keggin-type POM catalytic systems.

Entry	Catalyst ^a	Conv. (%)	Yield (%)					Carbon balance (%)
			2-HXL	2-HXN	DMTHF	HD	HX	
1	Pt/Cs _{2.5} H _{0.5} [PW ₁₂ O ₄₀]	100	54.5	1.0	36.1	0	8.0	100
2	Pt/K ₃ [PW ₁₂ O ₄₀]	94.3	46.5	20.1	23.7	0	4.7	100
3	Pt/H ₃ [PW ₁₂ O ₄₀]	99.5	50.2	1.5	29.4	0	11.8	93.7
4	Pt/H ₄ [SiW ₁₂ O ₄₀]	45.2	14.0	4.6	18.6	0.3	8.0	100
5	Pt/H ₃ [PMo ₁₂ O ₄₀]	3.2	0	0.3	0.5	1.1	0	98.9
6	Pt/Cu _{1.5} [PW ₁₂ O ₄₀]	6.7	0	0.4	2.3	3.0	0.3	99.2

^aPt (acac)₂ was used as platinum precursor for all experiments. Reaction conditions: 0.001 mol DMF, 10.0 mL decane as a solvent, 5% metal/cat – 2 mg Pt, 80 °C, 10 bar H₂, 770 rpm, 3 h.

the dehydration reaction of alcohols to alkenes followed by hydrogenation of the latter to alkanes. A quick glance at entry 5 shows that replacing some tungsten atoms with vanadium in the WD-type phosphotungstate has a negative effect on the activity of the catalyst. This can be illustrated by a lowered Brønsted acidity and reduction potential of the POM, as the vanadium reduces the acidity of the POM and decreases the reduction potential so the POM becomes less active.^{60,61} Moreover, using the K₃[PW₁₂O₄₀] POM alone as a catalyst (entry 8) did not give any conversion confirming Pt as the active species and the POM as a promotor. As a higher acidity of the POM might be the main reason for a higher catalytic activity of the Pt/K₃[PW₁₂O₄₀] catalyst in DMF hydrogenation to 2-HXL, we tried to optimize the POM compound accordingly.

Optimization of the Keggin-type POM component of the catalyst

Based on the results mentioned above, we tried to increase the acidity of the Keggin-type POMs further. We used

three different heteropolyacids with Keggin-type structure (Table 4, entries 3–5). We could clearly demonstrate that the phosphotungstic acid (entry 3) by far showed the best performance, achieving a 2-HXL yield of 50%. However, this was only slightly higher than that achieved with the K salt of the same heteropolyanion (Table 4, entry 2). Moreover, the Pt/H₃[PW₁₂O₄₀] showed a higher tendency for ring saturation hydrogenation leading to a larger amount (29%) of DMTHF as well as greater hexane formation (12%). Substituting P with Si in the heteropolyacid led to a drastically decreased performance (entry 4) with only 45% DMF conversion and with nearly unchanged selectivity. Using the phosphomolybdate as heteropolyanion (entry 5) again drastically decreased the performance to a conversion of only 3% because the phosphomolybdate lost its Keggin-structure during the reduction of the catalyst as illustrated (see Fig. S1 in the supporting information, Appendix S1), whereas the Pt/H₃[PW₁₂O₄₀] kept its structure during the reduction and after the reaction as show in Fig. S2 in Appendix S1. The reason for phosphotungstic acid being the most active Keggin-type structure is its highest acid

strength⁵⁴ (the ammonia desorption temperatures are indicated in degree C), which decreases in the following order: $H_3[PW_{12}O_{40}] > H_4[SiW_{12}O_{40}] > H_3[PMo_{12}O_{40}] > H_4[SiMo_{12}O_{40}] = 592 > 532 > 463 > 423$. Another important factor that plays a role is the higher reduction potential of the POM. Generally, as the valance of the central atom increases, or as the charge of the polyanion decreases, the reduction potential of the POM increases.⁶¹ The Pt/ $H_3[PW_{12}O_{40}]$ therefore showed higher reduction potential than Pt/ $H_4[SiW_{12}O_{40}]$.

Manipulating the content of the counter-cations in the $M_{3-y}H_y[PW_{12}O_{40}] \cdot xH_2O$ ($M = Cs^+$, $y = 0.5$; $M = Cu^{2+}$, $y = 0$) compounds led to the observation that the acidic Cs salt of the Keggin-type tungstophosphate (Table 4, entry 1) showed the highest conversion and tendency towards the formation of the desired product (2-HXL, 54%) compared with the heteropolyacids and the K and Cu salts. At the same time, like the Pt/ $H_3[PW_{12}O_{40}]$, the use of the Cs salt as the catalyst led to the generation of significant amounts of DMTHF (36%) and hexane (8%). We therefore focused on the K salt Pt/ $K_3[PW_{12}O_{40}]$ for further investigation as it showed the highest selectivity for the desired 2-HXL at lower DMTHF yield. Cs- (160 m²/g) and K salts (66 m²/g) of the Keggin-type phosphotungstates provide a larger surface area for Pt compared to the Cu salt (5 m²/g) being responsible for the higher catalytic activity.

Further improvement of the most selective Pt/ $K_3[PW_{12}O_{40}]$ catalyst

As was shown above, the Pt/ $K_3[PW_{12}O_{40}]$ catalyst (Table 3, entry 1) achieved the highest selectivity towards the formation of 2-HXL; however, further improvement of the solid two-component system seems possible. According to the literature, several modifications in the synthesis of the

Pt/POM catalyst or of the used POM structure may lead to structural changes in the resulting Pt/POM system, which, in turn, can cause the enhancement of its desired catalytic performance.⁴⁹ To test the effect of the POM synthetic procedure on the catalytic activity and selectivity of the resulting Pt/POM system, we used KCl instead of $KHCO_3$ as a source of the potassium ions during the preparation of $K_3[PW_{12}O_{40}]$. The use of KCl positively affects DMF conversion (100%), productivity (2-HXL, 57.8%) and selectivity (2-HXN, 16.3% and DMTHF, 19.4%) of the resulting Pt/ $K_3[PW_{12}O_{40}]$ catalytic system (Table 5, entry 3) in comparison with the catalyst obtained using $KHCO_3$ (Table 3, entry 1).

Another preparation parameter that may influence the catalytic activity is the solvent, which is used during wet merging of the Pt precursor with the POM species. Thus, for further improvement of the Pt/ $K_3[PW_{12}O_{40}]$ catalytic system we examined water versus acetone as the medium for the dispersion of $K_3[PW_{12}O_{40}]$ before mixing the resulting POM suspension with the Pt(acac)₂ acetone solution. According to the results (Table 5, entry 1) the use of water instead of acetone significantly improves the Pt/ $K_3[PW_{12}O_{40}]$ catalytic performance (2-HXL, 72.5%) due to the higher dispersion of Pt on the POM surface. The catalytic experiments were performed for two batches of the latter catalyst (Table 5, entry 2) to show the reproducibility of the results.

The influence of various Pt-sources on the activity of the resulting catalytic system was also tested. H_2PtCl_6 and $H\{Pt(NH_3)_4\}[PW_{11}O_{39}\{Pt(NH_3)_4\}_2]$ (see the supporting information for details) were chosen as alternative Pt sources to Pt(acac)₂ (see Table 5, entries 1–3). $H\{Pt(NH_3)_4\}[PW_{11}O_{39}\{Pt(NH_3)_4\}_2]$ was chosen as a promising Pt-POM precatalyst, as the studies mentioned above showed the ability of its reduced form to convert DMF to 2-HXL (2-HXL, 0.8%, Table S1, Appendix S1). However, the

Table 5. 2,5-Dimethylfuran conversion and product yields of the Pt/ $K_3[PW_{12}O_{40}]$ catalytic systems obtained by various synthetic methods.

Entry	Catalyst	Conv. (%)	Yield (%)					Carbon balance (%)
			2-HXL	2-HXN	DMTHF	HD	HX	
1	Pt/ $K_3[PW_{12}O_{40}]^a$	100	72.5	1.7	20.9	0	5.6	100
2	Pt/ $K_3[PW_{12}O_{40}]^a$	100	69	3.3	20.5	0	6.6	99.5
3	Pt/ $K_3[PW_{12}O_{40}]^b$	100	57.8	16.3	19.4	0	5.6	99
4	$H_2PtCl_6/K_3[PW_{12}O_{40}]$	100	32.1	38.4	24.5	0	6.2	100
5	$H\{Pt(NH_3)_4\}[PW_{11}O_{39}\{Pt(NH_3)_4\}_2]/K_3[PW_{12}O_{40}]$	57.6	17.3	20.9	17.2	0	5.0	100

^aKCl/water;

^bKCl/acetone.

Reaction conditions: 0.001 mol DMF, 10.0 mL decane as a solvent, 5% metal/cat – 2 mg Pt, 80 °C, 10 bar H₂, 770 rpm, 3 h.

results (Table 5, entries 4 and 5) confirmed Pt(acac)₂ as the most effective Pt precursor for selective ring opening to 2-HXL (Table 5, entry 1). A similar observation was reported by Alharbi *et al.*⁴⁹ using Pt(acac)₂ as a Pt source, showing much higher dispersion of Pt on the support than using H₂PtCl₆.

Performance comparison for the Pt/K₃PW₁₂O₄₀ catalyst with the commercial Pt/C catalyst for different substrates

After choosing the best performing Pt/POM catalyst (Pt/K₃[PW₁₂O₄₀]) from our previous investigations, we used different furanic substrates to compare the catalytic performance with the commercial (Pt/C) catalyst (see Table 6). First, full substrate conversion was achieved in each catalytic experiment. Using 2-methylfuran (MF) as a substrate lead to a mixture of 1-pentanol and 2-pentanol with 44.3% yield as alcoholic products using the Pt/POM catalyst whereby only 26.4% yield were achieved using the Pt/C catalyst. Furan hydrogenation with Pt/K₃PW₁₂O₄₀ gave product yields for 1-butanol of 59.7%, 17.5% tetrahydrofuran (THF) and 5.2% butane, detected in the liquid phase as well as traces (0.7%) of propane in the gas phase. Due to the low carbon balance we received from gas chromatography (GC) in case of furan, we also analyzed the liquid products with NMR, but no other products other than butanol and THF could be found (see Fig. S3 in Appendix S1). As a result, the low mass balance reported could be due to the low boiling point of the reactant furan (31 °C), which could be lost during the experiment preparation, pressure test, or purging with nitrogen. An optimization for the temperature, pressure, and stirrer speed may be beneficial for maximizing the alcohol yield for the two other furan substrates. However, it is thought that increasing the temperature by more than 80 °C will increase the selectivity to alkane production.

Characterization of the Pt/K₃PW₁₂O₄₀ and the commercial Pt/C catalyst

Various analytic techniques were used to try to explain the observed differences in performance of the different supported Pt catalysts. The characteristics of both catalysts were compared by using CO chemisorption for determination of Pt dispersion and Pt particle diameter. Moreover, N₂ physisorption was used for determining the total surface area and pore diameter, and the average pore volume of each catalyst. Transmission electron microscopy (TEM) was used to prove that Pt nanoparticles are well dispersed and uniformly distributed on the support surface without cluster formation, suggesting a good access of substrate to the active centers and good thermal stability. Furthermore, we have measured X-ray diffraction patterns in order to see the different crystal phases. Finally, we measured NH₃-TPD in order to quantify the surface acidity of the catalysts.

In Table 7, the textural properties determined by N₂-physisorption as well as the influence of the surface acidity measured by temperature-programmed desorption (TPD) using NH₃ of the commercial Pt/C catalyst is compared with the Pt/K₃[PW₁₂O₄₀] catalyst. The Pt/C shows a higher surface area (1284 versus 66 m²/g) together with a higher pore volume (0.37 versus 0.10 cm³/g) and a smaller pore diameter (36.8 versus 60.0 Å compared to the Pt/K₃[PW₁₂O₄₀] catalyst. We therefore conclude that no direct relationship between the textural properties and the catalytic performance can be given.

To examine if the acidity of the POM-support played an important role regarding the hydrogenation activity, the acidity of the prepared Pt/K₃[PW₁₂O₄₀] as well as the Pt/C catalyst was measured using NH₃-TPD and the results are included in Table 7. The POM-supported Pt catalyst showed a far higher number of acid sites whereas the Pt/C catalyst seems to be non-acidic as the results of TPD NH₃ suggest. The moderate total density of acid sites of K₃[PW₁₂O₄₀] was reported before by Soares.⁶² The role of the support K₃[PW₁₂O₄₀] as an acid site is to enhance

Table 6. Conversion and product yields for different furanic substrates.

Entry	Substrate	Catalyst	Conv. (%)	Yield (%)				Carbon balance (%)
				Alcohol	Ketone	Hydrogenated furan	Alkane	
1	DMF	Pt/K ₃ [PW ₁₂ O ₄₀]	100	72.5	1.7	20.9	5.6	100
2	MF	Pt/K ₃ [PW ₁₂ O ₄₀]	100	44.3	4.9	36.8	4.9	91
3	Furan	Pt/K ₃ [PW ₁₂ O ₄₀]	100	59.7	0	17.6	5.2	82.2
4	DMF	Pt/C	100	46.3	34.1	14.9	1	96.7
5	MF	Pt/C	100	26.4	18.9	41.1	0.4	87.2
6	Furan	Pt/C	100	25.5	0	49.6	-	75

Reaction conditions: 0.001 mol reactant, 10.0 mL decane as a solvent, 5% metal/cat – 2 mg Pt, 80 °C, 10 bar H₂, 770 rpm, 3 h.

Table 7. Textural properties and NH₃-TPD results of the different Pt catalysts.

Catalyst	BET surface area [m ² /g]	Pore vol. [cm ³ /g]	Av. pore diameter Å	Ads. NH ₃ [mmol/g]
5 wt% Pt/C	1284	0.37	36.8	0.05
5% Pt/ K ₃ [PW ₁₂ O ₄₀]	66	0.10	60.0	0.65

BET: (Brunauer, Emmett and Teller) specific surface.

C=O hydrogenation and overcome the rate-limiting step of 2-hexanone hydrogenation to 2-hexanol. The existence of Lewis acid sites in the support plays a major role in activating the C=O bond, where a charge transfer interaction between the oxygen atom in the carbonyl group and the cationic sites in the support creates a negative charge localized around carbonyl C, activating the latter for hydrogenation. Similar behavior was also observed for a selective hydrogenation of furfuraldehyde to furfuryl alcohol over Pt/TiO₂.⁶³

We also investigated the Pt content, the Pt dispersion and the Pt particle diameter by using inductively coupled plasma optical emission spectroscopy (ICP-OES) and CO chemisorption, respectively. Again, no explanation besides the different support acidity for the higher activity of the Pt/K₃[PW₁₂O₄₀] could be found, as the Pt/C catalyst showed higher Pt dispersion and a lower Pt particle diameter at the same Pt content (see Table 8).

Figure 1 shows representative TEM images of both the Pt/C catalyst (Fig. 1(a)) and the Pt/K₃[PW₁₂O₄₀] (Fig. 1(b)). In both catalysts, the Pt nanoparticles (small black dots) were well dispersed and uniformly distributed on the support surface without cluster formation, suggesting a good access of substrate to the active centers.

Figure 2 shows the X-ray diffraction (XRD) patterns of K₃[PW₁₂O₄₀] before Pt impregnation (blue), after Pt impregnation (red) and the commercial catalyst Pt/C (green). The Pt/C catalyst is amorphous while the Pt/K₃[PW₁₂O₄₀] is in a crystalline structure (cubic crystal lattice structure).⁶¹ The Pt in both cases did not show any obvious sharp peaks, which means it is finely dispersed on the support material as presented in the TEM images. All the sharp peaks in Pt/K₃[PW₁₂O₄₀] pattern belong to the K-POM salt structure. The diffractogram of K₃[PW₁₂O₄₀] did not show any evidence of phase segregation (i.e., presence of another phase of pure heteropolyacids) and is in agreement with literature.^{61,62}

Conclusion

Different bi-functional catalyst systems composed of Pt(acac)₂ as Pt precursor and Keggin as well as Wells–Dawson-type polyoxometalates (POMs) as acidic

Table 8. Elementary analysis and CO-chemisorption results of the 5% Pt/C and 5% Pt/K₃[PW₁₂O₄₀] catalysts.

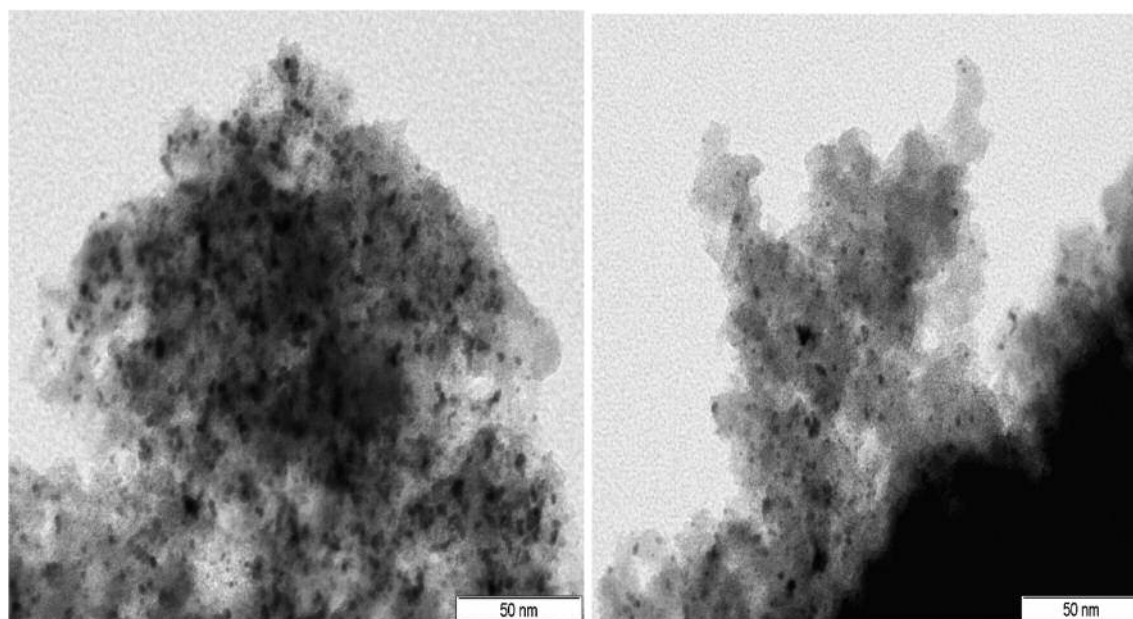
Catalyst	Pt content [wt%]	Pt dispersion, [%]	Pt particle diameter, [nm]
5 wt% Pt/C	4.6	42.4	2.7
5% Pt/ K ₃ [PW ₁₂ O ₄₀]	4.5	6.2	17.8

supports were prepared, characterized by ICP-OES, Fourier transform infrared spectroscopy (FTIR), and N₂-physisorption and successfully applied for the selective catalytic hydrogenation of 2,5 dimethylfuran (DMF) to 2-hexanol under mild reaction conditions of 80 °C and 10 bar H₂ using *n*-decane as a carrier liquid. The Keggin-type POM catalyst Pt/K₃[PW₁₂O₄₀] gave the highest yields of up to 72.5% 2-hexanol. Characterization of the Pt/POM and the Pt/C catalyst revealed several structural differences whereby the higher surface acidity of the POM support increases the catalytic performance. Interestingly, the Wells–Dawson type-POM catalyst Pt/K₆[α-P₂W₁₈O₆₂] was shown to be selective for 2-hexanone formation under identical reaction conditions. Moreover, modifications in the preparation procedure of the most selective Keggin-type Pt/K₃[PW₁₂O₄₀] POM-catalyst resulted in significantly higher yield of 2-hexanol (72.5%) compared with the commercial Pt/C catalyst (49%) at the same Pt loading. Finally, two other furanic compounds (2-methylfuran and furan) were also successfully hydrogenated to the corresponding alcohols (1-butanol (59.7% yield) and 1/2-pentanol (44.3% yield), respectively, under the same reaction conditions. This demonstrates the enhanced activity of the bi-functional catalyst system Pt/K₃[PW₁₂O₄₀] towards selective ring opening of furans in the liquid phase using mild reaction conditions.

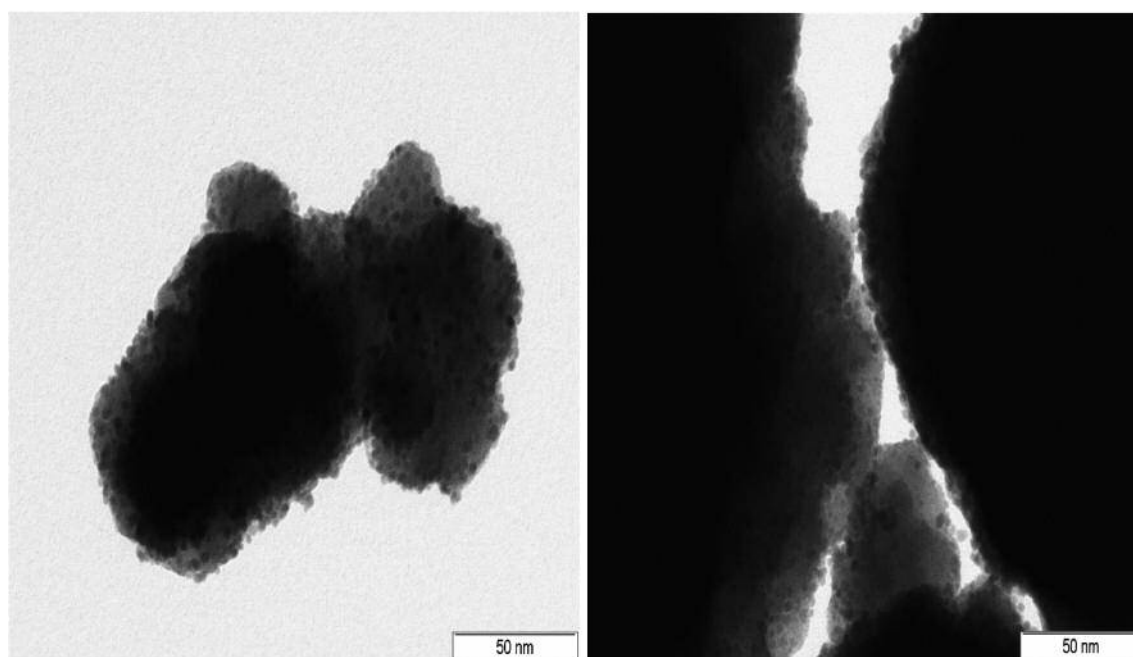
Experimental details

Materials

The following chemicals were commercially available (Sigma Aldrich, Munich, Germany) and used without further purification: 2,5-dimethylfuran (99% purity), 2-methylfuran (99 + % purity), furan (99% purity) as substrates, octane (99 + % purity), nonane (99 + % purity), decane (99 + % purity), hexadecane (99 + % purity) as carrier liquids, 5 wt% Pt/C, 5 wt% Ru/C, 5 wt% Pd + Re/C, 5 wt% Re/C as commercial reference catalysts, as well as H₂ (5.0) and N₂ (5.0) from Linde, Hamburg, Germany,



(A) TEM for Pt/C.

(B) TEM for Pt/K₃[PW₁₂O₄₀].Figure 1. (a) Transmission electron microscopy for Pt/C. (b) TEM for Pt/K₃[PW₁₂O₄₀].

AG as gases. Pt(acac)₂, H₂PtCl₆, H₄[SiW₁₂O₄₀] \cdot xH₂O as well as H₃[PW₁₂O₄₀] \cdot xH₂O were also purchased from a commercial supplier (Alfa Aesar, Kandel, Germany). H₃[PMo₁₂O₄₀] \cdot xH₂O,⁶⁴ H₂Pt(OH)₆ \cdot xH₂O,⁶⁵ K₆[α -P₂W₁₈O₆₂] \cdot 14H₂O,⁶⁶ K₁₄[NaP₅W₃₀O₁₁₀] \cdot 15H₂O,⁶⁶ K₇[α -PW₁₁O₃₉] \cdot 14H₂O,⁶⁷ K₈H[P₂W₁₅V₃O₆₂] \cdot 10H₂O⁶⁸ and K₆

[HSiW₉V₃O₄₀] \cdot 3H₂O⁶⁸ were synthesized according to procedures described in the literature. K₅[V₃W₃O₁₉], Cs_{2.5}H_{0.5}[PW₁₂O₄₀] and Cu_{1.5}[PW₁₂O₄₀] were obtained using slightly modified reported procedures (for details see 'Synthesis and characterization of the Pt-free POMs' in the supporting information).

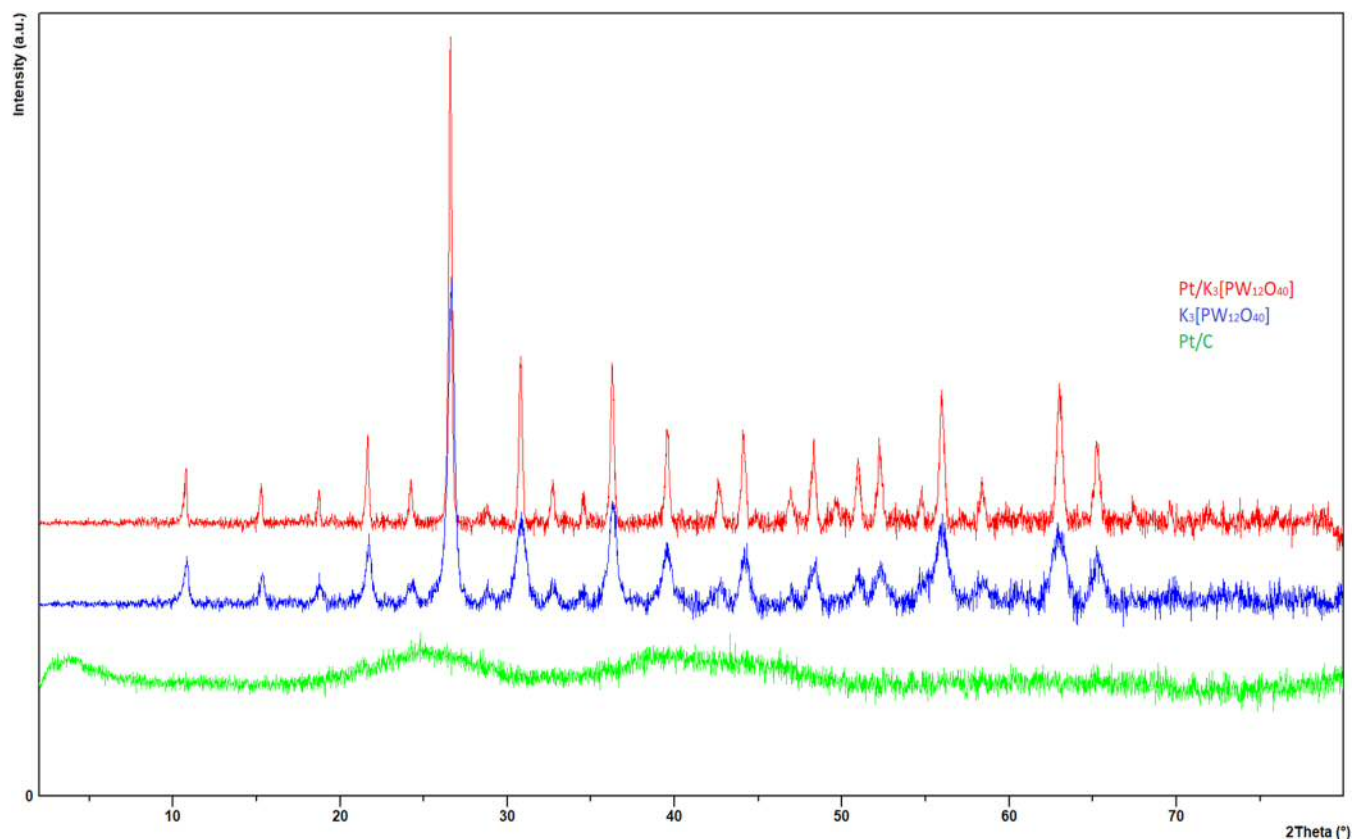


Figure 2. X-ray diffraction patterns of $K_3[PW_{12}O_{40}]$ in blue, $Pt/K_3[PW_{12}O_{40}]$ in red and Pt/C in green.

Catalyst synthesis

$Pt/Cs_{2.5}H_{0.5}[PW_{12}O_{40}]$ (5% Pt)

$Cs_{2.5}H_{0.5}[PW_{12}O_{40}]$ (0.148 g) was dispersed in 1 mL of acetone (Solution I) and $Pt(acac)_2$ (0.015 g) was dissolved in 2.5 mL of acetone (Solution II). Solution II was added dropwise to Solution I under vigorous stirring. The mixture obtained was stirred at room temperature for 1 h. After that the acetone was evaporated. The resulting precipitate was reduced in an oven with 10% H_2 flow (50 mL/min H_2 and 450 mL/min N_2) at 250 °C for 2 h.

Fourier transform infrared spectroscopy (cm^{-1}): 1621 (w), 1077 (s), 983 (s), 889 (s), 806 (br), 596 (m), 524 (s), 483 (w).

$Pt/K_6[\alpha-P_2W_{18}O_{62}]$, $Pt/K_{14}[NaP_5W_{30}O_{110}]$, $Pt/K_6[HSiW_9V_3O_{40}]$, $Pt/K_8H[P_2W_{15}V_3O_{62}]$, $Pt/K_5[V_3W_3O_{19}]$, $Pt/K_7[\alpha-PW_{11}O_{39}]$, $Pt/H_3[PW_{12}O_{40}]$, $Pt/H_4[SiW_{12}O_{40}]$, $Pt/H_3[PMo_{12}O_{40}]$ and $Pt/Cu_{1.5}[PW_{12}O_{40}]$

The catalysts were synthesized using the same procedure as for the $Pt/Cs_{2.5}H_{0.5}[PW_{12}O_{40}]$; however, instead of $Cs_{2.5}H_{0.5}[PW_{12}O_{40}]$ the corresponding POM compound was used.

Optimized synthetic procedure for the preparation of $Pt/K_3[PW_{12}O_{40}]$

$K_3[PW_{12}O_{40}] \cdot 10H_2O$ (abbreviated as $K_3[PW_{12}O_{40}]$)

KCl (0.357 g) was dissolved in 47.5 mL H_2O (Solution I). $H_3PW_{12}O_{40} \cdot xH_2O$ (4.6 g) was dissolved in 20 mL H_2O (Solution II). Solution I was added dropwise to the Solution II under vigorous stirring at 40 °C. The resulting suspension was further stirred for 1 h at 40 °C. Thereafter, the mixture obtained was kept undisturbed at room temperature for 24 h. After that, the upper aqueous phase was decanted. The resulting white precipitate was dried on air at room temperature. Yield: 4.2 g (91.3% based on W).

Fourier transform infrared spectroscopy (cm^{-1}): 3439 (br), 2360 (w), 1985 (w), 1621 (m), 1080 (s), 987 (s), 891 (s), 815 (br), 595 (m), 526 (s), 481 (w), 426 (w).

$Pt/K_3[PW_{12}O_{40}]$

$K_3[PW_{12}O_{40}]$ (1.425 g) was stirred in 10 mL of H_2O for 1 h at 40 °C (Suspension I). The solution of $Pt(acac)_2$ (0.151 g) in

25 mL of acetone (Solution II) was then added dropwise to Suspension I under vigorous stirring. The mixture obtained was stirred at 40 °C for 1 h in a closed vial. After that, the vial was opened and the mixture was kept under vigorous stirring at 40 °C until the volume was ~20 mL. The final suspension was dried with air. The resulting precipitate was reduced in an oven with 10% H₂ flow (50 mL/min H₂ and 450 mL/min N₂) at 250 °C for 2 h.

Elemental analysis (%) found: Pt 4.5, W 64.8, P 0.7, K 3.1, C 0.1, H 0.6.

Fourier transform infrared spectroscopy (cm⁻¹): 3464 (br), 2919 (w), 2354 (w), 1977 (w), 1613 (m), 1445 (w), 1386 (w), 1080 (s), 983 (s), 891 (s), 813 (br), 596 (m), 526 (s), 482 (w), 427 (w).

H₂PtCl₆/K₃[PW₁₂O₄₀]

K₃[PW₁₂O₄₀] (0.143 g) was stirred in 1 mL of H₂O for 1 h at 40 °C (Suspension I). Thereafter, the solution of H₂PtCl₆ (0.015 g) in 1 mL of H₂O (Solution II) was added dropwise to Suspension I under vigorous stirring. The mixture obtained was stirred at 40 °C for 1 h in a closed vial. After that, the vial was opened and the mixture was kept under vigorous stirring at room temperature for 6 h. The final suspension was dried with air. The resulting precipitate was reduced in an oven with 10% H₂ flow (50 mL/min H₂ and 450 mL/min N₂) at 250 °C for 2 h.

H{Pt(NH₃)₄}[PW₁₁O₃₉{Pt(NH₃)₄}₂]/K₃[PW₁₂O₄₀]

K₃[PW₁₂O₄₀] (0.143 g) was stirred in 1 mL of H₂O for 1 h at 40 °C (Suspension I). Thereafter, the suspension of H{Pt(NH₃)₄}[PW₁₁O₃₉{Pt(NH₃)₄}₂] (0.435 g) in 20 mL of H₂O (Suspension II) was added dropwise to Suspension I under vigorous stirring. The mixture obtained was stirred at 40 °C for 1 h in a closed vial. After that, the vial was opened and the mixture was kept under vigorous stirring at 40 °C until the volume was ~10 mL. The final suspension was dried with air. The resulting precipitate was reduced in an oven with 10% H₂ flow (50 mL/min H₂ and 450 mL/min N₂) at 250 °C for 2 h.

Elemental analysis (%) found: C 0.1, H 0.6, N 0.5.

Catalyst characterization techniques

Characterization of the synthesized catalysts has been carried out using different analytical techniques. Elemental analysis of the respective materials has been made using a *PerkinElmer Plasma 400* ICP-OES device (ICP). CHNS elemental analyses were performed on a UNICUBE analyzer.

The initial POM materials, Pt sources, and the resulting Pt/POM systems before and after catalytic reaction were

analyzed by FTIR spectroscopy at ambient conditions in KBr discs using a Jasco FT/IR-4100 spectrometer. The FTIR spectra were recorded with a resolution of 4 cm⁻¹ in the range between 4000 and 400 cm⁻¹. Thus, the changes in the POM structures after loading with Pt, reduction and catalytic reaction were controlled.

The Pt dispersion and an average Pt particle diameter of the Pt/C and Pt/K₃[PW₁₂O₄₀] catalysts were measured by CO-pulse-chemisorption on an Autochem II 2920 instrument from Micromeritics.

The specific surface area, pore volume and average pore diameter of the most active catalytic systems were determined by N₂-physisorption at 77 K on a Quantachrome instrument, model Quadrasorb SI. Before the measurement, the samples were outgassed in a vacuum at 523 K for 12 h.

The Pt/C and Pt/K₃[PW₁₂O₄₀] catalysts were characterized by XRD analyses performed in Empyrean diffractometer from PANalytical with a CuKα X-ray source operated at 40 kV and 40 mA. The data were collected over an angular 2θ range from 2° to 80° with a scan step time of 10.16 s and a step size of 0.0167°.

The TEM images were obtained by using a JEOL JEM 1011 Transmission Electron Microscope operated with a LaB6 filament with 100 kV accelerating voltage.

The NH₃-TPD measurements were carried out on a Micromeritics Autochem-II instrument.

Catalytic experiments

Hydrogenation reactions of different furanic compounds were carried out in a tenfold parallel reaction system in 21 mL stainless-steel (1.4571) high-pressure vessels equipped with magnetic stirring. For a typical reaction, alkane (10.0 mL) as a carrier liquid, catalyst (0.04 g, 2 mg active metal), and 0.001 mol of the substrate (0.1 g DMF, 0.082 g MF, 0.068 g furan) were charged into the reactor (the substrate to catalyst ratio was always kept constant at 100:1) and the system was purged with nitrogen gas (three times) to remove residual air before the hydrogen pressure was set to 10 bar. The stirrer speed was then adjusted to 330 rpm, because this is the speed of the rotating device (rounds per minute). When the desired reaction temperature (80 °C) was reached, the speed of the stirrer was adjusted to 770 rpm, because this is the speed of the rotating device. After the desired reaction time (3 h), the reactor was cooled down to room temperature and a gas-phase sample was collected from the reactor in a gas bag to be analyzed. Then the reactor was vented and purged with nitrogen gas (three times) before opening it. The catalyst was separated from the liquid phase by filtration and the liquid phase was analyzed by GC.

Product analysis

Gaseous samples were analyzed with a Varian GC 450-TCD-FID equipped with a Shin Carbon ST column (2 m × 0.75 mm internal diameter). The sample was injected using a gas bag and transported through the column with argon as the mobile phase at a pressure of 4.82 bar. The following temperature program was used for the column: 40 °C (1.5 min), 18 °C min⁻¹ to 250 °C, 250 °C (12 min). Analysis of the liquid phase was performed using a Varian CP-3900 gas chromatograph equipped with a flame ionization detector (FID). Product compounds were separated using a FactorFour capillary column (VF-WAXms, 30 m length, 0.25 mm diameter) coated with a 0.25 μm thick stationary phase with helium as a carrier gas. The following operating conditions were used: injection temperature of 250 °C, column temperature program: 40 °C (6 min), 10 °C min⁻¹ to 250 °C, 250 °C (2.5 min), detection temperature of 250 °C. Octane was used as external standard in all samples for liquid GC measurements except for the experiment in which octane was used as a carrier liquid and where decane was used as a standard. Substrate conversion and product yields were calculated as shown in Eqns (1) and (2). Mass balances were determined based on carbon balances of each reaction using both gas and liquid GC analysis.

$$\begin{aligned} \text{conversion (mol\%)} \\ &= \frac{\text{number of moles of substrate reacted}}{\text{number of moles of substrate loaded}} \times 100\% \end{aligned} \quad (1)$$

$$\begin{aligned} \text{yield (mol\%)} \\ &= \frac{\text{number of moles of product that actually formed}}{\text{maximum theoretical number of moles that can be produced}} \times 100\% \end{aligned} \quad (2)$$

Acknowledgements

M. Sh. acknowledges financial support from the Egyptian Ministry of Higher Education and Scientific Research (MHESR) and the German Academic Exchange Service (Deutscher Akademischer Austauschdienst, DAAD). J. A. and M. Sh. thank Patrick Schühle from Friedrich-Alexander-Universität Erlangen-Nürnberg (FAU) Erlangen-Nürnberg for performing NH₃-TPD measurements.

References

- Sutton AD, Waldie F, Wu R, Schlaf M, Silks L and Gordon J, The hydrodeoxygenation of bioderived furans into alkanes. *Nat Chem* **5**(5):428 (2013).
- Alonso DM, Bond JQ and Dumesic JA, Catalytic conversion of biomass to biofuels. *Green Chem* **12**(9):1493–1513 (2010).
- Zhang Y-HP, Reviving the carbohydrate economy via multi-product lignocellulose biorefineries. *J Ind Microbiol Biotechnol* **35**(5):367–375 (2008).
- Huber GW, Iborra S and Corma A, Synthesis of transportation fuels from biomass: chemistry, catalysts, and engineering. *Chem Rev* **106**(9):4044–4098 (2006).
- Xing R, Subrahmanyam AV, Olcay H, Qi W, van Walsum GP, Pendse H *et al.*, Production of jet and diesel fuel range alkanes from waste hemicellulose-derived aqueous solutions. *Green Chem* **12**(11):1933–1946 (2010).
- Maerten SG, Voß D, Liauw MA and Albert J, Selective catalytic oxidation of humins to low-chain carboxylic acids with tailor-made polyoxometalate catalysts. *ChemistrySelect* **2**(24):7296–7302 (2017).
- Voß D, Pickel H and Albert J, Improving the fractionated catalytic oxidation of lignocellulosic biomass to formic acid and cellulose by using design of experiments. *ACS Sustainable Chem. Eng.* **7**(11):9754–9762 (2019).
- Chen S, Wojcieszak R, Dumeignil F, Marceau E and Royer S, How catalysts and experimental conditions determine the selective hydroconversion of furfural and 5-hydroxymethylfurfural. *Chem Rev* **118**(22):11023–11117 (2018).
- Lange JP, van der Heide E, van Buijtenen J and Price R, Furfural—a promising platform for lignocellulosic biofuels. *ChemSusChem* **5**(1):150–166 (2012).
- He Z and Wang X, Hydrodeoxygenation of model compounds and catalytic systems for pyrolysis bio-oils upgrading. *Catal Sustainable Energy* **1**:28–52 (2012).
- Agirrezabal-Telleria I, Gandarias I and Arias P, Heterogeneous acid-catalysts for the production of furan-derived compounds (furfural and hydroxymethylfurfural) from renewable carbohydrates: a review. *Catal Today* **234**:42–58 (2014).
- Hu L, Zhao G, Hao W, Tang X, Sun Y, Lin L *et al.*, Catalytic conversion of biomass-derived carbohydrates into fuels and chemicals via furanic aldehydes. *RSC Adv* **2**(30):11184–11206 (2012).
- Körner S, Albert J and Held C, Catalytic low-temperature dehydration of fructose to 5-hydroxymethylfurfural using acidic deep eutectic solvents and polyoxometalate catalysts. *Front Chem* **7**:661 (2019).
- Román-Leshkov Y, Chheda JN and Dumesic JA, Phase modifiers promote efficient production of hydroxymethylfurfural from fructose. *Science* **312**(5782):1933–1937 (2006).
- Louie YL, Tang J, Hell AML and Bell AT, Kinetics of hydrogenation and hydrogenolysis of 2, 5-dimethylfuran over noble metals catalysts under mild conditions. *Appl Catal B* **202**:557–568 (2017).
- Gilkey MJ, Mironenko AV, Yang L, Vlachos DG and Xu B, Insights into the ring-opening of biomass-derived furanics over carbon-supported ruthenium. *ChemSusChem* **9**(21):3113–3121 (2016).
- Stevens JG, Bourne RA, Twigg MV and Poliakov M, Real-time product switching using a twin catalyst system for the hydrogenation of furfural in supercritical CO₂. *Angew Chem Int Ed* **49**(47):8856–8859 (2010).
- Wang T, Li K, Liu Q, Zhang Q, Qiu S, Long J *et al.*, Aviation fuel synthesis by catalytic conversion of biomass hydrolysate in aqueous phase. *Appl Energy* **136**:775–780 (2014).
- Chatterjee M, Ishizaka T and Kawanami H, Hydrogenation of 5-hydroxymethylfurfural in supercritical carbon dioxide–water: a tunable approach to dimethylfuran selectivity. *Green Chem* **16**(3):1543–1551 (2014).
- da Silva Trindade WR and dos Santos RG, Review on the characteristics of butanol, its production and use as fuel in internal combustion engines. *Renew Sustain Energy Rev* **69**:642–651 (2017).
- Scully SM and Orlygsson J, Biological production of alcohols, in *Advanced Bioprocessing for Alternative Fuels, Biobased Chemicals, and Bioproducts*. Woodhead Publishing, pp. 83–108 (2019).

22. Wei L, Cheung C and Huang Z, Effect of n-pentanol addition on the combustion, performance and emission characteristics of a direct-injection diesel engine. *Energy* **70**:172–180 (2014).
23. Frerot E, Esters comprising a secondary carbamoyl function and their use as odorant alcohol precursors. Google Patents EP1226113B1 (2004).
24. Hall JB, Sprecker MA, Shuster EJ, Schmitt FL, Vinals JF, Substituted dimethyl dihydroxy benzene and cyclohexadiene compounds and uses thereof for augmenting or enhancing the taste and/or aroma of consumable materials including tobaccos, perfumes and perfumed articles. Google Patents US4155867A (1978).
25. Wang T, Qiu S, Qin Y, Ma Y and Fang Y, Hydrothermal conversion of biomass to higher alcohol fuels for compression ignition engine. *Energy Procedia* **158**:249–253 (2019).
26. Luggren PJ, Apesteguía CR and Di Cosimo JI, Upgrading of biomass-derived 2-hexanol to liquid transportation fuels on Cu–Mg–Al mixed oxides. *Fuel* **177**:28–38 (2016).
27. Greene MI, Song R, Judzis Jr A, Conversion of alcohols to distillate fuels, Google Patents US9914672B2 (2018).
28. Bel'skii IF and Shuikin N, Catalytic hydrogenation and hydrogenolysis of furan compounds. *Russ Chem Rev* **32**(6):307 (1963).
29. Biswas P, Lin J-H, Kang J and Gulians VV, Vapor phase hydrogenation of 2-methylfuran over noble and base metal catalysts. *Appl Catal Gen* **475**:379–385 (2014).
30. Shuikin N and Bel'skii I, Catalytic hydrogenolysis of furan compounds. *Bull Acad Sci USSR, Div Chem Sci* **7**(3):293–298 (1958).
31. Wilson CL, Reactions of furan compounds. X. Catalytic reduction of methylfuran to 2-pentanone. *J Am Chem Soc* **70**(4):1313–1315 (1948).
32. Kliewer CJ, Aliaga C, Bieri M, Huang W, Tsung CK, Wood JB et al., Furan hydrogenation over Pt (111) and Pt (100) single-crystal surfaces and Pt nanoparticles from 1 to 7 nm: a kinetic and sum frequency generation vibrational spectroscopy study. *J Am Chem Soc* **132**(37):13088–13095 (2010).
33. Aliaga C, Tsung C-K, Alayoglu S, Komvopoulos K, Yang P and Somorjai GA, Sum frequency generation vibrational spectroscopy and kinetic study of 2-methylfuran and 2, 5-dimethylfuran hydrogenation over 7 nm platinum cubic nanoparticles. *J Phys Chem C* **115**(16):8104–8109 (2011).
34. Goto H, Takagaki A, Kikuchi R and Oyama ST, Hydrogenation of 2, 5-dimethylfuran on hexagonal-boron nitride- and silica-supported platinum catalysts. *Appl Catal Gen* **548**:122–127 (2017).
35. Runnebaum RC, Nimmanwudipong T, Doan J, Block DE and Gates BC, Catalytic conversion of furan to gasoline-range aliphatic hydrocarbons via ring opening and decarbonylation reactions catalyzed by Pt/γ-Al₂O₃. *Catal Lett* **142**(6):664–666 (2012).
36. Kang J, Liang X and Gulians VV, Selective hydrogenation of 2-methylfuran and 2, 5-dimethylfuran over atomic layer deposited platinum catalysts on multiwalled carbon nanotube and alumina supports. *ChemCatChem* **9**(2):282–286 (2017).
37. Jones D and Taylor A, Some aspects of furan and pyran chemistry. *Q Rev Chem Soc* **4**(2):195–216 (1950).
38. Albert J, Mehler J, Tucher J, Kastner K and Streb C, One-step synthesizable lindqvist–isopolyoxometalates as promising new catalysts for selective conversion of glucose as a model substrate for lignocellulosic biomass to formic acid. *ChemistrySelect* **1**(11):2889–2894 (2016).
39. Kozhevnikov IV, Catalysis by heteropoly acids and multicomponent polyoxometalates in liquid-phase reactions. *Chem Rev* **98**(1):171–198 (1998).
40. Wang S-S and Yang G-Y, Recent advances in polyoxometalate-catalyzed reactions. *Chem Rev* **115**(11):4893–4962 (2015).
41. Pope M, *Heteropoly and Isopoly Oxometalates*. Inorganic Chemistry Concepts, Vol. **8**. Springer, Heidelberg, (1983).
42. Bertleff B, Claußnitzer J, Korth W, Wasserscheid P, Jess A and Albert J, Extraction coupled oxidative desulfurization of fuels to sulfate and water-soluble sulfur compounds using polyoxometalate catalysts and molecular oxygen. *ACS Sustainable Chem Eng* **5**(5):4110–4118 (2017).
43. Kogan V, Aizenshtat Z and Neumann R, Preferential catalytic hydrogenation of aromatic compounds versus ketones with a palladium substituted polyoxometalate as pre-catalyst. *New J Chem* **26**(3):272–274 (2002).
44. Modvig A, Kumpidit C, Riisager A and Albert J, Ru-doped Wells–Dawson polyoxometalate as efficient catalyst for glycerol hydrogenolysis to propanediols. *Materials* **12**(13):2175 (2019).
45. Mai CT and Ng FT, Effect of metals on the hydrogenolysis of glycerol to higher value sustainable and green chemicals using a supported HSiW catalyst. *Org Process Res Dev* **20**(10):1774–1780 (2016).
46. Zhu S, Zhu S, Zhu Y, Hao S, Zheng H, Moab T et al., One-step hydrogenolysis of glycerol to biopropanols over Pt–H₄SiW₁₂O₄₀/ZrO₂ catalysts. *Green Chem* **14**(9):2607–2616 (2012).
47. Alhanash A, Kozhevnikova EF and Kozhevnikov IV, Hydrogenolysis of glycerol to propanediol over Ru: polyoxometalate bifunctional catalyst. *Catal Lett* **120**(3–4):307–311 (2008).
48. Alotaibi MA, Kozhevnikova EF and Kozhevnikov IV, Efficient hydrodeoxygenation of biomass-derived ketones over bifunctional Pt-polyoxometalate catalyst. *Chem Commun* **48**(57):7194–7196 (2012).
49. Alharbi K, Kozhevnikova E and Kozhevnikov I, Hydrogenation of ketones over bifunctional Pt-heteropoly acid catalyst in the gas phase. *Appl Catal Gen* **504**:457–462 (2015).
50. Kogan V, Aizenshtat Z and Neumann R, Polyoxometalates as reduction catalysts: Deoxygenation and hydrogenation of carbonyl compounds. *Angew Chem Int Ed* **38**(22):3331–3334 (1999).
51. Benaissa H, Davey PN, Khimyak YZ and Kozhevnikov IV, Heteropoly compounds as catalysts for hydrogenation of propanoic acid. *J Catal* **253**(2):244–252 (2008).
52. Jia S, Ma J, Wang D, Wang K, Zheng Q, Song C et al., Fast and efficient upgrading of levulinic acid into long-chain alkyl levulinate fuel additives with a tungsten salt catalyst at low temperature. *Sustainable Energy Fuels* **4**(4):2018–2025 (2020).
53. Zhang Y, Li WL, Zong S, Du HX and Shi XX, Clean synthesis process of 2, 5-hexanedione. *Adv Mater Res* **518–523**:3947–3950 (2012).
54. Li Y, Lv G, Wang Y, Deng T, Wang Y, Hou X et al., Synthesis of 2, 5-hexanedione from biomass resources using a highly efficient biphasic system. *ChemistrySelect* **1**(6):1252–1255 (2016).
55. Smith HA and Fuzek JF, Catalytic hydrogenation of furan and substituted furans on platinum. *J Am Chem Soc* **71**(2):415–419 (1949).
56. Wang S, Vorotnikov V and Vlachos DG, A DFT study of furan hydrogenation and ring opening on Pd (111). *Green Chem* **16**(2):736–747 (2014).
57. Mironenko AV, Gilkey MJ, Panagiotopoulou P, Facas G, Vlachos DG and Xu B, Ring activation of furanic compounds on ruthenium-based catalysts. *J Phys Chem C* **119**(11):6075–6085 (2015).
58. Vorotnikov V and Vlachos DG, Group additivity and modified linear scaling relations for estimating surface thermochemistry on transition metal surfaces: application to furanics. *J Phys Chem C* **119**(19):10417–10426 (2015).

59. Trinh T-K-H, de Hemptinne J-C, Lugo R, Ferrando N and Passarello J-P, Hydrogen solubility in hydrocarbon and oxygenated organic compounds. *J Chem Eng Data* **61**(1):19–34 (2016).
60. Kozhevnikov IV and Matveev KI, Heteropolyacids in catalysis. *Russ Chem Rev* **51**(11):1075 (1982).
61. Meller E, Gutkin V, Aizenshtat Z and Sasson Y, Catalytic hydrocracking-hydrogenation of castor oil fatty acid methyl esters over nickel substituted polyoxometalate catalyst. *ChemistrySelect* **1**(20):6396–6405 (2016).
62. Soares JCS, Gonçalves AHA, Zotin FMZ, Raddide Araújo LR and Gaspar AB, Cyclohexene to adipic acid synthesis using heterogeneous polyoxometalate catalysts. *Mol Catal* **458**:223–229 (2018).
63. Baker LR, Kennedy G, Van Spronsen M, Hervier A, Cai X, Chen S et al., Furfuraldehyde hydrogenation on titanium oxide-supported platinum nanoparticles studied by sum frequency generation vibrational spectroscopy: acid–base catalysis explains the molecular origin of strong metal–support interactions. *J Am Chem Soc* **134**(34):14208–14216 (2012).
64. Albert J, Lüders D, Bösmann A, Guldi DM and Wasserscheid P, Spectroscopic and electrochemical characterization of heteropoly acids for their optimized application in selective biomass oxidation to formic acid. *Green Chem* **16**:226–237 (2014).
65. Lee U and Sasaki Y, The geometrical isomerization on acidification in hexamolybdoheteropoly oxometalate. the crystal structure of $(\text{NH}_4)_4.5[\text{H}_3.5\alpha\text{-PtMo}_6\text{O}_{24}]\cdot 1.5\text{H}_2\text{O}$, $(\text{NH}_4)_4[\text{H}_4\beta\text{-PtMo}_6\text{O}_{24}]\cdot 1.5\text{H}_2\text{O}$ and $\text{K}_3.5[\text{H}_4.5\alpha\text{-PtMo}_6\text{O}_{24}]\cdot 3\text{H}_2\text{O}$. *Bull Korean Chem Soc* **15**:37–45 (1994).
66. Contant R, Inorganic Syntheses, in *Arly Transition Metal Polyoxoanions*, Vol. **27**, ed. by Ginsberg AP. John Wiley and Sons, New York, pp. 105–106 (1990).
67. Contant R, Relation between tungstophosphates related to the phosphorus tungsten oxide anion ($\text{PW}_{12}\text{O}_{40}^{3-}$). Synthesis and properties of a new lacunary potassium polyoxotungstophosphate ($\text{K}_{10}\text{P}_2\text{W}_{20}\text{O}_{70}\cdot 24\text{H}_2\text{O}$). *Can J Chem* **65**:568 (1987).
68. Finke RG, Rapko B, Saxton RJ and Domaille PJ, Trisubstituted heteropolytungstates as soluble metal oxide analogs. III. Synthesis, characterization, phosphorus-31, silicon-29, vanadium-51, and 1- and 2-D tungsten-183 NMR, deprotonation, and proton mobility studies of organic solvent solute forms of $\text{H}_x\text{Si}_x\text{W}_9\text{V}_3\text{O}_{40}\cdot 7$ and $\text{H}_x\text{P}_2\text{W}_{15}\text{V}_3\text{O}_{62}\cdot 9$. *J Am Chem Soc* **108**:2947–2960 (1986).



Magdy Sherbi

Magdy Sherbi completed his bachelor and master degrees in chemical engineering and petroleum refining at the faculty of Petroleum and Mining Engineering, Suez University, Egypt. After that he was awarded the DAAD (Deutscher Akademischer

Austauschdienst) scholarship to perform his PhD in Germany. In April 2019, he started working at the department of Chemical Reaction Engineering, FAU University, Germany. Since September 2020, he has been working in Professor Jakob Albert's group in Hamburg University in order to continue his research. As a part of his doctoral thesis, he is investigating the hydrogenation of biomass-derived furanes to bio-fuels using polyoxometalate catalysts.



Maria Stuckart

Dr Maria Stuckart studied analytic and physical chemistry at the Polytechnic University of Tomsk. Afterwards, she worked as a PhD student at Jacobs University Bremen on the 'Synthesis, Structure and Properties of Polyoxopalladates'.

After finishing her PhD in inorganic chemistry in 2011, she stayed at Jacobs and worked as a post-doc in the group of Professor Kortz. In 2015, she moved to Rheinisch-Westfälisch Technische Hochschule (RTWH) Aachen and Peter-Grünberg Institute (PGI-6) of the Forschungszentrum Jülich to study the synthesis and analysis of novel inorganic substances and materials for molecular electronics. In 2019, she joined the research group of Dr Albert at FAU Erlangen to focus on the synthesis and characterization of polyoxometalates for catalytic biomass conversion.



Jakob Albert

Professor Dr.-Ing. Jakob Albert has been professor for technical chemistry and deputy director of the Institute of Technical and Macromolecular Chemistry at Hamburg University since 2020. He holds a diploma (2011) and a PhD degree (2014) from

FAU Erlangen in chemical engineering. Afterwards, he became an independent group leader for biomass and sustainable production of platform chemicals at FAU's Institute of Chemical Reaction Engineering. Jakob's key activities are in the research fields of biomass valorization, power-to-X technologies, polyoxometalate catalysts, as well as scale-up and process design. He is an inventor on 23 patents, and has received numerous scientific awards e.g. the Promotionspreis of the Technical Faculty of the FAU in 2015, a Max Buchner scholarship in 2015, an EAM Starting Grant 2015, an Innovation MINT-Award 2016 and the Science sets Sail Award from the Excellence Cluster 'Engineering of Advanced Materials' in 2017.

Chapter 4. Modeling and optimization of bio-2-hexanol production from biomass derived dimethylfuran using Pt/K₃[PW₁₂O₄₀] by response surface methodology

This chapter is based on publication [224]. As introduced in chapter 3, the bifunctional catalyst system Pt/K₃[PW₁₂O₄₀], platinum supported on potassium phosphotungstate, showed high selectivity towards ring opening of various bio-derived furans like 2,5-dimethylfuran, 2-methylfuran and furan during the hydrogenation reaction under mild reaction conditions. In the present chapter, 2,5-dimethylfuran was chosen as a model compound for ring opening of furans and a response surface methodology (RSM) was employed on the hydrogenation reaction of it utilizing Pt/K₃PW₁₂O₄₀, with the objective of studying the reaction and identifying the optimal reaction conditions for maximizing alcohol production. RSM typically consists of several steps including experimental design, response surface modeling, statistical validation, diagnostics, experimental validation, and eventually optimization. Additional supporting information can be found in Appendix 10.5.

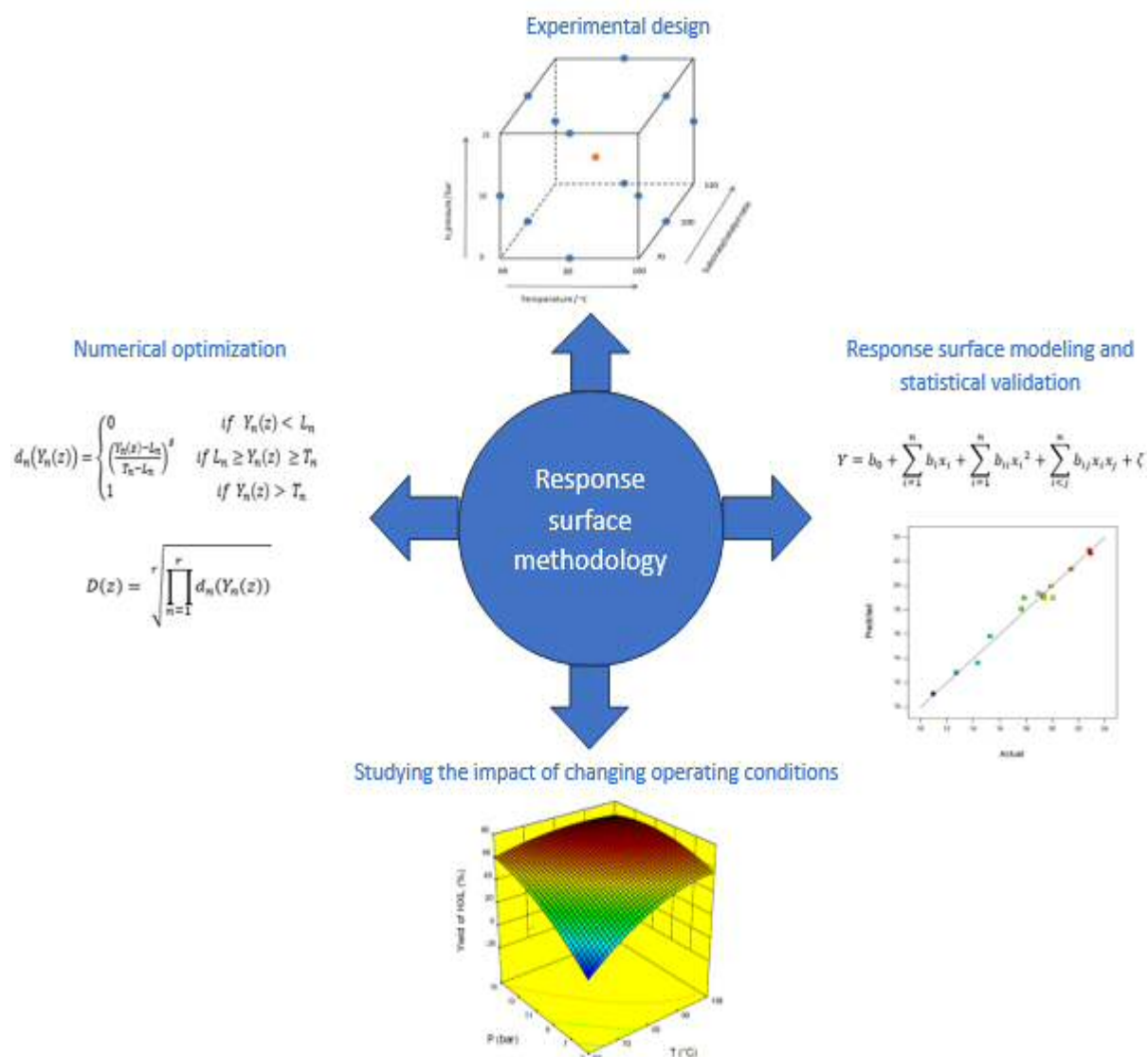


Figure 4.1 Response surface methodology steps implied in this chapter.



Modeling and optimization of bio-2-hexanol production from biomass derived dimethylfuran using Pt/K₃PW₁₂O₄₀ by response surface methodology

Magdy Sherbi, Jakob Albert*

Institute for Technical and Macromolecular Chemistry, University of Hamburg, Bundesstr. 45, Hamburg 20146, Germany

ARTICLE INFO

Article history:

Received 9 April 2021

Revised 9 September 2021

Accepted 12 September 2021

Available online 14 September 2021

Keywords:

Design of experiments

Response surface methodology

Selective catalytic hydrogenation

Polyoxometalates

Furan ring opening

ABSTRACT

Sustainable production of alcohols from renewable sources represents a very important environmental and industrial technology. In this work, response surface methodology (RSM) was employed to study the influence of various process parameters, such as temperature, pressure and substrate to catalyst ratio on the selective hydrogenation of dimethylfuran (DMF) as a model compound for bio-derived furans. The aim was to maximize the yield of the alcoholic product (2-hexanol) using a bifunctional catalyst system composed of platinum supported on a Keggin-polyoxometalate under mild hydrogenation conditions. Hereby, the RSM was used in order to build four predictive models capable of estimating the yield of each product resulting from the hydrogenation reaction. The performance of the prediction models was examined both statistically and experimentally confirming that the predictions are in an excellent agreement with the experimental data. Numerical optimization was performed to reveal the optimal operating conditions to achieve maximum yield of the alcoholic product. With the help of Design of Experiments (DoE) and desirability function approach for optimization, we were able to achieve 78% 2-hexanol yield at complete DMF conversion using a Pt/K₃PW₁₂O₄₀ catalyst under mild hydrogenation conditions of 80°C and 5–15 bar hydrogen pressure.

© 2021 Elsevier Ltd. All rights reserved.

1. Introduction

Alcohols from biogenic resources are discussed as suitable bio-fuels for aviation and transportation applications. Biomass-derived furans might be an attractive biogenic resource for sustainable alcohol production. In a previous study (Sherbi et al., 2021), we reported an efficient bifunctional catalyst system (Pt/K₃PW₁₂O₄₀), platinum supported on potassium phosphotungstate, for selective ring opening of various bio-derived furans like 2,5-dimethylfuran (DMF), methylfuran (MF) and furan showing high selectivities towards alcohol formation. In detail, we performed 2-hexanol (HXL) formation from DMF at 80 °C and 10 bar H₂ pressure using n-decane as a carrier liquid. Hereby, DMF represents a model compound for ring opening hydrogenolysis of furans.

Generally, the main products observed for DMF hydrogenation are 2,5-dimethyltetrahydrofuran (DMTHF) via a two-step ring-saturation hydrogenation of DMF with 2,5-dimethyl-dihydrofuran (DMDHF) as an intermediate, 2,5-hexanedione (HD) via oxidative ring opening to 3-ene-2,5 hexanedione followed by hydrogenation

to HD, 2-hexanone (HXN) via ring opening using two moles of hydrogen or the desired HXL via ring opening using three moles of hydrogen. HXL can be produced as a primary product directly from ring opening of DMF or as secondary product through hydrogenation of HXN. Moreover, HXL can undergo consecutive dehydration to 1-hexene which, in turn, can be hydrogenated to n-hexane (HX). A detailed explanation of the reaction network of DMF hydrogenation can be found in a previous study (Sherbi et al., 2021).

DMF hydrogenation in the liquid phase using mild reaction conditions has been investigated in terms of maximizing the yield of HXN (Louie et al., 2017) and DMTHF (Gilkey et al., 2016) before, but never for maximizing the yield of HXL as far as we know. The desired HXL is of major interest because it is discussed as a renewable C₆ platform molecule for full-performance jet and diesel fuels. HXL can be mixed with other alcohols produced from biomass and used directly in a compression ignition engine (Kumar and Saravanan, 2016; Wang et al., 2019). Moreover, it can be used as a co-feed with other C₂–C₁₁ alcohols for the production of jet and other heavy fuels (Greene et al., 2018). Cu–Mg–Al mixed oxides as catalyst where applied for gas-phase synthesis of high molecular weight compounds based on HXL, that can be used as liquid transportation fuels. The product pool was a mixture of ketones, alcohols and hydrocarbons with 160–200 g/mol average molecular

* Corresponding author.

E-mail address: jakob.albert@chemie.uni-hamburg.de (J. Albert).

Nomenclature

A	coded values of the independent variable temperature
B	coded values of the independent variable pressure
B_0, b_i, b_{ii}, b_{ij}	regression coefficients in the model
C	coded values of the independent variable Substrate/catalyst ratio
Df	degree of freedom
$dn(Yn(z))$	desirability function for each response
$D(z)$	total desirability function
K	number of factors (independent variables)
Ln	lower acceptable value of the response
MS	mean square
N	number of experimental runs
P	hydrogen pressure (bar)
p	number of terms in the model
Pred. R^2	predicted statistic coefficient
r	number of responses in desirability function
R_c	number of replicates for the central point
R^2	coefficient of multiple determination
$R^2_{adj.}$	adjusted statistic coefficient
s	importance degree of each response
SS	sum of squares of the regression model
S/C	Substrate/catalyst ratio (mol (DMF)/mol(Pt))
T	Operating temperature ($^{\circ}\text{C}$)
T_n	target value of the response
x_i	coded variables
Y, $Yn(z)$	predicted response
ζ	statistical error in regression model

weight, and up to 87% of the yield were obtained for compounds in the C_9 – C_{24} range. Around 70% of the products were C_9 – C_{15} compounds suitable for jet fuel applications and the rest as diesel substitutes (Luggren et al., 2016). HXL is also important for liquid phase C–C self-coupling that produces higher dimers with a yield of 79% and trimers with a yield of 11% at complete conversion (Shimura et al., 2013). Those C_{12} – C_{18} alkanes or alkenes that can be synthesized from HXL either by C–C self-coupling and hydrodeoxygenation, or dehydration and oligomerization can be connected to the production of diesel fuels (Liu et al., 2015; West et al., 2009). Furthermore, HXL can react with levulinic acid to produce around 82% yield of hexyl levulinate at full conversion. This long-chain levulinate ester is considered as a valuable synthetic fuel (or fuel additive) which has a theoretical calorific value of $6558.5 \text{ kJ mol}^{-1}$ and lower heating value (LHV) of 29.4 MJ L^{-1} which is very close to that of commercial gasoline (30 – 33 MJ L^{-1}) (Jia et al., 2020). Furthermore, HXL can also be used in the perfume (Frerot, 2004) and tobacco (Hall et al., 1978) industries.

The aim of the present study is to specify optimum reaction conditions for maximizing HXL production from DMF hydrogenation. Although the one-factor-at-a-time (OFAT) method, in which the effect of each variable on a process while holding the others constant is studied provides a way for finding suitable operating conditions, a better way for finding the optimum conditions is the response surface methodology (RSM) that involves statistical DoE where all variables are varied together over a set of experimental runs (Khayet et al., 2011). The main disadvantages of the (OFAT) method according to Czitrom (1999) are : (i) Interactions between experimental variables cannot be estimated using OFAT; (ii) The experimental information exists in a smaller region of the factor space. This deteriorates the prediction of the response, and makes process optimization less efficient as the optimal solution is searched for over a smaller region in the factor space. This is

the reason why RSM is considered as a more efficient way for optimization especially in chemical reactions where interactions between the variables under investigation always exist (Soravia and Orth, 2000). RSM also represents a very economic method in industry as it saves time and money through the lower number of experiments needed to extract the maximum amount of information about the system under investigation. It has been successfully applied in many different scientific fields such as technical chemistry, physics, biofuel production, CO_2 capture, food engineering, chemical engineering, petroleum refining and environmental protection (Bhran et al., 2016; Cepeda and Calvo, 2008; Khayet et al., 2011; Myers et al., 2016; Nuchitprasittichai and Cremaschi, 2011; Olsen et al., 2012; Ravikumar et al., 2005; Sherbi et al., 2020; Soto et al., 2016; Voß et al., 2019). RSM is a collection of mathematical and statistical methods for empirical model building, analyzing and optimization of a process. It implies three stages: (i) experimental design, (ii) response surface modeling in order to determine the relationship between the variables and the response through regression, (iii) optimization (Karacan et al., 2007). The design expert software version (10.0.3) has been chosen in our study for experimental design, modeling and optimization because it offers a wide range of different classes of design including factorials, fractional factorials and composite designs. In addition, it provides a large number of analytical and graphical techniques for model fitting, optimization and interpretation. The Box–Behnken experimental design has been chosen in this study for determining the relationship between the responses (yield of each product gained from DMF hydrogenation) and the variables (temperature, H_2 pressure and substrate/catalyst ratio). The Box–Behnken design was chosen in our study due to its higher efficiency reported by Ferreira et al. (2007) compared to other response surface designs like: central composite, Doehlert matrix and three-level full factorial design. Box–Behnken design is a three-level incomplete factorial design, described as a cube (see Fig. 1), which is composed of a central point and middle points of the edges, and requires number of experiments according to the relation $N = k^2 + k + R_c$, where (k) is the factor number and (R_c) is the number of replicates for the central point (Aslan and Cebeci, 2007). This means that in our case, three-level three-factorial Box–Behnken experimental design, 15 experimental runs, shown in Fig. 1, are needed.

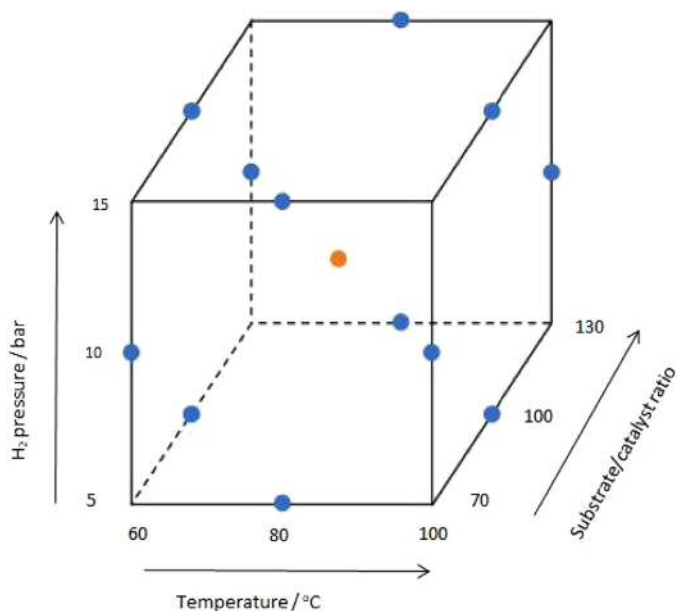


Fig. 1. Experimental points using the Box–Behnken design of experiments.

Consequently, a Box-Behnken experimental design is employed to model the relation between the yield of different products gained from DMF hydrogenation and the three process variables temperature, pressure and substrate/catalyst ratio. Statistical validation of the four models produced were performed using analysis of variance (ANOVA). The response surface and contour plots generated by design expert software version (10.0.3) were utilized in order to analyze the reaction system and gain as much valuable information as possible. Finally, optimization and experimental validation were performed, in order to validate the models and to find out the optimum conditions for maximizing the HXL yield.

2. Experimental details and methodology

2.1. Chemicals

The following chemicals were purchased from Sigma Aldrich and used without further purification: 2,5-dimethylfuran (99% purity) as substrate, decane (99+% purity) as carrier liquid, 5 wt% Pt/C as commercial reference catalyst, as well as H₂ (5.0) and N₂ (5.0) from Linde AG as gases. Pt(acac)₂, H₃[PW₁₂O₄₀]•xH₂O and KCl were used to synthesize the bi-functional catalyst (Pt/K₃PW₁₂O₄₀) as described in a previous study (Sherbi et al., 2021).

2.2. Catalytic experiments

Hydrogenation of DMF was carried out in a 10-fold parallel reaction system using 21 mL stainless-steel (1.4571) high-pressure vessels equipped with magnetic stirring. The autoclaves were connected in parallel to a single hydrogen supply line via individual couplings and placed inside a heating plate in order to adjust the required temperature. The heating plate was equipped with a magnetic stirrer whereby magnetic stirrer bars could be used for mixing. Additionally, each reactor was connected to a rupture disk with a burst pressure maximum of 90 bar. For a typical reaction, decane (10.0 mL) as a carrier liquid, 0.1 g (0.001 mol) DMF as a substrate and 0.04 g (Pt/K₃PW₁₂O₄₀) catalyst, (2 mg active Pt) were charged into the reactor providing a substrate to catalyst ratio of 100:1 mol (DMF)/mol (Pt). Afterwards, the system was purged three times with hydrogen gas to remove residual air. The stirrer speed was set to 330 rpm and electrical heating was switched on. When the desired reaction temperature was reached, the hydrogen pressure was increased to the required pressure and the stirring speed was set to 770 rpm in order to start the gas entrainment. This moment was set as starting time of the experiment. For the DoE studies, the temperature was varied from 60 to 100 °C, pressure from 5 to 15 bar and substrate to catalyst ratio from 70 to 130 mol (DMF)/mol (Pt). After the desired reaction time, the reactor was cooled down to room temperature, after that a gas-phase sample was collected from the reactor in a gas bag to be analyzed. Then the reactor was vented and purged with nitrogen gas (three times) before opening it. The catalyst was separated from the liquid phase by filtration and the liquid phase was analyzed by GC.

2.3. Product analysis

A Varian GC 450-TCD-FID equipped with a Shin Carbon ST column (2 m × 0.75 mm internal diameter) was used to analyze gaseous samples. Argon (pressure of 4.82 bar) was used as the mobile phase in the GC in order to transport the sample after injection through the column. The temperature program used for the column was: 40 °C (1.5 min), 18 °C min⁻¹ to 250, 250 °C (12 min). A Varian CP-3900 gas chromatograph (GC) equipped with a flame ionization detector (FID) was used for performing analysis of liquid products. Product compounds were separated using a Factor

Table 1
Independent variables and their coded values.

Independent variable	Symbol	Coded levels		
		-1	0	+1
Operating temperature (°C)	T	60	80	100
Hydrogen pressure (bar)	P	5	10	15
Substrate/catalyst ratio (mol (DMF)/mol(Pt))	S/C	70	100	130

Four capillary column (VF-WAXms, 30 m length, 0.25 mm diameter) coated with a 0.25 μm thick stationary phase with helium as a carrier gas. The operating conditions of the GC method used was: injection temperature of 250 °C, column temperature program: 40 °C (6 min), 10 °C min⁻¹ to 250, 250 °C (2.5 min), detection temperature of 250 °C. An external standard (octane) was used in all samples for liquid GC measurements. Conversion of DMF and product yields were calculated as presented below in Eqs. (1) and (2). Mass balance for all experiments, based on carbon balances of each reaction, was > 95% using the applied analytical methods

$$\text{Conversion (mol\%)} = \frac{\text{number of moles of substrate reacted}}{\text{number of moles of substrate loaded}} \times 100\% \quad (1)$$

$$\text{Yield (mol\%)} = \frac{\text{number of moles of product that actually formed}}{\text{maximum theoretical number of moles that can be produced}} \times 100\% \quad (2)$$

2.4. Design of experiments (DoE)

As stated before, the DoE employed has been performed considering three independent variables: reaction temperature T (°C), pressure p (bar) and substrate to catalyst ratio S/C (mol (DMF)/mol (Pt)). Table 1 presents the controllable factors and their different levels in coded and actual values.

The output response considered in the DOE is the yield (mole %) for each product in the reaction system calculated through Eq. (2). In order to investigate how the process variables affect the responses and to obtain models that represent the relationship between the responses and the variables, a Box-Behnken experimental design was performed with 3 factors and 3 levels. The 3-level 3-factorial Box-Behnken experimental design, shown in Table 2, consists of 15 runs with 12 design points (middle points of the edges) and 3 center points for replication.

Table 2
Box-Behnken design with coded values for the independent variables.

Entry	Coded level of variables		
	A (T) [°C] ^a	B (p) [bar] ^a	C (S/C) [mol/mol] ^a
1	(+1)	(-1)	(0)
2	(0)	(-1)	(+1)
3	(-1)	(+1)	(0)
4	(-1)	(0)	(-1)
5	(0)	(0)	(0)
6	(0)	(-1)	(-1)
7	(0)	(0)	(0)
8	(0)	(+1)	(+1)
9	(-1)	(-1)	(0)
10	(+1)	(+1)	(0)
11	(0)	(0)	(0)
12	(+1)	(0)	(-1)
13	(0)	(+1)	(-1)
14	(-1)	(0)	(+1)
15	(+1)	(0)	(+1)

^a -1 = minimum value, 0 = center value, +1 = maximum value.

A polynomial equation was used to produce the model predicting the response as a function of controllable variables. Usually a second-order polynomial model is used for Box-Behnken designs, so the responses become as follows (Khayet et al., 2011):

$$Y = b_0 + \sum_{i=1}^n b_i x_i + \sum_{i=1}^n b_{ii} x_i^2 + \sum_{i < j} b_{ij} x_i x_j + \zeta \quad (3)$$

where:

Y is the predicted response, x_i refers to the coded variables, b_0 , b_i , b_{ii} , b_{ij} are the regression coefficients and ζ is the statistical error.

For improving model's performance and ability for prediction in the current study, the model terms with insignificant coefficient depending on P -values were excluded. Also, some additional cubic terms were added to the models without overstressing the design or causing confounding (Soravia and Orth, 2000). The coefficients of the empirical models have been determined from the experimental data by the application of least square method using the Design Expert Software (version 10.0.3). Statistical validation and fit quality of produced models were examined by analyses of variance (ANOVA) using the same software. The coefficient of determination R^2 and the statistical significance of the models using the F -test were reported. Optimization of reaction conditions for maximizing HXL production was carried out using the software's numerical optimization. Since four responses were gained in the modeling of DMF hydrogenation as presented later, the simultaneous optimization of all of them resulted in a multi-objective optimization (MOO) problem. A numerical technique that can be used in case of several responses that should be optimized simultaneously is the desirability function approach, in which a multi-response problem is transformed into a single response problem (Soto et al., 2016). The desirability function approach consists usually of three steps: (i) Performing experiments and fitting the data for a number of responses; (ii) Defining an individual desirability function for each response; (iii) Defining the overall desirability and maximizing it in order to find optimum conditions. In our study, the experiments were performed according to Table 2, then the results were collected and used to produce the responses by response surface modeling. After all model responses $Y_n(z)$ are fitted to polynomial equations by response surface methodology, an individual desirability function $d_n(Y_n(z))$ is developed for each response as presented in Eq. (4).

$$d_n(Y_n(z)) = \begin{cases} 0 & \text{if } Y_n(z) < L_n \\ \left(\frac{Y_n(z) - L_n}{T_n - L_n}\right)^s & \text{if } L_n \leq Y_n(z) \leq T_n \\ 1 & \text{if } Y_n(z) > T_n \end{cases} \quad (4)$$

where z are the factors, L_n is the lower acceptable value of $Y_n(z)$, and T_n is the target value. The parameter s equals to unity for all responses in order to assign equal importance to each response. The total desirability function $D(z)$, can be defined as the geometric mean of the individual desirability functions obtained for the r responses of interest, as presented in Eq. (5) (Soravia and Orth, 2000; Soto et al., 2016).

$$D(z) = \sqrt[r]{\prod_{n=1}^r d_n(Y_n(z))} \quad (5)$$

Eq. (5) represents our single response problem that can be used for finding the optimum conditions for our reaction system.

3. Results and discussion

3.1. Response surface modeling of the product yields for DMF hydrogenation using Pt/K3PW12O40

In the first study (Table 3), we performed two reference experiments showing the superior activity of the Pt/K3PW12O40 catalyst (68.0% HXL-yield) compared to the commercial Pt/C catalyst (only 49.7% HXL-yield) under similar hydrogenation conditions. This data was set as reference point for further optimization.

In the next step, four predictive models were tested to estimate the product yields of DMF hydrogenation using the Pt/K3PW12O40 catalyst as a function of reaction temperature T ($^{\circ}\text{C}$), hydrogen pressure p (bar) and substrate to catalyst ratio S/C (mol (DMF)/mol (Pt)). The variables were changed from minimum to maximum values as presented in Tables 1 and 2 in order to build the Box-Behnken design shown in Table 4.

Based on the results of the Box-Behnken experimental design, the RSM was applied to find out the relation between the responses and the variables. In our case the best empirical models that can predict the yield of each product in terms of coded variables are given in Eqs. (6)–(9).

$$\begin{aligned} \text{Yield of HXL} = & 66.12 + 13.61 * A + 11.88 * B - 7.66 * C \\ & - 10.24 * AB + 6.97 * AC + 9.45 * BC - 8.64 * A^2 \\ & - 8.95 * B^2 + 3.62 * A^2 B - 7.97 * AC^2 \end{aligned} \quad (6)$$

$$\begin{aligned} \text{Yield of HXN} = & 9.6 - 6.72 * A - 16.5 * B + 11.78 * C + 3.75 * AB \\ & - 5.57 * AC - 10.82 * BC + 7.04 * B^2 + 3.25 * C^2 \\ & + 3.94 * A^2 B \end{aligned} \quad (7)$$

$$\begin{aligned} \text{Yield of HX} = & 6.01 + 1.01 * A + 0.66 * B - 1.95 * C - 1.3 * AC \\ & + 2.38 * A^2 + 1.24 * C^2 - 1.51 * A^2 C \end{aligned} \quad (8)$$

$$\begin{aligned} \text{Yield of DMTHF} = & 18.98 - 1.21 * A + 4.74 * B - 1.08 * C \\ & - 1.17 * AB + 0.57 * AC - 2.3 * B^2 \\ & + 0.82 * C^2 + 0.91 * AB^2 - 1.96 * BC^2 \end{aligned} \quad (9)$$

where A , B and C are the coded values of the independent variables (T , p , S/C), $60 \text{ }^{\circ}\text{C} \leq T \leq 100 \text{ }^{\circ}\text{C}$; $5 \leq p \leq 15 \text{ H}_2 \text{ bar}$ and $70 \leq \text{Sub/Catalyst} \leq 130 \text{ (mol (DMF)/mol (Pt))}$.

All analysis within the Design expert software are based on the coded equations presented in Eqs. (6)–(9). The empirical models obtained in terms of actual variables are presented in the supporting information (Eqs. (S1)–(S4)). The regression coefficients of the response models were calculated using the Multiple Linear Regression (MLR) method to minimize the sum of squares of the residuals. The best empirical model that fits the experimental yield data in each case was selected using a backward selection depending on the Bayesian Information Criterion (BIC). To improve the model performance, some terms were neglected depending on the P -value as the corresponding term will be more significant if its P -value is smaller than 0.05 (Cepeda and Calvo, 2008; Dc, 2001; Ravikumar et al., 2005). Some exceptions were done only if removing the term decreases the F -value or predicted R^2 significantly. For example, removing the term C^2 which has a P -value = 0.13, (see Table S10 in the supporting information) from DMTHF model will decrease the F -value of the model to 19, R^2 to 0.96, R^2_{adj} to 0.91 and Pred. R^2 to 0.48. On the other hand, if the term is included in the model the results will be of much higher significance as presented in Table 5. Also, some higher order interaction terms were introduced without overstressing the models in order to enhance

Table 3
DMF conversion and product yields using Pt/K3PW12O40 and Pt/C catalysts.

Entry	Catalyst	DMF-conversion (%)	Yield (%)			
			HXL	HXN	DMTHF	Hexane
1	5% Pt/C	100	49.7	30.6	14.3	0.7
2	5% Pt/K3PW12O40	100	68.0	5.7	19.7	6.3

Reaction conditions: 0.1 g DMF, 10.0 mL decane as a solvent, 0.04 g catalyst, 80 °C, 10 bar H₂, 770 rpm, 3 h.

Table 4
Box-Behnken design results for DMF hydrogenation using Pt/K3PW12O40.

Run no.	DOE Reaction Results				
	DMF-conversion %	Response 1HXL yield%	Response 2HXN yield%	Response 3HX yield%	Response 4DMTHF yield%
1	100	57.4	18.5	8.9	12.7
2	100	26.8	57.5	4.5	14.3
3	100	61.2	9.8	8.2	22.8
4	100	65.1	1.7	11.3	22.9
5	100	66.4	9.4	6.7	17.8
6	100	62.7	12.7	8.4	15.3
7	100	67.2	7.1	6	19.4
8	100	69.5	2.9	5.5	19.3
9	70.2	9.7	42.4	5.6	11
10	100	67.9	0.9	9.5	19.8
11	100	66.7	7.2	6.5	20
12	100	62.5	2.4	15.6	19.3
13	100	67.5	1.4	9.4	21.4
14	100	37.5	36.9	6.9	18.9
15	100	62.7	15.3	6	17.6

Reaction conditions: 0.1 g DMF, 10.0 mL decane as a solvent, 0.04 g catalyst, 770 rpm, 3 h.

Table 5
Analysis of variance (ANOVA) for the developed RSM models.

Source	SS	df	MS	F-value	F _{crit}	P-value	R ²	R ² _{adj.}	Pred. R ²	Adeq. Precision
a) HXL										
Model	4372.41	10	437.2	170.38	5.96	< 0.0001	0.998	0.992	0.875	44.9
Residual	10.27	4	2.57							
Lack of fit	9.89	2	4.95	26.59		0.0362				
Pure error	0.37	2	0.19							
Total	4382.67	14								
b) HXN										
Model	4050.92	9	450.1	45.46	4.77	0.0003	0.988	0.966	0.794	22.9
Residual	49.50	5	9.9							
Lack of fit	46.28	3	15.43	9.56		0.0962				
Pure error	3.23	2	1.61							
Total	4100.42	14								
c) HX										
Model	106.93	7	15.28	30.65	3.79	< 0.0001	0.968	0.937	0.778	20.9
Residual	3.49	7	0.50							
Lack of fit	3.23	5	0.65	4.92		0.1775				
Pure error	0.26	2	0.13							
Total	110.42	14								
d) DMTHF										
Model	166.27	9	18.47	24.18	4.77	0.0013	0.977	0.937	0.817	16.6
Residual	3.82	5	0.76							
Lack of fit	1.30	3	0.43	0.34		0.8011				
Pure error	2.52	2	1.26							
Total	170.09	14								

the prediction power. For example, the two significant terms A²B and AC² in the HXL prediction model have a P-value = 0.03 and 0.002, respectively). Without them the F-value, R², R²_{adj.} and Pred. R² are only 19.34, 0.96, 0.91 and 0.6, respectively. On the other hand, when they are included in the model the results of F-value, R², R²_{adj.} and Pred. R² were much better, (170.38, 0.998, 0.992, 0.875) respectively, as presented in Table 5.

3.2. Analysis of variance (ANOVA) or statistical analysis and validation

In order to statically validate the response surface models, see Eqs. (6)–(9) for adequacy, we used the analysis of variance

(ANOVA). All ANOVA tables for each model are presented in the supporting information (see Tables S1–S12). The most relevant information from the ANOVA tables for all of the models are summarized in Table 5.

The relationships used for determining the statistical estimators (i.e., F-value, P-value, R², R²_{adj.} and pred.R²) can be found elsewhere (Joyce, 1982; Tomescu et al., 1984). The F-test, shown in Eq. (10), was used to evaluate the statistical significance of the empirical models. In case that the calculated F-value is greater than the F_{crit}, the model gives a good prediction of the experimental data (Dc, 2001; Myers et al., 2016).

$$F_{value} > F_{crit}(p - 1, N - p, \gamma) \quad (10)$$

where p represents the number of terms in the model, N number of runs and $\gamma = 0.05$

In Table 5, the F -value for all models is found to be greater than the tabulated one ($F_{\text{crit}}(10,4,0.05)$ for HXL, $F_{\text{crit}}(9,5,0.05)$ for HXN, $F_{\text{crit}}(7,7,0.05)$ for HX, and $F_{\text{crit}}(9,5,0.05)$ for DMTHF). Moreover, the P -value for each model is used to judge whether the F -value is large enough to indicate statistical significance. For all of the models the P -value is smaller than 0.01 which indicates that they are statistically significant (Ravikumar et al., 2005). As already known the closer the determination coefficient (R^2) is to 1, the better the model fits the experimental data, and all of the models in our study have shown $R^2 \geq 0.968$. Moreover, the predicted R^2 values are in agreement with the R^2_{adj} values (i.e. The difference between them is less than 0.2). This implies that most of the significant terms have been inserted in the regression models (Khayet et al., 2011). The ANOVA table also presents the residual error for each model, which indicates the amount of variation in the response data left unexplained by the model (Ravikumar et al., 2005), and the lack of fit which is the weighted sum of squared deviations between the mean response at each factor level and the corresponding fitted value. A non-significant lack of fit (i.e. lack of fit P -value > 0.05) is desirable (Zafari et al., 2019), which is the case in all of the models except for the HXL-model. The significant lack of fit for the HXL-model can be ignored in our case because of the high $\text{pred.}R^2$ and the experimental validation that will be discussed later. "Adeq. Precision" is also reported for each model, which measures the signal to noise ratio and compares the range of the predicted values at the design points to the average prediction error. A ratio greater than 4 is desirable and represents indication for an adequate model discrimination, which is the case for all of the presented predictive models.

The analysis of variance (ANOVA) indicated that the proposed models are adequate to represent the relationship between the responses (Yield % for each product) and the significant variables (T , p , S/C). Residual analysis, presented in (Figs. S1–S4), is also performed for each model in order to check the linearity of the model and assure that the residuals are independent from one another, identically distributed and have a constant variance. The response values calculated using the empirical models were compared to the experimental results in Fig. 2 also confirming the adequacy of the models to fit the experimental data. Therefore, it can be concluded that the proposed models are validated from a statistical point of view and they can be considered suitable for making predictions and optimization.

3.3. Studying the impact of changing operating conditions on the product distribution

After the statistical validation of the developed models in the previous study and before performing the optimization in order to increase the amount of the desired product HXL, we investigated the influence of changing the variables T , p , S/C on the yield of each product using the response surface and contour plots generated by the Design Expert software in order to analyze the reaction system and to gain as much valuable information as possible.

Regarding HXL, Table S1 shows that all of the variables (T , p , S/C) are significant because they have a very low P -value. In order to investigate how each variable affects the yield of HXL, a response surface plot and contour plots were drawn. As can be seen from Fig. 3(a) at a medium value of $S/C = 100$, increasing the temperature at low pressure or increasing the pressure at low temperature increases the HXL yield. This is in good agreement with previous observations, that increasing the temperature favors the desired ring opening leading to HXL and HXN over ring saturation which produces mainly DMTHF (Louie et al., 2017). Increasing the H_2 pressure at constant T favors the consecutive hydrogenation

of the ring-opened intermediate HXN to HXL (Louie et al., 2017; Sen and Vannice, 1988) finally leading to a higher HXL-yield. Moreover, higher HXL-yields can be also achieved by increasing both of them simultaneously. To explore the effect of changing the S/C ratio, three contour plots presented in Fig. 3(a)–(c) were drawn at $S/C = 130$, 100, and 70, respectively. Obviously, decreasing the S/C ratio (i.e. increasing the catalyst amount) results in an enlarging domain containing high yield of HXL (red domain) and shifting the maximum achievable yield to lower values of p and T . It is worth to note that for $S/C = 70$ (Fig. 3(d)), increasing p and T to their maximum values simultaneously produces lower HXL-yield (yellow region) that can be attributed to the higher rate of dehydration of HXL to produce hexane. At higher S/C (Fig. 3(b)) the effect of increasing the temperature alone at low to moderate pressure becomes less significant and does not produce high yields of HXL unless the pressure is high as well.

Two 3D response surface plots for HXN at $S/C = 130$ and 70 respectively are presented in Fig. 4 in order to investigate the effect of each variable on the HXN yield. From Fig. 4(a), increasing temperature or pressure decreases the amount of HXN produced. As can be noticed from comparing Fig. 4(a) and (b), higher amounts of HXN can be produced only in case of high S/C ratio. This is related to the fact that HXN is an intermediate that can be further hydrogenated to HXL and the existence of higher amounts of the catalyst will always lead to the hydrogenation of HXN to HXL. From Fig. 4(a), it is obvious that H_2 pressure is a very significant variable. Decreasing p (H_2) will prevent subsequent hydrogenation to HXL and allow for the production of higher amounts of HXN. Regarding the temperature, it has less significance which is noticeable in Fig. 4(a) and (b) that agrees with the P -values of each variable presented in Table S4 as p , S/C have lower P -values (0.0001) than T which has (0.0018).

Regarding the HX yield, Table S7 in the supporting information presents the P -values of each factor. The p -value related to the pressure in the HX-model is 0.033. On the other hand, the P -values related to temperature and S/C ratio are (0.004, 0.0009, respectively) which are much lower and make them more significant, especially the S/C ratio. Therefore, only one 3D response surface plot between T and S/C is presented in order to investigate the HX product distribution. As shown in Fig. 5, decreasing the amount of S/C results in increasing the HX yield. Also, at low S/C ratio of 70, first increasing the temperature decreases the amount of HX until a temperature around 80 °C and then increases it again dramatically. The amount of HX increases to a maximum at very high temperature and low S/C . This behavior can be explained by the following behavior: (i) with increasing temperature, the amount of HXL produced increases which can further react to produce HX (Alharbi et al., 2015), (ii) low S/C ratio means that higher amounts of catalyst are present, therefore higher number of acid sites, which are responsible for dehydration of HXL, will exist in the reaction system and this will lead to higher HX yield (Alharbi et al., 2015; Aramendia et al., 1999).

As presented in Fig. 6(a)–(c), the effect of different variables on the DMTHF-yield can be seen. In general, increasing the temperature or decreasing S/C ratio increases the DMTHF yield slightly. However, the most significant factor that affects DMTHF production is the H_2 pressure. Increasing the latter significantly increases the DMTHF yield, because the rate of ring saturation increases much more with increasing the pressure rather than the rate of ring opening (Louie et al., 2017). This also agrees with the P -values presented in Table S10 in the supporting information, where the P -value related to the pressure has the lowest value which means it is the most significant variable on the DMTHF-yield.

A final conclusion after studying the effects of changing the variables on product distribution is that there is no conflict between the models and what is known from literature about the

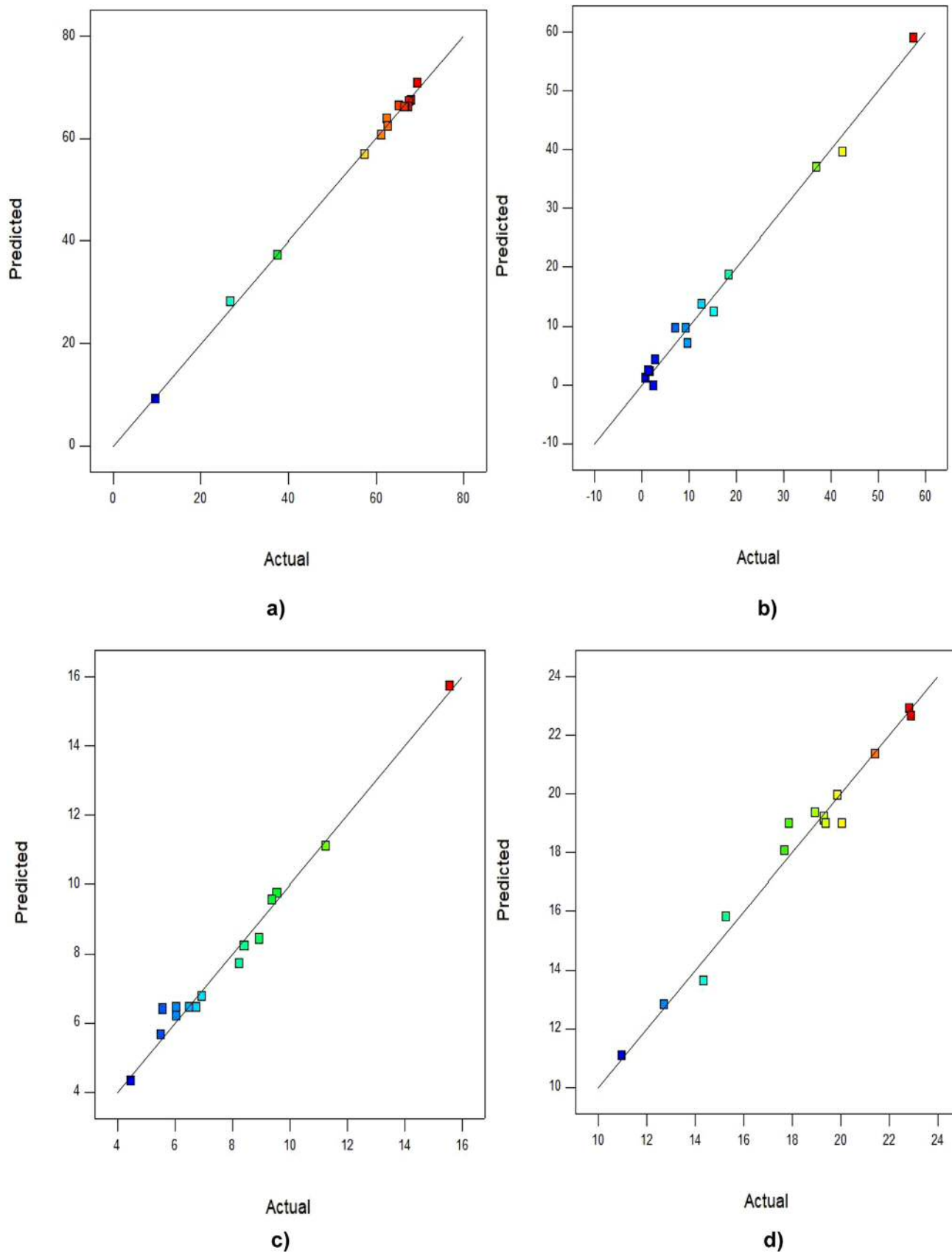


Fig. 2. Relation between experimental and predicted values of (a) HXL-yield, (b) HXN-yield, (c) HX-yield, (d) DMTHF yield.

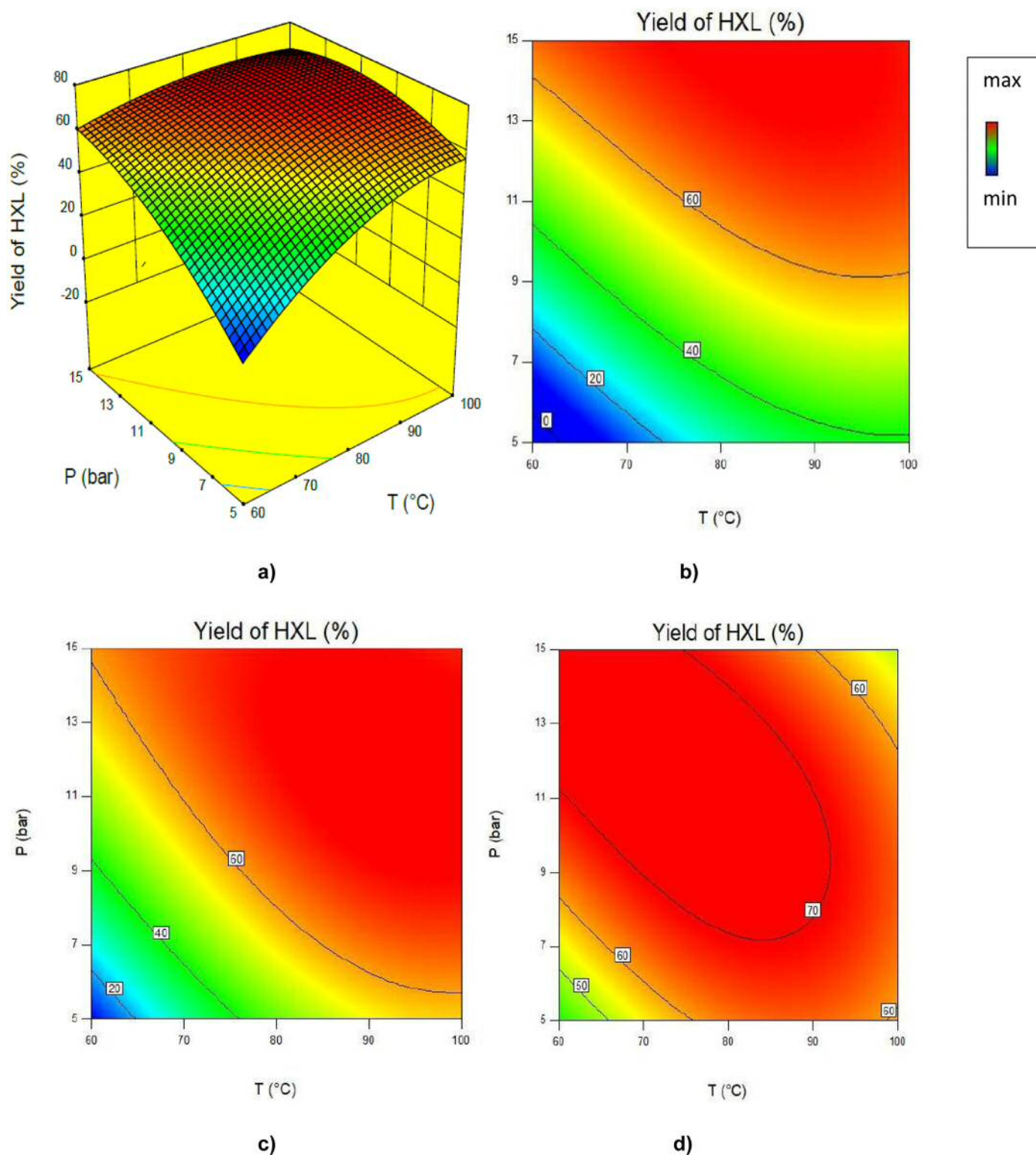


Fig. 3. (a) 3D response surface plot @ S/C = 100, (b) contour plot @ S/C = 130, (c) contour plot @ S/C = 100, (d) contour plot @ S/C = 70 of predicted HXL yield as a function of operating temperature and pressure.

reaction system, which is another good sign that allows us to use them for prediction and optimization.

3.4. Optimization and experimental validation of optimum conditions

Based on the aforementioned statistical validation of the models, we proceeded with optimization in order to find the optimum

conditions at which we can maximise our desired product HXL. Also, the ability of the proposed models to predict product yields has been confirmed in this study by performing additional runs under optimum conditions of maximizing HXL yield or minimizing the other products, as discussed later.

In order to show the importance of performing optimization using response surface modeling technique instead of one factor at

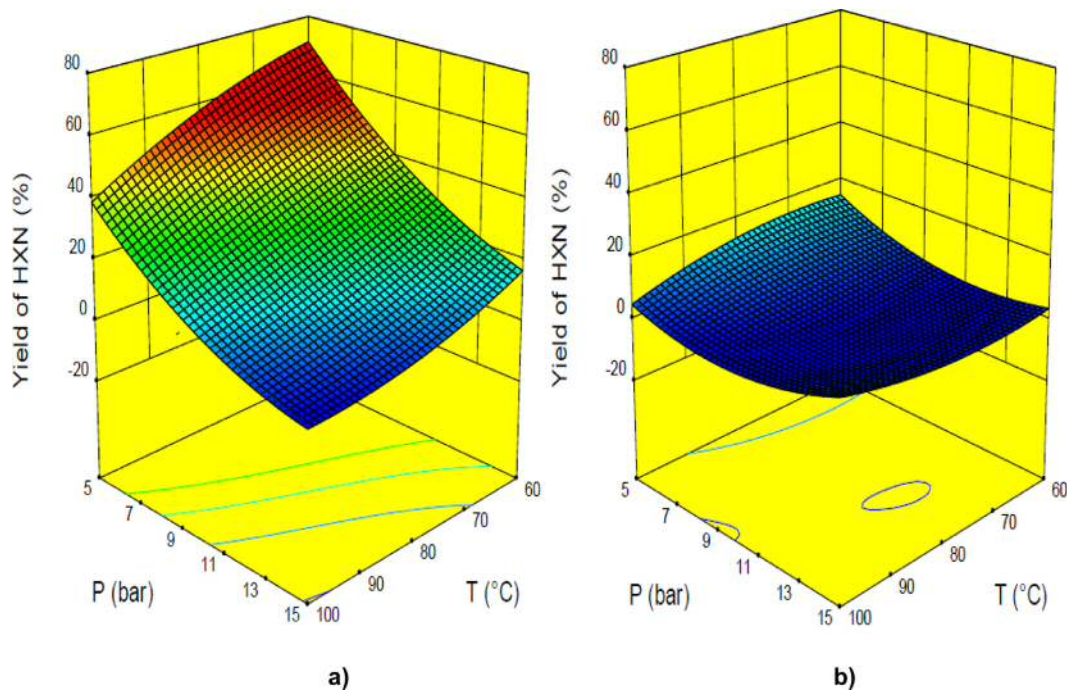


Fig. 4. 3D response surface plot of predicted HXN yield as a function of operating temperature and pressure (a) @ $S/C = 130$, (b) @ $S/C = 70$.

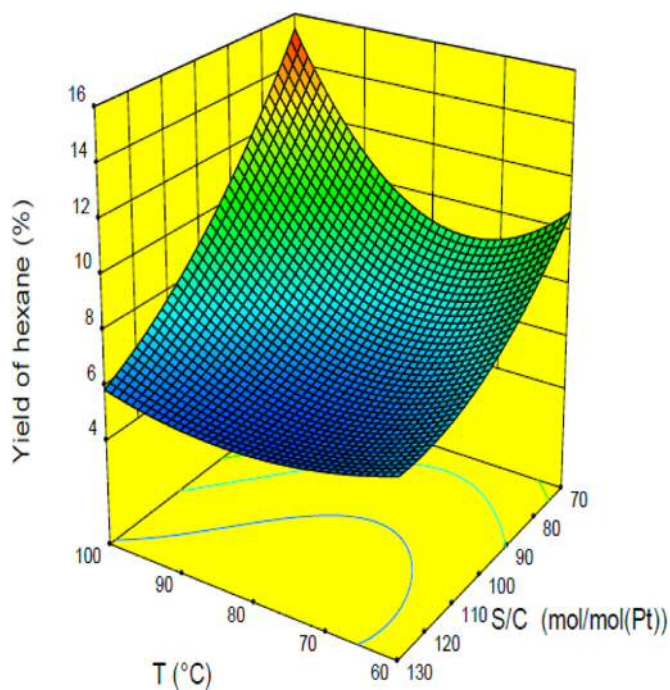


Fig. 5. 3D response surface plot of predicted HX yield as a function of operating temperature and substrate/catalyst ratio @ $p(\text{H}_2) = 10$ bar.

a time investigations (OFAT) technique, two interaction plots are presented for HXL-yield in Fig. 7(a)–(b), for $S/C = 100$ and 70 , respectively, investigating the effect of temperature at low and high hydrogen pressure. Regarding moderate $S/C = 100$ in Fig. 7(a): (i) at low $p = 5$ bar, increasing the temperature is desirable and we have maximum HXL-yield at maximum value of T . (ii) However, at higher $p = 15$ bar increasing temperature does not affect the yield significantly. Regarding lower S/C value $= 70$ (see Fig. 7(b)): (i) at low $p = 5$ bar, HXL yield is directly proportional to T . (ii) On

the other hand, at higher $p = 15$ bar, it is inversely proportional to T . Therefore, a compromise between different variables T , p , S/C should exist in order to achieve optimum conditions for maximizing HXL-yield, which is not a suitable task for one factor at a time investigations (OFAT), but can only be achieved using DoE.

The overall target of the optimization study is to find out the conditions that maximize HXL-yield and minimize other products. Simultaneous optimization of the four responses gained in the modeling of hydrogenation of DMF resulted in a multi-objective optimization (MOO) problem. The desirability function approach where a multi-response problem can be transformed into a single response problem is used to achieve this target in a three step process as discussed before in Section 2.4 using design expert software. In the first step, the experiments were performed and the data were fitted, and this resulted in four responses $Y_n(z)$ which represent Eqs. (6)–(9) in this study. Secondly, an individual desirability function $d_n(Y_n(z))$, ranging between 0 and 1, for each of the four responses was defined using Eq. (4). Finally, the overall desirability function $D(z)$ was defined as the geometric mean of the four individual desirability functions according to Eq. (5) and then maximized in order to find optimum conditions. The applied constrains to the experimental variables for the optimization of overall $D(z)$ were set to be at the same range of the experimental conditions: $60\text{ }^\circ\text{C} \leq T \leq 100\text{ }^\circ\text{C}$; $5 \leq p \leq 15\text{ H}_2\text{ bar}$ and $70 \leq \text{Sub/Catalyst} \leq 130\text{ (mol (DMF)/mol (Pt))}$. The constrains, target values, lower acceptable limits and the obtained numerical results for each individual desirability function and the overall desirability function are summarized in Tables S.13–14. Two different reaction condition sets, presented in entries 1 and 3 in Table 6, were obtained from optimizing the overall desirability function for maximizing the HXL-yield and minimizing other product yields. The predicted HXL-yields were 70.6% and 68.3%, respectively. We used those reaction condition sets in two different laboratory experiments (entries 2 and 4 Table 6) in order to validate the models experimentally at those optimum conditions. We managed to produce HXL-yield of 70.6, 68.9% experimentally as predicted from the model. As seen in entries 2 and 4 the yields of HX and DMTHF were still high, therefore we preformed another optimization task

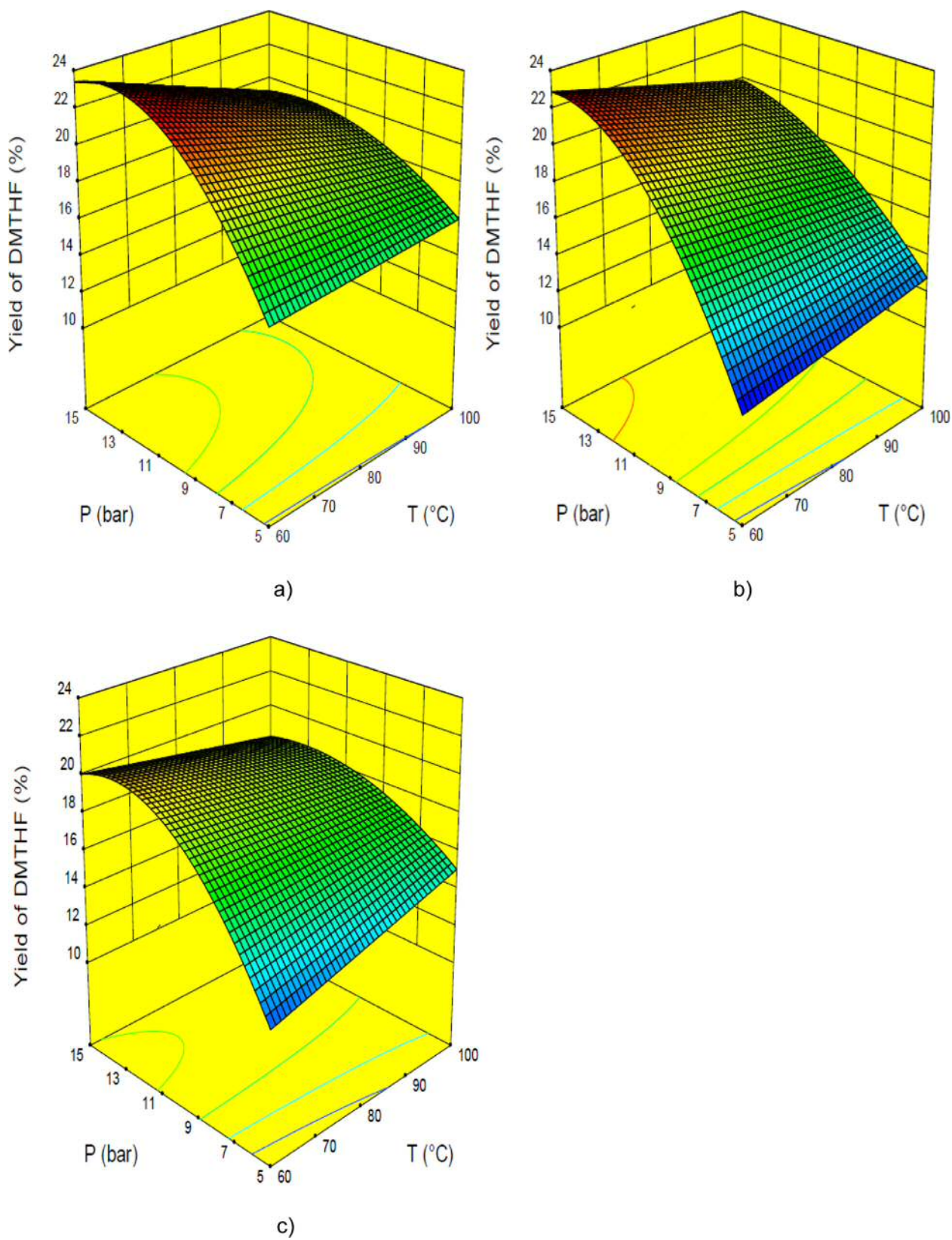


Fig. 6. 3D response surface plot of predicted DMTHF-yield as a function of operating temperature and pressure (a) @ S/C = 70, (b) @ S/C = 100, (c) S/C = 130.

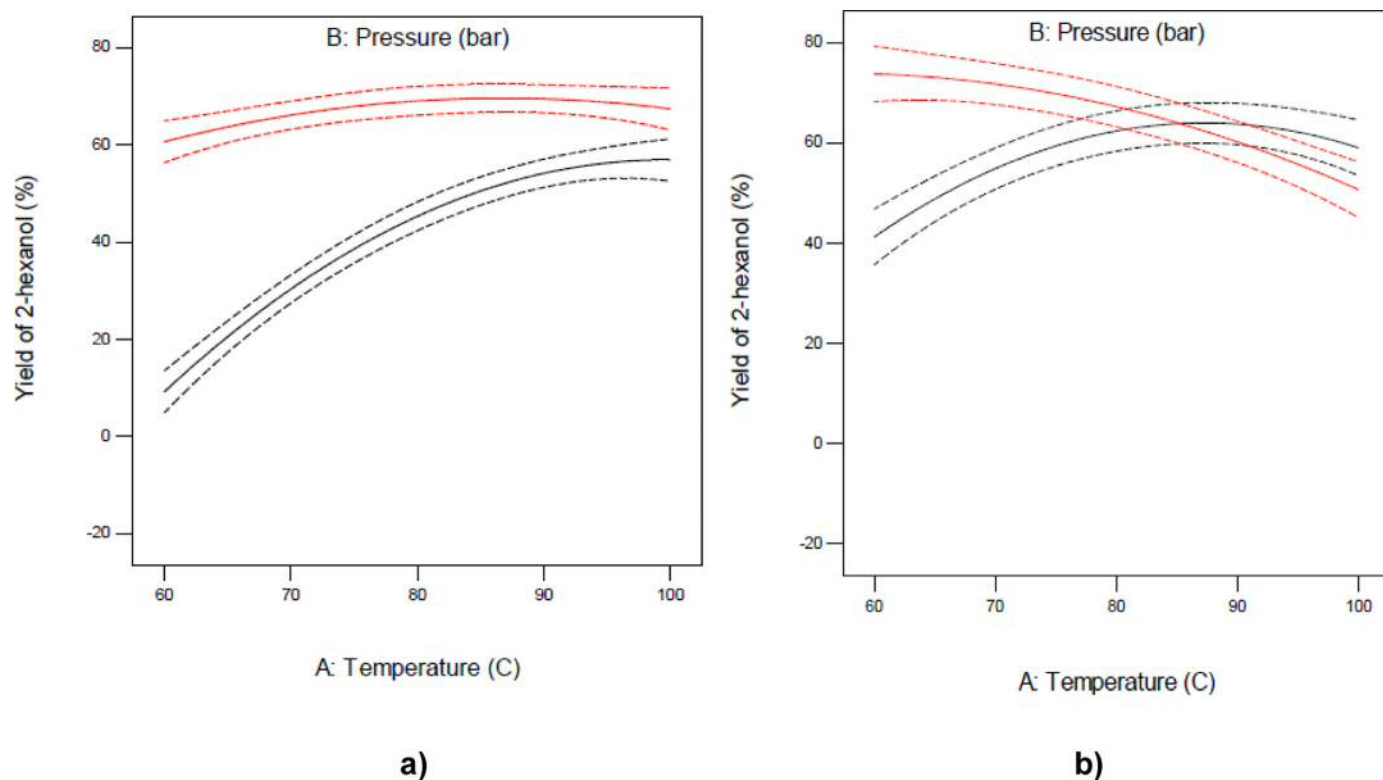


Fig. 7. Interaction plots of predicted HXL yield (a) @ S/C = 100, (b) @S/C = 70; red lines for $p = 15$ bar, black lines for $p = 5$ bar hydrogen.

Table 6

Optimum operating conditions and experimental validation for proposed models.

Entry	Type of run ^a	T (°C)	p(bar)	S/C (mol (DMF)/mol(Pt))	HXL yield %	HXN yield %	HX yield %	DMTHFyield %
1	Pred. ^b	91	15	130	70.6	0.9	6.0	18.7
2	Exp.	91	15	130	70.7	1.6	6.3	18.6
3	Pred. ^b	83	15	88	68.3	0.3	8.0	21.4
4	Exp.	83	15	88	68.9	0.6	8.9	21.5
5	Pred. ^b	83	5	88	54.8	23.3	6.6	13.0
6	Exp.	83	5	88	55	23.5	6.5	13.0
7	Exp.	83	5 then 15 ^c	88	77.4	1.1	6.2	15.5

Reaction conditions: 0.1 g DMF, 10.0 mL decane as a solvent, 770 rpm, 3 h.

^a type of the run: Pred. i.e. predicted by the models, Exp. i.e. experimentally performed

^b predicted values are reported here and the prediction intervals are reported in Table S.15

^c the H₂ pressure was maintained at 5 bar for 30 min then it was increased to 15 bar

Table 7

Conversion and product yields for different H₂ & N₂ pressure.

Entry	Pressure	Results				
		Conversion(%)	HXL yield (%)	HXN yield(%)	HX yield (%)	DMTHF yield (%)
1	5 bar H ₂	100	55.2	23.6	6.1	15.4
2	15 bar: (5 bar H ₂ , 10 bar N ₂)	100	65.5	10.6	7.8	15.4
3	15 bar H ₂	100	68.9	0.7	9	21.5
4	15 bar N ₂	0	-	-	-	-

Reaction conditions: 0.1 g DMF, 10.0 mL decane as a solvent, 5% Pt/K₃[PW₁₂O₄₀] (0.046 g), S/C = 88 (mol (DMF)/mol(Pt)), 83 °C, 770 rpm, 3 h.

where we minimized HXN, HX, DMTHF only without maximizing HXL-yield. As presented in entry 5, we obtained an optimum variable set of (83 °C for T , 5 bar for p (H₂) and 88 for S/C) as a solution for this optimization problem. Another experimental validation for the predicted yields was performed at similar reaction conditions (entry 6). The ability of the models to perform predictions at different product ranges can be confirmed through the experimental validation presented in Table 6 entries 1–6.

A quick glance at entries 3 and 6 shows that there is only one variable that is different in each case, namely the pressure (i.e. for minimizing the undesirable products low p is desirable and for maximizing our desired product HXL higher $p = 15$ is desirable). So, we decided to perform a further experiment, (entry 7), under similar reaction conditions starting with low $p = 5$ then increasing it to $p = 15$ after thirty minutes. As presented in entry 7, with the help of DoE and desirability function approach for

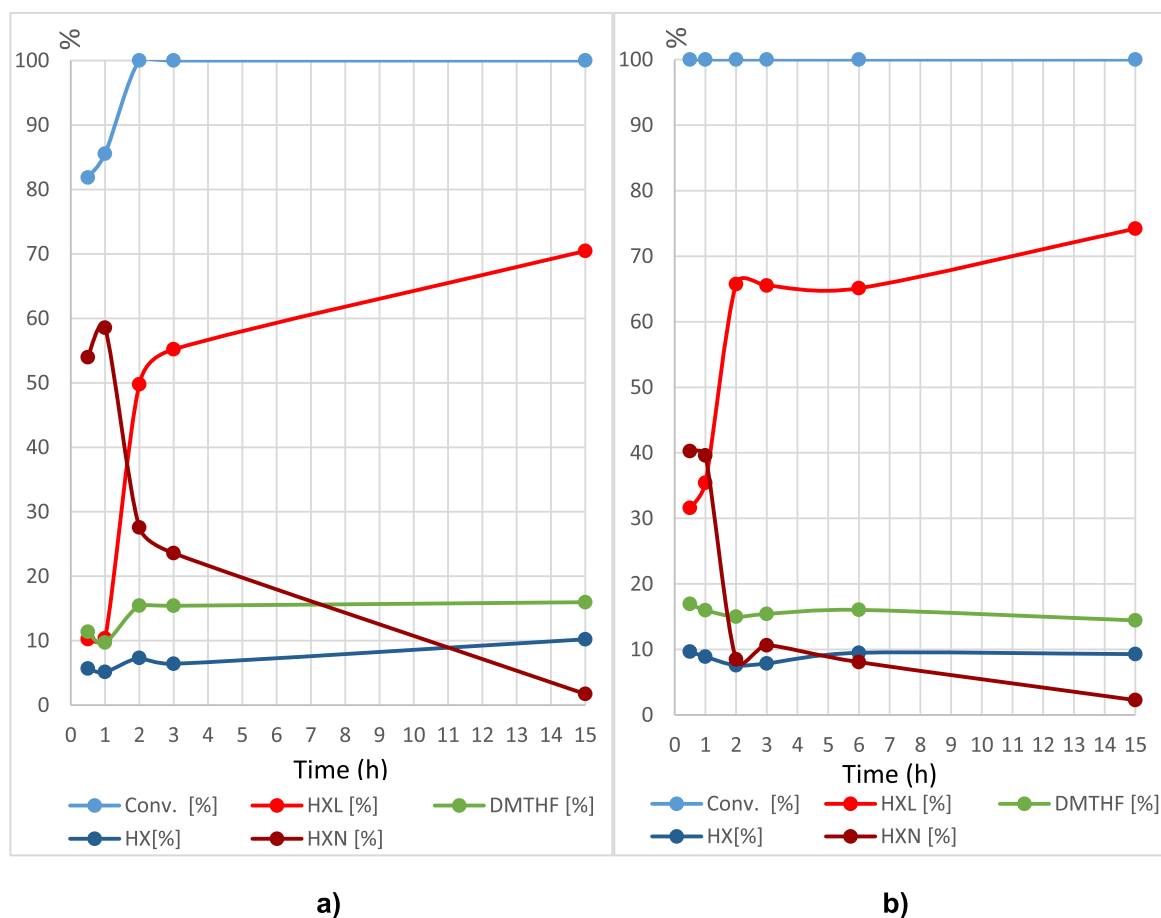


Fig. 8. Time-resolved conversion and product yields for DMF hydrogenation (a) at 5 bar H₂(b) at 15 bar (5 H₂ and 10 N₂). Reaction conditions: 0.1 g DMF, 10.0 mL decane as a solvent, 5% Pt/K₃[PW₁₂O₄₀] (0.046 g), S/C = 88 (mol (DMF)/mol(Pt)), 83 °C, 770 rpm.

optimization, we managed to achieve 77.4% HXL-yield at full DMF conversion.

3.5. Effect of H₂ pressure and time-resolved investigations

In the last set of experiments, the influence of different gas phase compositions on the hydrogenation of DMF was investigated. In detail, we wanted to find out the correlation between the partial pressure of hydrogen and the total pressure of the reaction system. Therefore, we used different dilutions with nitrogen in the gas phase. In the beginning, we used a low total pressure of 5 bar with pure hydrogen atmosphere leading to 55.2% HXL-yield and still 23.6% HXN-yield (entry 1). Moreover 15.4% DMTHF-yield shows that a significant amount of hydrogen is consumed in the undesired ring saturation reaction. Interestingly, increasing the total pressure to 15 bar by simply adding 10 bar of inert nitrogen gas further increased the HXL-yield to 65.5% by simultaneous decrease of the HXN-yield (entry 2). However, the amount of DMTHF remained unchanged. By further increasing the hydrogen pressure to 15 bar (entry 3), the yield of HXL was only slightly increased to 68.9% whereby DMTHF-yield increased to 21.5%. This goes hand in hand with a decreasing selectivity for the desired ring-opening reaction. A control experiment in pure nitrogen atmosphere (entry 4) did not show any DMF conversion as expected.

Moreover, further time-resolved experiments at extended reaction times were performed at different total pressures to study the kinetic effect of different gas atmospheres. A time-resolved experiment at a total pressure of 5 bar (pure H₂) is presented in Fig. 8(a). Hereby, we can observe full DMF conversion already after 2 h re-

action time. Moreover, HXN is formed as an intermediate with a maximum yield of 60% after 1 hour and a sharp decrease down to almost 20% after 3 h. Afterwards, its amount decreased constantly down to zero after 15 h. Furthermore, HXL is fastly formed after an initial phase of around 1 h by the consecutive hydrogenation of HXN upto almost 70% yield after 15 h. Additionally, small amounts of DMTHF (up to 15%) and HX (up to 10%) are slowly formed during the entire reaction time as side products.

In comparison, the time-resolved experiment at a total pressure of 15 bar (5 bar H₂ and 10 bar N₂) shown in Fig. 8(b) does not show significant differences in reaction kinetics except for the faster conversion of DMF (already full conversion after 1 h) and a faster formation of HXL directly after starting the reaction. Therefore, we can conclude that the total pressure increases hydrogen solubility in the carrier liquid decane according to Henry's law. This increases the kinetics of the desired ring-opening reaction leading to HXN as an intermediate and consecutive hydrogenation to HXL. However, the undesired ring saturation reaction leading to DMTHF is not affected by the overall pressure.

After this study and without any doubts, we can explain the reason for the highest yield of 77.4% HXL gained with the help of DoE in Table 6, entry 7. At the beginning of the reaction where most of the DMF conversion takes place and at low $p = 5$ H₂, the formation of DMTHF is limited to a minimum by parallel maximizing the ring opening reaction. After 30 min and with increasing the H₂ pressure to 15 bar in the system, we overcame the mass transfer limitation of H₂ and accelerated the rate limiting step, hydrogenation of ring-opened HXN to HXL, which increased the rate of HXL formation leading to a maximum overall HXL yield.

4. Conclusion

Four predictive models that estimate different product yields of DMF hydrogenation using the catalyst Pt/K₃PW₁₂O₄₀, in terms of temperature, pressure and substrate to catalyst ratio, were generated using response surface methodology applied to a Box-Behnken experimental design. The analysis of variance confirmed the adequacy of the models to fit the experimental data. Additionally, experimental validation of the models was performed at three different reaction condition sets. With the help of the response surface and contour plots generated by the Design Expert software, we were able to fully understand the effect of operating conditions on the yield of each product in the hydrogenation reaction. The desirability function approach for optimization was utilized in order to find the optimal conditions for maximizing HXL production. With those optimum reaction conditions reported in Table 6, entry 7 a maximum HXL yield of 77.4% was achieved at complete DMF conversion. Time-resolved experiments having two different total pressures managed to illustrate the reason for this high yield of HXL at the reported optimal condition. In addition, it revealed that DMF ring saturation and ring opening reactions occur in parallel not in series and that the ring opened products are produced directly from DMF not from DMTHF as an intermediate. Also, it showed that the rate-limiting step of the reaction leading to HXL as a product was the successive hydrogenation of the ring-opened product HXN to HXL, and that most of HXL produced resulted from the secondary reaction pathway, HXN hydrogenation to HXL, not from the primary reaction pathway of DMF ring opening and hydrogenation.

Declaration of Competing Interest

The authors declare that they have no known competing financial interests or personal relationships that could have appeared to influence the work reported in this paper.

CRediT authorship contribution statement

Magdy Sherbi: Writing – review & editing, Writing – original draft. **Jakob Albert:** Supervision, Writing – review & editing.

Acknowledgments

M. Sh. acknowledges financial support from the Egyptian Ministry of Higher Education and Scientific Research (MHESR) and the German Academic Exchange Service (Deutscher Akademischer Austauschdienst, DAAD).

Supplementary materials

Supplementary material associated with this article can be found, in the online version, at [doi:10.1016/j.compchemeng.2021.107546](https://doi.org/10.1016/j.compchemeng.2021.107546).

References

- Alharbi, K., Kozhevnikova, E., Kozhevnikov, I., 2015. Hydrogenation of ketones over bifunctional Pt-heteropoly acid catalyst in the gas phase. *Appl. Catal. A* 504, 457–462.
- Aramendia, M.A., Borau, V., Jiménez, C., Marinas, J.M., Romero, F.J., 1999. Synthesis and characterization of magnesium phosphates and their catalytic properties in the conversion of 2-hexanol. *J. Colloid Interface Sci.* 217, 288–298.
- Aslan, N., Cebeci, Y., 2007. Application of Box–Behnken design and response surface methodology for modeling of some Turkish coals. *Fuel* 86, 90–97.
- Bhran, A.A., Shoaib, A.M., Umana, B., 2016. Optimization of crude oil hydrotreating process as a function of operating conditions: application of response surface methodology. *Comput. Chem. Eng.* 89, 158–165.
- Cepeda, E., Calvo, B., 2008. Sunflower oil hydrogenation: study using response surface methodology. *J. Food Eng.* 89, 370–374.

- Czitrom, V., 1999. One-factor-at-a-time versus designed experiments. *Am. Stat.* 53, 126–131.
- Dc, M., 2001. *Design and Analysis of Experiments*. John Wiley and Sons, New York.
- Ferreira, S.C., Bruns, R., Ferreira, H., Matos, G., David, J., Brandão, G., da Silva, E.P., Portugal, L., Dos Reis, P., Souza, A., 2007. Box-Behnken design: an alternative for the optimization of analytical methods. *Anal. Chim. Acta* 597, 179–186.
- Frerot, E., 2004. Esters comprising a secondary carbamoyl function and their use as odorant alcohol precursors. US Patent 6677297.
- Gilkey, M.J., Mironenko, A.V., Yang, L., Vlachos, D.G., Xu, B., 2016. Insights into the ring-opening of biomass-derived furanics over carbon-supported ruthenium. *ChemSusChem* 9, 3113–3121.
- Greene, M. I., Song, R., & Judzis Jr, A. (2018). Conversion of alcohols to distillate fuels. In: Google Patents.
- Hall, J. B., Sprecker, M. A., Shuster, E. J., Schmitt, F. L., & Vinals, J. F. (1978). Substituted dimethyl dihydroxy benzene and cyclohexadiene compounds and uses thereof for augmenting or enhancing the taste and/or aroma of consumable materials including tobaccos, perfumes and perfumed articles. In: Google Patents.
- Jia, S., Ma, J., Wang, D., Wang, K., Zheng, Q., Song, C., Guo, X., 2020. Fast and efficient upgrading of levulinic acid into long-chain alkyl levulinate fuel additives with a tungsten salt catalyst at low temperature. *Sustain. Energy Fuels* 4, 2018–2025.
- Joyce, R., Akhnazarova, S., Kafarov, V., 1982. *Experiment Optimization in Chemistry and Chemical Engineering*, 312. Mir Publishers, Moscow and Chicago 372–372.
- Karacan, F., Ozden, U., Karacan, S., 2007. Optimization of manufacturing conditions for activated carbon from Turkish lignite by chemical activation using response surface methodology. *Appl. Therm. Eng.* 27, 1212–1218.
- Khayet, M., Zahrim, A., Hilal, N., 2011. Modeling and optimization of coagulation of highly concentrated industrial grade leather dye by response surface methodology. *Chem. Eng. J.* 167, 77–83.
- Kumar, B.R., Saravanan, S., 2016. Use of higher alcohol biofuels in diesel engines: a review. *Renew. Sustain. Energy Rev.* 60, 84–115.
- Liu, S., Okuyama, Y., Tamura, M., Nakagawa, Y., Imai, A., Tomishige, K., 2015. Production of renewable hexanols from mechanocatalytically depolymerized cellulose by using Ir-ReOx/SiO₂ catalyst. *ChemSusChem* 8, 628–635.
- Louie, Y.L., Tang, J., Hell, A.M., Bell, A.T., 2017. Kinetics of hydrogenation and hydrogenolysis of 2, 5-dimethylfuran over noble metals catalysts under mild conditions. *Appl. Catal. B* 202, 557–568.
- Luggren, P.J., Apesteguía, C.R., Di Cosimo, J.I., 2016. Upgrading of biomass-derived 2-hexanol to liquid transportation fuels on Cu–Mg–Al mixed oxides. Effect of Cu content. *Fuel* 177, 28–38.
- Myers, R.H., Montgomery, D.C., Anderson-Cook, C.M., 2016. *Response Surface Methodology: Process and Product Optimization Using Designed Experiments*. John Wiley & Sons.
- Nuchitprasittichai, A., Cremaschi, S., 2011. Optimization of CO₂ capture process with aqueous amines using response surface methodology. *Comput. Chem. Eng.* 35, 1521–1531.
- Olsen, C., Arantes, V., Saddler, J., 2012. The use of predictive models to optimize sugar recovery obtained after the steam pre-treatment of softwoods. *Biofuels Bioprod. Biorefin.* 6, 534–548.
- Ravikumar, K., Pakshirajan, K., Swaminathan, T., Balu, K., 2005. Optimization of batch process parameters using response surface methodology for dye removal by a novel adsorbent. *Chem. Eng. J.* 105, 131–138.
- Sen, B., Vannice, M.A., 1988. Metal-support effects on acetone hydrogenation over platinum catalysts. *J. Catal.* 113, 52–71.
- Sherbi, M., Stuckart, M., Albert, J., 2021. Selective catalytic hydrogenation of biomass derived furans to secondary alcohols using Pt/polyoxometalate catalysts under mild reaction conditions. *Biofuels Bioprod. Biorefin.* 15 (5), 1431–1446 2021.
- Sherbi, M.S., El-Maghraby, R.M., Shoaib, A.M., Bhran, A.A., 2020. Predictive correlations and optimization of atmospheric long residue hydrotreating process. *Pet. Coal* 62, 678–690.
- Shimura, K., Kon, K., Siddiki, S.H., Shimizu, K.I., 2013. Self-coupling of secondary alcohols by Ni/CeO₂ catalyst. *Appl. Catal. A* 462, 137–142.
- Soravia, S., Orth, A., 2000. *Design of experiments*. Ullmann's Encyclopedia of Industrial Chemistry. John Wiley & Sons, Inc..
- Soto, R., Fité, C., Ramírez, E., Bringué, R., Cunill, F., 2016. Equilibrium conversion, selectivity and yield optimization of the simultaneous liquid-phase etherification of isobutene and isomylenes with ethanol over Amberlyst™ 35. *Fuel Process. Technol.* 142, 201–211.
- Tomescu, M., Isaicmaniu, A., Cretu, S., Rachiteanu, G., 1984. Application of statistical-mathematical methods to the operation of chemical processes. *Rev. Chim.* 35, 1012–1017.
- Voß, D., Pickel, H., Albert, J., 2019. Improving the fractionated catalytic oxidation of lignocellulosic biomass to formic acid and cellulose by using design of experiments. *ACS Sustain. Chem. Eng.* 7, 9754–9762.
- Wang, T., Qiu, S., Qin, Y., Ma, Y., Fang, Y., 2019. Hydrothermal conversion of biomass to higher alcohol fuels for compression ignition engine. *Energy Procedia* 158, 249–253.
- West, R.M., Kunkes, E.L., Simonetti, D.A., Dumesic, J.A., 2009. Catalytic conversion of biomass-derived carbohydrates to fuels and chemicals by formation and upgrading of mono-functional hydrocarbon intermediates. *Catal. Today* 147, 115–125.
- Zafari, R., Abdouss, M., Zamani, Y., 2019. Application of response surface methodology for the optimization of light olefins production from CO hydrogenation using an efficient catalyst. *Fuel* 237, 1262–1273.

Part II: Hydroprocessing of biomass derived glycerol

In part I, the selective catalytic hydroprocessing of furans, derived from cellulose and hemicellulose was expounded. Part II* focuses on the selective catalytic hydroprocessing of glycerol, derived from oils and fats to 1,2-propanediol. This part contains one chapter (chapter 5). It is noteworthy to mention that the research on the hydrogenolysis of glycerol was initiated with a comprehensive screening of catalysts, which is presented in section.7.3.2 of chapter 7, in which the activity of Ru-based catalysts towards the hydroprocessing of glycerol and the effect of surface modification of Ru-based catalyst in changing its selectivity towards 1,2-propanediol production were reported.

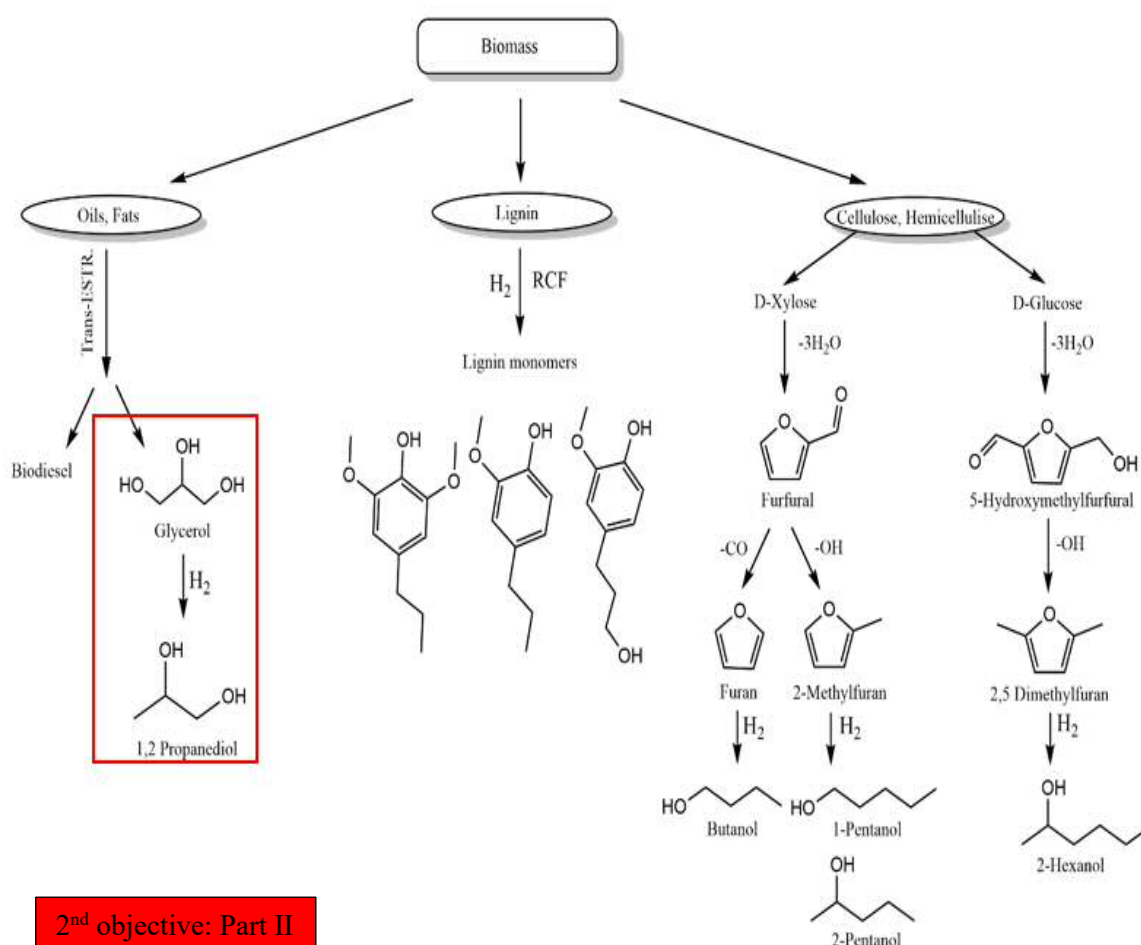


Figure 1.3 Scope of the thesis: 2nd objective (hydroprocessing of biomass derived glycerol).

* This part includes one publication, wherein the catalyst synthesis and characterization were undertaken and written by Anne Wesner and our cooperation partners from Hamburg University of Technology (TUHH).

Chapter 5. Superior CNT-supported bimetallic RuCu catalyst for the highly selective hydrogenolysis of glycerol to 1,2-propanediol

Chapter 5 is based on publication [217] and reports the selective production of 1,2-propanediol (1,2 PD) from glycerol (GL) using a bimetallic RuCu catalyst supported on carbon nanotubes (RuCu/CNT) under mild reaction conditions. The publication commences with an introductory section that underscores the significance of the conversion of GL into high-value products and outlines the various techniques and catalysts that have been employed to accomplish this goal. Among these approaches, the hydrogenolysis of GL into propanediols (PDs) is regarded as a particularly promising approach for the valorization of GL. According to section.7.3.2, it was observed that the surface modification of Ru-based catalysts with polyoxometalates (POMs) yielded positive outcomes in terms of enhancing the selectivity towards 1,2 PD. Building on this premise, the current investigation in chapter 5 focused on exploring the efficiency of surface modification of Ru-based catalysts with Cu and Fe, which are two of the most selective transition metals identified in the literature towards 1,2 PD. The findings of this investigation reveal a marked increase in selectivity towards 1,2-propanediol subsequent to the surface modification of Ru-based catalysts with both Fe and Cu. Notably, the utilization of Ru₁Cu₂/CNT catalyst for the hydrogenolysis of GL resulted in an outstanding 1,2 PD selectivity of 93.4%. Additional supporting information can be found in Appendix 10.6.

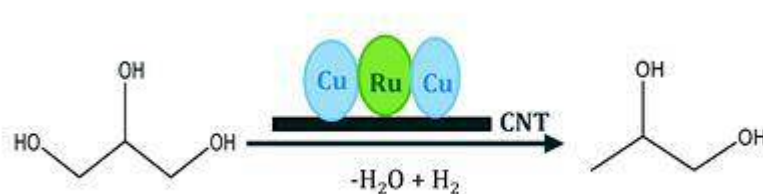


Figure 5.1 Selective hydrogenolysis of glycerol to 1,2-propanediol using Ru₁Cu₂/CNT.

Cite this: *Catal. Sci. Technol.*, 2021, 11, 6649Received 20th August 2021,
Accepted 17th September 2021

DOI: 10.1039/d1cy01518d

rsc.li/catalysis

Superior CNT-supported bimetallic RuCu catalyst for the highly selective hydrogenolysis of glycerol to 1,2-propanediol†

Magdy Sherbi,^a Anne Wesner,^a Valea Kim Wisniewski,^{id}^b Anna Bukowski,^a
Hristiana Velichkova,^{id}^b Bodo Fiedler^b and Jakob Albert^{id}^{*a}

Selective hydrogenation of glycerol to 1,2-propanediol (1,2-PD) is a promising route for sustainable production of platform chemicals. Herein, a bimetallic RuCu catalyst supported on multiwall carbon nanotubes (RuCu/MWCNT) is reported that shows superior catalytic performance leading to 93.4% 1,2-PD selectivity under mild reactions conditions.

To this date, the production of platform chemicals relies primarily on fossil resources. However, the increasing scarcity and negative environmental impact, that the use of fossil resources entails, show that the development of more sustainable production pathways is of paramount importance.¹

Glycerol (GL) is a major by-product of biodiesel manufacturing produced in an amount corresponding to around 10 wt% of the biodiesel production. Several catalytic transformations of GL into value-added chemicals have been reported including steam reforming, oxidation, dehydration, acetylation, esterification, etherification, carboxylation and chlorination.^{2–4} Nevertheless, hydrogenolysis of GL into propanediols (PDs) is one of the most attractive approaches for GL valorisation due to the wide applicability of PDs on a large scale.⁵ 1,2-Propanediol (1,2-PD), or propylene glycol, is an important chemical extensively used as a monomer for polyester resin. Other industrial applications are found in the food-, pharmaceutical-, cosmetic- and animal feed industries.^{6–8} Selective catalytic hydrogenolysis of GL provides an attractive, greener alternative to the current fossil-based manufacturing process of 1,2-PD.⁹

Hydrogenolysis of GL can be regarded as a two-step process involving acid-catalysed GL dehydration affording a

double bond, which is then selectively hydrogenated to yield the desired PD. The acidity of the applied catalyst effects the position of remaining hydroxyl groups on PD. Several heterogeneous catalysts (including carbon supported Ru, Pt, Ni and Cu) have been employed for GL hydrogenolysis with Ru being considered as the most effective.^{10–13}

However, several studies have shown that non-acidic Ru species mainly catalyse the undesired methanation reaction resulting from thermal-induced dehydration to acrolein followed by decomposition to CO and short chain alkanes.^{14,15} In comparison, acidic Ru species initialize the first protonation step followed by acid- and thermally-induced consecutive dehydration and subsequent keto-enol tautomerization leading to acetol as reaction intermediate. In the following step, selective hydrogenation to 1,2-PD takes place.¹⁶

Surface modification of Ru based catalysts either by adding sulphur for poisoning the active Ru sites or by adding another metal is reported in literature to increase the selectivity towards 1,2-PD.¹⁷ Bimetallic catalysts based on Ru and Fe as a promoter showed superior activity and selectivity for GL hydrogenolysis to PDs compared to monometallic Ru species, especially when supported on carbon nanotubes (CNTs).¹⁸ This can be explained by synergistic effects of the formation of Ru-Fe alloys and the interactions between RuFe bimetallic NPs and iron oxides on CNT surfaces. Moreover, several Cu-based catalysts have been applied for selective 1,2-PD formation. Hereby, mainly Cu chromite,¹⁹ Cu/ZnO²⁰ as well as Al₂O₃,²¹ SiO₂ (ref. 22) and MgO-supported²³ Cu nanoparticles where frequently reported. Additionally, also bimetallic CuAg²⁴ as well as CuPd²⁵ catalysts showed good activities for selective glycerol hydrogenolysis. From a mechanistic point of view, the conversion of glycerol to 1,2-PD using Cu as active species can be attributed to a selective cleavage of the C–O bond *via* a hydro-dehydrogenation mechanism proposed by Montassier *et al.*²⁶ Hereby, a proper balance between hydro-dehydrogenation centres and dehydration centres in Cu-based catalysts is required for a high 1,2-PD selectivity.

^a Universität Hamburg, Institut für Technische und Makromolekulare Chemie, Bundesstraße 45, 20146 Hamburg, Germany.

E-mail: jakob.albert@chemie.uni-hamburg.de

^b Technische Universität Hamburg, Institut für Kunststoffe und Verbundwerkstoffe, Denickestraße 15, 21073 Hamburg, Germany

† Electronic supplementary information (ESI) available. See DOI: 10.1039/d1cy01518d



The aim of our study was to find a suitable supported bimetallic catalyst for selective production of 1,2-PD through surface modification of Ru based catalysts. For efficient gas-liquid mass transfer, the micro-, meso- and macrostructure of the catalytic active surface has to be designed in an intelligent way to overcome mass and heat transport limitations by using CNT as catalyst support. We have now developed a superior CNT-supported bimetallic RuCu catalyst that specifically provides a very high selectivity for 1,2-propanediol. In this bimetallic catalyst, Ru is responsible for H₂ spillover which provides active hydrogen to the surface of the Cu nanoparticles and Cu is responsible for C–O cleavage through hydro-dehydrogenating properties.

The carbon nanotubes that were used as support for our new catalyst, are commercially available multi-walled CNT NC7000 by Nanocyl SA., Belgium, which is a nanoparticle powder widely applied in industrial scale CNT-modified materials. The catalysts were synthesised using an improved version of the wet impregnation method described by Asakura *et al.*¹⁸ A detailed description of the synthetic procedure can be found in the ESI.† Table 1 shows the surface properties of the synthesized materials. The total surface area slightly decreases after deposition of the metals on the CNT support. This might be caused by metal particles blocking the pores of CNTs. A similar behaviour was reported before for Ru–Cu supported on CNT.¹⁷ The decrease in surface area was higher in case of Ru₂Cu₁ and Ru₁Cu₂ catalysts, as Cu has a larger particle diameter compared to Ru and Fe. The only exception is for pure Cu which slightly increases the total surface area, possibly by forming separate particles instead of adhering to the CNT surface. The metallic surface area and metal dispersion as well as the active particle diameter were determined by CO-chemisorption. With respect to the metallic surface area, no significant differences between the synthesized materials could be observed.

The dispersion of Ru onto the CNTs is around 50% lower compared to the commercial Ru on carbon. This might be caused by the different surface properties of the CNT as they attract mainly acidic Ru species. Interestingly, the metal dispersion increases when Fe is added to the Ru/CNT catalyst but decreases when Cu is added instead. This correlates with the active particle diameter which increases when Cu is

added but decreases when Fe is added. Impregnation of the CNTs with Cu alone results in a very low metal dispersion and large diameter of the active particles. This is due to agglomeration of active Cu during the calcination step in catalyst synthesis.²⁷ Referring to Ru–Cu impregnation, it is assumed that the Cu adds partly to the Ru particles instead of directly to the CNTs. This results in larger particles with lower dispersion, whereas Fe and Ru independently form small particles on the CNT surface leading to a high dispersion and smaller particle size.

The transmission electron microscopy (TEM) micrographs and energy dispersive X-ray (EDX) mapping analysis of the Ru₂Cu₁-catalyst (Fig. 1) show that the catalysts obtained *via* wetness impregnation of the CNT surface with the catalytically active Ru and Cu nanoparticles retain the multiwall-CNT structure, which confirms the successful immobilization on the CNT support (Fig. 1a). EDX mapping analysis shows that all the chemical elements (C – Fig. 1b, Cu – Fig. 1c, Ru – Fig. 1d) are well represented in the material, which indicates a uniform distribution of the nanoparticles on the CNT surface.

The calcined catalysts were further characterised by powder-X-ray-diffraction (PXRD). In the diffractogram of the pure CNTs (Fig. 2a) only the 111 reflection of graphitic carbon is identifiable at 26°. Moreover, a small broad 111 reflection of orthorhombic Fe₂C is observable at 42°. Orthorhombic RuO₂ (Fig. 2b) is clearly identified by its 111 reflection at 28°, the merged 101 and 011 reflections at 35° and the combined 211 and 121 reflection at 55°, which are present in all three catalyst diffractograms. The diffractogram of Ru₁Cu₂ (Fig. 2c) additionally shows reflections for monoclinic CuO; the 002 and –111 reflections merge with the RuO₂ reflection at 35°, but the combined peak for the 111 and 200 reflections at 39° as well as the –222 reflection at 49° and the merged 022 and –311 reflection at 66° serve as clear identifiers. In the Ru₁Fe₂ diffractogram (Fig. 2d) trigonal Fe₂O₃ is identified by its 104 reflection at 33° and 024 reflection at 49°. Overall the PXRD data (complete PXRD data see ESI,† Fig. S1) confirms the presence of metal-oxide crystallites which are reduced to the respective metals prior to glycerol hydrogenolysis by treating the calcined catalysts in a tube furnace with a mixture of 5% H₂/95% N₂ for 8 h at 550 °C. Hereby, the close interaction of the noble Ru with the

Table 1 Textural properties of catalyst materials

Nominal catalyst composition ^a	Total surface area ^b [m ² g ⁻¹]	Metallic surface area ^c [m ² g ⁻¹ sample]	Metal dispersion ^c [%]	Active particle diameter ^c [nm]
Ru ₁ Cu ₂ /CNT	148	2.2	8.3	13.8
Ru ₂ Cu ₁ /CNT	164	1.9	8.9	14.0
Cu/CNT	248	1.1	3.4	30.7
Ru ₁ Fe ₂ /CNT	171	2.2	25.0	5.3
Ru ₂ Fe ₁ /CNT	175	2.3	15.7	8.4
Ru/CNT	182	2.0	11.1	11.9
Ru/C ^d	180	—	19.0	—
CNT	210	—	—	—

^a Determined by ICP-OES. ^b Measured by N₂-physisorption. ^c Determined by CO-chemisorption. ^d Provided by manufacturer.



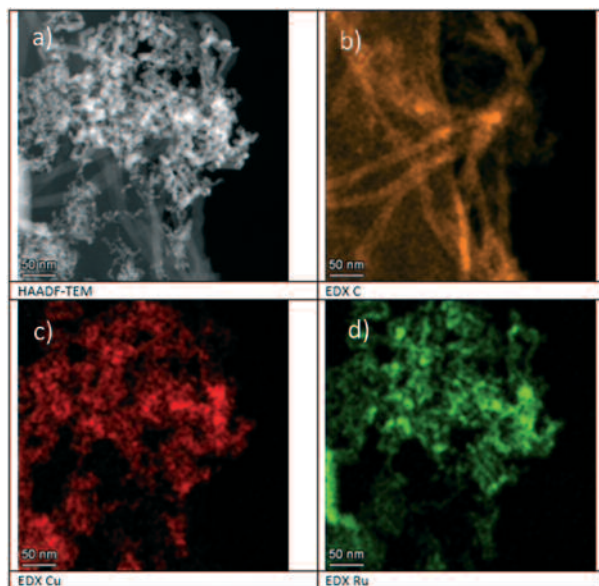


Fig. 1 a) HAADF-TEM image, and EDX elemental mapping images b)–d) of the Ru_2Cu_1 on CNT catalyst. Additional images can be found in the ESI,† Fig. S2–S5.

Fe or Cu inhibits the reduction of Ru and shifted the reduction peaks to higher temperatures. The H_2 -TPR profiles of the as-calcined samples with different metal loadings (see ESI,† Fig. S6) show significant differences between the Cu and Fe added Ru/CNT catalysts. Most significantly, the $\text{Ru}_1\text{Cu}_2/\text{CNT}$ catalyst shows the highest degree of reduction supporting the strong intermetallic effect between Cu and Ru. Furthermore, this is clearly shown by the three times higher reduction capacity of $\text{Ru}_1\text{Cu}_2/\text{CNT}$ compared to the other catalysts (Cu, Ru & Ru_1Fe_2 on CNT) with the same metal loading. This strong surface interaction between Cu and Ru metals was also previously reported using XPS studies by

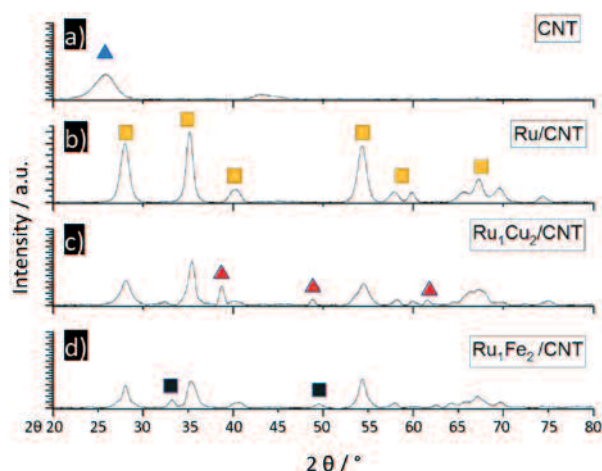


Fig. 2 PXRD-diffractograms of selected catalysts a)–d), measured with $\text{Cu-K}\alpha$ radiation, the blue triangle indicates reflexes for graphitic carbon, the yellow square for RuO_2 , the red triangle for CuO and the black square for Fe_2O_3 .

Jiang *et al.*²⁸ XPS showed shifts in binding energies of the active metal species and an electron transfer from Ru to Cu. This electron transfer leads to an inhibition of the undesired methanation reaction catalysed by Ru through C–C-bond cleavage. Therefore, the Cu-catalysed cleavage of the C–O bond, leading to the preferred 1,2-PD, is promoted.

The predominant product in the catalytic hydrogenolysis experiments was the desired 1,2-propanediol (1,2-PD) with up to 93% selectivity for the bimetallic $\text{Ru}_1\text{Cu}_2/\text{CNT}$ catalyst. Moreover, ethylene glycol (EG) was formed as the main liquid byproduct from initial C–C-bond cleavage with up to 21% using Fe/CNT . Other products in liquid phase were identified as hydroxyacetone (HA), propionic acid (PA) as well as iso- and *n*-propanol (iso-Pr, *n*-Pr), ethanol (EtOH), and methanol (MeOH). In the gas phase, mainly methane (up to 28% for Ru/C) as well as small amounts of ethane, propane and CO_2 were found. The formation of CO_2 in an otherwise reductive environment can be explained by an aqueous phase reforming mechanism.²⁹ Table 2 gives an overview of product selectivity and conversion for each catalyst. Moreover, the carbon balance could be closed to >90% for all catalytic runs showing the high accuracy of the used equipment. HPLC and GC were used to determine the mass balance and the product yields in the liquid and gaseous phases respectively as illustrated in the ESI.†

Control experiments without catalyst show that no glycerol conversion occurs by pure thermal activation. The CNTs themselves show almost no catalytic activity, a minimal conversion was recorded, which might be caused by metallic impurities like Al and Fe stemming from the CNT synthesis. (Characterisation of the CNTs is provided in the ESI.†). The comparison between the commercial Ru on C catalyst and Ru on CNT shows a huge improvement in the selectivity for 1,2-PD from 21 to around 52% accompanied by an increased glycerol conversion from 46% up to 74%, which can only be attributed to the beneficial interplay of the CNT support and the deposited Ru particles. We speculate that aside from a possible promoting effect of the metal impurities (mainly Al) in the CNTs, the CNT surface promotes a beneficial orientation of the metal crystallites on the surface.

The introduction of Fe has been reported to greatly enhance the performance of the Ru catalyst.¹⁸ However in our experiments, the addition of Fe did neither improve the conversion nor the selectivity for 1,2-PD significantly compared to pure Ru on CNT. Nevertheless, it is noteworthy that a larger Fe content (Ru_1Fe_2 on CNT) appears to limit the conversion (49% compared to 78% for Ru_2Fe_1 on CNT) while at the same time slightly increases the selectivity for 1,2-PD (59.5% vs. 44.8%). This might be due to the more efficient C–O bond cleavage caused by the synergistic effects of the resulting RuFe nanoparticles. As stated above, Cu based catalysts have previously shown a good selectivity for the formation of propanediols from glycerol.^{19–23}

A test with pure Cu on CNT shows a very high selectivity (>99%) for 1,2-PD, which is however accompanied by a very low activity (conversion of only 4%).



Table 2 Glycerol hydrogenolysis using different catalysts. Results from Ru/C and without catalyst are averaged over 7 experiments, results for Fe/CNT were taken from literature¹⁷

Catalyst-composition	Conversion [%]	Selectivity [%]											Carbon balance [%]	
		1,2-PD	EG	HA	PA	<i>i</i> -Pr	<i>n</i> -Pr	EtOH	MeOH	CH ₄	C ₂ H ₆	C ₃ H ₈		CO ₂
Ru ₁ Cu ₂ /CNT	18.0	93.4	4.1	0	0.7	0	1.0	0	0	2.5	<1	<1	<0.5	100
Ru ₂ Cu ₁ /CNT	21.2	83.6	5.0	0	2.1	0	1.5	0	0	3.5	<1	<1	<1	99
Cu/CNT	4.2	>99	2.1	<1	2.1	0	0	0	0	0	0	0	1.9	100
Ru ₁ Fe ₂ /CNT	49.1	59.5	9.9	0	4.5	<1	3.8	1.2	0	8.6	1.0	1.8	<1	96
Ru ₂ Fe ₁ /CNT	78.2	44.8	6.4	1.5	8.4	1.5	2.0	1.5	0	8.9	1.7	2.3	2.5	86
Fe/CNT ¹⁷	2.8	64.3	20.9	n.d.	n.d.	n.d.	n.d.	n.d.	n.d.	2.1	n.d.	n.d.	n.d.	n.d.
Ru/CNT	74.4	51.8	6.7	1.8	8.2	1.5	3.1	1.8	0	10.5	2.4	3.7	2.3	96
Ru/C	45.9	20.5	13.2	5.4	0	0	0	<1	1.3	27.7	3.6	2.1	2.4	89
CNT	0.3	0	0	0	0	0	0	0	0	4.5	0	0	0	100
No cat.	0	—	—	—	—	—	—	—	—	—	—	—	—	100

Reaction conditions: 2 g glycerol (10 mL of 20 wt% aqueous solution); catalyst amount = 200 mg; H₂ pressure = 5.0 MPa; T = 200 °C; stirring speed = 1000 rpm. t = 20 h.

As indicated above, pure Cu seems to form nanoparticles separately from the CNTs and therefore does not benefit from the promoting effect of the CNT support. The optimised catalyst system therefore contains both, Ru and Cu and provides very high selectivity for the desired product (up to 93%) as well as moderate catalyst activity (up to 21%). We have observed the highest selectivity with a catalyst of the composition 5% Ru₁Cu₂ on CNT (93.4%) while the catalyst with the composition 5% Ru₂Cu₁ on CNT provides a marginally higher conversion rate (21%) with a slightly lower selectivity for 1,2-PD (84%). Additionally, the active particle size for the pure Cu catalyst is comparatively large with around 31 nm while the metallic surface area is the lowest with only 1.1 m² g⁻¹ sample (Table 1). In contrast, the bimetallic Ru–Cu catalysts have well distributed metal nanocrystallites (confirmed by TEM pictures as well as EDX elemental mapping) with a metallic surface area similar to the bimetallic Ru–Fe catalysts of around 2 m² g⁻¹ sample. The larger active particle size and thereby lower dispersion of the Ru–Cu catalysts are probably the reason for the lower activity (conversion). The direct correlation between Cu content and selectivity for 1,2-PD indicates that the preference for C–O bond cleavage is an inherent property of the Cu particles. Future improvements in the catalyst synthesis procedure might improve the particle size and dispersion. Moreover, in combination with optimisation of the reaction parameters, high conversion can likely be achieved while maintaining the very high selectivity to the desired 1,2-PD.

To sum up, adding Cu to Ru nanoparticles dispersed on a CNT support by employing an improved wetness impregnation method significantly enhances the reducibility and modified the surface of the resulting Ru–Cu species. Hereby, the chemical composition of the resulting bimetallic Ru–Cu catalyst as well as the surface interaction between Cu and Ru led to a promoting effect resulting in a preference for C–O bond cleavage promoted by Cu over C–C bond cleavage catalysed by small Ru nanoparticles. By employing this catalyst for the hydrogenolysis of glycerol a superior 1,2-PD selectivity of 93.4% was achieved.

Conflicts of interest

There are no conflicts of interest to declare.

Notes and references

- 1 D. Voß, H. Pickel and J. Albert, *ACS Sustainable Chem. Eng.*, 2019, 7, 9754–9762.
- 2 S. Sandesh, P. Manjunathan, A. B. Halgeri and G. V. Shanbhag, *RSC Adv.*, 2015, 5, 104354–104362.
- 3 B. N. Zope, D. D. Hibbitts, M. Neurock and R. J. Davis, *Science*, 2010, 330, 74–78.
- 4 A. Corma, S. Iborra and A. Velty, *Chem. Rev.*, 2007, 107, 2411–2502.
- 5 D. Sun, Y. Yamada, S. Sato and W. Ueda, *Appl. Catal., B*, 2016, 193, 75–92.
- 6 A. M. Ruppert, K. Weinberg and R. Palkovits, *Angew. Chem., Int. Ed.*, 2012, 51, 2564–2601.
- 7 D. M. Alonso, S. G. Wettstein and J. A. Dumesic, *Chem. Soc. Rev.*, 2012, 41, 8075–8098.
- 8 Y. Wang, J. Zhou and X. Guo, *RSC Adv.*, 2015, 5, 74611–74628.
- 9 J. ten Dam and U. Hanefeld, *ChemSusChem*, 2011, 4, 1017–1034.
- 10 T. Miyazawa, Y. Kusunoki, K. Kunimori and K. Tomishige, *J. Catal.*, 2006, 240, 213–221.
- 11 W. Oberhauser, C. Evangelisti, R. P. Jumde, R. Psaro, F. Vizza, M. Bevilacqua, J. Filippi, B. F. Machado and P. Serp, *J. Catal.*, 2015, 325, 111–117.
- 12 A. Modvig, C. Kumpidit, A. Riisager and J. Albert, *Materials*, 2019, 12, 2175.
- 13 H. Zhao, L. Zheng, X. Li, P. Chen and Z. Hou, *Catal. Today*, 2020, 355, 84–95.
- 14 Y. Nakagawa and K. Tomishige, *Catal. Sci. Technol.*, 2011, 1, 179–190.
- 15 E. Maris and R. Davis, *J. Catal.*, 2007, 249, 328–337.
- 16 Z. Huang, F. Cui, H. Kang, J. Chen and C. Xia, *Appl. Catal., A*, 2009, 366, 288–298.
- 17 Z. Wu, Y. Mao, X. Wang and M. Zhang, *Green Chem.*, 2011, 13, 1311–1316.



- 18 B. Li, J. Wang, Y. Yuan, H. Ariga, S. Takakusagi and K. Asakura, *ACS Catal.*, 2011, **1**, 1521–1528.
- 19 C. Wang, H. Jiang, C. Chen, R. Chen and W. Xing, *Chem. Eng. J.*, 2015, **264**, 344–350.
- 20 Y. Du, C. Wang, H. Jiang, C. Chen and R. Chen, *J. Ind. Eng. Chem.*, 2016, **35**, 262–267.
- 21 C. Liu, C. Zhang, S. Hao, S. Sun, K. Liu, J. Xu, Y. Zhu and Y. Li, *Catal. Today*, 2016, **261**, 116–127.
- 22 S. Zhu, X. Gao, Y. Zhu, Y. Zhu, H. Zheng and Y. Li, *J. Catal.*, 2013, **303**, 70–79.
- 23 M. Balaraju, K. Jagadeeswaraiyah, P. S. S. Prasad and N. Lingaiah, *Catal. Sci. Technol.*, 2012, **2**, 1967–1976.
- 24 J. Zhou, L. Guo, X. Guo, J. Mao and S. Zhang, *Green Chem.*, 2010, **12**, 1835–1843.
- 25 A. N. Ardila, M. A. Sánchez-Castillo, T. A. Zepeda, A. L. Villa and G. A. Fuentes, *Appl. Catal., B*, 2017, **219**, 658–671.
- 26 C. Montassier, D. Giraud and J. Barbier, in *Studies in Surface Science and Catalysis*, Elsevier, 1988, vol. 41, pp. 165–170.
- 27 S. Zhu, X. Gao, Y. Zhu, W. Fan, J. Wang and Y. Li, *Catal. Sci. Technol.*, 2015, **5**, 1169–1180.
- 28 T. Jiang, Y. Zhou, S. Liang, H. Liu and B. Han, *Green Chem.*, 2009, **11**, 1000–1006.
- 29 M. Checa, S. Nogales-Delgado, V. Montes and J. M. Encinar, *Catalysts*, 2020, **10**, 1279.



Unpublished part of the dissertation

Part III: Hydroprocessing of lignin

In part I and part II, catalytic hydroprocessing of furans, derived from cellulose and hemicellulose, and glycerol, derived from fats and oils, were presented, respectively. Part III* focuses on catalytic hydroprocessing of lignin into aromatic monomers under mild reaction conditions and contains one chapter (chapter 6).

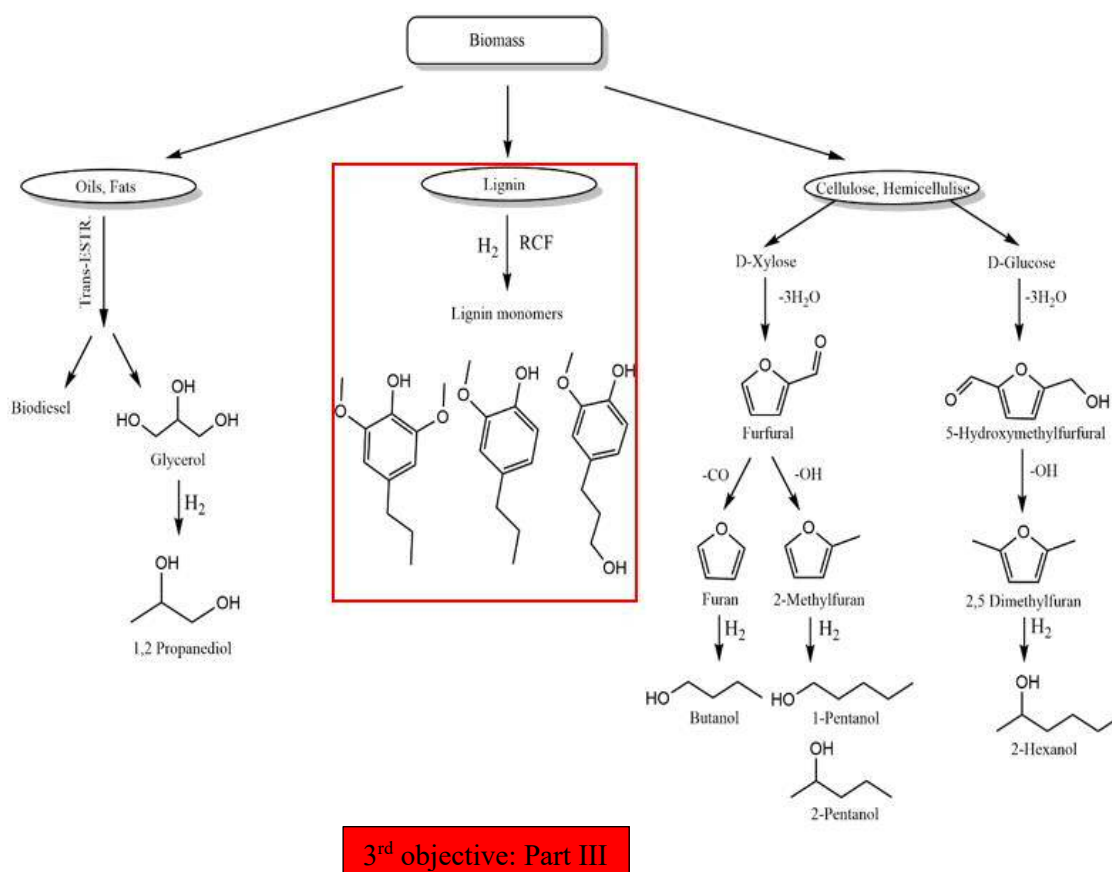


Figure 1.3 Scope of the thesis: 3rd objective (hydroprocessing of lignin)

* The experimental work included in Part III was a collaborative effort between the TMC Institute at the University of Hamburg and the IUE Institute at Hamburg University of Technology. The research is still ongoing and will be extended and published soon.

Chapter 6. Reductive catalytic fractionation for lignin valorization into aromatic monomers under mild reaction conditions

6.1. Introduction

Presently, the acquisition of aromatics is predominantly reliant on fossil raw materials [229]. In order to reduce the dependence on fossil resources, extensive scientific investigations focus on lignin as a renewable raw material for aromatic production. Various methodologies have been formulated for lignin valorization. These approaches are encompassed within the framework of "lignin-first" strategies [230], that avoid formation of technical lignin. Among these strategies, reductive catalytic fractionation (RCF) emerges as a noteworthy approach.

Figure 6.1 illustrates RCF, where lignocellulosic biomass is fractionated in an organic solvent (e.g. methanol or ethanol) at high temperatures (e.g. 200-250 °C) and pressures (e.g. 20-60 bar). Under these conditions, biomass undergoes solvolysis reactions, leading to the liberation of lignin fragments and monomers through the cleavage of ether bonds [188]. To preclude the recombination of these fragmented constituents hydrogen gas, often supplemented by a hydrogenation catalyst, are introduced, enabling the catalytic reduction of unsaturated double bonds, which ensures the stabilization of reactive lignin fragments [173].

Extensive investigations have already been conducted on RCF of diverse lignocellulosic biomass, encompassing a wide range of hardwoods such as birch and poplar [177, 231], softwoods like pine and spruce [192, 232], and herbaceous biomass such as corn stover and miscanthus [185, 233]. Notably, there is a dearth of research on RCF applied to biologically treated feedstock, such as digestates, which will serve as a focal point of investigation in the current work.

Digestates exhibit potential as a lignin-first substrate, primarily due to the partial degradation of various organic constituents (including fats, soluble sugars, hemicellulose, and cellulose) within the biomass during fermentation, which might result in an accumulation of lignin within the digestate. Therefore, the aim of this chapter was to investigate the applicability of straw digestates as a lignin first substrate in RCF. Furthermore, it aimed to investigate the impact of distinct catalysts, feedstock pretreatments, and operational parameters including time and H₂ pressure on the production and selectivity of aromatic monomers during RCF of digestates.

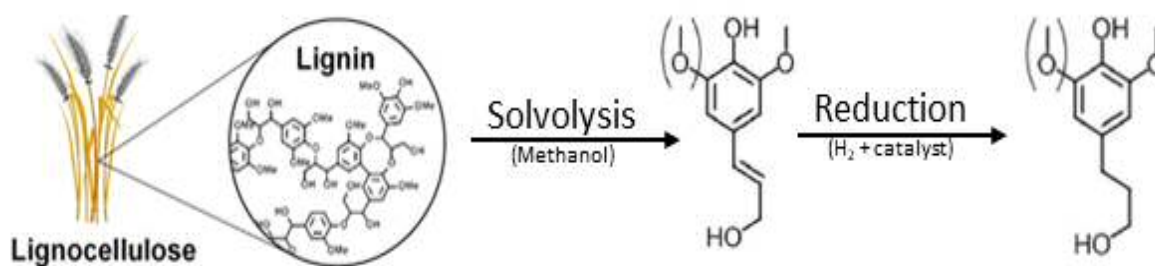


Figure 6.1 Main reaction steps involved in RCF of lignocellulosic biomass.

6.2. Experimental

6.2.1. Materials

In this study, various substrates were tested, namely beech wood, lab digestate, and industrial straw digestate. The industrial straw digestate refers to the solid fraction that remains after solid-liquid separation of the slurry leaving the fermenter. The beech wood chips, specifically "Räuchergold HBK 750-2000," were sourced from J. RETTENMAIER & SÖHNE GmbH + Co KG in Rosenberg, Germany. The rye straw, rye straw lab digestate, and industrial straw digestate were obtained from Verbio Vereinigte BioEnergie AG in Leipzig, Germany. Methanol (99+%) was purchased from Sigma Aldrich in Munich, Germany. Catalysts used include 5 wt.% Ru/C, 5 wt.% Pt/C, 5 wt.% Ru/Al₂O₃, and 5 wt.% Pt/Al₂O₃ which were purchased from Sigma Aldrich. 20 wt.% Ni/C and 20 wt.% Ni/Al₂O₃ were purchased from Riogen, Inc., New Jersey, USA, and 54 wt.% NiO/SiO₂-Al₂O₃ (NiSat) was purchased from Clariant specialty chemicals. All chemicals were used as received without any purification.

6.2.2. Substrate pre-treatment

To achieve a particle size below 1 mm, all biomasses were dry milled using a cutting mill (MF 10, IKA, Germany). In order to examine the impact of pre-treatment on industrial digestate, it underwent washing and alkaline treatment, as depicted in the following procedure. Beech wood was subjected to alkaline treatment as well for comparison purposes.

Washing

The digestate sample was subjected to drying in a convection oven maintained at a temperature of 45 °C. The residual straw digestate underwent a meticulous washing procedure with tap water, followed by multiple pressings using a hydraulic press (40 L, Speidel, Germany) until a visually transparent effluent was obtained. Subsequently, the obtained solids, known as washed industrial digestate, were dried in a convection oven set at 45 °C to ensure moisture removal. All straw and digestates utilized in this study underwent a washing process prior to being employed as a substrate in RCF, unless stated otherwise.

Alkaline treatment

A total of 0.4 g of biomass was combined with 20 mL of 1 M sodium hydroxide solution. The mixture was then placed in a dark environment and incubated for 24 hours at a temperature of 30 °C, with continuous shaking at a rate of 100 min⁻¹. To prevent oxidative degradation of the released phenolic acids, 50 mL centrifuge tubes were employed and purged with argon gas before sealing. To terminate the treatment, the samples were transferred to a water bath set at 4 °C. Subsequently, depending on the type of sample to be recovered, two distinct procedures were followed.

Procedure 1: To isolate the alkaline-insoluble residue resulting from the alkaline treatment, centrifugation was carried out at 4776×g for 20 minutes. The supernatant was discarded, and the remaining solids underwent two rounds of washing. Each washing step involved adding 40 mL of demineralized water, followed by centrifugation at 4776×g for 20 minutes.

Procedure 2: To recover the acid-insoluble residue following the alkaline treatment, 32 wt.% hydrochloric acid was added to adjust the pH to approximately 1. The mixture was

refrigerated overnight to induce the precipitation of dissolved lignin and hemicellulose. Subsequently, centrifugation was conducted at $4776\times g$ for 20 minutes. The supernatant was discarded, and the remaining solids underwent two cycles of washing, as previously mentioned in Procedure 1. For both procedures, the remaining samples were dried at $105\text{ }^{\circ}\text{C}$.

6.2.3. Catalytic experiments

The RCF reactions were performed in a batch reactor (10-fold hydrogen plant setup with 21 ml stainless-steel 1.4571 vessels equipped with magnetic stirring) mounted on a heating block on top of a stirrer (see Figure 6.2 and Figure 6.3). The reactors were filled with 7.93 ml of methanol as a solvent, 250 mg of substrates (beech wood, straw, lab digestate, or industrial digestate), and 50 mg of catalyst. The reactors were completely sealed and purged with N_2 three times. After that, a pressure test was conducted by filling 60 bar of N_2 for one hour. Following the pressure test, the reactors were purged with hydrogen gas two to three times before initiating the reaction. The system was then purged two times with H_2 and filled at room temperature with $2/3$ of the amount of H_2 pressure required. The reactors were heated to the final temperature of $200\text{ }^{\circ}\text{C}$, and then the pressure was adjusted to the desired H_2 pressure. In the case of performing reactions under very small H_2 pressures, the reactors were filled with the theoretical amount of H_2 that is equivalent to the required pressure at $200\text{ }^{\circ}\text{C}$. The stirrer speed was set to 300 rpm during the heating phase, after which the reaction was initiated by vigorous stirring at 1000 rpm. Hydrogen was pressurized between 5-50 bars for pressure studies, typically set to 50 bars at 200°C . The reaction time (t) ranged from 30 minutes to 48 hours, typically lasting 24 hours. After the reaction time, the stirrer speed was reduced to 300 rpm, and the heating block was let to be cooled to room temperature. Once the reactor had completely cooled down, the pressure was released by collecting the gas phase for GC analysis, (see Table S2 in SI section 10.7), and the exhaust gas was released through the outlet vent. The reactor was then purged three times with N_2 before being opened. The contents of the reactor were then collected by filtering to separate the solid residue (pulp and catalyst) from the liquid product mixture. The liquid phase was then analyzed using GC-MS.



Figure 6.2 Ten-fold parallel reaction system used for hydroprocessing reactions.

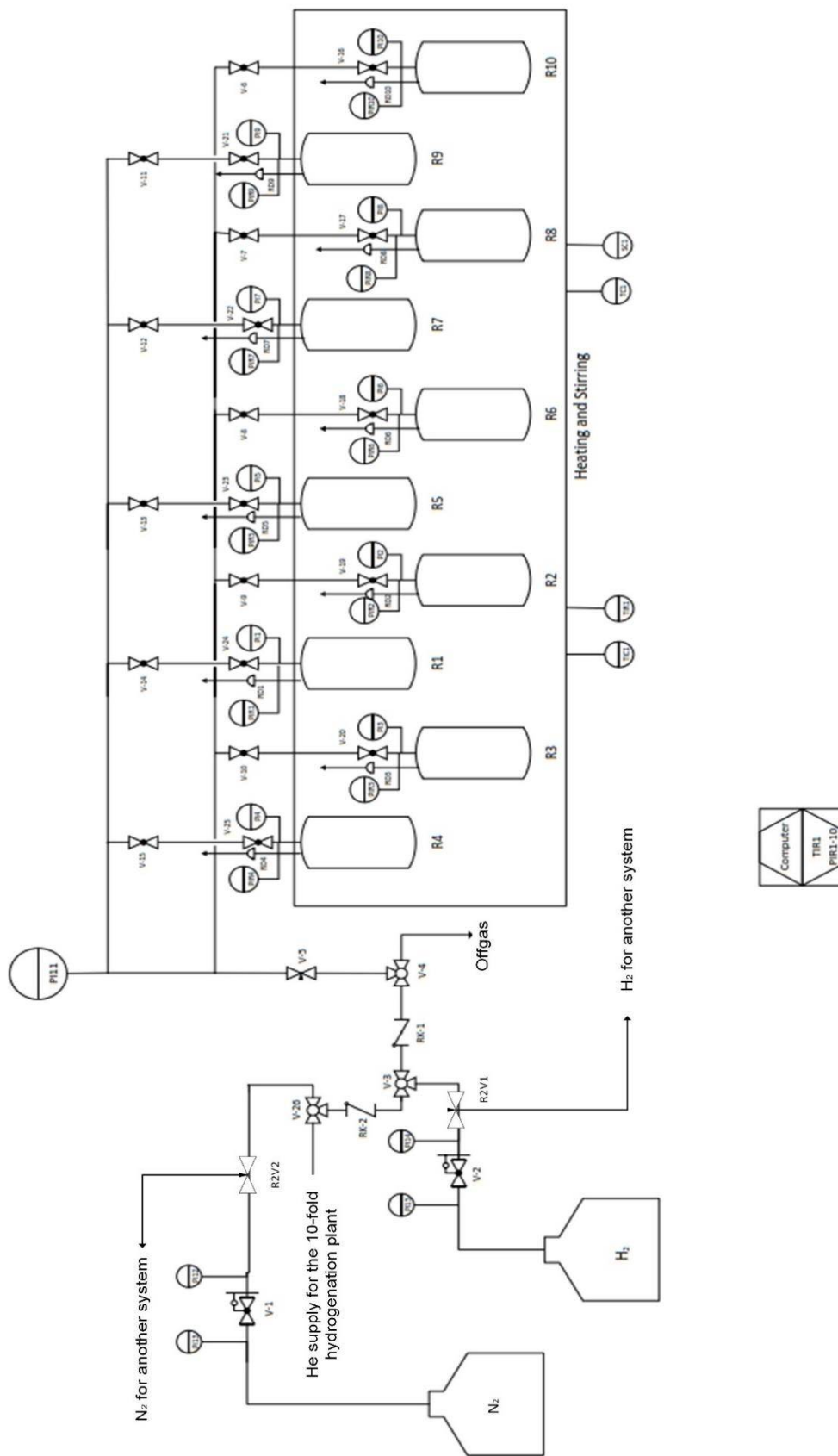

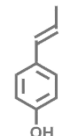
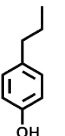
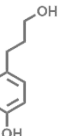
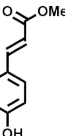
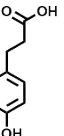
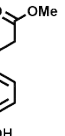
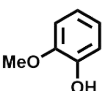
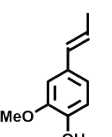
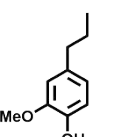
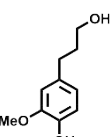
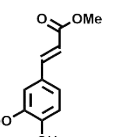
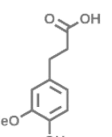
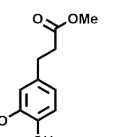
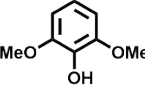
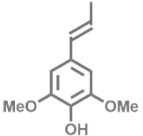
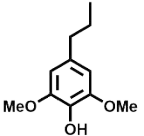
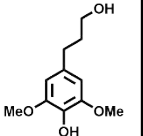
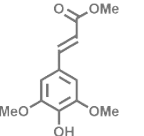
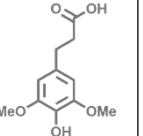
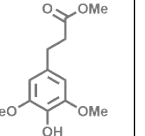


Figure 6.3 P&I Diagram for 10-fold parallel reaction system used for hydroprocessing reactions.

6.2.4. Product analysis

Through RCF, the lignin fraction of biomass undergoes depolymerization, resulting in the production of an oil comprising monomers and oligomers. In this chapter, the focus was specifically on characterizing the monomer fraction of the oil, as it contains the most valuable products. Table 6.1 presents all monomers that can be obtained through RCF of biomass substrates, which can be directly associated with the three fundamental building blocks of lignin: coniferyl alcohol, sinapyl alcohol, and para-coumaryl alcohol. They exhibit variations in terms of the basic aromatic building block, which can be either H (with a single OH-group), G (with one hydroxyl and one methoxy group), or S (with one hydroxyl and two methoxy groups). Furthermore, they differ in the presence of unsaturated C-C double bonds in the aliphatic side chain and the presence of an OH-group at the γ -position of the aliphatic side chain. In addition to the conventional alcoholic monolignols, the lignin polymer also includes phenolic acids. During the RCF process using methanol, these phenolic acids are predominantly obtained in the form of methyl esters. Key products detected from RCF in our investigations include: 4-propylphenol (HP), 4-propyl guaiacol (GP), 4-propyl syringol (SP), 4-propanol guaiacol (GPOH), 4-propanol syringol (SPOH), hydroxy-benzenepropanoic acid methyl ester (HPaMe), 3-(4-hydroxyphenyl)-2-propenoic acid methyl ester (HPeaMe), 3-(4-hydroxy-3-methoxyphenyl)-propanoic acid methyl ester (GPaME), and 3-(4-hydroxy-3-methoxyphenyl)-2-propenoic acid methyl ester (GPeaMe).

Table 6.1 Typical monomers obtained from RCF*.

Basic aryl group	Aliphatic side chain					
	Derived from alcoholic monolignols			Derived from phenolic acids		
	-propen	-propane	-propanol	-propenoic acid methyl ester	-propanoic acid	-propanoic acid methyl ester
 H-	 HPe (not calib.)	 HP (calib.)	 HPOH (not calib.)	 HPeaMe (calib.)	 HPa (calib.)	 HPaMe (calib.)
 G-	 GPe (calib.)	 GP (calib.)	 GPOH (calib.)	 GPeaMe (calib.)	 GPa (not calib.)	 GPaMe (calib.)
 S-	 SPe (not calib.)	 SP (calib.)	 SPOH (calib.)	 SPeMe (not calib.)	 SPa (not calib.)	 SPaMe (not calib.)

* Only the compounds in black were quantitatively measured using GC-MS.

GC-MS analysis

The liquid phase obtained from the RCF process was subjected to analysis using a GC Agilent system 6890 coupled with an Agilent 5975C mass spectrometer. The system was equipped with an OPTIMA 5-MS capillary column from MACHERY-NAGEL, which had dimensions of 30 m length, 0.25 mm inner diameter, and 0.25 μm film thickness. Helium was employed as the carrier gas. To ensure accurate quantification, a known quantity of the internal standard (isopropyl phenol) was added to the liquid sample containing the monomers. Subsequently, the reaction mixture was diluted with methanol. The GC program employed the following conditions: an initial oven temperature of 50 °C was maintained for 2 minutes, followed by a heating rate of 15 °C/min up to 150 °C. From there, the temperature was increased at a rate of 10 °C/min to reach 220 °C, and then further increased at a rate of 15 °C/min until reaching 250 °C, where it was held for additional 3 minutes. The inlet temperature was set to 250 °C, and a split mode with a split ratio of 25:1 was employed, maintaining a constant column flow of 1 mL/min.

GC analysis for gas phase

The gaseous samples were subjected to analysis using a Varian GC 450-TCD-FID system, which was equipped with a Shin Carbon ST column (2m x 0.75mm internal diameter). The sample was injected into the system using a gas bag and transported through the column with argon serving as the mobile phase at a pressure of 4.82 bar. The column oven was programmed to follow a specific temperature program, which consisted of an initial temperature of 40°C maintained for 1.5 minutes. Subsequently, the temperature was increased at a rate of 18°C per minute until reaching 250°C, where it was held for 12 minutes.

6.2.5. Calculations:

Monomer yield (Y) was calculated based on lignin-basis in (wt. %), as follows:

$$Y = \frac{\sum_i m_i}{m_{\text{biomass,dry}}(\text{g}) * \text{lignin content}_{\text{biomass}}}$$

m_i = weight of each monomer released as being calculated using GC-MS in (g)

For comparison reasons, three shares (in mol.%) were used through our investigations, and can be defined as follows:

- 1) Share of S-monomers share:

$$\text{S-monomers} = \frac{n_{SP} + n_{SPOH}}{n_{SP} + n_{SPOH} + n_{GP} + n_{GPOH}}$$

- 2) Share of γ -OH-monomers:

$$\gamma\text{-OH-monomers} = \frac{n_{GPOH} + n_{SPOH}}{n_{SP} + n_{SPOH} + n_{GP} + n_{GPOH}}$$

- 3) Share of phenolic acid monomers:

$$\text{Phen. acid monomers} = \frac{n_{HPeMe} + n_{HPaMe} + n_{GPeMe} + n_{GPaMe}}{n_{HPeMe} + n_{HPaMe} + n_{GPeMe} + n_{GPaMe} + n_{SP} + n_{SPOH} + n_{GP} + n_{GPOH}}$$

n_i = number of moles released for each monomer after RCF

6.3. Results and discussion

6.3.1. Substrate composition

This study utilized various biomass for investigation. Apart from beech wood, which is a well-studied substrate for RCF, rye straw and a solid digestate obtained after anaerobic digestion of rye straw in lab-scale (rye straw digestate) were also employed. Additionally, a digestate from an industrial straw mono-fermentation plant was used as a substrate for comparison. For a first evaluation of the suitability of the straw and its digestates as RCF substrates, compositional analysis of lignin content, along with CHNS analysis, were conducted as outlined in the Supplementary information (section 10.7). These results were then compared to those of the typical RCF substrate, beech wood. According to Table 6.2, rye straw exhibited a low lignin content of 15.2%, whereas the digestates showed high lignin contents of 28.3% and 25.6%, respectively, which are similar to or even higher than that of beech wood (24.6%). This indicates the accumulation of lignin in the digestates resulting from straw fermentation, suggesting a higher degradation of carbohydrates than lignin during fermentation.

Table 6.2: Lignin content of all biomasses that were used as substrates for RCF.

	Beech wood	Rye straw	Washed rye straw digestate	Washed industrial straw digestate
	in wt.% (based on dry mass)			
Lignin content	24.6 ± 0.5	15.2 ± 0.2	28.3 ± 0.2	25.6 ± 0.4

The CHNS compositional analysis results comparing straw and its digestates to beech wood are presented in Table 6.3. The carbon content of the two digestates was found to be (46.7% and 47.6%), which is comparable to the carbon content of beech wood (48.5%). Only rye straw exhibited a slightly lower carbon content of 44.5%. The nitrogen, hydrogen, and sulfur contents were also similar for all four biomasses.

Table 6.3 CHNS analysis of all biomasses that were used as substrates for RCF.

	N %	C %	H %	S %
Beech wood	0.8	48.5	6.3	< 0.2
Rye straw	0.8	44.5	6.0	< 0.2
Washed rye straw digestate	1.8	46.7	6.1	0.3
Washed industrial straw digestate	0.7	47.6	6.4	< 0.2

The results of the compositional analysis presented in both Table 6.2 and Table 6.3 confirm that the two straw digestates exhibit similar CHNS composition and lignin content to the typical RCF substrate, beech wood. This indicates that the straw digestate has the potential to be a promising substrate for RCF as well.

6.3.2. Catalyst screening:

The objective of this investigation was to evaluate various commercial catalysts with different metal sites and supports, aiming to identify a suitable catalyst for RCF that produces

high monomer yields (Y) and exhibits enhanced selectivity towards propanol-substituted phenols (γ -OH-monomers). These γ -OH-monomers, characterized by their functional groups, hold significant appeal for the chemical industry, as OH-functionalities are often essential in the production of polymers [182]. Throughout this series of catalyst screening experiments, beech wood, a commonly used substrate for RCF, was employed as a substrate.

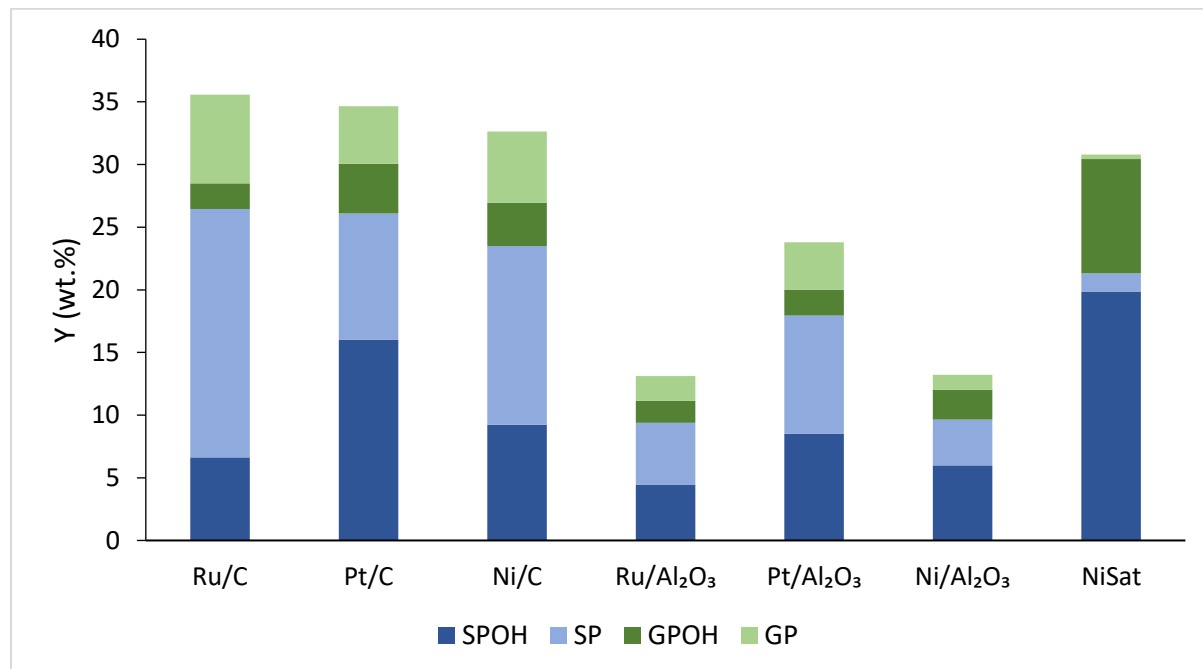


Figure 6.4 Monomer yields for RCF of beech wood with different catalysts. Reaction conditions: 10 mL methanol, 250 mg beech wood, 50 mg catalyst, $T=200\text{ }^{\circ}\text{C}$, $P=50\text{ bars H}_2$, $t=24\text{ h}$.

Figure 6.4 presents a comparison of the total monomer yield generated using different catalysts, including Ru/C, Pt/C, Ni/C, Ru/Al₂O₃, Pt/Al₂O₃, Ni/Al₂O₃, and NiSat. In general, for the same active element with the same metal loading (5 wt.%), higher monomer yields were obtained using C-supported catalysts than alumina (Al₂O₃) supported catalysts. The monomer yields using Ru/C, Pt/C and Ni/C were 35.7 %, 34.7 %, 32.7 %, respectively. On the other hand, Ru/Al₂O₃, Pt/Al₂O₃, Ni/Al₂O₃ produced yields of 13.9 %, 24.2 %, 13.5 %, respectively. This is attributed to the higher acidity of Al₂O₃ support, which enhances repolymerization of monomers through favoring C-C and C-O bonds formation, as reported by Lan et al. [152]. A similar trend was observed by Renders et al., where for all investigated noble metals (Ru, Pd, Pt, Rh), the alumina catalysts exhibited lower lignin monomer yields compared to their carbon-supported analogues [231]. Renders et al. detected a higher amount of a high molecular weight fraction in the lignin oils from the Al₂O₃-based catalysts. This high molecular weight fraction could also be explained by repolymerization reactions that became more pronounced due to higher acidity of the alumina support.

Regardless of support and with the same metal loading (5 wt.%), the active metal site appeared to play a vital role in determining γ -OH-monomers yield. Among the metal supported catalysts, Pt showed higher γ -OH-monomers yields followed by Ni and Ru. For instance, the γ -OH-monomers yield of Pt/C, Ni/C, Ru/C were 20%, 12.7%, 8.6 %, respectively. Similarly, when supported on Al₂O₃, the yields of γ -OH-monomers were 10.6 %, 8.4 %, 6.2 % for Pt/Al₂O₃, Ni/ Al₂O₃, Ru/ Al₂O₃, respectively.

NiSat is an industrial metal oxide supported catalyst with a higher metal content of 54 wt.%, which makes it different from the other tested metal supported catalysts. It also showed high monomer yield of (30.8 %), which is slightly less than the carbon supported metal catalysts and largely higher than the alumina supported metal catalysts. Additionally, it showed the highest selectivity towards the γ -OH-monomers with a γ -OH-monomer yield of 29 wt.% and a γ -OH monomers share of 93.7 mol.%. Therefore, it was chosen for further investigation in the substrate screening (section 6.3.3). NiSat produced monomers containing aliphatic OH-groups, whereas Ni/C and Ru/C produced monomers without aliphatic OH-groups. The specific reasons for this observation were not further investigated, but it could be attributed to either the higher Ni content in NiSat (54 wt.%) or the lower ability of the NiSat in hydrogenolysis of the C-O bond. Similarly, in another study conducted by Van den Bosch et al., it was observed that Pd/C resulted in significantly higher amounts of monomers with aliphatic OH-groups compared to Ru/C. This difference was attributed to the higher C-O hydrogenolysis activity of Ru in comparison with Pd [182].

In the absence of a hydrogenation catalyst, primarily unsaturated monomers were released, yielding only about 0.25 wt.% (Table S1 section 10.7). This emphasizes the critical role of the catalyst in RCF. Similarly, when only the supports without any active element were added, very low yields of 0.31 wt.% for alumina and 2 wt.% for carbon were observed (Table S1 section 10.7).

6.3.3. Substrate screening:

The objective of this investigation was to evaluate the suitability of straw and its digestates for the RCF and to compare their performance with the traditional beech wood substrate. NiSat was selected as a catalyst for this comparison, and the reactions were conducted under the following conditions: 10 mL of methanol as a solvent, 250 mg of substrate, 50 mg of NiSat, a reaction temperature of 200 °C, 50 bar H₂ pressure and a reaction time of 24 hours. Figure 6.5 illustrates the comparison of monomer yields obtained from straw, its digestates, and beech wood substrates.

According to Figure 6.5, straw and straw digestates showed a product distribution typical for herbaceous substrates. As a result, certain products derived from phenolic acids and obtained as methyl esters such as HPaMe and GPaMe were detected. The findings indicate that straw and its digestates yielded lower but comparable amounts of total monomers compared to beech wood. This difference in yield is attributed to the higher complexity of the lignin structure in herbaceous materials compared to beech wood. Specifically, when using the NiSat catalyst, beech wood yielded 31 wt.%, while rye straw, rye straw digestate, and industrial straw digestate produced yields of 25 wt.%, 18 wt.%, and 21 wt.%, respectively.

Additionally, rye straw produced a greater total monomer yield per (g) of lignin compared to its digestates. This strongly suggests that lignin degradation or structural changes occur during the fermentation and processing of straw. This degradation primarily impacts hydroxycinnamates or phenolic acids incorporated into the lignin structure rather than the alcoholic monolignols, as shown in Table 6.4. When subjecting rye straw to RCF, a yield of 15.9 wt.% monomers derived from alcoholic monolignols was obtained. RCF of digestates resulted in yields of 13.8 wt.% for rye straw digestate and 15.4 wt.% for industrial digestate, showing comparable outcomes. In contrast, RCF of rye straw produced a higher yield of

9.4 wt.% monomers derived from phenolic acids, nearly twice the amount obtained when rye straw digestate (4.4 wt.%) and industrial digestate (5.3 wt.%) were used as substrates. This highlights the differential impact of the degradation on the various components of lignin.

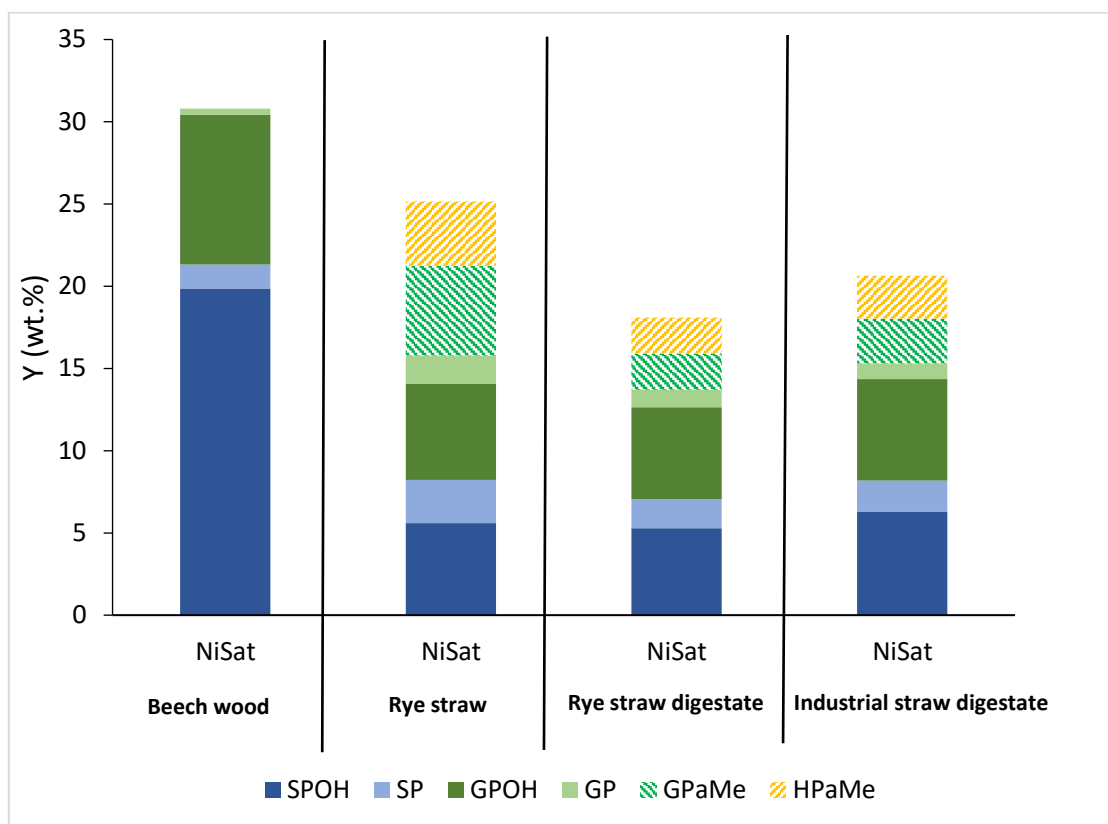


Figure 6.5 Monomer yields for RCF of rye straw, rye straw digestate or industrial straw digestate under reaction conditions of 10 mL methanol, 250 mg substrate, 50 mg NiSat, T= 200 °C, P=50 bars H₂, and t= 24 h.

Table 6.4 Monomer yields derived from alcoholic monolignols and phenolic acids incorporated in lignin structure during RCF of straw and its digestates

	Monomers yield derived from alcoholic monolignols (wt.%)	Monomers yield derived from phenolic acids (wt.%)
Rye straw	15.9	9.4
Rye straw digestate	13.8	4.4
Industrial straw digestate	15.3	5.3

*Reaction conditions of 10 mL methanol, 250 mg substrate, 50 mg NiSat, T= 200 °C, P=50 bars H₂, t= 24 h.

6.3.4. Investigating the impact of substrate pretreatment and changing the reaction conditions on the RCF of industrial digestate

These investigations focused on assessing the influence of substrate pretreatment, reaction time, and H₂ pressure on RCF of straw digestate. As a promising substrate for RCF, the industrial straw digestate, which represents a by-product of straw fermentation, was selected. For comparison purposes, alkaline-pretreatment investigations were performed on beech wood as well. NiSat was selected as a catalyst for these investigations due to its ability to yield high monomer outputs, along with its selectivity towards monomers containing aliphatic OH-groups.

6.3.4.1. Effect of pretreatment

The objective of this investigation was to examine the impact of two different types of pretreatment steps on the monomer yield obtained from RCF of industrial digestate, employing the NiSat catalyst.

1) Effect of washing digestate fibers

Table 6.5 compares the results of washed and unwashed industrial straw digestates utilized for RCF using the NiSat catalyst. The washed industrial digestate underwent a thorough washing process using tap water, as outlined in section 6.2.2, until a completely clear effluent was achieved. The washing process was found to have a substantial impact on the yields of monomers, resulting in 21 wt.% monomer yield, and also on γ -OH monomers share, reaching 80.5 mol.%. In contrast, the unwashed industrial straw digestate yielded approximately 10 wt.% monomers and had a γ -OH monomer share of 56 mol.%. This significant improvement in monomer yields and γ -OH monomer share after washing can be attributed to the removal of impurities such as minerals, ammonia, and microorganisms present in the digestate. These impurities persist in the digestate even after separating the digestate fibers from the liquid phase through decantation following the anaerobic digestion of straw in industry [14].

Table 6.5 Monomer yields produced from RCF of washed and unwashed industrial straw digestate using NiSat catalyst.

	HP	GP	SP	GPOH	SPOH	GPaMe	HPaMe	Monomer yield (wt.%)
Washed industrial straw digestate	0.03	0.95	1.9	6.18	6.28	2.72	2.6	20.7
Unwashed industrial straw digestate	0.024	0.92	1.72	1.53	2.17	2.23	1.76	10.4

*Reaction conditions of 10 mL methanol, 250 mg substrate, 50 mg NiSat, T= 200 °C, P=50 bars H₂, t= 24 h.

2) Effect of alkaline pretreatment

Figure 6.6 presents a comparative analysis of monomer yields obtained from RCF of untreated industrial straw digestate, the alkaline insoluble residue, and the acid insoluble residue. The acid insoluble residue was obtained by subjecting the alkaline-treated digestate to a rapid pH reduction to approximately pH~1 after the alkaline treatment. The untreated industrial digestate produced a monomer yield of 21 wt.%. In contrast, the alkaline insoluble residue, which represents the portion of the digestate's lignin that remains insoluble after alkaline treatment, exhibited a significantly lower monomer yield of only 2.7 wt.%. However, after precipitating the alkali-soluble lignin using acid as described in section 6.2.2, the monomer yield produced from RCF remarkably increased to 19 wt.%. This observation confirms that the lignin present in the industrial straw digestate is predominantly alkaline-soluble, as evidenced by the limited amount of lignin-derived monomers obtained from RCF of the alkaline insoluble residue.

Figure 6.7, on the other hand, focuses on beech wood lignin and illustrates that a substantial portion of it is alkaline-insoluble parts. Consequently, the alkaline-insoluble residue from

beech wood produced a considerable amount of lignin monomers, approximately 19 wt.%. In comparison, the untreated beech wood produced a higher monomer yield of 30.8 wt.%. As observed with the industrial digestate, the precipitation of alkali-soluble beech wood lignin led to an increase in lignin monomer yield, from 19 wt.% to 28.5 wt.%.

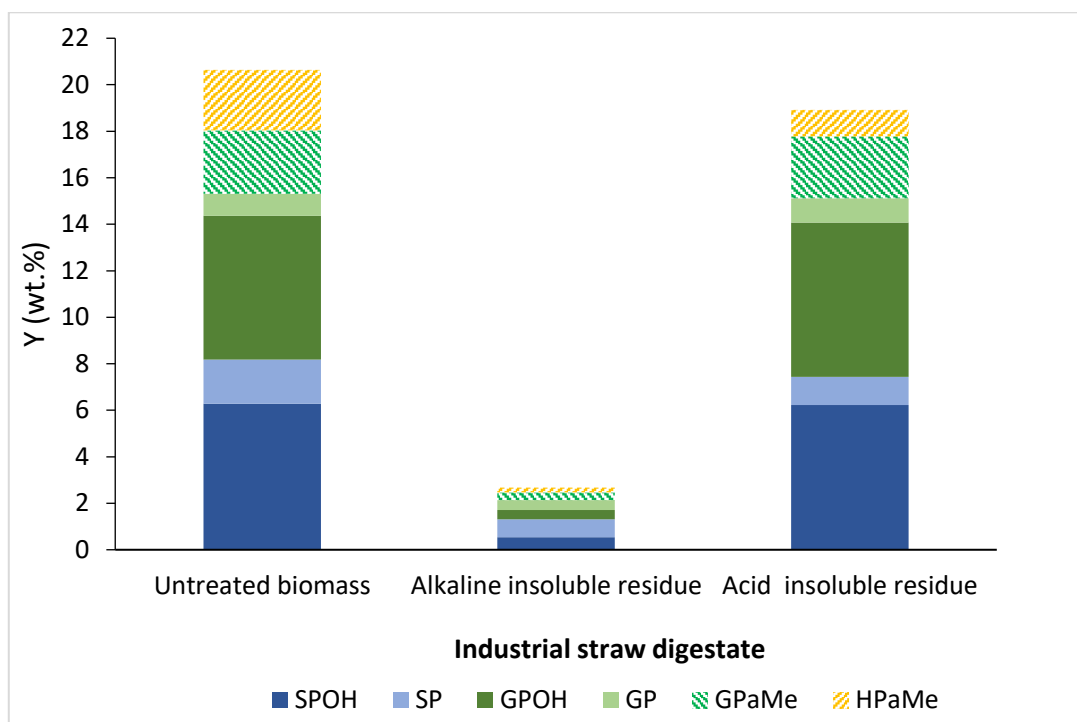


Figure 6.6 Effect of alkaline pretreatment on the monomer yields obtained by RCF of industrial straw digestate. Reaction conditions: 10 mL methanol, 250 mg substrate, 50 mg NiSat, T= 200 °C, P=50 bars H₂, and t= 24 h.

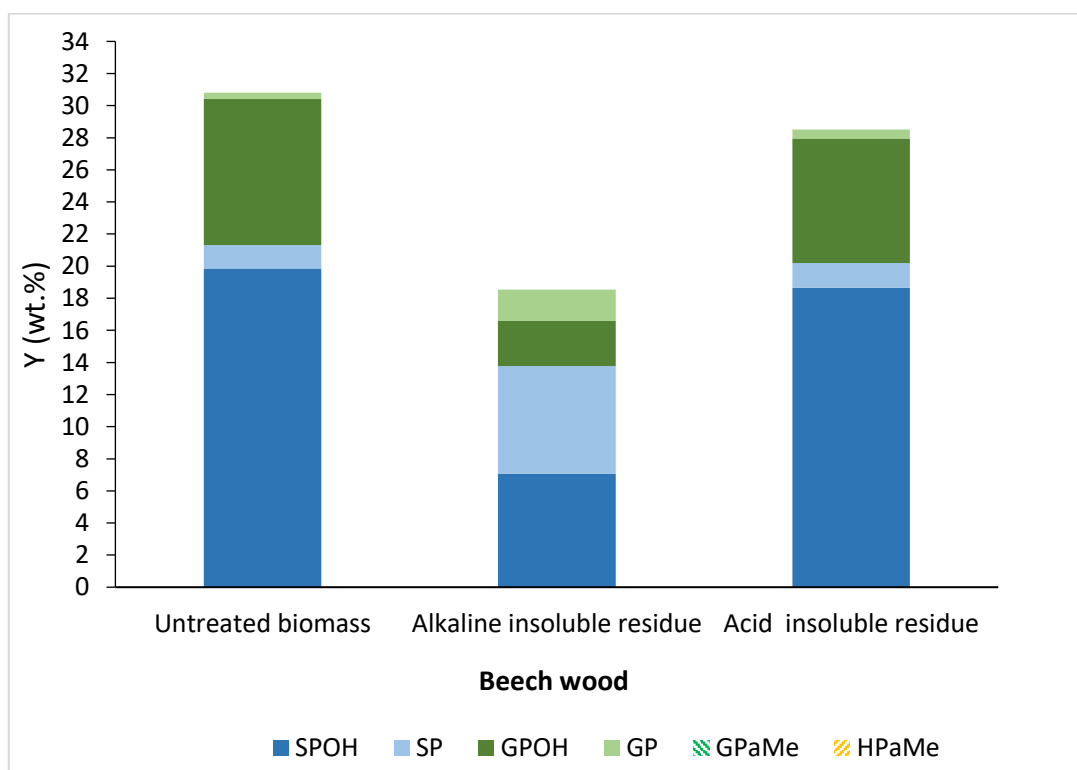


Figure 6.7 Effect of alkaline pretreatment on the monomer yields obtained by RCF of beech wood. Reaction conditions: 10 mL methanol, 250 mg substrate, 50 mg NiSat catalyst, T= 200 °C, P=50 bars H₂, and t= 24 h.

6.3.4.2. Effect of reaction time

The aim of these investigations was to examine the impact of extending the reaction time from 30 minutes to 48 hours on the yields of monomers obtained through RCF of industrial straw digestate. Figure 6.8 illustrates the outcome in terms of total monomer yield and the different monomer shares as defined in section 6.2.5.

During the initial 7 hours of reaction, the monomer yield showed a pronounced increase with extending reaction times, rising from 9.4 wt.% at 30 minutes to 21.3 wt.% at 7 hours. Subsequently, as the reaction time extended further, the monomer yield reached a nearly constant level, suggesting the establishment of an equilibrium state between the degradation reactions, which lead to monomer formation, and the repolymerization reactions, which consume these monomers. The γ -OH monomers share demonstrated a decreasing trend with increasing reaction time. For instance, the γ -OH monomer share was approximately 87 mol.% at 30 minutes, and it reduced to 77 mol.% after 7 hours. A gradual decline from 77 to 69 mol.% was further observed during the subsequent 41 hours. This phenomenon arose due to the secondary reaction in RCF that involves the hydrogenolysis of γ -OH monomers to form γ -H monomers. Moreover, the share of phenolic acid monomers exhibited an increasing trend during the initial 7 hours, reaching up to 23.7 mol.%. However, after this period, there was only a marginal increase, with the share reaching 24.7% at 48 hours. The share of S-monomers remained relatively constant, accounting for approximately 46-49 mol.% throughout the 48-hours reaction time. This observation indicated that the depolymerization kinetics to form G- and S-monomers were not significantly different in RCF of industrial straw digestate.

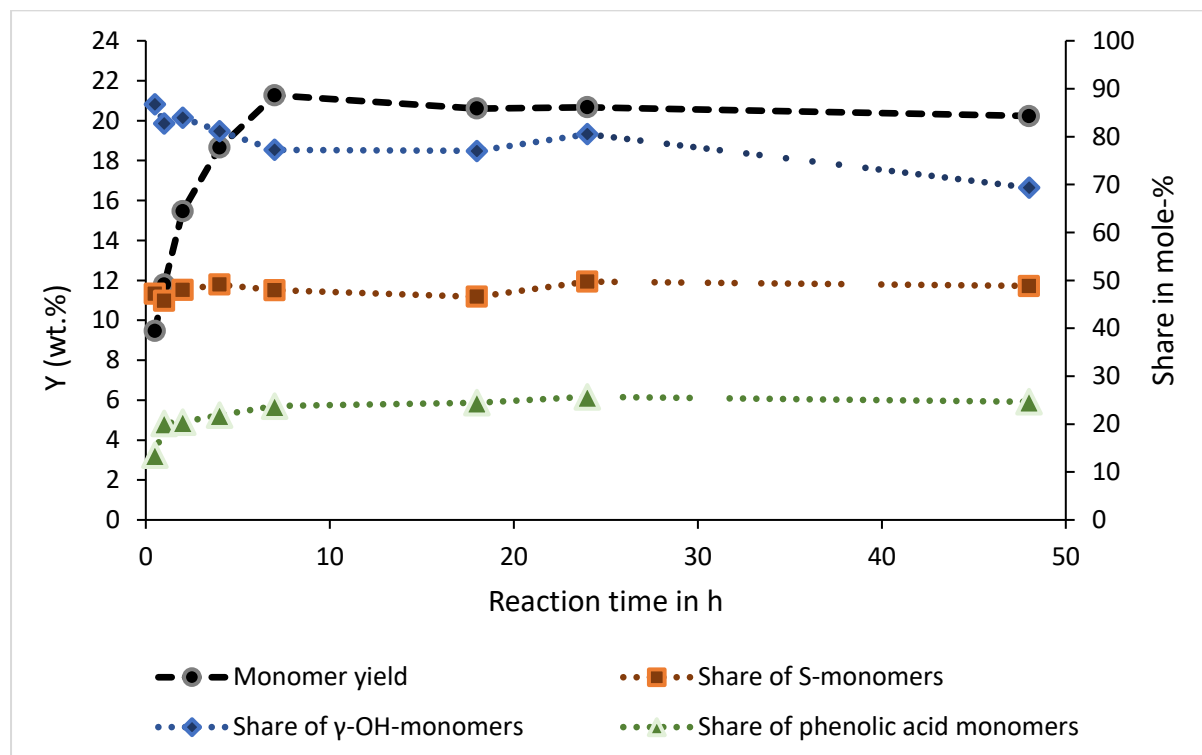


Figure 6.8 Effect of the reaction time on the total monomer yield (left y-axis) and the shares of S-monomers, γ -OH monomers and phenolic acid monomers (the right y-axis) obtained by RCF of washed industrial straw digestate. Reaction conditions: 10 mL methanol, 250 mg substrate, 50 mg NiSat, T= 200 °C, P=50 bars H₂, and different reaction times.

6.3.4.3. Effect of H₂ pressure

As depicted in Figure 6.9, the primary aim of these investigations was to examine the impact of varying the H₂ pressure, ranging from 5 bar to 50 bar, on both the total monomer yield and the γ -OH monomers share obtained through RCF of washed industrial straw digestate. No considerable changes were observed for other monomer shares; hence, they were not included. A gradual rise in monomer yield was observed, ranging from 13.7 wt.% at 5 bar H₂ pressure to 21.2 wt.% at 50 bar H₂ pressure. Additionally, there was a significant increase in the share of γ -OH monomers, from 30 mol% to 83 mol%, as the H₂ pressure increased from 5 bar to 50 bar. These findings can be attributed to the distinctive hydrogen-dependent properties of hydrogenolysis and hydrogenation reactions [155, 172], as presented in Figure 2.16 in chapter 2. At lower pressures, the dominant pathway in RCF involves the hydrogenolysis of monolignols, leading to the formation of propenyl-substituted phenols (GPe and SPe), followed by the hydrogenation of unsaturated double bonds to generate GP and SP. In contrast, at elevated pressures, the direct hydrogenation of monolignols to form γ -OH monomers (GPOH and SPOH) becomes predominant. The observed increase in γ -OH monomers share at high H₂ pressures is concomitant with a rise in monomer yield. This can be attributed to the nature of the direct hydrogenation pathway of monolignols to γ -OH monomers, which does not involve side repolymerization reactions. In contrast, the hydrogenolysis pathway of monolignols generates intermediates such as GPe and SPe that are considerably more prone to repolymerization reactions that consume monomers and, consequently, reduce the overall monomer yield.

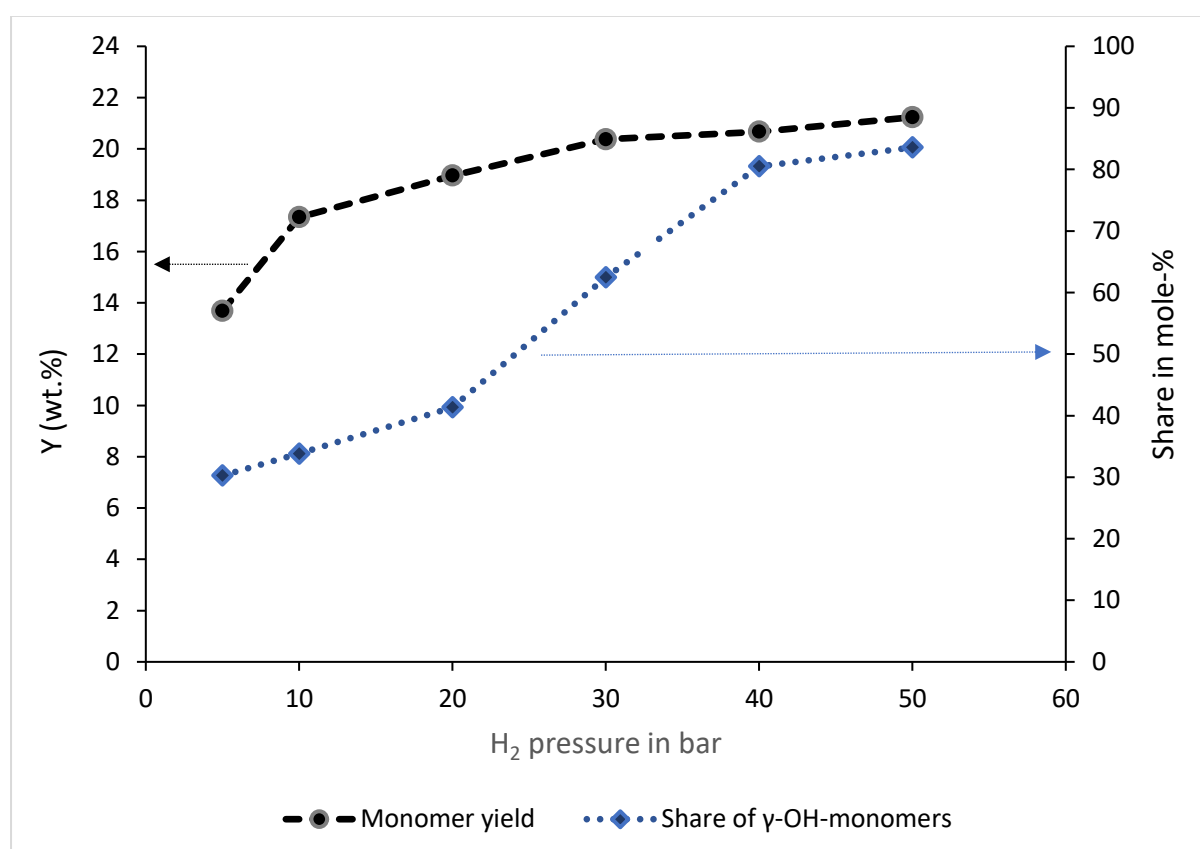


Figure 6.9 Effect of the reaction time on the total monomer yield (left y-axis) and the γ -OH monomers share (right y-axis) obtained by RCF of washed industrial straw digestate. Reaction conditions: 10 mL methanol, 250 mg substrate, 50 mg NiSat, T= 200 °C, and different H₂ pressures for 24 h.

6.4. Conclusion

The utilization of fermentation byproduct, namely straw industrial digestate, as a lignin-rich substrate for lignin valorization through RCF, shows promising prospects. The RCF applied to industrial digestate achieved 70 % of the monomer yield produced when the conventional beech wood substrate was utilized. Among the various catalysts tested using beech wood as a substrate, NiSat demonstrated the highest selectivity toward γ -OH monomers, with a significant γ -OH monomer share of 93.7 mol.%. Observations from the experimental analysis indicate that lignin degradation, affecting hydroxycinnamates incorporated into the lignin structure of straw, occurs during the fermentation and processing of straw. Consequently, the RCF of industrial straw digestate resulted in a monomer yield of 21 wt.%, which is slightly lower by 4 wt.% compared to rye straw. Further investigations examining the impact of various pretreatment steps and reaction conditions revealed that the lignin present in the industrial straw digestate is predominantly alkaline-soluble, and that the initial washing of the substrate, along with reduced reaction times and conducting the reaction under a hydrogen-rich atmosphere at elevated pressure, are essential factors for increasing the selectivity towards γ -OH monomers.

Part IV: Influence of polyoxometalates (POMs) in hydrogenation of furans, glycerol hydrogenolysis, and lignin valorization via reductive catalytic fractionation

This part is centered on investigating the impact of applying POMs in the hydroprocessing reaction medium and includes one chapter (chapter 7). This chapter presents first an introductory overview of the theoretical background, followed by an experimental analysis that aims to reveal the influence of POMs in the three biomass hydroprocessing reactions discussed in parts I, II and III.

Chapter 7. Assessing the influence of polyoxometalates in hydrogenation of furans, glycerol hydrogenolysis, and lignin valorization via reductive catalytic fractionation

7.1. Introduction

Currently, the majority of platform chemicals are obtained from non-renewable fossil resources. However, the limited availability of these resources and their detrimental impact on the environment have raised concerns and stimulated interest in exploring alternative and sustainable production pathways, such as the utilization of biomass resources. In particular, hydroprocessing reactions are promising routes for the conversion of biomass-derived furans into alcohols, glycerol into 1,2 propanediol, and lignin into phenolic monomers.

In the realm of hydroprocessing reactions, catalysts can generally be categorized into two groups based on the metal site employed: transition metal catalysts and noble metal catalysts. The commonly utilized metal sites for these reactions include Ru, Pt, Rh, Pd, Cu, Ni, Fe, and Co. It is important to note that, aside from the metal site, the catalyst support, modifiers, and the presence of acidic or basic additives can also exert a significant impact on the conversion and selectivity towards the desired products.

Several studies in the literature have reported the positive impact of incorporating acidic properties into hydroprocessing reactions, either by using acidic support, acidic co-catalyst, or additive, on the conversion of the aforementioned three reactions and selectivity towards specific products. For example, Kang et al. [119] reported that Pt deposited on multi-walled carbon nanotubes and alumina using atomic layer deposition exhibited strong acid sites, resulting in deep hydrogenation of 2,5 dimethylfuran (DMF) to hexane (HX) in gas phase. In light of these findings, we aimed to tune the acidity in our work to enhance selectivity towards 2-hexanol (HXL) which represents the intermediate responsible for HX production.

Regarding 1,2 propanediol (1,2 PD) production from glycerol (GL), the combination of Ru/C with solid acids has been found to be effective in the simultaneous dehydration and hydrogenation steps involved in GL hydrogenolysis [207, 234]. The addition of a homogenous acid catalyst H_2SO_4 to the reaction medium has been shown to increase the activity of Ru/C and double the selectivity towards 1,2 PD [207]. Alhanash et al. [93] reported a selectivity of 96% to 1,2 PD at 21% GL conversion using ruthenium-doped (5 wt.%) acidic heteropoly salt $Cs_{2.5}H_{0.5}PW_{12}O_{40}$.

Moreover, as mentioned in section 2.4.4, the addition of acidic co-catalysts or additives, such as H_3PO_4 , has shown great potential in enhancing the delignification of some lignocellulosic biomass feedstocks and increasing phenolic monomer yields [14, 168]. The use of acidic POMs ($H_4SiW_{12}O_{40}$) in a second reaction step after reductive catalytic fractionation (RCF) of lignin provided a feasible route to integrate RCF-based biorefinery processes into existing petro-refinery schemes, as illustrated in section 2.4.6.

Polyoxometalates (POMs) possess distinctive physicochemical properties, including modifiable Brønsted/Lewis-acidity and redox properties. Therefore, the aim of this chapter was to investigate the impact of utilizing acidic POMs, especially the Keggin-structure (Figure 7.1), in the aforementioned three RCF reactions (hydrogenation of furans, glycerol hydrogenolysis, and lignin valorization via RCF).

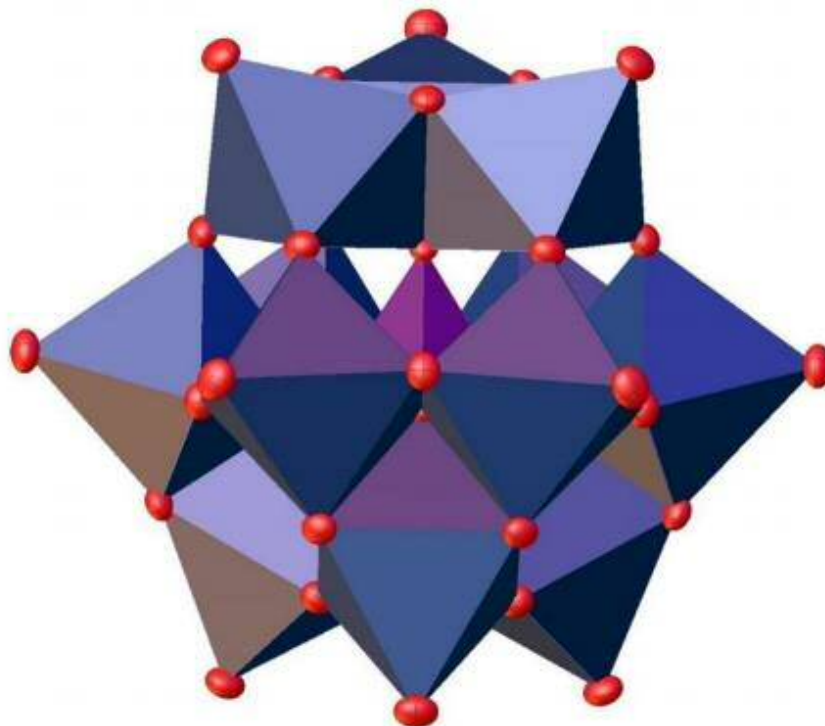


Figure 7.1 Schematic representation of the Keggin-type POM anion $[ZM_{12}O_{40}]^{3-}$ [235].

7.2. Experimental

7.2.1. Catalytic experiments

The same 10-fold parallel reaction system, depicted in Figure 6.2 and Figure 6.3, was used to carry out hydroprocessing reactions. For each run, the reactor was filled with 10 ml of the solvent, substrate, catalyst, and POMs additive if present. After closing the reactor, it was placed in a heating block above a magnetic stirrer and connected to the gas supply. To remove any residual air, the system was purged three times with N_2 and then pressure tested at 70 bar N_2 . The system was then purged two times with H_2 and filled at room temperature with 2/3 of the amount of H_2 pressure required. The reactors were heated to the final temperature, and then the pressure was adjusted to the desired H_2 pressure. The stirrer speed was set to 330 rpm during the heating phase, after which the reaction was initiated by vigorous stirring at 770 rpm. Upon completion of the reaction time, the stirring was reduced to 330 rpm, and the reactors were cooled to room temperature. Gas samples for GC analysis were then taken from the reactors using gas bags. The reactors were subsequently vented and purged three times with nitrogen gas before opening. The catalyst was filtered off, and the liquid phase was analyzed.

7.2.2. Product analysis

In addition to the various analytical techniques employed and discussed in chapters 3-6, such as gas chromatography (GC), high-performance liquid chromatography (HPLC), gas chromatography-mass spectrometry (GC-MS), and catalyst characterization techniques such as X-ray diffraction (XRD), transmission electron microscopy (TEM), temperature-

programmed desorption of ammonia (NH₃-TPD), and nitrogen physisorption (N₂-physisorption), Fourier Transform Infrared Spectroscopy (FTIR), gel permeation chromatography (GPC) was utilized in these investigation to obtain more comprehensive information on the degree of lignin depolymerization and the distribution of the molar mass of the lignin products in the RCF of beech wood and straw industrial digestate when POMs were introduced into the reaction medium.

The GPC analyses were carried out at 25 °C using a Knauer K-4002 degasser and a smartline 3800 autosampler equipped with a PLgel 10 µm guard column and two PLgel 10 µm MIXED-B columns by Agilent, operating at a flow rate of 1 (mL.min⁻¹) with tetrahydrofuran (THF) as the solvent and a Schambeck SFD GmbH RI 2000 detector.

7.3. Results and discussion

7.3.1. Effect of adding POMs in hydrogenation of furans

Chapter 3 of this thesis provides a detailed account of the impact of POM catalysts on the hydrogenation of furan. However, it will be briefly discussed here. The products observed during the reaction were HXL, 2-hexanone (HXN), 2,5-dimethyltetrahydrofuran (DMTHF), 2,5-hexanedione (HD), and HX. As previously shown in chapter 3, Pt/C demonstrated the highest selectivity towards the desired furan ring-opening reaction and achieved a yield of 49.7% HXL at complete DMF conversion. Based on this, Pt was selected as the preferred metal site for subsequent investigations.

Table 7.1 provides a concise summary of the impact of incorporating POMs into the reaction medium. Initially, the efficiency of utilizing a POM salt, K₃[PW₁₂O₄₀], exclusively as a reduction catalyst was evaluated, as outlined in (Table 7.1, entry 16), and it was found to exhibit no conversion, indicating the lack of reduction ability of POMs alone under the utilized reaction conditions, and thus necessitating the use of Pt as the active species. Subsequent experiments were conducted to evaluate the activity of various Pt-substituted POMs, both in their original forms and after reduction in a hydrogen environment, as potential heterogeneous catalysts for DMF hydrogenation in a slurry system. Regrettably, no significant DMF conversion was achieved under the applied reaction conditions (Table 7.1, entry 10-15).

As a result of the limited success of Pt-substituted POMs in the previous experiments, an alternative approach was taken to investigate the potential of a bi-functional catalyst for selective DMF hydrogenation. This involved the impregnation of Pt onto three heteropolyacids that possess a Keggin-type structure. These Pt-free POMs were combined with a Pt-precursor to generate bi-functional catalysts, as presented in (Table 7.1, entry 4-6). Our findings indicate that the utilization of Pt-free POMs in conjunction with a Pt-precursor were able to generate a bi-functional catalyst that showed potential for selective DMF hydrogenation. Results indicated that Pt/phosphotungstic acid (entry 4) demonstrated superior performance, achieving a yield of 50% for HXL. However, it displayed a higher tendency for ring saturation hydrogenation, leading to an increased production of DMTHF (29%), as well as greater hexane formation (12%) through dehydration of HXL. The introduction of silicon (Si) in place of phosphorus (P) in the heteropolyacid led to a significant decline in

performance (entry 5) with only 45% DMF conversion observed. The application of phosphomolybdate as a heteropolyanion (entry 6) resulted in a significant decline in the catalyst's performance with only 3% conversion achieved. This outcome is attributed to the loss of the Keggin structure of the phosphomolybdate during reduction. On the other hand, Pt/H₃[PW₁₂O₄₀] retained its structure after reduction and reaction, as shown in (Fig. S1, S2 in Appendix 10.4).

The superior activity of H₃[PW₁₂O₄₀] (HPW) compared to the other tested Keggin-type acids H₄SiW₁₂O₄₀ (HSiW) and H₃[PMo₁₂O₄₀] (HPMo) can be attributed to its higher acid strength [236], as evidenced by the ammonia desorption temperatures (indicated in degrees Celsius) in the following order: HPW > HSiW > HPMo = 592 > 532 > 463. Pt was also supported on WD-type acidic potassium POMs salts, such as Pt/K₆[α -P₂W₁₈O₆₂], (Table 7.1, entry 7), which showed slightly lower conversion compared to Pt supported on Keggin type POMs (Table 7.1, entry 1,4). However, it exhibited high selectivity to HXN (56%) instead of HXL. On the other hand, when Pt was supported on mono vacant potassium salt (K₇[α -PW₁₁O₃₉]), (Table 7.1, entry 9), the performance was drastically decreased, compared to Pt supported on Keggin type POMs, with only 1.8% DMF conversion.

The results presented till now demonstrated that the choice of POMs as the catalyst support provides a significant impact on the performance of the catalyst in selective hydrogenation of DMF. The most active catalysts were found to be Pt-supported on Keggin-type POMs, with phosphotungstic acid H₃[PW₁₂O₄₀] showing the best performance. Manipulating the content of the counter-cations in H₃[PW₁₂O₄₀], (Table 7.1, entry 1-3), led to the observation that the acidic Cs-salt of the Keggin-type tungstophosphate (Table 7.1, entry 2) showed high conversion and tendency towards the formation of the desired product (HXL, 54 %) compared to the heteropoly acids and Cu-salts. However, similarly to the Pt/H₃[PW₁₂O₄₀], the Cs-salt led to the generation of significant amounts of the undesired DMTHF (36 %) and HX (8 %).

The moderate acidic K-salt of Keggin-type tungstophosphate (Pt/K₃[PW₁₂O₄₀]), (Table 7.1, entry 1), was found to be most selective catalyst towards HXL production with approximately 72.5% yield. The Pt/K₃[PW₁₂O₄₀] and Pt/C catalyst were characterized, revealing several structural differences. Additionally, the POM support's moderate surface acidity, as measured by NH₃-TPD, enhances the catalytic performance and selectivity towards HXL. The K₃[PW₁₂O₄₀] support acts as a moderate acid site, enhancing C=O hydrogenation and overcoming the rate-limiting step of HXN hydrogenation to HXL, without exhibiting a high degree of HXL dehydration that produces HX. The presence of acid sites in the support plays a crucial role in activating the C=O bond. A charge transfer interaction between the oxygen atoms in the carbonyl group and the cationic sites in the support generates a negative charge localized around carbonyl C, activating it for hydrogenation. A similar behavior was observed for selective hydrogenation of furfuraldehyde to furfuryl alcohol over Pt/TiO₂ [237].

Table 7.1 DMF conversion and product yields of different Pt-POM catalytic systems.

Entry	Catalyst	Conv. (%)	Yield (%)					Carbon balance (%)
			HXL	HXN	DMTHF	HD	HX	
1	Pt/K ₃ [PW ₁₂ O ₄₀]	100	72.5	1.7	20.9	0	5.6	100
2	Pt/Cs _{2.5} H _{0.5} [PW ₁₂ O ₄₀]	100	54.5	1.0	36.1	0	8.0	100
3	Pt/Cu _{1.5} [PW ₁₂ O ₄₀]	6.7	0	0.4	2.3	3.0	0.3	99.2
4	Pt/H ₃ [PW ₁₂ O ₄₀]	99.5	50.2	1.5	29.4	0	11.8	93.7
5	Pt/H ₄ [SiW ₁₂ O ₄₀]	45.2	14.0	4.6	18.6	0.3	8.0	100
6	Pt/H ₃ [PMo ₁₂ O ₄₀]	3.2	0	0.3	0.5	1.1	0	98.9
7	Pt/K ₆ [α -P ₂ W ₁₈ O ₆₂]	95.2	17	56.4	14.0	0.6	3.6	96.5
8	Pt/K ₆ [HSiW ₉ V ₃ O ₄₀]	5.0	0.7	0.3	0.9	1.1	2.4	100
9	Pt/K ₇ [α -PW ₁₁ O ₃₉]	1.8	0	0.3	0.4	1.5	0	100
10	Reduced K ₃ [{Pt(en) ₂ } ₂ PW ₁₁ O ₃₉]*	4.7	0	1.0	2.2	0.6	0	99.7
11	Reduced H{Pt(NH ₃) ₄ }-[PW ₁₁ O ₃₉ {Pt(NH ₃) ₄ } ₂]*	3.9	0.8	1.7	2.3	0.7	0.3	100
12	Reduced Na ₅ [H ₂ PtV ₉ O ₂₈]*	1.2	0	0	0.5	0.7	0.3	100
13	K ₃ [{Pt(en) ₂ } ₂ PW ₁₁ O ₃₉]	0.4	0	0	0	0.4	0	100
14	H{Pt(NH ₃) ₄ }-[PW ₁₁ O ₃₉ {Pt(NH ₃) ₄ } ₂]	1.4	0	0	0	0.4	0	100
15	Na ₅ [H ₂ PtV ₉ O ₂₈]	0.3	0	0	0	0.3	0	100
16	K ₃ [PW ₁₂ O ₄₀]	0	0	0	0	0	0	100

Reaction conditions: 0.001 mol DMF, 10.0 mL decane as a solvent, 2 mg Pt, 80° C, 10 bar H₂, 770 rpm, 3 h.

*The Pt-substituted POMs were used after reduction in an oven with 10 % H₂ flow (50 mL/min H₂ and 450 mL/min N₂) at 250°C for 2 h (abbreviated as “Reduced [POM]”)

7.3.2. Effect of adding POMs in hydrogenolysis of glycerol

This section represents the basis of the publication in chapter 5. In this section, several metal-sites supported on carbon were tested for their activity and selectivity in GL hydrogenolysis. After that, the effect of adding POMs to the reaction medium was investigated. The typical products observed during the hydrogenolysis of GL were 1,2 PD, ethylene glycol (EG), hydroxyacetone (HA), 1-propanol (n-Pr), 2-propanol (i-Pr), methanol (MeOH), ethanol (EtOH), methane and some other gases including CO₂.

The metal components of the catalysts play an important role in activating hydrogen during the reaction. Therefore, in the first set of experiments, we wanted to investigate which metal is the most suitable metal site for hydrogenolysis of glycerol and the selective production of 1,2 PD under the chosen reaction conditions. Based on previous studies [216, 238], we focused on carbon as a support material and mild reaction conditions of 200°C and 50 bar H₂ were used during the reaction. In each run, equal amounts (10 mg) of each metal were tested to allow a direct comparison of the different catalysts, except for Ni which was 4 times greater than Pt and Ru.

The catalyst's metal site screening results are presented in Table 7.2 and shows that Ru/C (entry 1) acquires the highest activity among the different tested catalysts with a conversion of 44.5 % under the applied reaction conditions. A selectivity of only 21.7 % towards 1,2 PD formation was obtained using the same catalyst. The high amounts of methane produced provide evidence that Ru/C is active for the scission of C-C bonds. On the other hand, Pt/C (entry 2) showed significantly lower activity with a conversion of 7.6 %, but a higher selectivity of 55.9 % towards 1,2 PD formation. These results suggest that a higher tendency of Ru towards C-C bond cleavage exists which is not the case in Pt systems. This tendency is consistent with the results reported by Ryneveld et.al [216] of Ru and Pt catalyst systems. Notably, Ni/C did not show any activity for glycerol hydrogenolysis under the same reaction conditions although the amount of Ni was 4 times higher than Ru and Pt.

The high conversion of glycerol with Ru/C was also confirmed by other publications in literature [207, 216, 238] and is attributed to its activity for both the scission of C-O and C-C bonds. Ru also proved to be the most effective catalyst in hydrogenation of the intermediate HA to 1,2 PD [207]. Based on this, we decided to proceed with Ru as an active metal site in our further investigations and search for a way to increase the selectivity towards 1,2 PD.

Table 7.2 Glycerol conversion and product selectivity during hydrogenolysis using different active metal sites supported on carbon.

Catalyst	Conversion [%]	Selectivity [%]										Carbon balance [%]
		1,2-PD	EG	HA	i-Pr	EtOH	MeOH	CH ₄	C ₂ H ₆	C ₃ H ₈	CO ₂	
Ru/C	44.5	21.7	14	5.6	0	0.5	1.3	31.8	4.1	2.4	2.8	93
Pt/C	7.6	55.9	9.4	0	1.6	0	0	0.7	0.6	0.3	0	97.7
Ni/C	0	-	-	-	-	-	-	-	-	-	-	100
No cat.	0	-	-	-	-	-	-	-	-	-	-	100

Reaction conditions: 2 g glycerol (10 mL of 20 wt.% aqueous solution); catalyst amount = 200 mg; H₂ pressure = 5.0 MPa; T= 200°C; stirring speed = 1000 rpm; t=20h.

Based on the results mentioned above, and since Ru/C gave the highest conversion, it was decided to screen some solid acid POMs in a combination with Ru/C to study the effect of this acidic environment on glycerol hydrogenolysis and to determine whether this will increase the selectivity towards 1,2 PD by promoting the dehydration step. Three different heteropolyacids with Keggin-type structure, HPMo, HPW, and HSiW (Table 7.3, entries 1–3) were added to the reaction medium at the same reaction conditions. We could clearly demonstrate that the combination of POMs with Ru/C increased the selectivity towards 1,2 PD formation and decreased undesired methane formation.

HPMo as an additive (entry 1) showed the best performance, achieving an increase in selectivity towards 1,2 PD from 21.7 % up to 70.6 % and decrease in CH₄ selectivity from 31.8 % to only 2.2 %. The higher selectivity of n-Pr in comparison with the other runs results from the higher yield of 1,2 PD, as n-Pr is mainly formed from hydrogenolysis of 1,2 PD. The lower yield of EG formed is attributed to the decrease of Ru/C tendency for C-C bond cleavage during the reaction. The addition of HPW and HSiW (entry 2,3) increased the selectivity towards 1,2 PD from 21.7 % to 31.1 % and 26.3 %, respectively. A decrease in CH₄ and EG formation was notable as well.

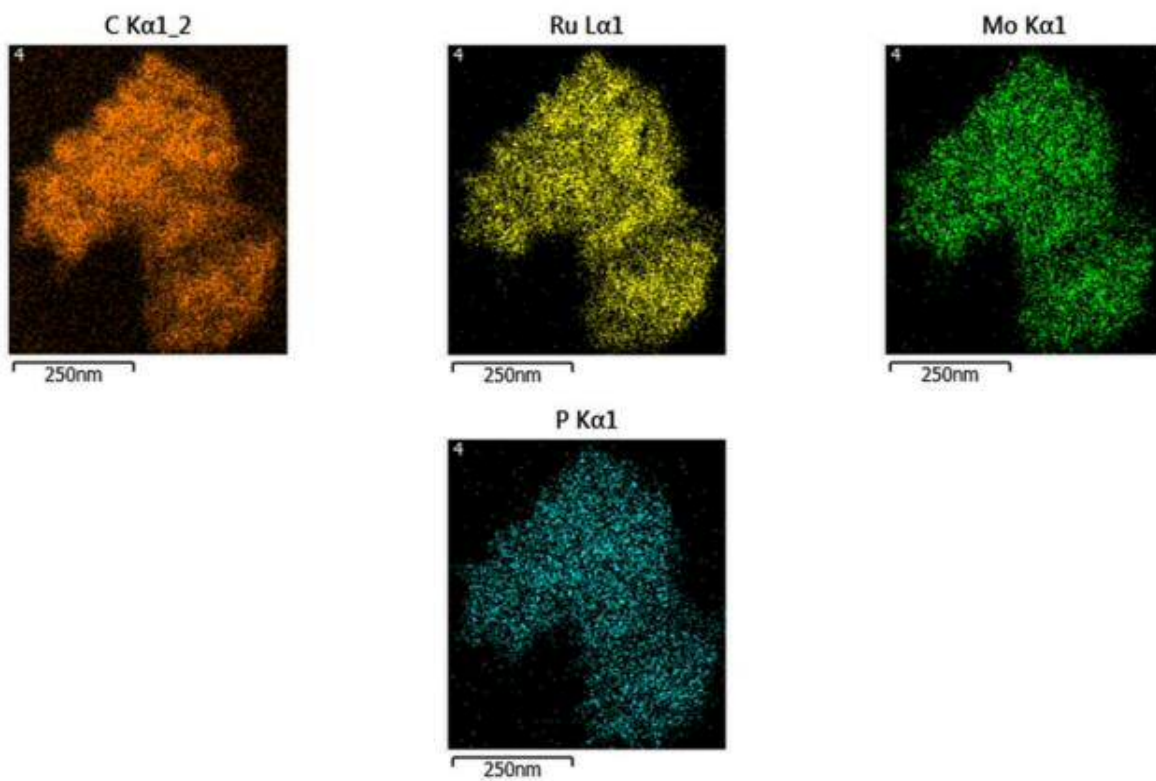
The high acidity of the POMs might be responsible for enhancing the dehydration step in the reaction mechanism of glycerol hydrogenolysis, outlined in section 2.5.5, which led to higher production of 1,2 PD. However, this explanation cannot account for all observations, such as the decreased tendency of Ru/C for C-C bond cleavage during the reaction and the highest selectivity towards 1,2 PD exhibited by the Ru/C + HPMo combination, despite HPMo having the lowest acid strength among the tested heteropolyacids [4]. Therefore, the Ru/C spent catalyst was collected from the filter paper after the reaction, when HPMo was used as an additive, and analyzed using TEM-EDX and FTIR, in order to determine how the addition of POMs affects the catalyst.

Table 7.3 Glycerol hydrogenolysis catalyzed by 5% Ru/C + POMs.

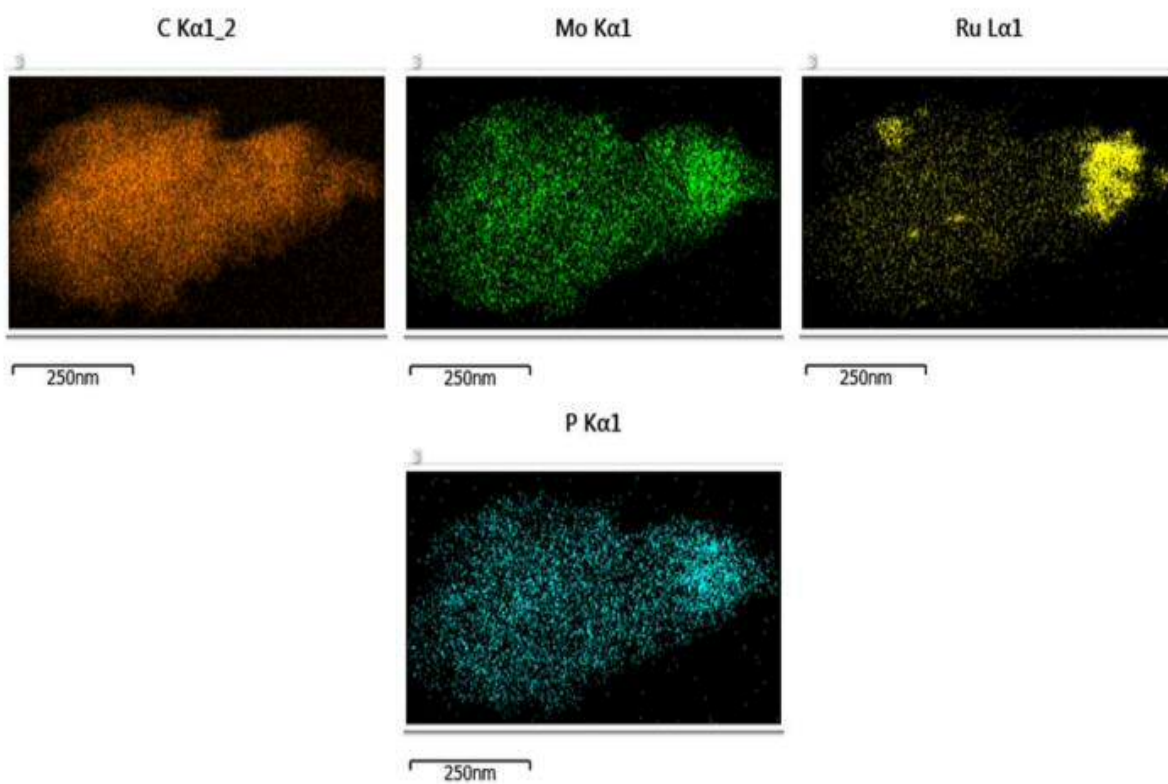
Entry	Catalyst	Conversion [%]	Selectivity [%]				Carbon balance [%]
			1,2 PD	EG	n-Pr	CH ₄	
1	Ru/C+ HPMo	30.5	70.6	1.6	11.9	2.2	99.5
2	Ru/C+ HPW	49.8	31.1	8.1	2.6	15.7	82
3	Ru/C+ HSiW	45.7	26.3	8	3	19.3	83.3
4	Ru/C	44.5	21.7	14	0	31.8	93

Reaction conditions: 2 g glycerol (10 mL of 20 wt.% aqueous solution); 5% Ru/C = 200 mg; POM=200 mg; H₂ pressure = 5.0 MPa; T= 200°C; stirring speed = 1000 rpm; t=20h.

TEM-EDX analysis of the spent catalyst revealed the presence of Mo on the surface of the carbon support, as depicted in Figure 7.2. The ratio of Ru/Mo on the surface calculated using TEM ranges from 1/2 to 1/6. These findings suggest that Mo and W species present in the POM complex, or possibly the entire POM complex, precipitated on the surface of the Ru/C catalyst during the reaction. A synergetic effect between the POM precipitates and Ru on the surface might be responsible for the higher selectivity towards 1,2 PD, compared to Ru/C alone.



a)



b)

Figure 7.2 TEM-EDX for Ru/C spent catalyst when HPMo was added to reaction medium.

Comparative analysis between HPMo and Ru/C spent catalyst when HPMo was added to reaction medium using FTIR is presented in Figure 7.3. All the characteristic bands of Keggin anion in the region of 1100-550 cm^{-1} exist in the spectra, which supports our claim that the entire POM complex was precipitated on the surface of the Ru/C catalyst during the reaction. TEM-EDX analysis presented in Figure 7.2 (a, b) suggests also that the POMs remained intact and undecomposed following precipitation, due to the nearly identical surface distribution of Mo and P. Furthermore, the Ru species were found to be sometimes partially covered by the POMs precipitate, suggesting that $\text{H}_3[\text{PMo}_{12}\text{O}_{40}]$ was not only evenly attached to the carbon support, but also partial covered Ru metals.

In a related study, Song et al. reported the precipitation of HPW on another noble metal supported on C, (Pd/C) [100]. Their study revealed that the active Pd was partially covered and modified by POMs, which was crucial for the hydrogenolysis of lactone intermediates to aldehydes/alcohols during the HDO of δ -furfurylidenelevulinic acid (FDLA) into alkanes. In our investigations, this partial coverage of Ru in addition to interaction between precipitated POMs with Ru, might be the reason for the observed reduction of C-C bond cleavage (lower methane formation) and increasing HDO of glycerol to form 1,2 PD.

The higher selectivity towards 1,2 PD of HPMo in combination with Ru/C followed by HPW and HSiW acids, is consistent with the order of HDO ability of those heteropolyacids $[\text{SiW}_{12}\text{O}_{40}]^{4-} < [\text{PW}_{12}\text{O}_{40}]^{3-} < [\text{PMo}_{12}\text{O}_{40}]^{3-}$, as reported previously in literature [67].

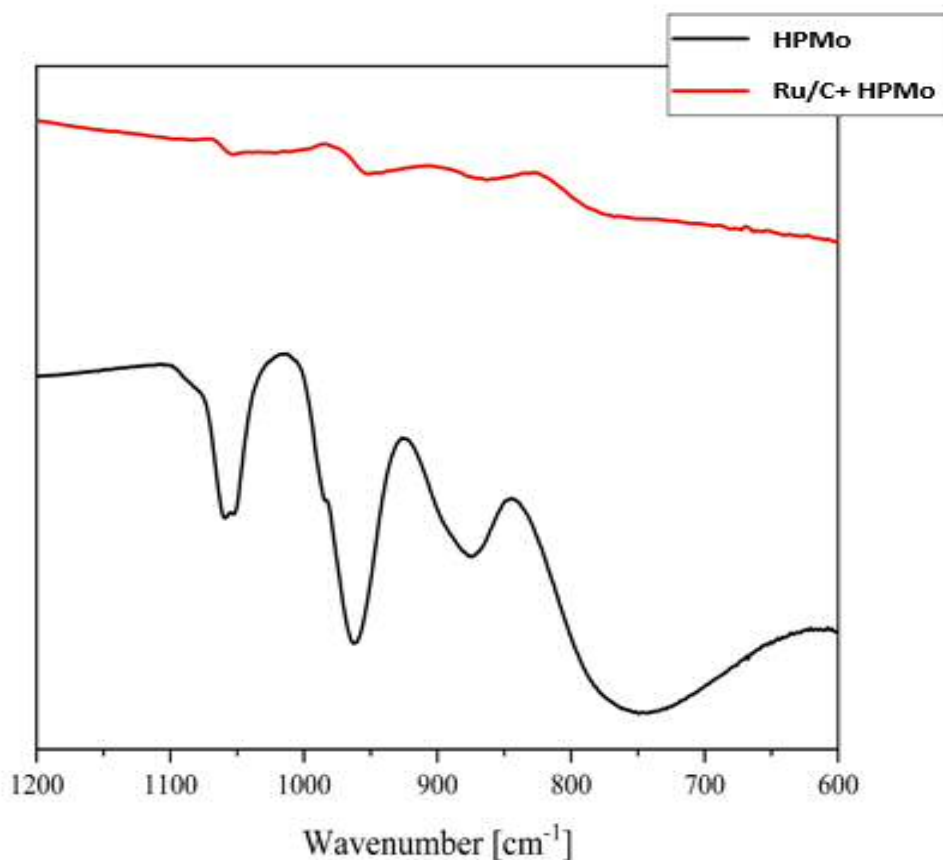


Figure 7.3 FTIR spectra of HPMo (black) and Ru/C spent catalyst when HPMo was added to reaction medium (red).

7.3.3. Effect of adding POMs in reductive catalytic fractionation

As expounded in section 2.4, the RCF represents a novel technique for the conversion of lignin into phenolic aromatics. Chapter 5 has demonstrated the potential of using straw industrial digestate as a lignin first substrate for RCF process. The target in this part of the studies was to investigate the effect of applying POM catalysts on monomer yield and selective production of propanol-substituted phenols (GPOH and SPOH) from Lignin fraction of beech wood and straw industrial digestate. The utilization of POM catalysts played a crucial role in enhancing a newly developed integration approach between RCF and petrorefinery [195], as presented in section 2.4.6. RCF is first employed as a step for the fractionation of lignin, followed by the utilization of POM acid HSiW as a co-catalyst in the subsequent step for the selective production of naphtha from the cellulose and hemicellulose fractions of biomass. So, we investigated here the effect of incorporating POMs into our system, with the aim of augmenting the yields of SPOH and GPOH monomers from the lignin fraction of biomass, which can give an opportunity for maximizing γ -OH monomers from lignin fraction and naphtha from cellulose and hemicellulose fractions in a single step.

As illustrated in chapter 6, Nickel (Ni) was identified as the optimal metal site for elevating the yield of monomers and enhancing selectivity towards SPOH and GPOH. Subsequently, numerous Ni-substituted POMs were synthesized and examined in the RCF process of beech wood (Table 7.4, entry 3-6). However, the Ni-substituted POMs were found to be ineffective in our reaction system when compared to commercial Ni/C and NiSat.

Table 7.4 Comparison between commercial Ni catalysts with some Ni- substituted POMs for RCF of beech wood.

Entry	Catalyst	Metal site in catalyst to-biomass-ratio g:g	GP	SP	GPOH	SPOH	Monomer Yield (wt.%)
1	Ni/C	1:100	5.7	14.2	3.5	9.2	32.7
2	NiSat	12:100	0.36	1.46	9.1	19.9	30.8
3	H ₁₁ PMnNiMo ₁₀ O ₄₀	0.8:100	0.04	0.08	0.12	0.16	0.45
4	H ₈ PVNiMo ₁₀ O ₄₀	0.7:100	0.04	0.04	0.08	0.08	0.24
5	H ₇ PNiMo ₁₁ O ₄₀	0.7:100	0.04	0.08	0.08	0.12	0.37
6	H ₁₁ PNi ₂ Mo ₁₀ O ₄₀	1.5:100	0.04	0.08	0.08	0.08	0.32

Reaction conditions: 10 ml (methanol) as a solvent, 250 mg substrate, 50 mg catalyst, 200 °C, 50 bar H₂, and t = 24 h.

The addition of POMs as additives in combination with the commercial catalysts to the reaction medium was also investigated, as presented in Figure 7.4. Various heteropolyacids, namely HPMo, HSiW, and HPW were also examined as additives in conjunction with Ru/C, NiSat and Ni/C. With beech wood as a substrate, none of them led to an increase in monomer yield. In contrast, all of the POMs resulted in reduced yields, with a distinct pattern in which the addition of HPMo consistently caused the most significant decrease, while the addition of HSiW resulted in the lowest decrease in monomer yield. Additionally, there was a noticeable trend in which the inclusion of these additives induced a shift in the product selectivity,

consistently leading to a decrease in γ -OH monomer share when compared to the experiments conducted without the additives. Similar trends were observed when using straw industrial digestate as a substrate.

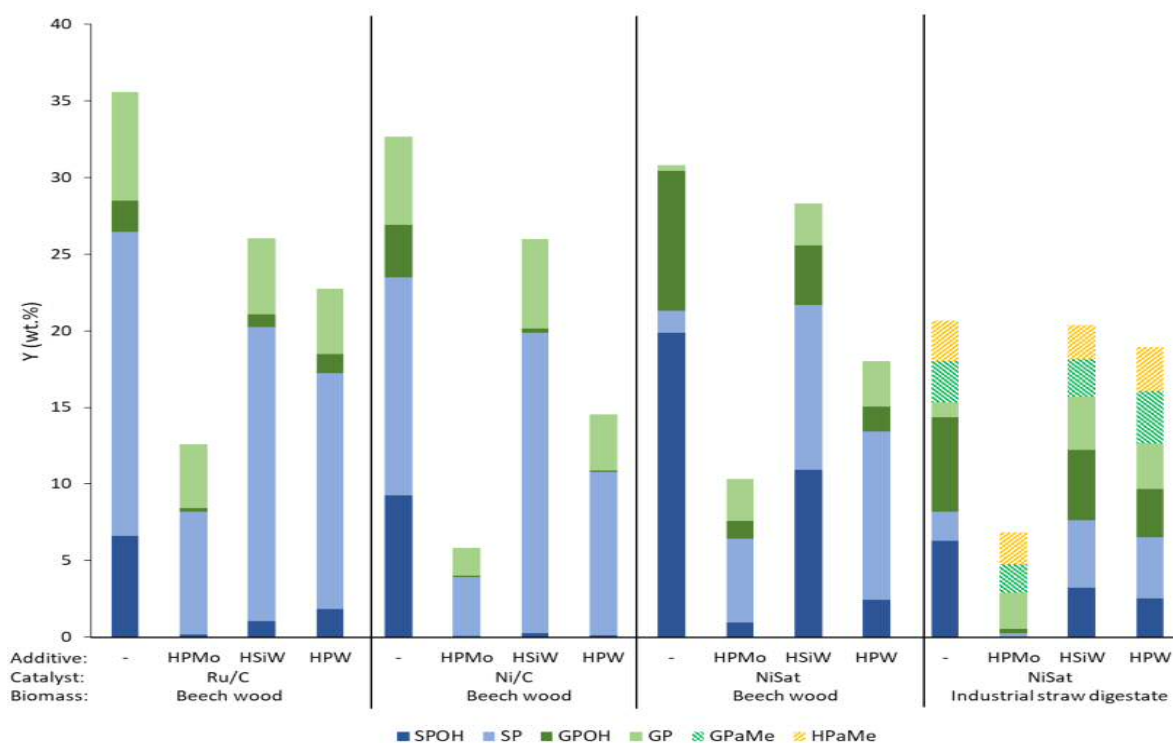


Figure 7.4 Effect of the addition of the POMs during the RCF using different catalysts (NiSat, Ni/C, or Ru/C). Reaction conditions: 10 ml (methanol) as a solvent, 250 mg substrate, 50 mg catalyst, 50 mg additive, 200 °C, 50 bar H₂, and t = 24 h.

The results of our investigations can be attributed to two distinct characteristics of POMs: their acid properties and hydrodeoxygenation capability. Renders et al. [231] proposed that the production of GP/SP and GPOH/SPOH, (Figure 7.5), occurs through two parallel reaction pathways (R2, R3 followed by R6), with the catalyst system properties dictating which pathway is favored. For example, Ru/C exhibited 75% selectivity towards GP/SP due to efficient hydrogenolysis of C γ -OH, whereas Pd/C favored the formation of GPOH, SPOH with 91% selectivity [182].

The observed results suggest that the addition of POMs to the reaction medium leads to preferential cleavage of hydroxyl groups located in the sidechains of monolignols and SPOH/GPOH through the hydrodeoxygenation (HDO) capability of POMs. This HDO capability of POMs has been reported in several publications, such as Yang et al.'s study on HDO of lignin-derived phenolic compounds using Ru/C-HPW [82] and Anderson et al.'s work on HDO of 4-propylguaiacol using HPMo/TiO₂ [80]. The cleavage of hydroxyl groups in the sidechains of monolignols intermediates and SPOH/GPOH, by POMs HDO capability, leads to the production of GPe and SPe (R3) and SP/GP (R5), respectively. These GPe and SPe can further undergo hydrogenation (R6) to increase the yield of GP/SP or participate in repolymerization reactions (R7) to form dimers and oligomers. Now with the presence of acidic properties, such as POMs, in the reaction medium, C-C and C-O bonds formation are favored which increases the repolymerization pathways (R4,R7), as reported by Lan et al. [152], thus lower monomer yields are produced. This explains why the monomer yield

decreased upon the addition of POMs, as it resulted in a reduction of the yields of SPOH and GPOH, and an increase in repolymerization reactions.

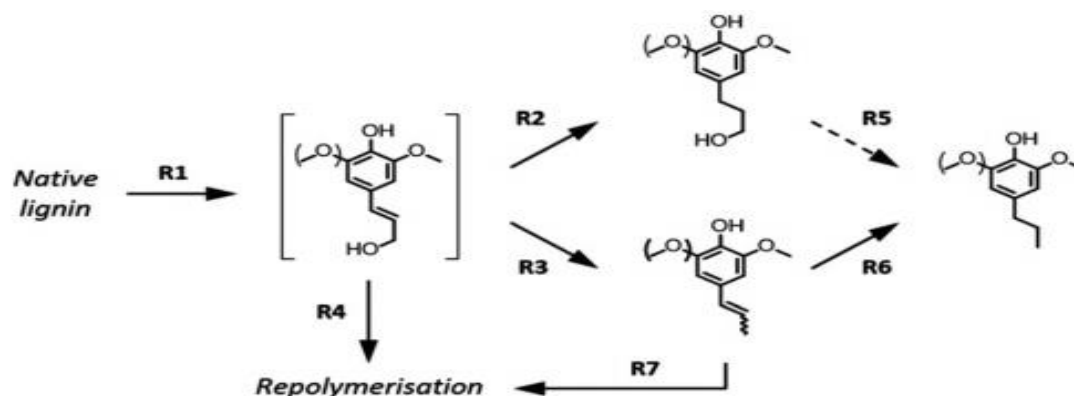


Figure 7.5 Reaction pathways in RCF [231].

The reason for HPMo exhibiting the lowest total monomer yield can be attributed to its superior HDO capability, as compared to other tested POMs. On the other hand, HSiW, which produced the highest monomer yield, had the lowest HDO capability among the POMs examined. The order of catalytic activity in HDO, as previously reported by Kogan et al. [67], was found to be $[\text{SiW}_{12}\text{O}_{40}]^{4-} < [\text{PW}_{12}\text{O}_{40}]^{3-} < [\text{PMo}_{12}\text{O}_{40}]^{3-}$ when benzophenone was used as the substrate. This order was found to be correlated with the reducibility of the POMs with H_2 , as well as their oxidation potentials. The validity of this illustration has been augmented through the implementation of GPC analysis, which was conducted on the liquid product obtained from the conversion of beech wood and industrial digestate using diverse heteropolyacids as additives. As depicted in Figure 7.6, the GPC results show that HPMo as additive yields the highest peak corresponding to dimers that are formed through repolymerization. This is followed by HPW, which provides a plausible explanation for their relatively lower monomer yields observed in Figure 7.4 as determined by GC-MS analysis.

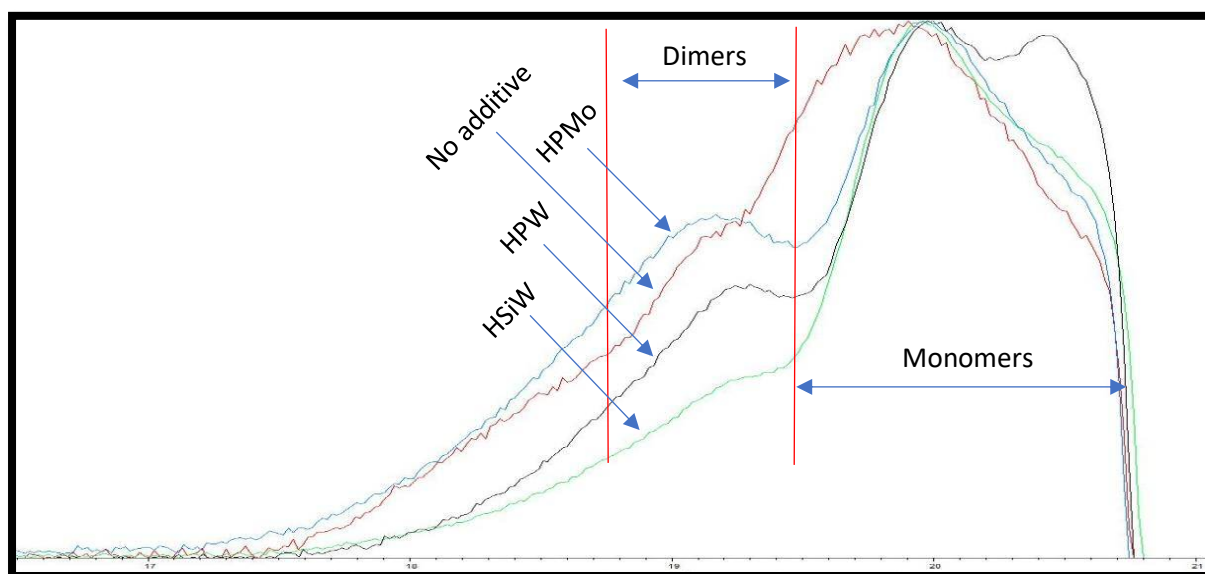


Figure 7.6 GPC for different lignin oils produced from RCF of beech wood, with and without POMs additives, comparing molecular weight distribution in function of time, where x-axis represents retention time (min) and y-axis represents the signal.

It is noteworthy that the acidic properties are also reported to be responsible for promoting hemicellulose and cellulose dissolution [14], which is consistent with the higher levels of biomass mass loss observed during the RCF experiments conducted with HSiW and HPW additives.

7.4. Conclusion

POMs were investigated for their potential applications in several hydroprocessing reactions for biomass valorization. The addition of POMs as an acidic support along with a metal function or as an additive with another catalyst in the reaction medium significantly altered the selectivity towards specific products, as compared to using POMs alone or employing metal POM composites as reductive catalysts. For the hydrogenation of furans, a Pt-supported on moderate acid Keggin salt ($K_3[PW_{12}O_{40}]$) exhibited superior performance, with a selectivity of up to 72.5% towards HXL production. In the hydrogenolysis of glycerol under mild reaction conditions, the combination of Ru/C with $H_3[PMo_{12}O_{40}]$ resulted in a significant increase in selectivity towards 1,2 PD (70.6%). The observed higher selectivity towards 1,2 PD was attributed to surface modification of Ru/C due to the addition of $H_3[PMo_{12}O_{40}]$ to the reaction medium. However, in the case of RCF, the addition of POMs had a negative impact due to their high acidic properties and HDO capabilities, leading to a shift in selectivity away from desired GPOH and SPOH towards the formation of GP, SP, and oligomers.

Chapter 8. Comprehensive discussion

Catalytic hydroprocessing is a crucial reaction class in the conversion of biomass molecules into a diverse range of fuels and chemicals. The objective of this study was to valorize various types of biomass classes into chemicals and fuels using selective hydroprocessing techniques, including hydrogenation of furans derived from cellulose and hemicellulose into alcohols, hydrogenolysis of glycerol derived from oils into 1,2-propanediol, and reductive catalytic fractionation for lignin valorization into phenolic monomers.

8.1. Hydrogenation of furans

The hydrogenation of furans began with the selection of DMF as a model substrate, followed by screening of different catalysts to identify the most suitable active metal site for selective ring opening and production of HXL. The results showed that Pt was the most selective metal site for the desired furan ring opening reaction among the tested metal sites, under the reaction conditions of 80°C and 10 bar H₂. This was attributed to the preferred adsorption configuration of furans on Pt, which is σ_{cc} . The influence of the carrier liquid was also investigated, and n-decane was found to be the optimal liquid carrier in our system, among the tested liquid carriers, owing to its higher H₂ solubility and its suitable viscosity.

Despite several attempts to use Pt-substituted POMs as heterogeneous catalysts for DMF hydrogenation, no significant DMF conversion could be achieved under the applied reaction conditions. Therefore, an alternative approach was taken to investigate the potential of a bifunctional catalyst for selective DMF hydrogenation. This involved the impregnation of Pt onto three heteropolyacids possessing a Keggin-type structure. Pt/phosphotungstic acid demonstrated superior performance, achieving a yield of 50% for HXL. However, it displayed a higher tendency for ring saturation hydrogenation, leading to an increased production of DMTHF (29%), as well as greater HX formation (12%) through dehydration of HXL. The introduction of silicon (Si) in place of phosphorus (P) in the heteropolyacid led to a significant decline in performance, with only 45% DMF conversion observed. The application of HPMo as a heteropolyanion resulted in a significant decline in the catalyst's performance, with only 3% conversion achieved. The exceptional activity of HPW acid among the Keggin-type structures could be attributed to its higher acid strength, which is evident from the ammonia desorption temperatures (in degrees Celsius) arranged in the following order: H₃[PW₁₂O₄₀] > H₄[SiW₁₂O₄₀] > H₃[PMo₁₂O₄₀] > H₄[SiMo₁₂O₄₀] = 592 > 532 > 463 > 423. It is important to note that HPMo lost its Keggin structure during reduction, whereas Pt/H₃[PW₁₂O₄₀] retained its structure after reduction and further reaction.

Additionally, Pt was supported on WD-type acidic potassium POMs salts, such as Pt/K₆[α P₂W₁₈O₆₂], which exhibited slightly lower conversion than Pt supported on Keggin type POMs, but demonstrated high selectivity towards HXN over HXL. When Pt was supported on mono vacant potassium salt, Pt/K₇[α PW₁₁O₃₉], the catalyst's performance significantly decreased compared to Pt supported on Keggin type POMs, resulting in only 1.8 % DMF conversion.

By manipulating the content of counter-cations in H₃[PW₁₂O₄₀], it was observed that the Cs-salt of Keggin-type tungstophosphate exhibited high conversion and a tendency towards the

formation of the desired product (HXL, 54%) in comparison to heteropoly acids and Cu-salts. However, similar to Pt/H₃[PW₁₂O₄₀], the Cs-salt resulted in the generation of substantial amounts of DMTHF (36%) and hexane (8%), which could be attributed to the very high Brønsted acidity of Cs salt POMs and H₃[PW₁₂O₄₀].

Optimizing the synthesis of Pt supported on the moderately acidic K-salt of Keggin-type tungstophosphate (Pt/K₃[PW₁₂O₄₀]) was found to produce the most selective catalyst for HXL production, yielding approximately 72.5%. The investigations showed that modifying the synthesis of the Pt/POM catalyst or the POM structure resulted in structural changes in the resulting Pt/POM system, which can lead to enhanced catalytic performance. For instance, the use of KCl instead of KHCO₃ as a source of potassium ions during the preparation of K₃[PW₁₂O₄₀], and water as a solvent instead of acetone during the wet merging of the Pt precursor with the POM species, significantly improved the Pt/K₃[PW₁₂O₄₀] catalytic performance due to the higher dispersion of Pt on the POM surface. Furthermore, Pt(acac)₂ as a Pt precursor showed better results than using H₂PtCl₆, which is attributed to the better dispersion of Pt on the surface in case of Pt(acac)₂.

Subsequent to identifying the most effective Pt/POM catalyst (Pt/K₃[PW₁₂O₄₀]) through prior investigations, we conducted further experiments using diverse furanic substrates (DMF, MF, furan) to compare its catalytic performance against that of the commercially available (Pt/C) catalyst. The results showed that Pt/K₃[PW₁₂O₄₀] outperformed commercial Pt/C in alcohol production, achieving yields of (72.5%), (44.3%) and (59.7%) for 2-hexanol, 1/2-pentanol, and 1-butanol, respectively.

The Pt/K₃[PW₁₂O₄₀] and Pt/C catalysts were subjected to various analytical techniques such as CO chemisorption, N₂ physisorption, TEM, XRD, and NH₃-TPD to explain the observed variations in the performance of these supported Pt catalysts. These analyses revealed several structural disparities. Furthermore, the moderate surface acidity of the POM support, as measured by NH₃-TPD, was found to enhance catalytic performance and selectivity towards HXL. The K₃[PW₁₂O₄₀] support functioned as a moderate acid site, augmenting C=O hydrogenation and surmounting the rate-limiting step of HXN hydrogenation to HXL, without showing a high degree of HXL dehydration that results in HX production. The presence of acid sites in the support plays a crucial role in activating the C=O bond, where a charge transfer interaction between the oxygen atoms in the carbonyl group and the cationic sites in the support generates a negative charge localized around carbonyl C, activating it for hydrogenation.

The next studies employed RSM to investigate the influence of key process parameters, such as temperature (T), pressure (P), and substrate-to-catalyst ratio (S/C), on the selective hydrogenation of DMF, which served as a representative model compound for bio-derived furans. To achieve optimization of the reaction, DoE and a desirability function approach were implemented, and with the help of them, we were able to achieve a 78% yield of HXL at complete DMF conversion using the Pt/K₃PW₁₂O₄₀ catalyst.

The implementation of RSM involved the selection of a Box-Behnken design in our study due to its higher efficiency compared to other response surface designs. Following the design

selection, a total of 15 laboratory runs were performed by altering the temperature, pressure, and substrate-to-catalyst ratio. The next step involved constructing four statistical models to establish the relationships between the various parameters and the yield of HXL, HXN, DMTHF, and HX. Backward selection methods were employed for automatic model building, and selection criteria included P-value and Bayesian information criterion. The models were statistically validated using ANOVA, and all statistical estimators, including F-value, P-value, R^2 , $R^2_{adj.}$, $pred.R^2$, and lack of fit, were reported. Additional experiments were conducted to experimentally validate the models, which confirmed that the four models accurately represented the yield of each product and could be utilized for analysis and predictions.

Response surface and contour plots, generated using the DesignExpert software, were employed to explore the effect of T, p, and S/C on the yield of each product. Results indicated that all variables were significant in the formation of HXL, as evidenced by their low P-values. Increasing T at low p or increasing p at low T enhanced the yield of HXL, in accordance with previous observations, which suggests that a higher temperature leads to the desired ring opening process that yields HXL and HXN, whereas a higher pressure favors the consecutive hydrogenation of ring-opened intermediate HXN to HXL. An interaction between the S/C ratio, pressure, and temperature was observed, wherein at a high S/C ratio of 130, an increase in P and T leads to an increase in HXL yield. However, at a low S/C ratio of 70, increasing P and T to their maximum values simultaneously results in a lower HXL yield.

In the case of HX, S/C ratio was found to be the most significant variable. Higher amounts of catalyst containing more acid sites can lead to an increased HX yield. Regarding DMTHF, increasing the temperature or decreasing S/C ratio increases the DMTHF yields slightly. However, the H_2 pressure is found to be the most significant factor influencing DMTHF production. A substantial increase in DMTHF yield is observed upon increasing H_2 pressure, as the rate of ring saturation increases much more than the rate of ring opening with increasing the H_2 pressure.

After that, a numerical optimization technique utilizing the desirability function theory was utilized to determine the optimum reaction conditions for maximizing the desired HXL production. An impressive yield of approximately 78% HXL was achieved at full DMF conversion, using a $Pt/K_3PW_{12}O_{40}$ catalyst under the following conditions: 83°C, S/C ratio of 88 (mol (DMF)/mol(Pt)), and a starting H_2 pressure of 5 bar, which was increased to 15 bar after 30 minutes.

Finally, time-resolved investigations were conducted to elucidate the underlying reason for the high yield of HXL (77.4%) achieved with the help of DoE by increasing the pressure from 5 to 15 bar after 30 minutes. The initial stages of the reaction at low H_2 pressure of 5 bars, where most of the DMF conversion occurred, resulted in limited formation of DMTHF, favoring instead the ring-opening reaction. With increasing H_2 pressure to 15 bar after 30 minutes, the mass transfer limitation of H_2 was overcome, and the rate-limiting step of hydrogenation of ring-opened HXN to HXL was accelerated, significantly increasing the rate of HXL formation, and maximizing the overall HXL yield.

8.2. Hydrogenolysis of glycerol

The catalyst's metal site screening results indicated that Ru/C demonstrated the highest activity among the tested catalysts with a conversion rate of 44.5% under the reaction conditions applied. This is attributed to its efficiency in scission of both C-O and C-C bonds. Moreover, the addition of POMs to the reaction medium increased the selectivity towards 1,2-PD from 21.7% to 70% for HPMo. Among the tested POMs, HPMo exhibited the highest selectivity towards 1,2 PD, followed by HPW and HSiW. TEM-EDX and FTIR analyses of the spent catalyst provided evidence for POMs precipitation during the reaction, as demonstrated by the presence of Mo and P. The surface modification of Ru due to POMs precipitation is likely responsible for the observed increase in selectivity towards 1,2 PD. The selectivity towards 1,2 PD increased in an order which is constituent with the order of their HDO ability $[\text{SiW}_{12}\text{O}_{40}]^{4-} < [\text{PW}_{12}\text{O}_{40}]^{3-} < [\text{PMo}_{12}\text{O}_{40}]^{3-}$. TEM-EDX and FTIR analyses showed that the POMs remained intact and undecomposed following precipitation, as evidenced by the nearly identical surface distribution of Mo and P, and the existence of all the characteristic bands of Keggin anion in the region of 1100-550 cm^{-1} in the spectra of Ru/C spent catalyst. Furthermore, the Ru was occasionally partially covered by the POMs.

In further investigation, the surface modification of Ru based catalyst with other transition metals like Fe and Cu, which are two of the most selective transition metals towards 1,2 PD identified in the literature, was investigated. The results showed a significant increase in selectivity towards 1,2 PD subsequent to the surface modification of Ru-based catalysts with both Fe and Cu. Remarkably, the utilization of the $\text{Ru}_1\text{Cu}_2/\text{CNT}$ catalyst for the hydrogenolysis of glycerol resulted in a 1,2 PD selectivity of 93.4%. Adding Cu to Ru nanoparticles dispersed on a CNT support significantly enhanced the reducibility and modified the surface of the resulting catalyst. The chemical composition of the resulting bimetallic Ru-Cu catalyst, as well as the surface interaction between Cu and Ru, led to a promoting effect resulting in a preference for C-O bond cleavage promoted by Cu over C-C bond cleavage catalyzed by small Ru nanoparticles.

8.3. Reductive catalytic fractionation for lignin valorization

The present study aimed to assess the viability of straw digestate as a lignin-rich substrate for RCF, and to compare it with beech wood, for the production of phenolic monomers. Compositional analysis revealed that the lignin content in the digestate was comparable to or higher than that in beech wood. Moreover, the digestate contained a significant amount of phenolic esters (ferulate and p-coumarate), which are typical of herbaceous biomass, in contrast to beech wood.

RCF was performed on beech wood as a substrate using different catalysts to investigate the effect of metal site and support during the reaction. It was observed that catalysts supported on C produced higher amounts of monomers than those supported on alumina, possibly due to the higher acidity of alumina that enhances condensation reactions. The Ru-based catalyst exhibited a preference for the production of GP/SP, whereas NiSat showed selectivity towards SPOH/GPOH.

Further investigations were conducted to extend the application of RCF to straw and straw digestate substrates, using NiSat catalyst. Interestingly, two additional monomers GPaMe and HPaMe were obtained from straw and digestate compared to beech wood. Observations from

the experimental analysis indicate that lignin degradation, affecting hydroxycinnamates incorporated into the lignin structure of straw, occurs during the fermentation and processing of straw. Consequently, the RCF of industrial straw digestate resulted in a monomer yield of 21 wt.%, which is slightly lower by 4 wt.% compared to rye straw.

The investigation of POMs as additives in combination with commercial catalysts in the reaction medium was also explored. Various heteropolyacids, including HPMo, HSiW, and HPW, were examined in conjunction with Ru/C, Ni/Sat, and Ni/C, using beech wood and straw industrial digestate as substrates. Results showed that none of the POMs led to an increase in monomer yield from beech wood, and instead resulted in reduced yields, with HPMo consistently causing the most significant decrease while HSiW resulted in the lowest decrease. Additionally, the inclusion of these additives induced a shift in product selectivity, leading to a decrease in the γ -OH: γ -H ratio when compared to experiments conducted without any additives. Similar trends were observed when using straw industrial digestate as a substrate. The observed results could be attributed to two distinct characteristics of POMs: their acid properties and hydrodeoxygenation capability. Adding POMs to the reaction medium led to preferential cleavage of hydroxyl groups located in the sidechains of monolignols and SPOH/GPOH through the HDO capability of POMs. The cleavage of hydroxyl groups in the sidechains of monolignols intermediates and SPOH/GPOH, by POMs HDO capability, led to the production of GPe/Spe and SP/GP, respectively. These GPe/Spe can further undergo hydrogenation to increase the yield of GP/SP or participate in repolymerization reactions to form dimers and oligomers. The presence of acidic properties in the reaction medium, such as POMs, favored C-C and C-O bond formation, which increased the repolymerization tendency during the reaction. The order of monomer yield produced when POMs were added was HPMo<HPW<HSiW, which is consistent with the order of catalytic activity in HDO $[\text{SiW}_{12}\text{O}_{40}]^{4-}$ < $[\text{PW}_{12}\text{O}_{40}]^{3-}$ < $[\text{PMo}_{12}\text{O}_{40}]^{3-}$. The validity of this illustration has been augmented through the implementation of GPC analysis, which showed that HPMo as additive yielded the highest peak corresponding to dimers that are formed through repolymerization, followed by HPW and HSiW.

Additionally, different other parameters were investigated for RCF, including the effect of alkaline treatment, pre-washing, reaction time, and H₂ pressure. The alkaline treatment showed that a significant portion of the lignin in the straw digestate is solubilized by alkaline treatment, and hardly any lignin remains in the solid biomass during alkaline treatment. Conversely, a large part of the beech wood lignin is alkali-insoluble, and from the alkali-insoluble residue, a large amount of lignin monomers is obtained. Pre-washing was found to be a crucial step in maximizing the monomer yield in RCF of industrial digestate. Increasing the reaction time up to 7 hours was observed to enhance the monomer yield produced, although the γ -OH monomer share tended to decrease, indicating that the cleavage of γ -OH in SPOH and GPOH to form SP/GP was a secondary reaction. Additionally, an increase in the H₂ pressure was found to increase the monomer yield, as well as the selectivity towards γ -OH monomers.

Chapter 9. Bibliography

1. Zhang, Y.P., *Reviving the carbohydrate economy via multi-product lignocellulose biorefineries*. Journal of industrial microbiology and biotechnology, 2008. **35**(5): p. 367-375.
2. Behr, A. and T. Seidensticker, *Chemistry of Renewables: An Introduction*. 2020: Springer Nature.
3. Baskar, C., S. Baskar, and R.S. Dhillon, *Biomass conversion: The interface of biotechnology, chemistry and materials science*. 2012: Springer Science & Business Media.
4. Sherbi, M., M. Stuckart, and J. Albert, *Selective catalytic hydrogenation of biomass derived furans to secondary alcohols using Pt/polyoxometalate catalysts under mild reaction conditions*. Biofuels, Bioproducts and Biorefining, 2021. **15**(5): p. 1431-1446.
5. Kumpidet, C., *Transformation of biomass to platform chemicals using homogeneous polyoxometalate catalysts*. 2020, Friedrich-Alexander-Universität Erlangen-Nürnberg (FAU).
6. Voß, D., *Selektive katalytische Umsetzung biogener Rohstoffe zu organischen Säuren unter Einsatz von Polyoxometallat-Katalysatoren*. 2020, Friedrich-Alexander-Universität Erlangen-Nürnberg (FAU).
7. Klemm, D., et al., *Cellulose: fascinating biopolymer and sustainable raw material*. Angewandte chemie international edition, 2005. **44**(22): p. 3358-3393.
8. Huang, Y.-B. and Y. Fu, *Hydrolysis of cellulose to glucose by solid acid catalysts*. Green Chemistry, 2013. **15**(5): p. 1095-1111.
9. Geboers, J.A., et al., *Chemocatalytic conversion of cellulose: opportunities, advances and pitfalls*. Catalysis Science & Technology, 2011. **1**(5): p. 714-726.
10. Alonso, D.M., J.Q. Bond, and J.A. Dumesic, *Catalytic conversion of biomass to biofuels*. Green chemistry, 2010. **12**(9): p. 1493-1513.
11. Bukowski, A., *Anwendung von redoxaktiven Polyoxometallaten in technisch relevanten Prozessen zur stofflichen und energetischen Biomasseumsetzung*. 2021, Friedrich-Alexander-Universität Erlangen-Nürnberg (FAU).
12. Melro, E., et al., *Revisiting lignin: A tour through its structural features, characterization methods and applications*. New Journal of Chemistry, 2021. **45**(16): p. 6986-7013.
13. Ralph, J., *Hydroxycinnamates in lignification*. Phytochemistry Reviews, 2010. **9**(1): p. 65-83.
14. Anderson, E.M., et al., *Reductive catalytic fractionation of corn stover lignin*. ACS Sustainable Chemistry & Engineering, 2016. **4**(12): p. 6940-6950.
15. Chakar, F.S. and A.J. Ragauskas, *Review of current and future softwood kraft lignin process chemistry*. Industrial crops and products, 2004. **20**(2): p. 131-141.
16. Vanholme, R., et al., *Lignin engineering*. Current opinion in plant biology, 2008. **11**(3): p. 278-285.
17. Korányi, T.I., et al., *Development of 'Lignin-First' approaches for the valorization of lignocellulosic biomass*. Molecules, 2020. **25**(12): p. 2815.
18. Ragauskas, A.J., et al., *Lignin valorization: improving lignin processing in the biorefinery*. science, 2014. **344**(6185): p. 1246843.
19. Zakzeski, J., et al., *The catalytic valorization of lignin for the production of renewable chemicals*. Chemical reviews, 2010. **110**(6): p. 3552-3599.

20. Rogalska, E., et al., *Stereoselective hydrolysis of triglycerides by animal and microbial lipases*. Chirality, 1993. **5**(1): p. 24-30.
21. Karmakar, G., P. Ghosh, and B.K. Sharma, *Chemically modifying vegetable oils to prepare green lubricants*. Lubricants, 2017. **5**(4): p. 44.
22. Endisch, M., T. Kuchling, and J. Roscher, *Process balances of vegetable oil hydrogenation and coprocessing investigations with middle-distillates*. Energy & fuels, 2013. **27**(5): p. 2628-2636.
23. Rinaldi, R., *Catalytic hydrogenation for biomass valorization*. 2015: Royal Society of Chemistry.
24. Ye, S., et al., *Chemical energy storage*. 2022: Walter de Gruyter GmbH & Co KG.
25. Rinaldi, R. and F. Schüth, *Design of solid catalysts for the conversion of biomass*. Energy & Environmental Science, 2009. **2**(6): p. 610-626.
26. Schüth, F., *Hydrogen: economics and its role in biorefining*. 2014.
27. Kobayashi, H., H. Ohta, and A. Fukuoka, *Noble-Metal Catalysts for Conversion of Lignocellulose under Hydrogen Pressure*. Catalytic Hydrogenation for Biomass Valorization, 2014. **13**: p. 52.
28. Kaltschmitt, M. and W. Streicher, *Energie aus biomasse*. 2009: Springer.
29. Kaltschmitt, M., *Energy from organic materials (biomass): a volume in the encyclopedia of sustainability science and technology*. 2019: Springer.
30. Vispute, T.P., et al., *Renewable chemical commodity feedstocks from integrated catalytic processing of pyrolysis oils*. Science, 2010. **330**(6008): p. 1222-1227.
31. Román-Leshkov, Y., et al., *Production of dimethylfuran for liquid fuels from biomass-derived carbohydrates*. Nature, 2007. **447**(7147): p. 982-985.
32. Chen, S., et al., *How catalysts and experimental conditions determine the selective hydroconversion of furfural and 5-hydroxymethylfurfural*. Chemical reviews, 2018. **118**(22): p. 11023-11117.
33. Sutton, A.D., et al., *The hydrodeoxygenation of bioderived furans into alkanes*. Nature chemistry, 2013. **5**(5): p. 428-432.
34. Louie, Y.L., *Synthesis, Hydrogenation, and Hydrodeoxygenation of Biomass-Derived Furans for Diesel Fuel*. 2017: University of California, Berkeley.
35. Hengst, K., et al., *Hydrodeoxygenation of lignocellulose-derived platform molecules*, in *Catalytic Hydrogenation for Biomass Valorization*. 2014, The Royal Society of Chemistry: Cambridge, UK. p. 125-150.
36. Louie, Y.L., et al., *Kinetics of hydrogenation and hydrogenolysis of 2, 5-dimethylfuran over noble metals catalysts under mild conditions*. Applied Catalysis B: Environmental, 2017. **202**: p. 557-568.
37. Renders, T., et al., *Reductive catalytic fractionation: state of the art of the lignin-first biorefinery*. Current opinion in biotechnology, 2019. **56**: p. 193-201.
38. RETNOARDIYANTI, A. and H.J. HEERES, *Catalytic hydrotreatment of fast pyrolysis oils using supported metal catalysts*. Catalytic Hydrogenation for Biomass Valorization, 2015(13): p. 151.
39. Gomes, J.R., et al., *Biofuels Generation via Hydroconversion of Vegetable Oils and Animal Fats*. Catalytic Hydrogenation for Biomass Valorization, 2014(13): p. 204.
40. Chaminand, J., et al., *Glycerol hydrogenolysis on heterogeneous catalysts*. Green chemistry, 2004. **6**(8): p. 359-361.
41. Bertleff, B., *Extractive catalytic oxidative desulfurization and denitrogenation of fuels using vanadium substituted heteropolyacids and molecular oxygen*. 2020, Friedrich-Alexander-Universität Erlangen-Nürnberg (FAU).
42. Rhule, J.T., et al., *Polyoxometalates in medicine*. Chemical Reviews, 1998. **98**(1): p. 327-358.

43. Pope, M.T. and A. Müller, *Polyoxometalate chemistry: an old field with new dimensions in several disciplines*. Angewandte Chemie International Edition in English, 1991. **30**(1): p. 34-48.
44. Wang, S.-S. and G.-Y. Yang, *Recent advances in polyoxometalate-catalyzed reactions*. Chemical reviews, 2015. **115**(11): p. 4893-4962.
45. Zhong, J., J. Pérez-Ramírez, and N. Yan, *Biomass valorisation over polyoxometalate-based catalysts*. Green Chemistry, 2021. **23**(1): p. 18-36.
46. Hill, C.L. and C.M. Prosser-McCartha, *Homogeneous catalysis by transition metal oxygen anion clusters*. Coordination Chemistry Reviews, 1995. **143**: p. 407-455.
47. Pope, M.T. and A. Müller, *Chemie der Polyoxometallate: Aktuelle Variationen über ein altes Thema mit interdisziplinären Bezügen*. Angewandte Chemie, 1991. **103**(1): p. 56-70.
48. Ammam, M., *Polyoxometalates: formation, structures, principal properties, main deposition methods and application in sensing*. Journal of Materials Chemistry A, 2013. **1**(21): p. 6291-6312.
49. Pope, M.T., Y. Jeannin, and M. Fournier, *Heteropoly and isopoly oxometalates*. Vol. 8. 1983: Springer.
50. Borrás-Almenar, J.J., et al., *Polyoxometalate molecular science*. Vol. 98. 2003: Springer Science & Business Media.
51. Li, G., et al., *New progress of Keggin and Wells–Dawson type polyoxometalates catalyze acid and oxidative reactions*. Journal of Molecular Catalysis A: Chemical, 2007. **262**(1-2): p. 67-76.
52. Khenkin, A.M. and R. Neumann, *Aerobic Oxidation of Vicinal Diols Catalyzed by an Anderson-Type Polyoxometalate, [IMo6O24] 5-*. Advanced Synthesis & Catalysis, 2002. **344**(9): p. 1017-1021.
53. López, X., et al., *Structure, properties and reactivity of polyoxometalates: a theoretical perspective*. Chemical Society Reviews, 2012. **41**(22): p. 7537-7571.
54. Kozhevnikov, I.V., *Catalysis by heteropoly acids and multicomponent polyoxometalates in liquid-phase reactions*. Chemical reviews, 1998. **98**(1): p. 171-198.
55. Lopez, X., et al., *Electronic properties of polyoxometalates: A DFT study of α/β -[XM12O40] n-relative stability (M= W, Mo and X a main group element)*. Journal of the American Chemical Society, 2001. **123**(39): p. 9571-9576.
56. Pettersson, L., et al., *Multicomponent polyanions. 46. Characterization of the isomeric Keggin decamolybdovanadophosphate ions in aqueous solution by 31P and 51V NMR*. Inorganic Chemistry, 1994. **33**(5): p. 982-993.
57. Okuhara, T., N. Mizuno, and M. Misono, *Catalytic chemistry of heteropoly compounds*, in *Advances in catalysis*. 1996, Elsevier. p. 113-252.
58. Hill, C.L., *Introduction: polyoxometalates multicomponent molecular vehicles to probe fundamental issues and practical problems*. Chemical Reviews, 1998. **98**(1): p. 1-2.
59. Modvig, A., et al., *Ru-doped wells–dawson polyoxometalate as efficient catalyst for glycerol hydrogenolysis to propanediols*. Materials, 2019. **12**(13): p. 2175.
60. Voß, D., H. Pickel, and J. Albert, *Improving the fractionated catalytic oxidation of lignocellulosic biomass to formic acid and cellulose by using design of experiments*. ACS Sustainable Chemistry & Engineering, 2019. **7**(11): p. 9754-9762.
61. Albert, J., et al., *Spectroscopic and electrochemical characterization of heteropoly acids for their optimized application in selective biomass oxidation to formic acid*. Green Chemistry, 2014. **16**(1): p. 226-237.

62. Maerten, S., et al., *Glucose oxidation to formic acid and methyl formate in perfect selectivity*. Green Chemistry, 2020. **22**(13): p. 4311-4320.
63. Albert, J., et al., *One-step synthesizable lindqvist– isopolyoxometalates as promising new catalysts for selective conversion of glucose as a model substrate for lignocellulosic biomass to formic acid*. ChemistrySelect, 2016. **1**(11): p. 2889-2894.
64. Bertleff, B., et al., *Extractive Catalytic Oxidative Denitrogenation of Fuels and Their Promoting Effect for Desulfurization Catalyzed by Vanadium Substituted Heteropolyacids and Molecular Oxygen*. Energy & Fuels, 2020. **34**(7): p. 8099-8109.
65. Gao, G., et al., *CO₂ coordination by inorganic polyoxoanion in water*. Journal of the American Chemical Society, 2008. **130**(33): p. 10838-10839.
66. Putluru, S.S.R., et al., *Heteropoly acid promoted Cu and Fe catalysts for the selective catalytic reduction of NO with ammonia*. Catalysis today, 2011. **176**(1): p. 292-297.
67. Kogan, V., Z. Aizenshtat, and R. Neumann, *Polyoxometalates as reduction catalysts: Deoxygenation and hydrogenation of carbonyl compounds*. Angewandte Chemie International Edition, 1999. **38**(22): p. 3331-3334.
68. North, J., et al., *Efficient hydrodesulfurization catalysts based on Keggin polyoxometalates*. Applied Catalysis A: General, 2015. **508**: p. 16-24.
69. Benaissa, H., et al., *Heteropoly compounds as catalysts for hydrogenation of propanoic acid*. Journal of Catalysis, 2008. **253**(2): p. 244-252.
70. Benaissa, H., et al., *Gas-phase hydrogenation of hexanoic acid over P–Mo–V heteropoly compounds in comparison with the constituent Mo and V oxides*. Applied Catalysis A: General, 2008. **351**(1): p. 88-92.
71. Kogan, V., Z. Aizenshtat, and R. Neumann, *Preferential catalytic hydrogenation of aromatic compounds versus ketones with a palladium substituted polyoxometalate as pre-catalyst*. New Journal of Chemistry, 2002. **26**(3): p. 272-274.
72. Srivani, A., P. Prasad, and N. Lingaiah, *Reductive amination of carbonyl compounds over silica supported palladium exchanged molybdophosphoric acid catalysts*. Catalysis letters, 2012. **142**(3): p. 389-396.
73. Poole, O., et al., *Hydrodeoxygenation of 3-pentanone over bifunctional Pt-heteropoly acid catalyst in the gas phase: Enhancing effect of gold*. Applied Catalysis B: Environmental, 2017. **202**: p. 446-453.
74. Hetterley, R.D., E.F. Kozhevnikova, and I.V. Kozhevnikov, *Multifunctional catalysis by Pd-polyoxometalate: one-step conversion of acetone to methyl isobutyl ketone*. Chemical communications, 2006(7): p. 782-784.
75. da Silva Rocha, K.A., et al., *Pd-heteropoly acid as a bifunctional heterogeneous catalyst for one-pot conversion of citronellal to menthol*. Applied Catalysis A: General, 2007. **317**(2): p. 171-174.
76. Liu, Y. and M. Misono, *Hydroisomerization of n-butane over platinum-promoted cesium hydrogen salt of 12-tungstophosphoric acid*. Materials, 2009. **2**(4): p. 2319-2336.
77. Branytska, O., L.J. Shimon, and R. Neumann, *Tandem pinacol coupling–rearrangement of aromatic aldehydes with hydrogen catalyzed by a combination of a platinum complex and a polyoxometalate*. Chemical communications, 2007(38): p. 3957-3959.
78. Almohalla, M., et al., *Cooperative action of heteropolyacids and carbon supported Ru catalysts for the conversion of cellulose*. Catalysis Today, 2018. **301**: p. 65-71.
79. Zhu, S., et al., *One-pot conversion of furfural to alkyl levulinate over bifunctional Au–H₄SiW₁₂O₄₀/ZrO₂ without external H₂*. Green Chemistry, 2016. **18**(20): p. 5667-5675.

80. Anderson, E., et al., *Bifunctional Molybdenum Polyoxometalates for the Combined Hydrodeoxygenation and Alkylation of Lignin-Derived Model Phenolics*. ChemSusChem, 2017. **10**(10): p. 2226-2234.
81. Alharbi, K., et al., *Deoxygenation of ethers and esters over bifunctional Pt–heteropoly acid catalyst in the gas phase*. ACS Catalysis, 2016. **6**(3): p. 2067-2075.
82. Yang, Z., et al., *Synergistic effect of active metal–acid sites on hydrodeoxygenation of lignin-derived phenolic compounds under mild conditions using Ru/C-HPW catalyst*. Fuel, 2022. **319**: p. 123617.
83. Alharbi, K., E. Kozhevnikova, and I. Kozhevnikov, *Hydrogenation of ketones over bifunctional Pt-heteropoly acid catalyst in the gas phase*. Applied Catalysis A: General, 2015. **504**: p. 457-462.
84. Mai, C.T. and F.T. Ng, *Effect of Cs⁺ on the hydrogenolysis of glycerol to higher value sustainable and green chemicals using a supported Ni-HSiW catalyst*. Catalysis Today, 2017. **291**: p. 195-203.
85. Mai, C.T. and F.T. Ng, *Effect of metals on the hydrogenolysis of glycerol to higher value sustainable and green chemicals using a supported HSiW catalyst*. Organic Process Research & Development, 2016. **20**(10): p. 1774-1780.
86. Zhu, S., et al., *One-step hydrogenolysis of glycerol to biopropanols over Pt–H₄SiW₁₂O₄₀/ZrO₂ catalysts*. Green Chemistry, 2012. **14**(9): p. 2607-2616.
87. Liu, M., et al., *Polyoxometalate-supported ruthenium nanoparticles as bifunctional heterogeneous catalysts for the conversions of cellobiose and cellulose into sorbitol under mild conditions*. Chemical communications, 2011. **47**(34): p. 9717-9719.
88. García-Bosch, N., et al., *Tracking the paths for the sucrose transformations over bifunctional Ru-POM/AC catalysts*. Catalysis Today, 2020. **357**: p. 113-121.
89. Gawade, A.B., M.S. Tiwari, and G.D. Yadav, *Biobased green process: Selective hydrogenation of 5-hydroxymethylfurfural to 2, 5-dimethyl furan under mild conditions using Pd-Cs₂. 5H₀. 5PW₁₂O₄₀/K-10 clay*. ACS Sustainable Chemistry & Engineering, 2016. **4**(8): p. 4113-4123.
90. Alotaibi, M.A., E.F. Kozhevnikova, and I.V. Kozhevnikov, *Efficient hydrodeoxygenation of biomass-derived ketones over bifunctional Pt-polyoxometalate catalyst*. Chem Commun (Camb), 2012. **48**(57): p. 7194-6.
91. Zhu, S., et al., *Hydrogenolysis of glycerol to 1, 3-propanediol over bifunctional catalysts containing Pt and heteropolyacids*. Catalysis today, 2013. **212**: p. 120-126.
92. Zhu, S., et al., *Alkaline metals modified Pt–H₄SiW₁₂O₄₀/ZrO₂ catalysts for the selective hydrogenolysis of glycerol to 1, 3-propanediol*. Applied catalysis B: environmental, 2013. **140**: p. 60-67.
93. Alhanash, A., E.F. Kozhevnikova, and I.V. Kozhevnikov, *Hydrogenolysis of glycerol to propanediol over Ru: polyoxometalate bifunctional catalyst*. Catalysis Letters, 2008. **120**(3): p. 307-311.
94. Op de Beeck, B., et al., *Conversion of (ligno) cellulose feeds to isosorbide with heteropoly acids and Ru on carbon*. ChemSusChem, 2013. **6**(1): p. 199-208.
95. Geboers, J., et al., *Efficient catalytic conversion of concentrated cellulose feeds to hexitols with heteropoly acids and Ru on carbon*. Chemical Communications, 2010. **46**(20): p. 3577-3579.
96. Geboers, J., et al., *Hydrolytic hydrogenation of cellulose with hydrotreated caesium salts of heteropoly acids and Ru/C*. Green Chemistry, 2011. **13**(8): p. 2167-2174.
97. Palkovits, R., et al., *Heteropoly acids as efficient acid catalysts in the one-step conversion of cellulose to sugar alcohols*. Chemical Communications, 2011. **47**(1): p. 576-578.

98. de Beeck, B.O., et al., *Direct catalytic conversion of cellulose to liquid straight-chain alkanes*. Energy & Environmental Science, 2015. **8**(1): p. 230-240.
99. Tai, Z., et al., *Catalytic conversion of cellulose to ethylene glycol over a low-cost binary catalyst of Raney Ni and tungstic acid*. ChemSusChem, 2013. **6**(4): p. 652-658.
100. Li, S., et al., *One-pot hydrodeoxygenation of biomass furan derivatives into decane under mild conditions over Pd/C combined with phosphotungstic acid*. Green Chemistry, 2020. **22**(9): p. 2889-2900.
101. ten Dam, J., et al., *Pt/Al₂O₃ catalyzed 1, 3-propanediol formation from glycerol using tungsten additives*. ChemCatChem, 2013. **5**(2): p. 497-505.
102. Balaraju, M., et al., *Influence of solid acids as co-catalysts on glycerol hydrogenolysis to propylene glycol over Ru/C catalysts*. Applied Catalysis A: General, 2009. **354**(1-2): p. 82-87.
103. He, Z. and X. Wang, *Hydrodeoxygenation of model compounds and catalytic systems for pyrolysis bio-oils upgrading*. Catalysis for sustainable energy, 2012. **1**(2013): p. 28-52.
104. Agirrezabal-Telleria, I., I. Gandarias, and P. Arias, *Heterogeneous acid-catalysts for the production of furan-derived compounds (furfural and hydroxymethylfurfural) from renewable carbohydrates: A review*. Catalysis Today, 2014. **234**: p. 42-58.
105. Lange, J.P., et al., *Furfural—a promising platform for lignocellulosic biofuels*. ChemSusChem, 2012. **5**(1): p. 150-166.
106. Román-Leshkov, Y., J.N. Chheda, and J.A. Dumesic, *Phase modifiers promote efficient production of hydroxymethylfurfural from fructose*. Science, 2006. **312**(5782): p. 1933-1937.
107. Stevens, J.G., et al., *Real-time product switching using a twin catalyst system for the hydrogenation of furfural in supercritical CO₂*. Angewandte Chemie International Edition, 2010. **49**(47): p. 8856-8859.
108. Wang, T., et al., *Aviation fuel synthesis by catalytic conversion of biomass hydrolysate in aqueous phase*. Applied energy, 2014. **136**: p. 775-780.
109. Chatterjee, M., T. Ishizaka, and H. Kawanami, *Hydrogenation of 5-hydroxymethylfurfural in supercritical carbon dioxide–water: a tunable approach to dimethylfuran selectivity*. Green Chemistry, 2014. **16**(3): p. 1543-1551.
110. Djokic, M., et al., *The thermal decomposition of 2, 5-dimethylfuran*. Proceedings of the Combustion Institute, 2013. **34**(1): p. 251-258.
111. Fábos, V., et al., *Bio-oxygenates and the peroxide number: a safety issue alert*. Energy & Environmental Science, 2009. **2**(7): p. 767-769.
112. Christensen, E., et al., *Experimental and theoretical study of oxidative stability of alkylated furans used as gasoline blend components*. Fuel, 2018. **212**: p. 576-585.
113. McCormick, R.L., et al., *Properties of oxygenates found in upgraded biomass pyrolysis oil as components of spark and compression ignition engine fuels*. Energy & Fuels, 2015. **29**(4): p. 2453-2461.
114. Williams, C.L., et al., *Cycloaddition of biomass-derived furans for catalytic production of renewable p-xylene*. ACS Catalysis, 2012. **2**(6): p. 935-939.
115. Uslamin, E.A., et al., *Co-Aromatization of furan and methanol over ZSM-5—a pathway to bio-aromatics*. ACS Catalysis, 2019. **9**(9): p. 8547-8554.
116. Li, G., et al., *Synthesis of renewable diesel with the 2-methylfuran, butanal and acetone derived from lignocellulose*. Bioresource technology, 2013. **134**: p. 66-72.
117. Ding, F., et al., *Synthesis and catalytic performance of Ni/SiO₂ for hydrogenation of 2-methylfuran to 2-methyltetrahydrofuran*. Journal of Nanomaterials, 2015. **16**(1): p. 60-60.

118. Gilkey, M.J., et al., *Insights into the ring-opening of biomass-derived furanics over carbon-supported ruthenium*. ChemSusChem, 2016. **9**(21): p. 3113-3121.
119. Kang, J., X. Liang, and V.V. Guliyants, *Selective Hydrogenation of 2-Methylfuran and 2, 5-Dimethylfuran over Atomic Layer Deposited Platinum Catalysts on Multiwalled Carbon Nanotube and Alumina Supports*. ChemCatChem, 2017. **9**(2): p. 282-286.
120. da Silva Trindade, W.R. and R.G. dos Santos, *Review on the characteristics of butanol, its production and use as fuel in internal combustion engines*. Renewable and Sustainable Energy Reviews, 2017. **69**: p. 642-651.
121. Scully, S.M. and J. Orlygsson, *Biological production of alcohols*, in *Advanced bioprocessing for alternative fuels, biobased chemicals, and bioproducts*. 2019, Elsevier. p. 83-108.
122. Wei, L., C.S. Cheung, and Z. Huang, *Effect of n-pentanol addition on the combustion, performance and emission characteristics of a direct-injection diesel engine*. Energy, 2014. **70**: p. 172-180.
123. Frerot, E., *Esters comprising a secondary carbamoyl function and their use as odorant alcohol precursors*. 2004, Google Patents.
124. Hall, J.B., et al., *Substituted dimethyl dihydroxy benzene and cyclohexadiene compounds and uses thereof for augmenting or enhancing the taste and/or aroma of consumable materials including tobaccos, perfumes and perfumed articles*. 1979, Google Patents.
125. De Pours, M.V., et al., *1-Hexanol as a sustainable biofuel in DI diesel engines and its effect on combustion and emissions under the influence of injection timing and exhaust gas recirculation (EGR)*. Applied Thermal Engineering, 2017. **113**: p. 1505-1513.
126. Heufer, K., J. Bugler, and H. Curran, *A comparison of longer alkane and alcohol ignition including new experimental results for n-pentanol and n-hexanol*. Proceedings of the Combustion Institute, 2013. **34**(1): p. 511-518.
127. Pandian, A.K., et al., *Emission and performance analysis of a diesel engine burning cashew nut shell oil bio diesel mixed with hexanol*. Petroleum Science, 2018. **15**: p. 176-184.
128. Runnebaum, R.C., et al., *Catalytic conversion of furan to gasoline-range aliphatic hydrocarbons via ring opening and decarbonylation reactions catalyzed by Pt/ γ -Al₂O₃*. Catalysis letters, 2012. **142**: p. 664-666.
129. Sutton, A.D., et al., *The hydrodeoxygenation of bioderived furans into alkanes*. Nature chemistry, 2013. **5**(5): p. 428-432.
130. Balakrishnan, M., E.R. Sacia, and A.T. Bell, *Selective hydrogenation of furan-containing condensation products as a source of biomass-derived diesel additives*. ChemSusChem, 2014. **7**(10): p. 2796-2800.
131. Jensen, C.M. and W.C. Troglor, *Catalytic hydration of terminal alkenes to primary alcohols*. Science, 1986. **233**(4768): p. 1069-1071.
132. Yin, M.-Y., et al., *Asymmetric hydrogenation of ketones catalyzed by a silica-supported chitosan-palladium complex*. Journal of Molecular Catalysis A: Chemical, 1999. **147**(1-2): p. 93-98.
133. Pham, T.T., et al., *Hydrogenation and Hydrodeoxygenation of 2-methyl-2-pentenal on supported metal catalysts*. Journal of Catalysis, 2009. **266**(1): p. 9-14.
134. Aliaga, C., et al., *Sum frequency generation vibrational spectroscopy and kinetic study of 2-methylfuran and 2, 5-dimethylfuran hydrogenation over 7 nm platinum cubic nanoparticles*. The Journal of Physical Chemistry C, 2011. **115**(16): p. 8104-8109.

135. Kang, J., A. Vonderheide, and V.V. Guliants, *Deuterium-Labeling Study of the Hydrogenation of 2-Methylfuran and 2, 5-Dimethylfuran over Carbon-Supported Noble Metal Catalysts*. ChemSusChem, 2015. **8**(18): p. 3044-3047.
136. Kliewer, C.J., et al., *Furan hydrogenation over Pt (111) and Pt (100) single-crystal surfaces and Pt nanoparticles from 1 to 7 nm: a kinetic and sum frequency generation vibrational spectroscopy study*. Journal of the American Chemical Society, 2010. **132**(37): p. 13088-13095.
137. Vorotnikov, V. and D.G. Vlachos, *Group additivity and modified linear scaling relations for estimating surface thermochemistry on transition metal surfaces: Application to furanics*. The Journal of Physical Chemistry C, 2015. **119**(19): p. 10417-10426.
138. Wang, S., V. Vorotnikov, and D.G. Vlachos, *A DFT study of furan hydrogenation and ring opening on Pd (111)*. Green Chemistry, 2014. **16**(2): p. 736-747.
139. Bel'skii, I.F. and N. Shuikin, *Catalytic hydrogenation and hydrogenolysis of furan compounds*. Russian Chemical Reviews, 1963. **32**(6): p. 307.
140. Biswas, P., et al., *Vapor phase hydrogenation of 2-methylfuran over noble and base metal catalysts*. Applied Catalysis A: General, 2014. **475**: p. 379-385.
141. Shuikin, N. and I. Bel'skii, *Catalytic hydrogenolysis of furan compounds*. Bulletin of the Academy of Sciences of the USSR, Division of chemical science, 1958. **7**(3): p. 293-298.
142. Wilson, C.L., *Reactions of furan compounds. X. Catalytic reduction of methylfuran to 2-pentanone*. Journal of the American Chemical Society, 1948. **70**(4): p. 1313-1315.
143. Jones, D. and A. Taylor, *Some aspects of furan and pyran chemistry*. Quarterly Reviews, Chemical Society, 1950. **4**(2): p. 195-216.
144. Brunner, E., *Solubility of hydrogen in 10 organic solvents at 298.15, 323.15, and 373.15 K*. Journal of chemical and Engineering Data, 1985. **30**(3): p. 269-273.
145. Wainwright, M.S., et al., *Solubility of hydrogen in alcohols and esters*. Journal of Chemical and Engineering Data, 1987. **32**(1): p. 22-24.
146. Ralph, J., C. Lapierre, and W. Boerjan, *Lignin structure and its engineering*. Current opinion in biotechnology, 2019. **56**: p. 240-249.
147. Cao, Y., et al., *Advances in lignin valorization towards bio-based chemicals and fuels: Lignin biorefinery*. Bioresource technology, 2019. **291**: p. 121878.
148. Galkin, M.V. and J.S. Samec, *Lignin valorization through catalytic lignocellulose fractionation: a fundamental platform for the future biorefinery*. ChemSusChem, 2016. **9**(13): p. 1544-1558.
149. Lancefield, C.S., et al., *Investigation of the chemocatalytic and biocatalytic valorization of a range of different lignin preparations: the importance of β -O-4 content*. ACS Sustainable Chemistry & Engineering, 2016. **4**(12): p. 6921-6930.
150. Dhyani, V. and T. Bhaskar, *A comprehensive review on the pyrolysis of lignocellulosic biomass*. Renewable energy, 2018. **129**: p. 695-716.
151. Rahman, M.M., R. Liu, and J. Cai, *Catalytic fast pyrolysis of biomass over zeolites for high quality bio-oil—a review*. Fuel Processing Technology, 2018. **180**: p. 32-46.
152. Lan, W. and J.S. Luterbacher, *Preventing lignin condensation to facilitate aromatic monomer production*. Chimia, 2019. **73**(7-8): p. 591-591.
153. Ghoreishi, S., T. Barth, and H. Derribsa, *Stirred and non-stirred lignin solvolysis with formic acid in aqueous and ethanolic solvent systems at different levels of loading in a 5-L reactor*. Biofuel research journal, 2019. **6**(1): p. 937.
154. Mottweiler, J., et al., *Iron-catalysed oxidative cleavage of lignin and β -O-4 lignin model compounds with peroxides in DMSO*. Green Chemistry, 2015. **17**(11): p. 5001-5008.

155. Liu, X., et al., *Recent advances in the catalytic depolymerization of lignin towards phenolic chemicals: a review*. ChemSusChem, 2020. **13**(17): p. 4296-4317.
156. Voithl, T. and P. Rudolf von Rohr, *Oxidation of lignin using aqueous polyoxometalates in the presence of alcohols*. ChemSusChem: Chemistry & Sustainability Energy & Materials, 2008. **1**(8-9): p. 763-769.
157. Bujanovic, B., et al., *Polyoxometalates in oxidative delignification of chemical pulps: Effect on lignin*. Materials, 2010. **3**(3): p. 1888-1903.
158. Gale, M., C.M. Cai, and K.L. Gilliard-Abdul-Aziz, *Heterogeneous Catalyst Design Principles for the Conversion of Lignin into High-Value Commodity Fuels and Chemicals*. ChemSusChem, 2020. **13**(8): p. 1947-1966.
159. Ha, J.-M., et al., *Recent progress in the thermal and catalytic conversion of lignin*. Renewable and Sustainable Energy Reviews, 2019. **111**: p. 422-441.
160. Dawange, M., M.V. Galkin, and J.S. Samec, *Selective aerobic benzylic alcohol oxidation of lignin model compounds: Route to aryl ketones*. ChemCatChem, 2015. **7**(3): p. 401-404.
161. Cheng, C., et al., *Catalytic oxidation of lignin in solvent systems for production of renewable chemicals: A review*. Polymers, 2017. **9**(6): p. 240.
162. Meng, X., et al., *Chemical transformations of poplar lignin during cosolvent enhanced lignocellulosic fractionation process*. ACS Sustainable Chemistry & Engineering, 2018. **6**(7): p. 8711-8718.
163. Wang, S., et al., *Selective Fragmentation of Biorefinery Corncob Lignin into p-Hydroxycinnamic Esters with a Supported Zinc Molybdate Catalyst*. ChemSusChem, 2018. **11**(13): p. 2114-2123.
164. Parto, S.G., et al., *Solvent assisted catalytic conversion of beech wood and organosolv lignin over NiMo/ γ -Al₂O₃*. Sustainable Energy & Fuels, 2020. **4**(4): p. 1844-1854.
165. Van den Bosch, S., et al., *Reductive lignocellulose fractionation into soluble lignin-derived phenolic monomers and dimers and processable carbohydrate pulps*. Energy & environmental science, 2015. **8**(6): p. 1748-1763.
166. Parsell, T., et al., *A synergistic biorefinery based on catalytic conversion of lignin prior to cellulose starting from lignocellulosic biomass*. Green Chemistry, 2015. **17**(3): p. 1492-1499.
167. Anderson, E.M., et al., *Kinetic studies of lignin solvolysis and reduction by reductive catalytic fractionation decoupled in flow-through reactors*. ACS Sustainable Chemistry & Engineering, 2018. **6**(6): p. 7951-7959.
168. Renders, T., et al., *Influence of acidic (H₃PO₄) and alkaline (NaOH) additives on the catalytic reductive fractionation of lignocellulose*. ACS Catalysis, 2016. **6**(3): p. 2055-2066.
169. Yan, N., et al., *Selective degradation of wood lignin over noble-metal catalysts in a two-step process*. ChemSusChem: Chemistry & Sustainability Energy & Materials, 2008. **1**(7): p. 626-629.
170. Huang, X., et al., *Effective release of lignin fragments from lignocellulose by Lewis acid metal triflates in the lignin-first approach*. ChemSusChem, 2016. **9**(23): p. 3262-3267.
171. Jastrzebski, R., et al., *Tandem catalytic depolymerization of lignin by water-tolerant Lewis acids and rhodium complexes*. ChemSusChem, 2016. **9**(16): p. 2074-2079.
172. Bernas, H., et al., *Influence of reaction parameters on the hydrogenolysis of hydroxymatairesinol over carbon nanofibre supported palladium catalysts*. Catalysis letters, 2008. **125**: p. 8-13.

173. Van den Bosch, S., et al., *Integrating lignin valorization and bio-ethanol production: on the role of Ni-Al₂O₃ catalyst pellets during lignin-first fractionation*. Green Chemistry, 2017. **19**(14): p. 3313-3326.
174. Yoo, C.G., et al., *The critical role of lignin in lignocellulosic biomass conversion and recent pretreatment strategies: A comprehensive review*. Bioresource technology, 2020. **301**: p. 122784.
175. Rinaldi, R., et al., *Lignin-first biorefining of lignocellulose: The impact of process severity on the uniformity of lignin oil composition*. Journal of the Brazilian Chemical Society, 2019. **30**: p. 479-491.
176. Thornburg, N.E., et al., *Mesoscale Reaction–Diffusion Phenomena Governing Lignin-First Biomass Fractionation*. ChemSusChem, 2020. **13**(17): p. 4495-4509.
177. Ferrini, P. and R. Rinaldi, *Catalytic biorefining of plant biomass to non-pyrolytic lignin bio-oil and carbohydrates through hydrogen transfer reactions*. Angewandte Chemie, 2014. **126**(33): p. 8778-8783.
178. Sultan, Z., et al., *Membrane Fractionation of Liquors from Lignin-First Biorefining*. ChemSusChem, 2019. **12**(6): p. 1203-1212.
179. Sun, Z., et al., *Complete lignocellulose conversion with integrated catalyst recycling yielding valuable aromatics and fuels*. Nature catalysis, 2018. **1**(1): p. 82-92.
180. Song, Y., *Lignin valorization via reductive depolymerization*. Chemical Catalysts for Biomass Upgrading, 2020: p. 395-437.
181. Pepper, J. and Y. Lee, *Lignin and related compounds. I. A comparative study of catalysts for lignin hydrogenolysis*. Canadian Journal of Chemistry, 1969. **47**(5): p. 723-727.
182. Van den Bosch, S., et al., *Tuning the lignin oil OH-content with Ru and Pd catalysts during lignin hydrogenolysis on birch wood*. Chemical communications, 2015. **51**(67): p. 13158-13161.
183. Chen, J., et al., *High yield production of natural phenolic alcohols from woody biomass using a nickel-based catalyst*. ChemSusChem, 2016. **9**(23): p. 3353-3360.
184. Huang, X., et al., *Selective production of mono-aromatics from lignocellulose over Pd/C catalyst: the influence of acid co-catalysts*. Faraday Discussions, 2017. **202**: p. 141-156.
185. Torr, K.M., et al., *Mild hydrogenolysis of in-situ and isolated Pinus radiata lignins*. Bioresource technology, 2011. **102**(16): p. 7608-7611.
186. Kaplunova, T., et al., *Hydrogenolysis of rice husk lignin. IV*. Chemistry of Natural Compounds, 1993. **29**(4): p. 530-532.
187. Klein, I., B. Saha, and M.M. Abu-Omar, *Lignin depolymerization over Ni/C catalyst in methanol, a continuation: effect of substrate and catalyst loading*. Catalysis Science & Technology, 2015. **5**(6): p. 3242-3245.
188. Song, Q., et al., *Lignin depolymerization (LDP) in alcohol over nickel-based catalysts via a fragmentation–hydrogenolysis process*. Energy & Environmental Science, 2013. **6**(3): p. 994-1007.
189. Ouyang, X., et al., *Catalytic conversion of lignin in woody biomass into phenolic monomers in methanol/water mixtures without external hydrogen*. ACS Sustainable Chemistry & Engineering, 2019. **7**(16): p. 13764-13773.
190. Li, C., et al., *One-pot catalytic hydrocracking of raw woody biomass into chemicals over supported carbide catalysts: simultaneous conversion of cellulose, hemicellulose and lignin*. Energy & Environmental Science, 2012. **5**(4): p. 6383-6390.
191. Graham-Forsythe, W., *Catalytic depolymerisation of suberin rich biomass with precious metal catalysts*. Green Chemistry, 2018. **20**(12): p. 2702-2705.

192. Renders, T., et al., *Synergetic effects of alcohol/water mixing on the catalytic reductive fractionation of poplar wood*. ACS Sustainable Chemistry & Engineering, 2016. **4**(12): p. 6894-6904.
193. Schutyser, W., et al., *Influence of bio-based solvents on the catalytic reductive fractionation of birch wood*. Green Chemistry, 2015. **17**(11): p. 5035-5045.
194. Wu, X., et al., *Lignin-First Monomers to Catechol: Rational Cleavage of C–O and C–C Bonds over Zeolites*. ChemSusChem, 2022. **15**(7): p. e202102248.
195. Deneyer, A., et al., *Direct upstream integration of biogasoline production into current light straight run naphtha petrorefinery processes*. Nature Energy, 2018. **3**(11): p. 969-977.
196. Dusselier, M.J., B.O. De Beeck, and B.F. Sels, *Biphasic solvent catalytic process for the direct production of light naphtha from carbohydrate-containing feedstock*. 2019, Google Patents.
197. Leoneti, A.B., V. Aragão-Leoneti, and S.V.W.B. De Oliveira, *Glycerol as a by-product of biodiesel production in Brazil: alternatives for the use of unrefined glycerol*. Renewable Energy, 2012. **45**: p. 138-145.
198. Fukuda, H., A. Kondo, and H. Noda, *Biodiesel fuel production by transesterification of oils*. Journal of bioscience and bioengineering, 2001. **92**(5): p. 405-416.
199. Bagnato, G., et al., *Glycerol Production and Transformation: A Critical Review with Particular Emphasis on Glycerol Reforming Reaction for Producing Hydrogen in Conventional and Membrane Reactors*. Membranes (Basel), 2017. **7**(2): p. 17.
200. Pagliaro, M., et al., *From glycerol to value-added products*. Angewandte Chemie International Edition, 2007. **46**(24): p. 4434-4440.
201. Bagheri, S., N.M. Julkapli, and W.A. Yehye, *Catalytic conversion of biodiesel derived raw glycerol to value added products*. Renewable and Sustainable Energy Reviews, 2015. **41**: p. 113-127.
202. CJ, S., *Propanediols*. Ullmann's encyclopedia of industrial chemistry. Wi-ley-VCH Verlag, 1993. **20**(0): p. 0.
203. Cortright, R., M. Sanchez-Castillo, and J. Dumesic, *Conversion of biomass to 1, 2-propanediol by selective catalytic hydrogenation of lactic acid over silica-supported copper*. Applied Catalysis B: Environmental, 2002. **39**(4): p. 353-359.
204. Dasari, M.A., et al., *Low-pressure hydrogenolysis of glycerol to propylene glycol*. Applied Catalysis A: General, 2005. **281**(1-2): p. 225-231.
205. Behr, A., et al., *Improved utilisation of renewable resources: New important derivatives of glycerol*. Green Chemistry, 2008. **10**(1): p. 13-30.
206. Kusunoki, Y., et al., *Highly active metal–acid bifunctional catalyst system for hydrogenolysis of glycerol under mild reaction conditions*. Catalysis Communications, 2005. **6**(10): p. 645-649.
207. Miyazawa, T., et al., *Glycerol conversion in the aqueous solution under hydrogen over Ru/C+ an ion-exchange resin and its reaction mechanism*. Journal of Catalysis, 2006. **240**(2): p. 213-221.
208. Wang, Y., J. Zhou, and X. Guo, *Catalytic hydrogenolysis of glycerol to propanediols: a review*. RSC Advances, 2015. **5**(91): p. 74611-74628.
209. Ten Dam, J. and U. Hanefeld, *Renewable chemicals: dehydroxylation of glycerol and polyols*. ChemSusChem, 2011. **4**(8): p. 1017-1034.
210. Montassier, C., D. Giraud, and J. Barbier, *Polyol conversion by liquid phase heterogeneous catalysis over metals*, in *Studies in Surface Science and Catalysis*. 1988, Elsevier. p. 165-170.
211. Wang, S., et al., *Glycerol hydrogenolysis to propylene glycol and ethylene glycol on zirconia supported noble metal catalysts*. ACS Catalysis, 2013. **3**(9): p. 2112-2121.

212. Shinmi, Y., et al., *Modification of Rh/SiO₂ catalyst for the hydrogenolysis of glycerol in water*. Applied Catalysis B: Environmental, 2010. **94**(3-4): p. 318-326.
213. Nakagawa, Y., et al., *Direct hydrogenolysis of glycerol into 1, 3-propanediol over rhenium-modified iridium catalyst*. Journal of Catalysis, 2010. **272**(2): p. 191-194.
214. Amada, Y., et al., *Reaction mechanism of the glycerol hydrogenolysis to 1, 3-propanediol over Ir-ReO_x/SiO₂ catalyst*. Applied Catalysis B: Environmental, 2011. **105**(1-2): p. 117-127.
215. Gandarias, I., et al., *Hydrogenolysis of glycerol to propanediols over a Pt/ASA catalyst: The role of acid and metal sites on product selectivity and the reaction mechanism*. Applied Catalysis B: Environmental, 2010. **97**(1-2): p. 248-256.
216. van Ryneveld, E., et al., *Direct hydrogenolysis of highly concentrated glycerol solutions over supported Ru, Pd and Pt catalyst systems*. Catalysis letters, 2011. **141**(7): p. 958-967.
217. Sherbi, M., et al., *Superior CNT-supported bimetallic RuCu catalyst for the highly selective hydrogenolysis of glycerol to 1, 2-propanediol*. Catalysis Science & Technology, 2021. **11**(20): p. 6649-6653.
218. Zhao, H., et al., *Hydrogenolysis of glycerol to 1, 2-propanediol over Cu-based catalysts: A short review*. Catalysis Today, 2020. **355**: p. 84-95.
219. Nakagawa, Y. and K. Tomishige, *Heterogeneous catalysis of the glycerol hydrogenolysis*. Catalysis Science & Technology, 2011. **1**(2): p. 179-190.
220. Feng, J., et al., *Effect of base additives on the selective hydrogenolysis of glycerol over Ru/TiO₂ catalyst*. Chemistry letters, 2007. **36**(10): p. 1274-1275.
221. Li, B., et al., *Carbon nanotube-supported RuFe bimetallic nanoparticles as efficient and robust catalysts for aqueous-phase selective hydrogenolysis of glycerol to glycols*. Acs Catalysis, 2011. **1**(11): p. 1521-1528.
222. SABERI, M.A.M.B.M., *Comparison between Method of One-Factor-At-A-Time (Ofat) & Design of Experiment (Doe) in Screening of Immunoglobulin Production Stimulating Factors*. 2010, Universiti Malaysia Pahang.
223. Czitrom, V., *One-factor-at-a-time versus designed experiments*. The American Statistician, 1999. **53**(2): p. 126-131.
224. Sherbi, M. and J. Albert, *Modeling and optimization of bio-2-hexanol production from biomass derived dimethylfuran using Pt/K3PW12O40 by response surface methodology*. Computers & Chemical Engineering, 2021. **155**: p. 107546.
225. Lazic, Z.R., *Design of experiments in chemical engineering: a practical guide*. 2006: John Wiley & Sons.
226. Bhran, A.A., A.M. Shoaib, and B. Umana, *Optimization of crude oil hydrotreating process as a function of operating conditions: Application of response surface methodology*. Computers & Chemical Engineering, 2016. **89**: p. 158-165.
227. Sherbi, M.S., et al., *Predictive Correlations and Optimization of Atmospheric Long Residue Hydrotreating Process*. Petroleum & Coal, 2020. **62**(3).
228. Esser, T., et al., *Development of an efficient downstream process for product separation and catalyst recycling of a homogeneous polyoxometalate catalyst by means of nanofiltration membranes and design of experiments*. Chemical Engineering Research and Design, 2022. **185**: p. 37-50.
229. Pérez-Uresti, S.I., et al., *Techno-economic assessment of benzene production from shale gas*. Processes, 2017. **5**(3): p. 33.
230. Abu-Omar, M.M., et al., *Guidelines for performing lignin-first biorefining*. Energy & Environmental Science, 2021. **14**(1): p. 262-292.

231. Renders, T., et al., *Catalytic lignocellulose biorefining in n-butanol/water: a one-pot approach toward phenolics, polyols, and cellulose*. *Green Chemistry*, 2018. **20**(20): p. 4607-4619.
232. Galkin, M.V., et al., *Hydrogen-free catalytic fractionation of woody biomass*. *ChemSusChem*, 2016. **9**(23): p. 3280-3287.
233. Taran, O.P., et al., *Reductive Catalytic Fractionation of Spruce Wood over Ru/C Bifunctional Catalyst in the Medium of Ethanol and Molecular Hydrogen*. *Catalysts*, 2022. **12**(11): p. 1384.
234. Miyazawa, T., et al., *Glycerol hydrogenolysis to 1, 2-propanediol catalyzed by a heat-resistant ion-exchange resin combined with Ru/C*. *Applied Catalysis A: General*, 2007. **329**: p. 30-35.
235. Raabe, J.-C., et al., *H8 [PV5Mo7O40](HPA-5)-a unique polyoxometalate for acid and RedOx catalysis: synthesis, characterization, and modern applications in green chemical processes*. *ChemSusChem*, 2023: p. e202300072.
236. Kozhevnikov, I.V.e. and K.I. Matveev, *Heteropolyacids in catalysis*. *Russian Chemical Reviews*, 1982. **51**(11): p. 1075.
237. Baker, L.R., et al., *Furfuraldehyde hydrogenation on titanium oxide-supported platinum nanoparticles studied by sum frequency generation vibrational spectroscopy: acid-base catalysis explains the molecular origin of strong metal-support interactions*. *J Am Chem Soc*, 2012. **134**(34): p. 14208-16.
238. Feng, J., et al., *Hydrogenolysis of glycerol to glycols over ruthenium catalysts: Effect of support and catalyst reduction temperature*. *Catalysis Communications*, 2008. **9**(6): p. 1458-1464.

Chapter 10. Appendix

10.1. List of hazardous substances used according to GHS

Table 10.1 List of hazardous materials used according to globally harmonized system of classification and labelling of chemicals (GHS).

Material	GHS-Symbol	Hazard statement	Precautionary statement
2,5-Dimethyl-furan	GHS02, GHS07	H225, H302, H315, H317, H319, H335	P210, P233, P280, P301, P312, P303, P361, P353, P305, P351, P338
2,5-Dimethyltetrahydrofuran	GHS02	H226	-
2,5-Hexanedione	GHS07, GHS08	H302, H315, H319, H361f, H373	P201, P202, P301, P312, P302, P352, P305, P351, P338, P308, P313
2-Hexanol	GHS02	H226	P210, P233, P340, P241, P242, P243
2-Hexanone	GHS02, GHS07, GHS08	H226, H336, H361f, H372	P201, P210, P308, P313
2-Methoxy-4-propyl-phenol	GHS05, GHS07	H315, H317, H318, H335	P261, P264, P271, P280, P302, P352, P305, P351, P338
2-Methylfuran	GHS02, GHS06	H225, H301, H330,	P210, P233, P304, P340, P312
3-(4-Hydroxy-3-methoxyphenyl)-propanoic acid methyl ester	GHS07	H302, H319	P264, P270, P280, P312, P305, P351, P338, P337, P313
3-(4-Hydroxy-3-methoxyphenyl)-1-propanol	GHS07	-	P264, P280, P363, P313, P338, P351
3-(4-Hydroxy-3-methoxyphenyl)-1-propanol	GHS07	H315, H317, H335	P261, P264, P264, P265, P271, P280, P302, P352, P304, P340, P305, P351, P338, P319, P321, P332, P317, P337, P317, P362, P364, P403, P233, P405, P501
4-Hydroxy-benzenepropanoic acid methyl ester	GHS09	H411	P273, P391, P501
C ₂ H ₆	GHS04, GHS02	H220, H280	P210, P377, P381, P410, P403
C ₃ H ₈	GHS04, GHS02	H220, H280	P210, P377, P381, P410, P403
Carbon nano tubes	-	-	P304, P312, P304, P340, P361, P353, P338, P260, P233
CH ₄	GHS04, GHS02	H220, H280	P210, P377, P381, P410, P403, P403,
CO ₂	GHS04	H280	P410, P403
Cs ₂ CO ₃	GHS08, GHS05	H318, H361f, H373	P201, P261, P280, P302, P352, P305, P351, P338, P310

Table 10.1 List of hazardous materials used according to (GHS) continued.

Material	GHS-Symbol	Hazard statement	Precautionary statement
$\text{Cu}(\text{NO}_3)\cdot\text{H}_2\text{O}$	GHS03, GHS07, GHS09	H272, H302, H315, H319, H410	P220, P373, P280, P302, P352, P305, P351, P338
$\text{Cu}(\text{NO}_3)_2$	GHS03, GHS05, GHS09	H272, H314, H410	P210, P260, P280, P303, P361, P353, P305, P351, P338
Decane	GHS02, GHS08	H226, H304	P210, P301, P310, P331, P370, P378, P403, P235, P501
Ethanol	GHS02, GHS07	H225, H319	P210, P233, P305, P351, P338
Ethylene glycol	GHS07, GHS08	H302, H373	P260, P270, P301, P312
$\text{Fe}(\text{NO}_3)_3$	GHS05	H314	P260, P280, P303, P361, P353, P305, P351, P338, P321, P501
Furan	GHS02, GHS08, GHS07	H224, H302, H332, H315, H341, H350, H373, H412	P210, P233, P273, P304, P340, P312, P308, P313, P403, P233
Glycerol	-	-	P313, P352, P353, P340
H_2	GHS02, GHS04	H220, H280, EUH018	P103, P102, P101, P210, P377, P410, P403
$\text{H}_2\text{Pt}(\text{OH})_6\cdot x\text{H}_2\text{O}$	GHS07	H315, H319, H317, H335	P264, P280, P261, P272, P271, P340, P310, P350, P362, P364, P332, P313, P351, P338, P403, P233, P405, P501
H_2PtCl_6	GHS06, GHS08, GHS05, GHS09	H290, H300, H314, H317, H334, H372, H410, EUH071	P280, P284, P301, P330, P331, P303, P361, P353, P305, P351, P338, P310
$\text{H}_3[\text{PMo}_{12}\text{O}_{40}]\cdot x\text{H}_2\text{O}$	GHS05, GHS03	H272, H290, H314	P220, P280, P301, P330, P331, P303, P361, P353, P305, P351, P338, P310
$\text{H}_3[\text{PW}_{12}\text{O}_{40}]\cdot x\text{H}_2\text{O}$	GHS05, GHS09, GHS07	H302, H314, H411	P260, P273, P280, P301, P312, P303, P361, P353, P305, P351, P338
$\text{H}_4[\text{SiW}_{12}\text{O}_{40}]\cdot x\text{H}_2\text{O}$	GHS05	H314, H412	P301, P330, P331, P305, P351, P338, P280, P310, P303, P361, P353
Hexadecane	GHS08	H304	P301, P310, P331, P405, P501
Hydroxyacetone	GHS02	H226	P210, P233, P241, P280, P303, P361, P353, P403, P235
iso-Propanol	GHS02, GHS07	H225, H319, H336	P210, P305, P351, P338, P312, P370, P378, P403, P233, P403, P235, P501
KCl	-	-	P304, P340, P302, P350, P330, P331, P403, P235
Methanol	GHS02, GHS06, GHS08	H225, H301, H311, H331, H370	P101, P102, P103, P280, P264, P270, P261, P210, P350, P310, P363, P340, P405, P403
N_2	GHS04	H280	P103, P102, P101, P410, P403

Table 10.1 List of hazardous materials used according to (GHS) continued.

Material	GHS-Symbol	Hazard statement	Precautionary statement
n-Hexane	GHS02, GHS07, GHS08, GHS09	H225, H304, H315, H336, H361f, H373, H411	P202, P280, P303, P361, P353, P304, P340, P308, P313
Ni/C	GHS07, GHS08	H317, H351, H372, H412	P201, P260, P280, P308, P313, P314, P501
NiO/SiO ₂ -Al ₂ O ₃	GHS07, GHS08	H317, H350i, H351, H372, H412	P202, P260, P273, P280, P302, P352, P308, P313
Nonane	GHS07, GHS08, GHS09	H226, H304, H315, H336, H410, H412	P210, P273, P301, P310, P303, P361, P353, P304, P340
n-Propanol	GHS02, GHS05, GHS07	H225, H318, H336	P210, P233, P280, P305, P351, P338, P310
Octane	GHS09, GHS08, GHS07, GHS02	H225, H304, H315, H336, H410	P210, P280, P301, P310, P302, P352, P331, P403, P233
Pd/Al ₂ O ₃	-	-	P304, P340, P350, P301, P330, P331, P261
Pd/C	-	-	P304, P340, P360, P233, P231, P281
Propionic acid	GHS02, GHS07, GHS05	H226, H314, H335	P210, P260, P280, P302, P352, P305, P351, P338, P310
Pt(acac) ₂	GHS07, GHS08	H302, H312, H332, H315, H319, H335, H361	P201, P280, P301, P312, P330, P302, P352, P32, P304, P340, P312, P308, P313
Pt/Al ₂ O ₃	GHS02	H228	P210, P240, P241, P280, P370, P378
Pt/C	GHS02	H228	P210, P240, P241, P280
Ru/C	-	-	P341, P350
RuCl ₃	GHS05, GHS07	H302, H314, H412	P280, P30, P330, P331, P303, P361, P353, P305, P351, P338, P310

10.2. List of figures

Figure 1.1 Reserves for C raw materials [2].	1
Figure 1.2 Biomass as a renewable and clean resource for fuel and chemical production, modified from [3].	2
Figure 1.3 Scope of the thesis: in which three different reaction systems were investigated for biomass valorization into chemicals and fuels through selective hydroprocessing.	3
Figure 2.1 Main ingredients of biomass (in wt.%) [2].	6
Figure 2.2 Structural section of cellulose [10].	7
Figure 2.3 Structural section of hemicellulose [10].	7
Figure 2.4 a) The methoxylated phenylpropane building blocks of lignin b) Coumaric acid and ferulic acid incorporated in lignin structure of herbaceous biomass [14].	8
Figure 2.5 Hypothetical molecular structure of lignin [12].	9
Figure 2.6 Molecular structure of triglycerides.	9
Figure 2.7 Oxygen and hydrogen content of biomass components compared to fossil resources and other traditional chemicals, modified from [25].	10
Figure 2.8 Structure of hetero-POMs a) Keggin structure b) Wells–Dawson structure c) Anderson structure, brown clusters represent heteroanions in POMs structure, adapted from [53].	12
Figure 2.9 Graphical illustration of the five rotational isomers of the Keggin structure, adapted from [41, 53].	13
Figure 2.10 a) Wells–Dawson structure POMs b) Metal incorporated in Wells–Dawson structure POMs, blue clusters represent heteroanions (ZO_4), grey cluster represent Ru, Pt or Pd cluster [59].	13
Figure 2.11 Furan, MF, and DMF production from cellulose and hemicellulose.	20
Figure 2.12 Alcohol production from furans.	22
Figure 2.13 Proposed reaction network for the hydrogenation of DMF into ring saturated and ring opened products [36].	23
Figure 2.14 Solubility of hydrogen in some organic solvents [23, 144, 145].	24
Figure 2.15 Mechanisms for reductive catalytic fractionation of lignocellulosic biomass [14].	27
Figure 2.16 Reaction pathways and the typical products of RCF [155].	28
Figure 2.17 Two “lignin first” biorefinery strategies, depending on solvent choice [155].	32
Figure 2.18 Schematic representation for integrating RCF-based biorefinery process and (LPCtoN) technology into existing petrorefinery, adapted from [195].	33
Figure 2.19 Transesterification reaction for biodiesel and glycerol production, adapted from [199].	34
Figure 2.20 Glycerol valorization through different reactions into value-added products, adapted from [200].	35
Figure 2.21 Hydrogenolysis of propylene oxide to form 1,2 PD [202].	35
Figure 2.22 Two stage commercial 1,2 PD production from glycerol [202].	36
Figure 2.23 Dehydration- hydrogenation mechanism [208].	36
Figure 2.24 Glyceraldehyde-based mechanism [208].	37
Figure 2.25 Hydride-attack mechanism a) from glycerol to form 1,3 PD b) from glycerol to form 1,2 PD [214].	37
Figure 2.26 Reaction scheme of glycerol hydrogenolysis [59, 208, 210, 215, 216].	38
Figure 3.1 Selective catalytic hydrogenation of 2,5-dimethylfuran (DMF), 2-methylfuran (MF) and furan to the corresponding alcohols 2-hexanol, 1/2-pentanol and 1-butanol, respectively, using $Pt/K_3[PW_{12}O_{40}]$ catalyst under mild reaction conditions.	42
Figure 4.1 Response surface methodology steps implied in this chapter.	59
Figure 5.1 Selective hydrogenolysis of glycerol to 1,2-propanediol using Ru_1Cu_2/CNT .	74
Figure 6.1 Main reaction steps involved in RCF of lignocellulosic biomass.	81

Figure 6.2 Ten-fold parallel reaction system used for hydroprocessing reactions.....	83
Figure 6.3 P&I Diagram for 10-fold parallel reaction system used for hydroprocessing reactions.....	84
Figure 6.4 Monomer yields for RCF of beech wood with different catalysts. Reaction conditions: 10 mL methanol, 250 mg beech wood, 50 mg catalyst, T= 200 °C, P=50 bars H ₂ , t= 24 h.	88
Figure 6.5 Monomer yields for RCF of rye straw, rye straw digestate or industrial straw digestate under reaction conditions of 10 mL methanol, 250 mg substrate, 50 mg NiSat, T= 200 °C, P=50 bars H ₂ , and t= 24 h.	90
Figure 6.6 Effect of alkaline pretreatment on the monomer yields obtained by RCF of industrial straw digestate. Reaction conditions: 10 mL methanol, 250 mg substrate, 50 mg NiSat, T= 200 °C, P=50 bars H ₂ , and t= 24 h.....	92
Figure 6.7 Effect of alkaline pretreatment on the monomer yields obtained by RCF of beech wood. Reaction conditions: 10 mL methanol, 250 mg substrate, 50 mg NiSat catalyst, T= 200 °C, P=50 bars H ₂ , and t= 24 h.	92
Figure 6.8 Effect of the reaction time on the total monomer yield (left y-axis) and the shares of S-monomers, γ-OH monomers and phenolic acid monomers (the right y-axis) obtained by RCF of washed industrial straw digestate. Reaction conditions: 10 mL methanol, 250 mg substrate, 50 mg NiSat, T= 200 °C, P=50 bars H ₂ , and different reaction times.	93
Figure 6.9 Effect of the reaction time on the total monomer yield (left y-axis) and the γ-OH monomers share (right y-axis) obtained by RCF of washed industrial straw digestate. Reaction conditions: 10 mL methanol, 250 mg substrate, 50 mg NiSat, T= 200 °C, and different H ₂ pressures for 24 h.	94
Figure 7.1 Schematic representation of the Keggin-type POM anion [ZM ₁₂ O ₄₀] ³⁻ [235].....	98
Figure 7.2 TEM-EDX for Ru/C spent catalyst when HPMo was added to reaction medium.....	104
Figure 7.3 FTIR spectra of HPMo (black) and Ru/C spent catalyst when HPMo was added to reaction medium (red).....	105
Figure 7.4 Effect of the addition of the POMs during the RCF using different catalysts (NiSat, Ni/C, or Ru/C).	107
Figure 7.5 Reaction pathways in RCF [231].....	108
Figure 7.6 GPC for different lignin oils produced from RCF of beech wood, with and without POMs additives, comparing molecular weight distribution in function of time, where x-axis represents retention time (min) and y-axis represents the signal.	108

10.3. List of tables

Table 2.1 Examples for biomass valorization processes that use hydrogen as a (co-)feedstock.	11
Table 2.2 POMs applications in hydroprocessing reactions.	14
Table 2.3 Application of heteropolyacids, their salts and metal-POMs composites in biomass valorization via hydroprocessing.	16
Table 2.4 Application of bifunctional catalysts composed of metal site and acid POMs site in biomass valorization via hydroprocessing.	17
Table 2.5 Application of adding POMs to the reaction medium combined with other metal catalysts in biomass valorization via hydroprocessing.	19
Table 2.6 Some examples for catalysts utilized in glycerol hydrogenolysis.	39
Table 6.1 Typical monomers obtained from RCF.	85
Table 6.2: Lignin content of all biomasses that were used as substrates for RCF.	87
Table 6.3 CHNS analysis of all biomasses that were used as substrates for RCF.	87
Table 6.4 Monomer yields derived from alcoholic monolignols and phenolic acids incorporated in lignin structure during RCF of straw and its digestates.	90
Table 6.5 Monomer yields produced from RCF of washed and unwashed industrial straw digestate using NiSat catalyst.	91
Table 7.1 DMF conversion and product yields of different Pt-POM catalytic systems.	101
Table 7.2 Glycerol conversion and product selectivity during hydrogenolysis using different active metal sites supported on carbon.	102
Table 7.3 Glycerol hydrogenolysis catalyzed by 5% Ru/C + POMs.	103
Table 7.4 Comparison between commercial Ni catalysts with some Ni- substituted POMs for RCF of beech wood.	106
Table 10.1 List of hazardous materials used according to globally harmonized system of classification and labelling of chemicals (GHS).	128

10.4. Online ESI of 1st publication (chapter 3)

Content

Supporting Notes:

- 1- Catalyst synthesis
- 2- Catalytic activity tests
- 3- POM catalyst characterization
- 4- NMR analysis for furan hydrogenation liquid products

Supplementary information

Catalyst synthesis

Pt-substituted POMs

$K_3\{Pt^{II}(CH_2CH_2(NH_2)_2)_2PW_{11}O_{39}\} \cdot 3H_2O$ (abbreviated as $K_3\{Pt(en)_2\}_2PW_{11}O_{39}$)

The compound was obtained using the following procedure:

$Pt(en)Cl_2$ (0.130 g, 0.4 mmol) was added to the solution of $K_7[\alpha-PW_{11}O_{39}] \cdot 14H_2O$ (0.638 g (0.2 mmol) in 40 mL of H_2O). The resulting mixture was stirred at room temperature for 24 h. After that the solution was filtered and 1.5 g of KCl was added to the filtrate with vigorous stirring. The solution was stirred at room temperature for 12 h. The resulting yellow precipitate (Product I) was collected by filtration. Yield: 0.288 g (43 % based on Pt).

The tiny needle-like crystals (Product II) unfortunately unsuitable for the single-crystal XRD analysis were obtained from the solution without the addition of KCl after ca. 24 hours.

The FT-IR spectra of Products I and II revealed the identity of the both products.

The formula of the compound was proposed based on the results of elemental analyses.

FT-IR (cm^{-1}): 3545 (br), 3472 (br), 3208 (s), 3142 (m), 3069 (w), 2350 (w), 1617 (s), 1451 (m), 1398 (w), 1383 (w), 1362 (w), 1316 (w), 1306 (m), 1234 (w), 1173 (m), 1099 (s), 1046 (s), 972 (sh), 954 (s), 922 (sh), 890 (sh), 858 (s), 797 (s), 749 (s), 726 (sh), 593 (w), 585 (w), 508 (m), 486 (sh).

Elemental analysis (%) calculated (found): W 60.2, (60.6); Pt 11.6, (12.5); P 0.9, (1.2); H 0.7, (1.1); N 1.7, (1.5); C 1.4, (1.5); K 3.5, (3.9).

$H\{Pt^{II}(NH_3)_4\}[PW_{11}O_{39}\{Pt^{II}(NH_3)_4\}_2] \cdot 8H_2O$ (abbreviated as $H\{Pt(NH_3)_4\}[PW_{11}O_{39}\{Pt(NH_3)_4\}_2]$)

$H\{Pt(NH_3)_4\}[PW_{11}O_{39}\{Pt(NH_3)_4\}_2]$ was obtained using the synthetic strategy, which was previously published for the preparation of $Cs_3[\alpha-PW_{11}O_{39}\{cis-Pt(NH_3)_2\}_2] \cdot 8H_2O$ (ref. C. N. Kato, Y. Morii, S. Hattori, R. Nakayama, Y. Makino, H. Uno, *Dalton Trans.*, **2012**, 41, 10021-10027).

$Pt(NH_3)_4Cl_2 \cdot xH_2O$ (0.2672 g, 0.8 mmol) was dissolved in 150 mL H_2O (Solution I).

$K_7[\alpha-PW_{11}O_{39}] \cdot 14H_2O$ (0.638 g, 0.2 mmol) was dissolved in 40 mL H_2O (Solution II).

The Solution I was added to the Solution II with vigorous stirring at room temperature. At that a white precipitate appeared. The resulting solution was stirred at room temperature for 1 h. The precipitate was collected by filtration. The formula of the compound was proposed based on the results of elemental analyses. Yield: 0.666 g (95 % based on W).

FT-IR (cm^{-1}): 3514 (br), 3457 (br), 3283 (s), 3211 (sh), 2675 (w), 2442 (w), 2355 (w), 2203 (w), 2124 (w), 1620 (s), 1338 (s), 1080 (s), 1037 (s), 960 (sh), 946 (s), 892 (w), 853 (m), 804 (br), 739 (br), 622 (w), 589 (w), 511 (m), 432 (w).

Elemental analysis (%) calculated (found): W 56.0, (46.6); Pt 16.2, (16.1); P 0.9, (1.06); H 1.5, (1.5); N 4.7, (4.8); Na 0, (0.38 %); K 0, (0 %).

$Na_5[H_2Pt^{IV}V_9O_{28}] \cdot 21H_2O$ (abbreviated as $Na_5[H_2PtV_9O_{28}]$)

$Na_5[H_2PtV_9O_{28}]$ was prepared using the published procedure (U. Lee, H.-C. Joo, K.-M. Park, S. S. Mal, U. Kortz, B. Keita, L. Nadjo, *Angew. Chem. Int. Ed.* **2008**, 47, 793–796).

The identification of the compound was done using FT-IR and ^{51}V NMR spectroscopy.

IR (KBr pellet, cm^{-1}): 3534 (br), 3409 (br), 2309 (br), 1617 (s), 1383 (s), 1150 (w), 986 (br), 972 (br), 846 (s), 750 (s), 649 (w), 589 (sh), 536 (br), 438 (w).

^{51}V NMR (ppm): -372, -452, -476.

Pt-free POMs

K₅[V₃W₃O₁₉]·8H₂O (abbreviated as K₅[V₃W₃O₁₉])

The hydrated potassium salt of the Lindqvist-type polyanion [V₃W₃O₁₉]⁵⁻ POM was prepared using a slightly modified published procedure (J. Albert, J. Mehler, J. Tucher, K. Kastner, C. Streb, *Chem. Sel.* 2016, 1, 2889–2894.).

The mixture of K₂WO₄ (12.73 g) and V₂O₅ (3.52 g) in 10 mL H₂O was heated at 80 °C for 10 min. The pH of the solution was adjusted to 12 with aqueous KOH (5 M) and the mixture was heated at 80 °C until the solution turned colourless. 2 M HCl was dropwise added to the colourless solution till pH 5.5. At that the colour of the solution changed from colourless to yellow, followed by orange and finally to red. Solid KCl (5.00 g) was added to the resulting solution. The mixture was stirred for 45 min at 80 °C. After cooling to the room temperature the solution was filtered and placed in acetone bath for diffusion. After 1-2 days the orange crystals were collected. Yield: 10.35 g (63 % based on W).

Elemental analysis (%) calculated (found): W 40.9, (35.4); V 11.3, (8.0); H 1.2, (1.2), K 14.5, (14.1).

Elemental analysis (%): W 35.4; V 8.0; H 1.2; K 14.5.

IR (KBr pellet, cm⁻¹): 3446 (br), 1635 (m), 953 (s), 787 (s), 590 (m), 432 (s), 415 (s).

⁵¹V NMR (ppm): -423, -497, -504, -510, -513, -517, -575.

Cs_{2.5}H_{0.5}[PW₁₂O₄₀]·xH₂O (abbreviated as Cs_{2.5}H_{0.5}[PW₁₂O₄₀])

Cs_{2.5}H_{0.5}[PW₁₂O₄₀] was prepared using a slightly modified published procedure (T. Okuhara, H. Watanabe, T. Nishimura, K. Inumaru, M. Misono, “Microstructure of Cesium Hydrogen Salts of 12-Tungstophosphoric Acid Relevant to Novel Acid Catalysis”, *Chem. Mater.* 2000, 12, 2230-2238).

Cs₂CO₃ (0.61 g) was dissolved in 47.5 mL H₂O (Solution I). H₃[PW₁₂O₄₀] (4.32 g) was dissolved in 20 mL H₂O Solution II). The Solution I was added dropwise to the Solution II under vigorous stirring at 40°C. The resulting suspension was further stirred for 30 min at 40°C. Thereafter, the obtained mixture was kept undisturbed at room temperature for 1 h. After that the upper aqueous phase was decanted. The resulting white precipitate was dried on air at room temperature.

Cu_{1.5}[PW₁₂O₄₀]·xH₂O (simplified formula, abbreviated as Cu_{1.5}[PW₁₂O₄₀])

Cu_{1.5}[PW₁₂O₄₀] was prepared using a slightly modified published procedure (S. R. Bajpe, S. Henke, J.-H. Lee, P. D. Bristowe, A. K. Cheetham, “Disorder and polymorphism in Cu(II)-polyoxometalate complexes: [Cu_{1.5}(H₂O)_{7.5}PW₁₂O₄₀]·4.75H₂O, *cis*- & *trans*-[Cu₂(H₂O)₁₀SiW₁₂O₄₀]·6H₂O”, *CrystEngComm*, 2016, 18, 5327-5332).

Cu(NO₃)·H₂O (2.8 g) was dissolved in 20 mL of the 50% water / 50% ethanol solution. To this solution H₃[PW₁₂O₄₀] (1.5 g) was added under vigorous stirring. The resulting mixture was stirred until all the acid dissolved. After that, the solution was heated at 40°C till the formation of blue precipitate. Thereafter, the obtained mixture was kept undisturbed at room temperature for 1 h. The resulting powder was isolated by filtration and dried on air at room temperature.

Catalytic activity tests

Pt-substituted POMs

The Pt-substituted POMs were used directly or after reduction in an oven with 10 % H₂ flow (50 mL/min H₂ and 450 mL/min N₂) at 250°C for 2 h (abbreviated as “Reduced [POM]” as catalysts for DMF conversion.

Table S1. DMF conversion and product yields for the initial and reduced Pt-substituted POMs.

Entry	Catalyst	Conv. (%)	Yield (%)						Carbon balance (%)
			2-HXL	2-HXN	DMTHF	HD	HX	gases	
1.1	Reduced K ₃ [{Pt(en) ₂ } ₂ PW ₁₁ O ₃₉]	4.7	0	1.0	2.2	0.6	0	0	99.7
1.2	K ₃ [{Pt(en) ₂ } ₂ PW ₁₁ O ₃₉]	0.4	0	0	0	0.4	0	0	100
2.1	Reduced H{Pt(NH ₃) ₄ }-[PW ₁₁ O ₃₉ {Pt(NH ₃) ₄ } ₂]	3.9	0.8	1.7	2.3	0.7	0.3	0	100
2.2	H{Pt(NH ₃) ₄ }-[PW ₁₁ O ₃₉ {Pt(NH ₃) ₄ } ₂]	1.4	0	0	0	0.4	0	1.0	100
3.1	Reduced Na ₅ [H ₂ PtV ₉ O ₂₈]	1.2	0	0	0.5	0.7	0.3	0	100
3.2	Na ₅ [H ₂ PtV ₉ O ₂₈]	0.3	0	0	0	0.3	0	0	100

Reaction conditions: 0.001 mol DMF, 10.0 mL decane as a solvent, each catalyst contains the same amount of Pt = 2 mg, 80° C, 10 bar hydrogen, 770 rpm, 3 h.

Pt precursors

Table S2. DMF conversion and product yields using pure Pt precursors (reduced in oven with 10 % H₂ flow (50 mL/min H₂ and 450 mL/min N₂) at 250°C for 2 h).

Entry	Catalyst	Conv. (%)	Yield (%)					Carbon balance (%)
			2-HXL	2-HXN	DMTHF	HD	HX	
1	Pt(acac) ₂	1	0	0	0	1	0	99
2	H ₂ PtCl ₆	0	0	0	0	0	0	100
3	H ₂ Pt(OH) ₆	0	0	0	0	0	0	100
4	Pt(acac) ₂ (doubled amount)	1	0	0	0	1	0	99

Reaction conditions: 0.001 mol DMF, 10.0 mL decane as a solvent, each catalyst contains the same amount of Pt = 2 mg except for entry (4) which contains 4 mg, 80° C, 10 bar H₂, 770 rpm, 3 h.

POM catalyst characterization

FTIR for Pt/H₃[PMo₁₂O₄₀]

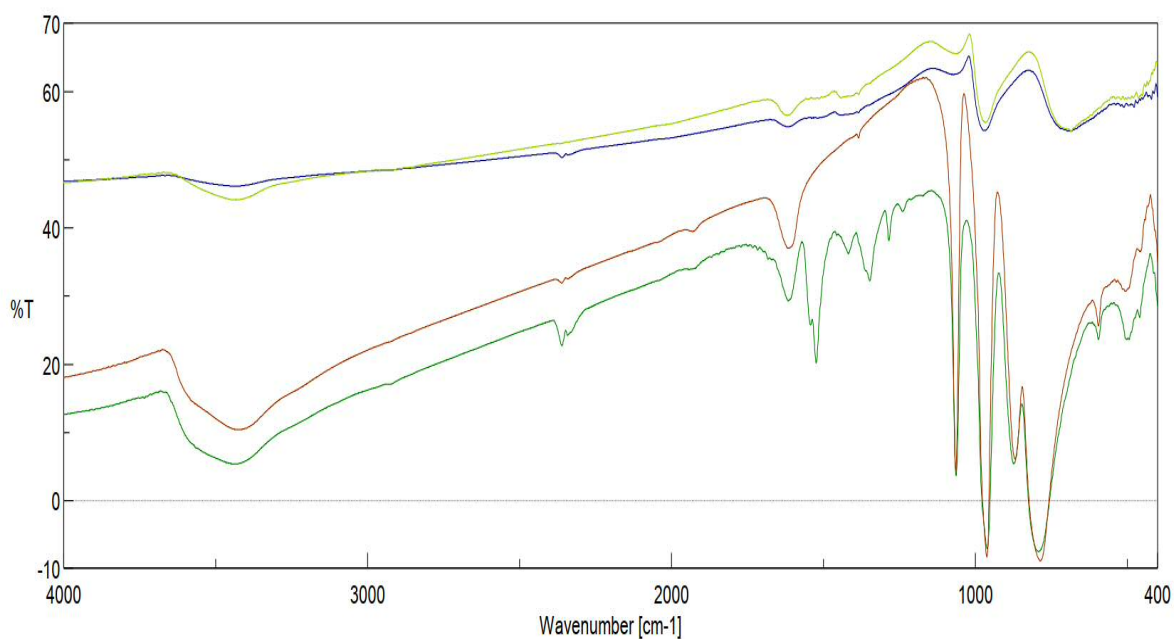


Fig S1. FT-IR spectra of the H₃PMo₁₂O₄₀ (brown line), of Pt(acac)₂/H₃PMo₁₂O₄₀ before (green line) and after reduction with hydrogen (blue line) and after the catalytic reaction (yellow line).

FTIR for Pt/H₃[PW₁₂O₄₀]

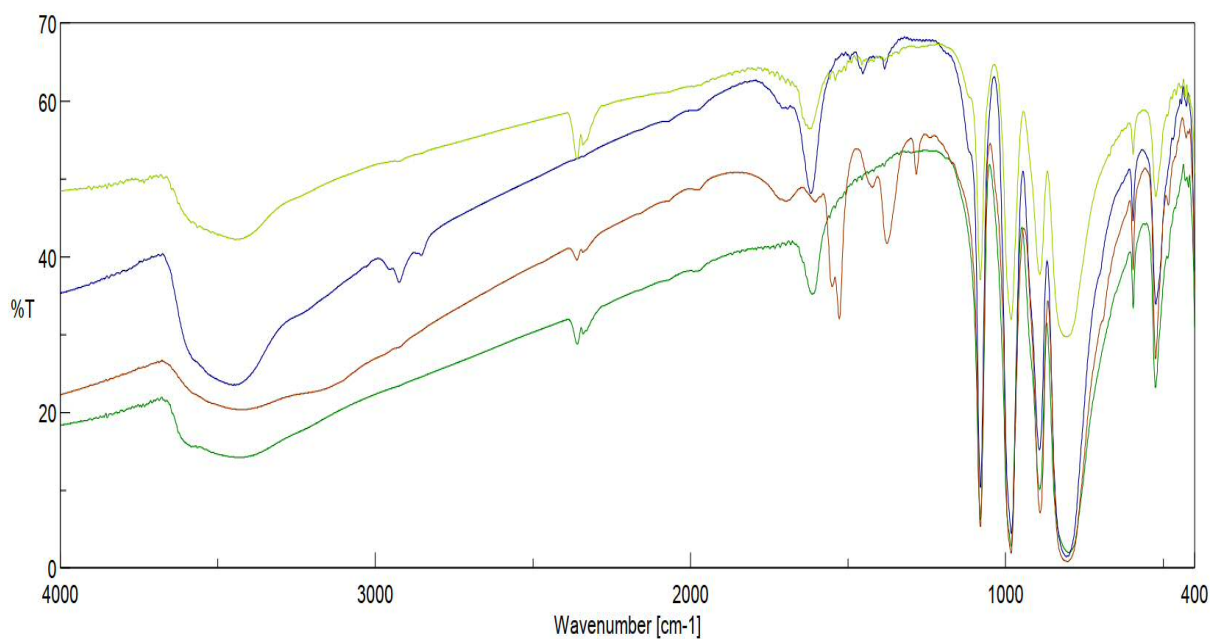


Fig S2. FT-IR spectra of the H₃PW₁₂O₄₀ (green line), of Pt(acac)₂/H₃PW₁₂O₄₀ before (brown line) and after reduction with hydrogen (yellow line) and after the catalytic reaction (blue line).

FTIR for Pt/K₃[PW₁₂O₄₀]

All the characteristic bands of Keggin anion in the region of 1100-550 cm⁻¹ exist in the spectra. The typical Keggin anion bands of tungsten POMs are the PO₄ central tetrahedron bands at 1077 cm⁻¹, W = O at 978 cm⁻¹, W-O-W edge sharing at 756 cm⁻¹, W-O-W corner sharing at 884 cm⁻¹ and O-P-O at 595 cm⁻¹ [69,70]. This confirms that the Keggin structure was maintained unchanged after the substitution of protons with potassium and after the impregnation with Pt on K₃[PW₁₂O₄₀].

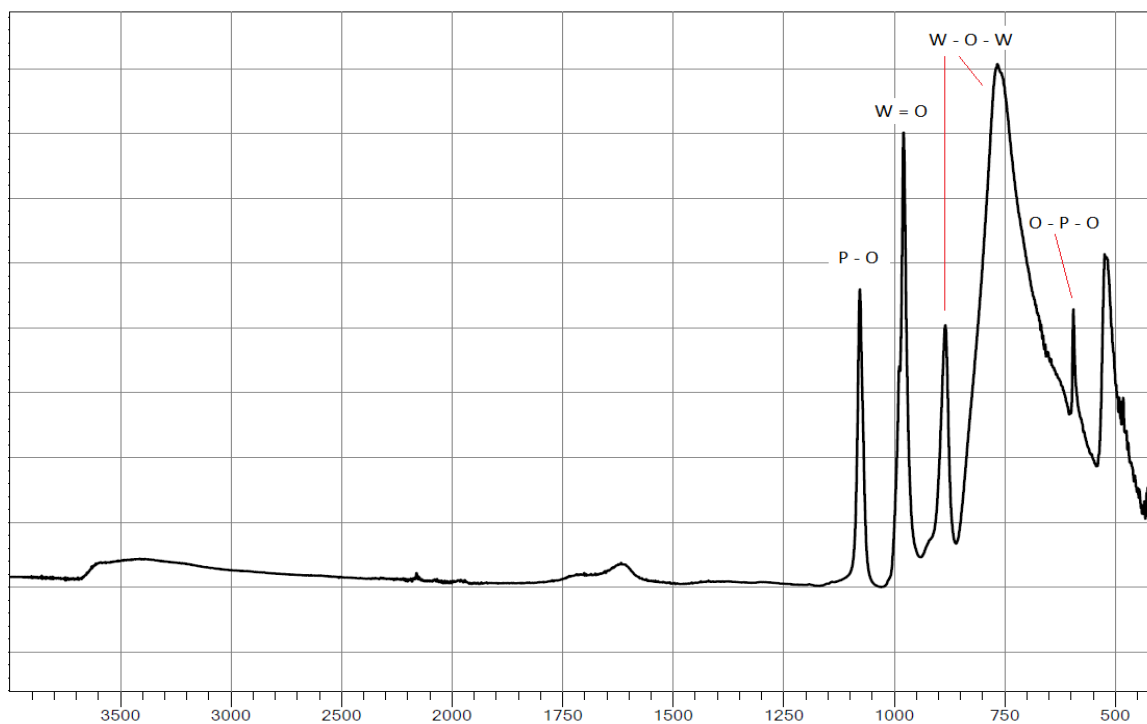


Fig.S3 The FTIR spectra of Pt/K₃[PW₁₂O₄₀]

NMR analysis of the liquid product phase using furan as a substrate

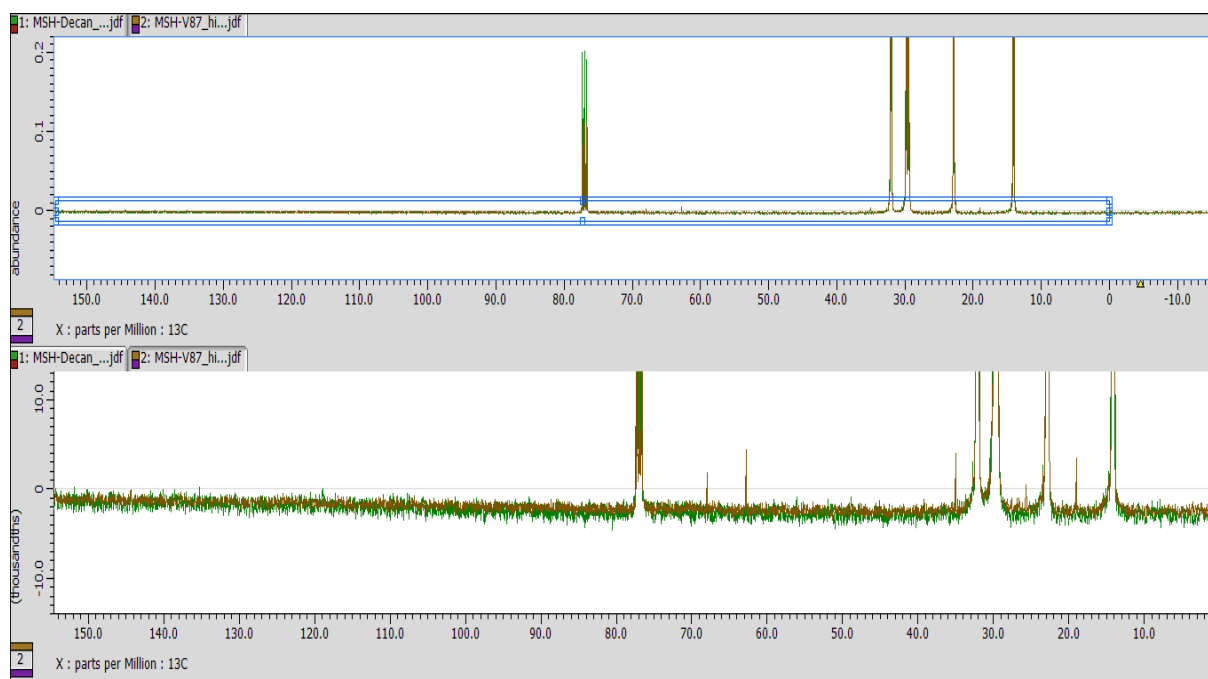


Fig S4. ¹H-NMR analysis of the liquid product solution for furan hydrogenation (top spectra: pure decane, bottom spectra: product solution using furan as a substrate in decane)

10.5. Online ESI of 2nd publication (chapter 4)

Content

Supporting Notes:

- 1- Models with actual variables
- 2- Complete ANOVA tables for 2-hexanol (HXL)
- 3- Complete ANOVA tables for 2-hexanone (HXN)
- 4- Complete ANOVA tables for n-hexan (HX)
- 5- Complete ANOVA tables for DMTHF
- 6- Residual plots
- 7- Further optimization and experimental validation tables

Supplementary information

Models with actual variables

$$\begin{aligned} \text{Yield of 2-Hexanol} = & -189.669 + 6.48334 * T + 23.1551 * P - 1.81517 * (S/C) - 0.392375 * T \\ & * P + 0.0175444 * T * (S/C) + 0.0630167 * P * (S/C) - 0.0401447 * T^2 - 0.364515 * P^2 + \\ & 0.0018125 * T^2 * P - 2.9618e-005 * T * (S/C)^2 \end{aligned} \quad (\text{eq.S1})$$

$$\begin{aligned} \text{Yield of 2-Hexanone} = & -22.3622 + 0.217417 * T + 0.672572 * P + 1.07684 * (S/C) - \\ & 0.0967397 * T * P - 0.00927917 * T * (S/C) - 0.0721333 * P * (S/C) + 0.291917 * P^2 + \\ & 0.00389768 * (S/C)^2 + 0.000838842 * T^2 * P \end{aligned} \quad (\text{eq.S2})$$

$$\begin{aligned} \text{Yield of n-hexan} = & 122.169 - 2.6957 * T + 0.132 * P - 0.973094 * (S/C) + 0.0179513 * T * \\ & (S/C) + 0.0185183 * T^2 + 0.00138297 * (S/C)^2 - 0.000125729 * T^2 * (S/C) \end{aligned} \quad (\text{eq.S3})$$

$$\begin{aligned} \text{Yield of DMTHF} = & 2.06078 + 0.142417 * T + 6.5888 * P - 0.294632 * (S/C) - 0.0481 * T * P + \\ & 0.000958333 * T * (S/C) - 0.237446 * P^2 + 0.00105565 * (S/C)^2 + 0.00182 * T * P^2 - \\ & 1.45818e-005 * P * (S/C)^2 \end{aligned} \quad (\text{eq.S4})$$

where: $60 \text{ }^\circ\text{C} \leq T \leq 100 \text{ }^\circ\text{C}$, $5 \leq P \leq 15 \text{ bar}$, and $70 \leq \text{Sub/Catalyst} \leq 130$.

Complete ANOVA tables for 2-Hexanol (HXL)

Table S1. Analysis of variance (ANOVA) for 2-Hexanol model

Source	Sum of Squares	df	Mean Square	F Value	p-value Prob > F
Model	4372.41	10	437.24	170.38	< 0.0001 Significant
<i>A-Temperature</i>	<i>741.20</i>	<i>1</i>	<i>741.20</i>	<i>288.82</i>	<i>< 0.0001</i>
<i>B-Pressure</i>	<i>564.78</i>	<i>1</i>	<i>564.78</i>	<i>220.08</i>	<i>0.0001</i>
<i>C-Sub/Cat ratio</i>	<i>469.40</i>	<i>1</i>	<i>469.40</i>	<i>182.91</i>	<i>0.0002</i>
<i>AB</i>	<i>419.23</i>	<i>1</i>	<i>419.23</i>	<i>163.36</i>	<i>0.0002</i>
<i>AC</i>	<i>194.46</i>	<i>1</i>	<i>194.46</i>	<i>75.78</i>	<i>0.0010</i>
<i>BC</i>	<i>357.40</i>	<i>1</i>	<i>357.40</i>	<i>139.27</i>	<i>0.0003</i>
<i>A²</i>	<i>277.52</i>	<i>1</i>	<i>277.52</i>	<i>108.14</i>	<i>0.0005</i>
<i>B²</i>	<i>297.45</i>	<i>1</i>	<i>297.45</i>	<i>115.91</i>	<i>0.0004</i>
<i>A²B</i>	<i>26.28</i>	<i>1</i>	<i>26.28</i>	<i>10.24</i>	<i>0.0329</i>
<i>AC²</i>	<i>127.04</i>	<i>1</i>	<i>127.04</i>	<i>49.50</i>	<i>0.0022</i>
Residual	10.27	4	2.57		
<i>Lack of Fit</i>	<i>9.89</i>	<i>2</i>	<i>4.95</i>	<i>26.59</i>	<i>0.0362 significant</i>
<i>Pure Error</i>	<i>0.37</i>	<i>2</i>	<i>0.19</i>		
Cor Total	4382.67	14			

Table S2. Fit statistics for the 2-hexanol yield model

Std. Dev.	1.60	R-Squared	0.9977
Mean	56.74	Adj R-Squared	0.9918
C.V. %	2.82	Pred R-Squared	0.8749
PRESS	548.26	Adeq Precision	44.959
-2 Log Likelihood	36.88	BIC	66.67
		AICc	146.88

Table S3. Coefficients in terms of coded factors and their standard error for Model 1

Factor	Coefficient		Standard Error	95% CI		VIF
	Estimate	df		Low	High	
Intercept	66.12	1	0.77	63.98	68.26	
A-Temperature	13.61	1	0.80	11.39	15.84	2.00
B-Pressure	11.88	1	0.80	9.66	14.11	2.00
C-Sub/Cat ratio	-7.66	1	0.57	-9.23	-6.09	1.00
AB	-10.24	1	0.80	-12.46	-8.01	1.00
AC	6.97	1	0.80	4.75	9.20	1.00
BC	9.45	1	0.80	7.23	11.68	1.00
A ²	-8.64	1	0.83	-10.95	-6.34	1.01
B ²	-8.95	1	0.83	-11.26	-6.64	1.01
A ² B	3.62	1	1.13	0.48	6.77	2.00
AC ²	-7.97	1	1.13	-11.12	-4.82	2.00

Complete ANOVA tables for 2-Hexanon (HXN)

Table S4. Analysis of variance (ANOVA) for 2-hexanone model

Source	Sum of Squares	df	Mean Square	F Value	p-value Prob > F	
Model	4050.92	9	450.10	45.46	0.0003	significant
<i>A-Temperature</i>	<i>360.73</i>	<i>1</i>	<i>360.73</i>	<i>36.44</i>	<i>0.0018</i>	
<i>B-Pressure</i>	<i>1088.34</i>	<i>1</i>	<i>1088.34</i>	<i>109.93</i>	<i>0.0001</i>	
<i>C-Sub/Cat ratio</i>	<i>1110.38</i>	<i>1</i>	<i>1110.38</i>	<i>112.15</i>	<i>0.0001</i>	
<i>AB</i>	<i>56.18</i>	<i>1</i>	<i>56.18</i>	<i>5.67</i>	<i>0.0630</i>	
<i>AC</i>	<i>123.99</i>	<i>1</i>	<i>123.99</i>	<i>12.52</i>	<i>0.0166</i>	
<i>BC</i>	<i>468.29</i>	<i>1</i>	<i>468.29</i>	<i>47.30</i>	<i>0.0010</i>	
<i>B²</i>	<i>184.08</i>	<i>1</i>	<i>184.08</i>	<i>18.59</i>	<i>0.0076</i>	
<i>C²</i>	<i>39.23</i>	<i>1</i>	<i>39.23</i>	<i>3.96</i>	<i>0.1032</i>	
<i>A²B</i>	<i>31.01</i>	<i>1</i>	<i>31.01</i>	<i>3.13</i>	<i>0.1370</i>	
Residual	49.50	5	9.90			
<i>Lack of Fit</i>	<i>46.28</i>	<i>3</i>	<i>15.43</i>	<i>9.56</i>	<i>0.0962</i>	<i>not significant</i>
<i>Pure Error</i>	<i>3.23</i>	<i>2</i>	<i>1.61</i>			
Cor Total	4100.42	14				

Table S5. Fit statistics for the 2-hexanone yield model

Std. Dev.	3.15	R-Squared	0.9879
Mean	15.09	Adj R-Squared	0.9662
C.V. %	20.85	Pred R-Squared	0.7936
PRESS	846.49	Adeq Precision	22.990
-2 Log Likelihood	60.48	BIC	87.56
		AICc	135.48

Table S6. Coefficients in terms of coded factors and their standard error for Model 2

Factor	Coefficient		Standard Error	95% CI		VIF
	Estimate	df		Low	High	
Intercept	9.60	1	1.51	5.72	13.49	
A-Temperature	-6.72	1	1.11	-9.57	-3.86	1.00
B-Pressure	-16.50	1	1.57	-20.54	-12.45	2.00
C-Sub/Cat ratio	11.78	1	1.11	8.92	14.64	1.00
AB	3.75	1	1.57	-0.30	7.79	1.00
AC	-5.57	1	1.57	-9.61	-1.52	1.00
BC	-10.82	1	1.57	-14.86	-6.78	1.00
B ²	7.04	1	1.63	2.84	11.24	1.01
C ²	3.25	1	1.63	-0.95	7.45	1.01
A ² B	3.94	1	2.22	-1.78	9.66	2.00

Complete ANOVA tables for n-Hexan (HX)

Table S7. Analysis of variance (ANOVA) for n-hexane model

Source	Sum of Squares	df	Mean Square	F Value	p-value Prob > F	
Model	106.93	7	15.28	30.65	< 0.0001	significant
<i>A-Temperature</i>	<i>8.22</i>	<i>1</i>	<i>8.22</i>	<i>16.50</i>	<i>0.0048</i>	
<i>B-Pressure</i>	<i>3.48</i>	<i>1</i>	<i>3.48</i>	<i>6.99</i>	<i>0.0332</i>	
<i>C-Sub/Cat ratio</i>	<i>15.24</i>	<i>1</i>	<i>15.24</i>	<i>30.58</i>	<i>0.0009</i>	
<i>AC</i>	<i>6.75</i>	<i>1</i>	<i>6.75</i>	<i>13.55</i>	<i>0.0079</i>	
<i>A²</i>	<i>21.01</i>	<i>1</i>	<i>21.01</i>	<i>42.15</i>	<i>0.0003</i>	
<i>C²</i>	<i>5.75</i>	<i>1</i>	<i>5.75</i>	<i>11.55</i>	<i>0.0115</i>	
<i>A²C</i>	<i>4.55</i>	<i>1</i>	<i>4.55</i>	<i>9.14</i>	<i>0.0193</i>	
Residual	3.49	7	0.50			
<i>Lack of Fit</i>	<i>3.23</i>	<i>5</i>	<i>0.65</i>	<i>4.92</i>	<i>0.1775</i>	<i>not significant</i>
<i>Pure Error</i>	<i>0.26</i>	<i>2</i>	<i>0.13</i>			
Cor Total	110.42	14				

Table S8. Fit statistics for the n-hexane yield model

Std. Dev.	0.71	R-Squared	0.9684
Mean	7.95	Adj R-Squared	0.9368
C.V. %	8.88	Pred R-Squared	0.7776
PRESS	24.56	Adeq Precision	20.879
-2 Log Likelihood	20.69	BIC	42.35
		AICc	60.69

Table S9. Coefficients in terms of coded factors and their standard error for Model 3

Factor	Coefficient		Standard Error	95% CI		VIF
	Estimate	df		Low	High	
Intercept	6.01	1	0.34	5.21	6.82	
A-Temperature	1.01	1	0.25	0.42	1.60	1.00
B-Pressure	0.66	1	0.25	0.070	1.25	1.00
C-Sub/Cat ratio	-1.95	1	0.35	-2.79	-1.12	2.00
AC	-1.30	1	0.35	-2.13	-0.46	1.00
A ²	2.38	1	0.37	1.51	3.24	1.01
C ²	1.24	1	0.37	0.38	2.11	1.01
A ² C	-1.51	1	0.50	-2.69	-0.33	2.00

Complete ANOVA tables for DMTHF

Table S10. Analysis of variance (ANOVA) for DMTHF model

Source	Sum of Squares	df	Mean Square	F Value	p-value Prob > F	
Model	166.27	9	18.47	24.18	0.0013	significant
<i>A-Temperature</i>	<i>5.90</i>	<i>1</i>	<i>5.90</i>	<i>7.73</i>	<i>0.0389</i>	
<i>B-Pressure</i>	<i>89.87</i>	<i>1</i>	<i>89.87</i>	<i>117.62</i>	<i>0.0001</i>	
<i>C-Sub/Cat ratio</i>	<i>9.33</i>	<i>1</i>	<i>9.33</i>	<i>12.21</i>	<i>0.0174</i>	
<i>AB</i>	<i>5.48</i>	<i>1</i>	<i>5.48</i>	<i>7.17</i>	<i>0.0440</i>	
<i>AC</i>	<i>1.32</i>	<i>1</i>	<i>1.32</i>	<i>1.73</i>	<i>0.2454</i>	
<i>B²</i>	<i>19.58</i>	<i>1</i>	<i>19.58</i>	<i>25.63</i>	<i>0.0039</i>	
<i>C²</i>	<i>2.49</i>	<i>1</i>	<i>2.49</i>	<i>3.26</i>	<i>0.1308</i>	
<i>AB²</i>	<i>1.66</i>	<i>1</i>	<i>1.66</i>	<i>2.17</i>	<i>0.2009</i>	
<i>BC²</i>	<i>7.72</i>	<i>1</i>	<i>7.72</i>	<i>10.11</i>	<i>0.0246</i>	
Residual	3.82	5	0.76			
<i>Lack of Fit</i>	<i>1.30</i>	<i>3</i>	<i>0.43</i>	<i>0.34</i>	<i>0.8011</i>	<i>not significant</i>
<i>Pure Error</i>	<i>2.52</i>	<i>2</i>	<i>1.26</i>			
Cor Total	170.09	14				

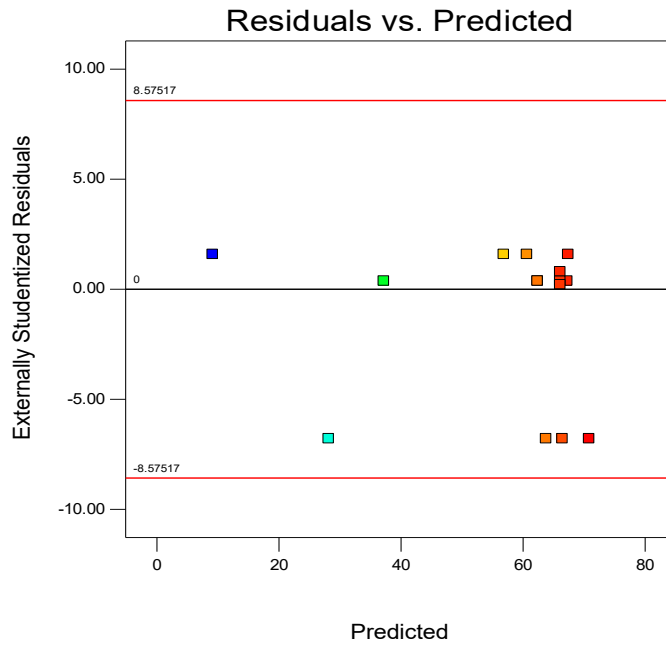
Table S11. Fit statistics for DMTHF yield model

Std. Dev.	0.87	R-Squared	0.9775
Mean	18.19	Adj R-Squared	0.9371
C.V. %	4.81	Pred R-Squared	0.8174
PRESS	31.06	Adeq Precision	16.562
-2 Log Likelihood	22.05	BIC	49.13
		AICc	97.05

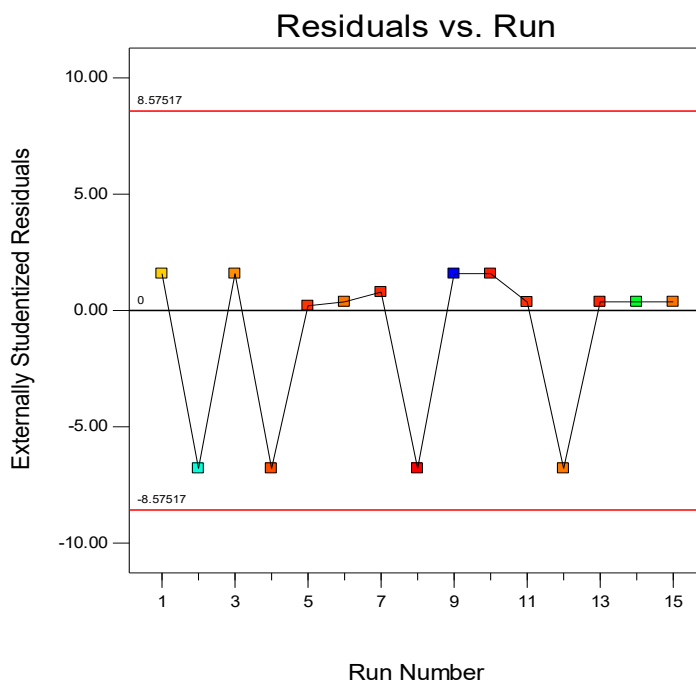
Table S12. Coefficients in terms of coded factors and their standard error for Model 4

Factor	Coefficient		Standard Error	95% CI		VIF
	Estimate	df		Low	High	
Intercept	18.98	1	0.42	17.90	20.06	
A-Temperature	-1.21	1	0.44	-2.34	-0.092	2.00
B-Pressure	4.74	1	0.44	3.62	5.86	2.00
C-Sub/Cat ratio	-1.08	1	0.31	-1.87	-0.29	1.00
AB	-1.17	1	0.44	-2.29	-0.047	1.00
AC	0.57	1	0.44	-0.55	1.70	1.00
B ²	-2.30	1	0.45	-3.46	-1.13	1.01
C ²	0.82	1	0.45	-0.35	1.98	1.01
AB ²	0.91	1	0.62	-0.68	2.50	2.00
BC ²	-1.96	1	0.62	-3.55	-0.38	2.00

Residual plots



a)



b)

Fig.S1 Residual analysis for HXL model a) Residuals vs. Predicted plot, b) Residuals vs. Run plot

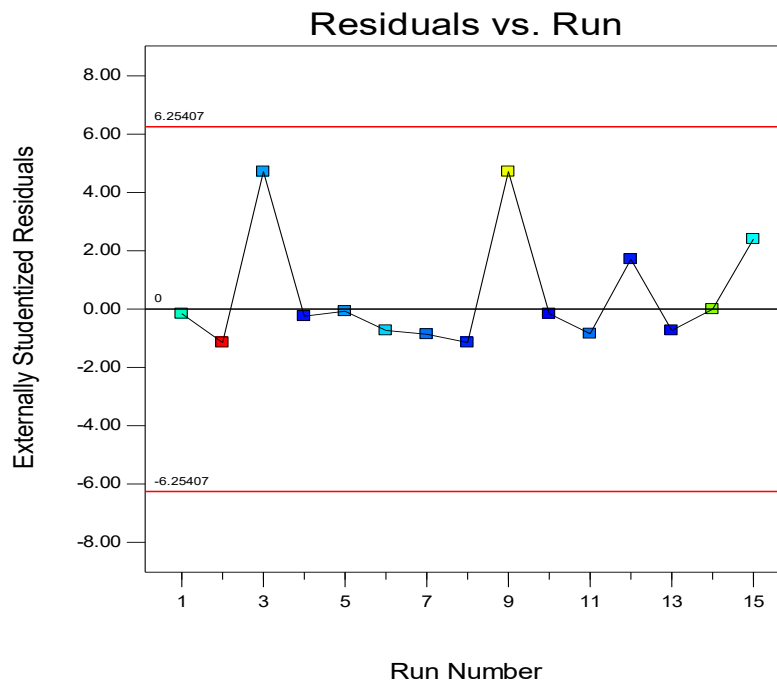
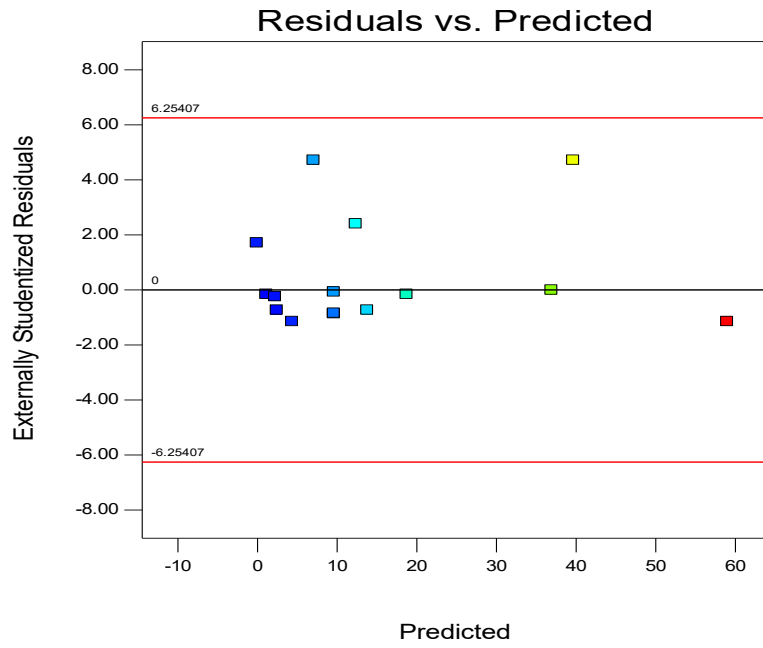
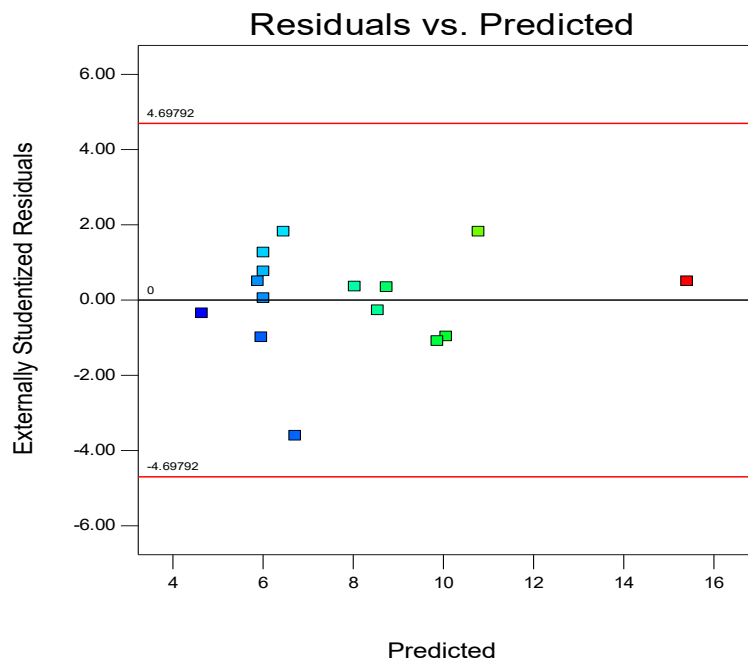
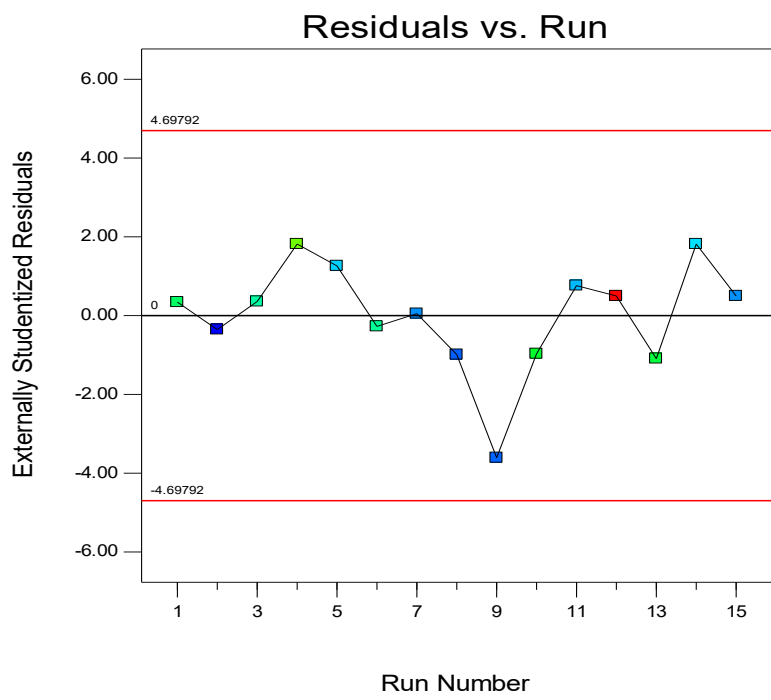


Fig.S2 Residual analysis for HXN model a) Residuals vs. Predicted plot, b) Residuals vs. Run plot

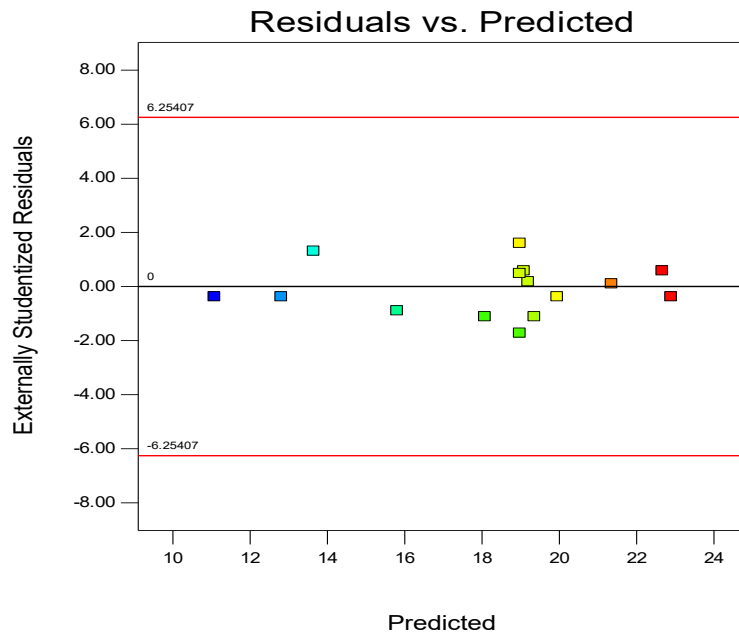


a)

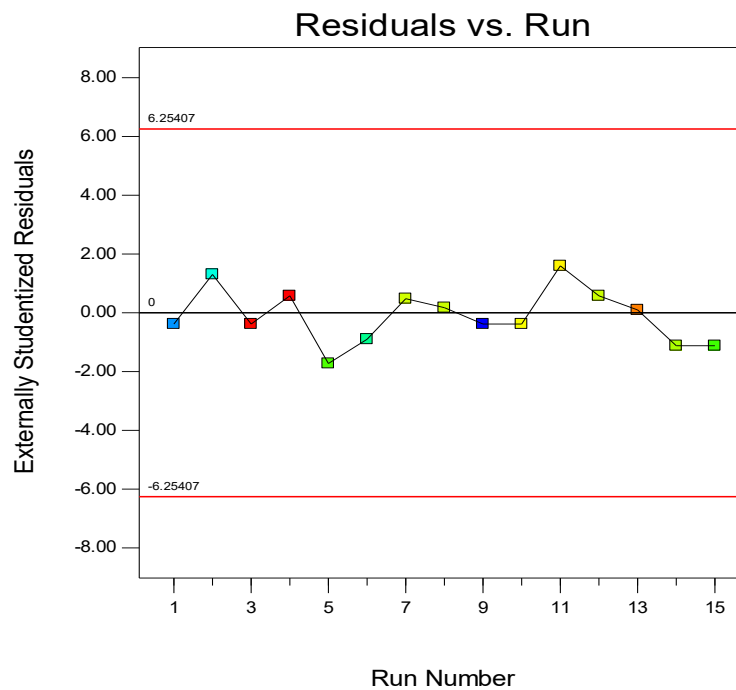


b)

Fig.S3 Residual analysis for HX model a) Residuals vs. Predicted plot, b) Residuals vs. Run plot



a)



b)

Fig.S4 Residual analysis for DMTHF model a) Residuals vs. Predicted plot, b) Residuals vs. Run plot

Further optimisation and experimental validation tables

Table S.13 Constrains of the experimental variables, lower acceptable limits and target values for optimization of overall desirability function $D(z)$

Name	Lower limit	Upper limit
T (°C)	60	100
P (bar)	5	15
S/C (mol (DMF)/mol(Pt))	70	130
Yield of HXL	9.7	69.5
Yield of HXN	0.9	57.5
Yield of Hexane	4.5	15.6
Yield of DMTHF	11	22.9

Table S.14 Obtained numerical results for individual desirability function $d_n(Y_n(z))$ and the overall desirability function $D(z)$ for the optimal experimental conditions reported in table 6.

T (°C)	P (bar)	S/C (mol(DMF)/mol(Pt))	$d(Y_{HXL})$	$d(Y_{HXN})$	$d(Y_{HX})$	$d(Y_{DMTHF})$	$D(z)$
91	15	130	1	1	0.9	0.3	0.7
83	15	88	1	1	0.7	0.1	0.6
83	5	88	-	0.6	0.8	0.8	0.7

Table S.15 Prediction intervals for the mentioned predictions in Table.6.

Response	Predicted value	95 % PI low	95 % PI high
a) Entry 1: T = 91 C, P=15 bar, S/C = 130 (mol (DMF)/mol(Pt))			
Yield of 2-hexanol	70.6363	64.53	76.74
Yield of 2-hexanone	0.854248	-10.30	12.01
Yield of n-hexan	6.07233	4.02	8.13
Yield of DMTHF	18.7019	15.69	21.71
b) Entry 3: T = 83 C, P=15 bar, S/C = 88 (mol (DMF)/mol(Pt))			
Yield of 2-hexanol	68.3211	62.68	73.56
Yield of 2-hexanone	0.259334	-9.53	10.05
Yield of n-hexan	7.95069	6.01	9.89
Yield of DMTHF	21.4159	18.78	24.05
c) Entry 5: T = 83 C, P=5 bar, S/C = 88 (mol (DMF)/mol(Pt))			
Yield of 2-hexanol	54.8262	49.39	60.27
Yield of 2-hexanone	23.2919	13.50	33.08
Yield of n-hexan	6.63069	4.69	8.57
Yield of DMTHF	12.9157	10.28	15.55

Reaction conditions: 0.1 g DMF, 10.0 mL decane as a solvent, 770 rpm, 3 h.

10.6. Online ESI of 3rd publication (chapter 5)

Content

Supporting Notes:

- 1- Catalysts synthesis
- 2- Description of catalyst characterization techniques
- 3- Experimental details of catalyst testing
- 4- Detailed catalyst characterization
- 5- References

Superior CNT-supported bimetallic RuCu catalyst for the highly selective hydrogenolysis of glycerol to 1,2-propanediol

Magdy Sherbi ^a, Anne Wesner ^a, Valea Kim Wisniewski ^b, Anna Bukowski ^a, Hristiana Velichkova ^b, Bodo Fiedler ^b, Jakob Albert ^{a*}

a) Universität Hamburg, Institute for Technical and Macromolecular Chemistry, Bundesstraße 45, 20146 Hamburg, Germany.

b) Technische Universität Hamburg, Institut für Kunststoffe und Verbundwerkstoffe, Denickestraße 15, 21073 Hamburg, Germany.

* Corresponding author: Prof. Dr.-Ing. Jakob Albert

Tel.: +49 40 42838-4209

E-Mail: jakob.albert@chemie.uni-hamburg.de

We gratefully acknowledge Jan-Paul Grass for carrying out N₂ physisorption measurements, Nina Heene-Würl for performing CO-Chemisorption measurements and Dr. Bo-Magnus Elfers for performing elemental analysis as well as Isabelle Nevoigt for XRD and Sebastian Sichert for H₂-TPR measurements.

Supporting Information

Catalysts synthesis

Carbon-Nano-Tubes (CNT)

The used CNT are commercially available MWCNT NC7000 by Nanocyl SA., Belgium. The CNTs were used without further treatment as received for all functionalization steps. The following properties have been determined for the catalyst support: The surface area according to BET characterization is 210 m²/g, the average diameter is 12 ±3 nm with a length of 0.1-10 μm having cylindrical shape. The overall composition determined by EDX is in wt% is C(92.15), O(5.96), Al(1.81), Si(0.08). The total amount of impurities determined by TGA was around 10 wt%. The TGA residues were analysed by SEM-EDX to show a composition of O (50 wt%), Al(40 wt%), Fe(2 wt%), C(8 wt%), Co(2 wt%).²

Synthesis of Catalysts

The catalysts were synthesized using an improved version of the wet impregnation method described by Y. Yuan *et al.*¹ The CNTs (3.80 g) were suspended in water (500-750 mL) and aqueous solutions of the metal precursors (RuCl₃, Fe(NO₃)₃, or Cu(NO₃)₂ respectively) were added. The overall metal loading was kept constant at 5 wt-%, the atomic ratio of the metals was varied accordingly. After mixing for 4 hours in a rotary evaporator with 100 rpm under a reduced pressure of 800 mbar, the solvent was removed under reduced pressure (200 mbar, 80 °C at 100 rpm). The material was then dried at 110 °C for 12 hours and calcined at 400 °C for 4 hours.

Description of catalyst characterisation techniques

Determination of elemental composition via ICP-OES

Inductive-coupled plasma (ICP-OES) analysis was carried out on a Perkin Elmer Optima 8300 DV at the central analytics department of TUHH (working group Dr. rer. nat. Elfers). 10 mg of the samples were dissolved in nitric acid and hydrochloric acid in a mixing ratio of 1 :3 (aqua regia) followed by threatening for 1.5 h at 260°C. For determining the concentration the following wavelengths have been used: 238,204 nm (Fe), 327,393 nm (Cu), 240,272 (Ru).

Powder X-Ray Diffraction Measurements (PXRD)

Powder X-Ray Diffraction Measurements (PXRD) were performed by the X-Ray Service Facility of the University Hamburg, using a X'Pert Pro MPD diffractometer from PANalytical with a theta-theta/Bragg-Brentano geometry and a Cu X-ray source.

Transmission Electron Microscopy (TEM)

Transmission electron microscopy (TEM) and elemental mapping via STEM-EDX characterization were performed using a FEI Talos F200X with acceleration voltage of 200 kV at BeEM, TUHH. Samples were prepared by pulsed ultrasonic dispersion for 30 s at 30 % amplitude in Hexane with a Bandelin Sonopuls (200 W, KE 76 cone tip). Drops of the dispersion were deposited on a Lacey carbon film gold grid.

Determination of the surface area according to the Brunauer-Emmett-Teller (BET) Method

The determination of the specific surface area of all catalysts were carried out by N₂-physisorption at 77.3 °K on a Quantachrome instrument, model Quadrasorb SI. Before the measurement, the samples were pre-treated and outgassed in a vacuum at 473 °K for 12 h.

CO-Chemisorption

The metal dispersion of (Ru, Cu, Fe) and an average metal particle diameter of each catalyst were measured by CO-pulse-chemisorption on an Autochem II 2920 instrument from Micromeritics.

H₂-Temperature Programmed Reduction (TPR)

H₂-TPR was measured with an Autosorb IQ instrument from Anton Parr. For a typical measurements 80-90 mg of the sample was pretreated in nitrogen (300°C for 30 min) and then cooled down to room temperature. A mixture von 10% H₂ in Nitrogen was employed at a flow rate of 60 ml/min and a heating rate of 10 K/min to 900°C. TCD monitored the H₂ consumption.

Experimental details of catalyst testing

Description of the experimental procedure

Hydrogenolysis of Glycerol for selective production of 1,2 propanediol was performed in a 10-fold parallel reaction system using 21 mL high-pressure stainless-steel (1.4571) vessels equipped with magnetic stirring. Immediately prior to the reaction, approx. 200 mg of the catalyst were reduced using a mixture of 5 vol% H₂ in N₂ (100 L/h) at 550 °C for 8 hours. For a typical run, each reactor was filled with 10 g of the substrate solution (20 wt% glycerol in water), the pre-reduced catalyst, and a PTFE-coated stirrer bar. The reactor was then closed and placed in a heating block above a magnetic stirrer, and connected to the gas supply.

The reactors were first purged three times with N₂ in order to remove residual air, then pressure tested at 70 bar N₂, purged again two times with H₂ and eventually filled with approx. 35 bar of H₂ at room temperature. Then the reactors were heated to 200 °C, upon which the pressure reached approx. 50 bar. The stirrer speed was set to 330 rpm during the heating. After reaching the desired reaction temperature (200 °C) the reaction was then started by vigorous stirring at 770 rpm. After 20 hours the stirring was reduced (330 rpm) and the reactors were allowed to cool to room temperature.

Description of Analytical Methods

Gas samples for analysis by gas chromatography (GC) were taken from the reactors using gas bags. Then the reactors were vented and purged with nitrogen gas (three times) before opening. Subsequently, the catalyst was filtered off and the liquid phase was analysed with high pressure liquid chromatography (HPLC). Additionally, ¹H and ¹³C NMR spectra were measured of the liquid phase to confirm the identity of the products.

The analysis of the gaseous by-products was performed using a Varian GC 450-TCD-FID equipped with a Shin Carbon ST column (2 m × 0.75 mm internal diameter) and both a thermal conductivity detector and a flame ionisation detector. The mobile phase used in the GC was Argon (pressure of 5 bar) and the temperature program used for the measurement was: holding at 40 °C for 1.5 min., heating with a rate of 18 °C min.⁻¹ up to 250 °C, holding at 250 °C for 12 min.

Liquid phase quantitative analysis was carried out using a HPLC system from SHIMADZU equipped with Aminex HPX-87H 300 mm × 7.8 mm BIORAD Column and a refractive index detector. The eluent for the measurements was 5 mmol of an aqueous sulfuric acid solution.

NMR Spectra were measured by the Division of NMR Spectroscopy in the Department of Chemistry of the University Hamburg using a Bruker Avance I 400 MHz spectrometer. Samples were prepared by combining 0.8 mL of the reaction solution with 0.1 mL D₂O.

Formulas for Calculations

$$\text{Conversion (\%)} = \frac{n(\text{Glycerol initial}) - n(\text{Glycerol after Reaction})}{n(\text{Glycerol initial})} \times 100$$

$$\text{Selectivity (\%)} = \frac{n(\text{Product}) \times \text{Number of C atoms in Product}}{(n(\text{Glycerol initial}) - n(\text{Glycerol after Reaction})) \times 3} \times 100$$

$$\text{Carbon Balance (\%)} = \frac{(n(\text{Product}) \times \text{Number of C atoms in Product})}{n(\text{Glycerol initial}) \times 3} \times 100$$

Detailed catalyst characterisation

Powder-XRD diffractograms of synthesized catalysts

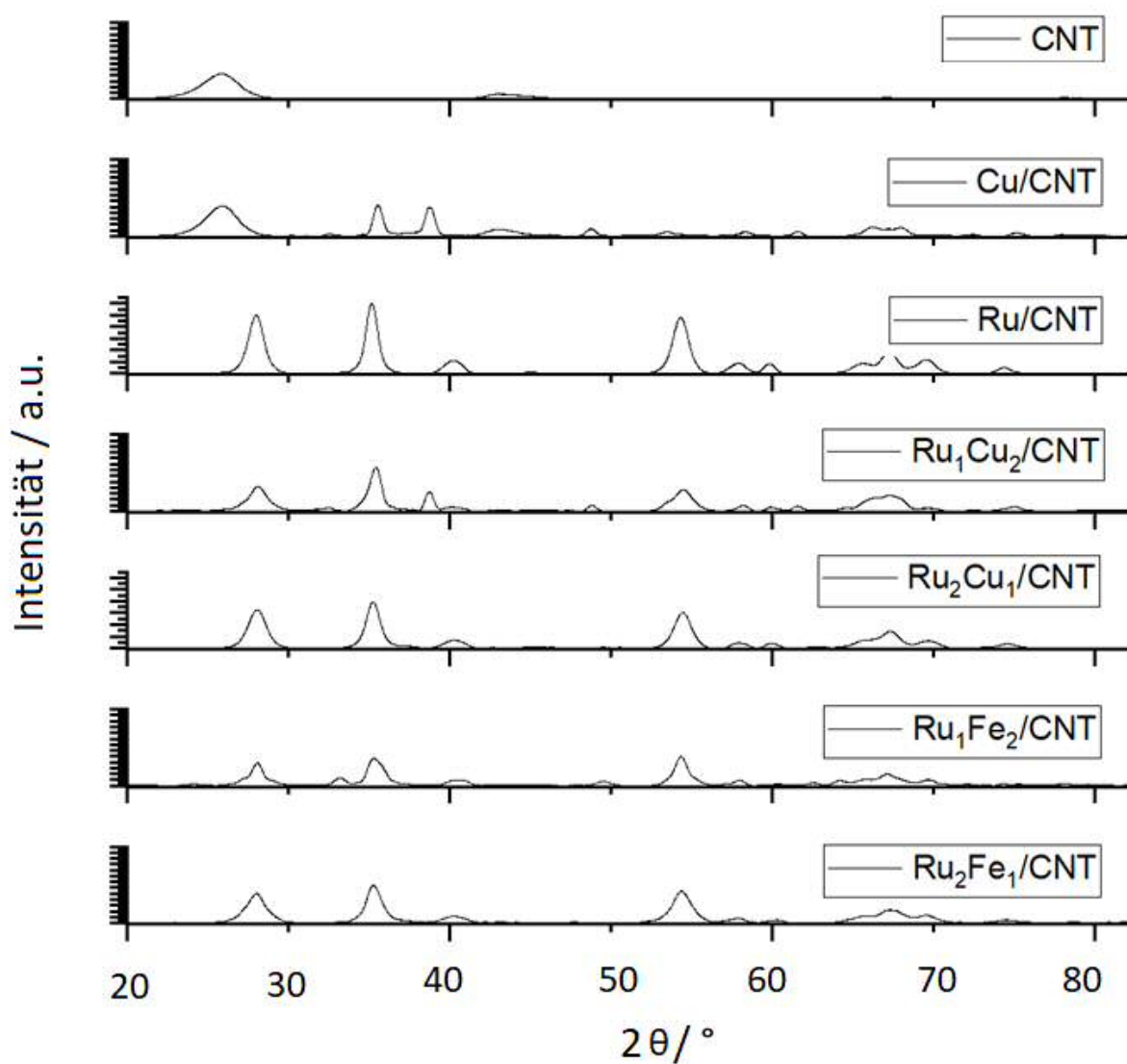


Figure S1: PXRD-diffractograms of all catalysts, measured with Cu-K α radiation, the blue triangle indicates reflexes for graphitic carbon, the yellow square for RuO₂, the red triangle for CuO and the black square for Fe₂O₃

TEM images and EDX-elemental mapping of various catalysts

CNT:

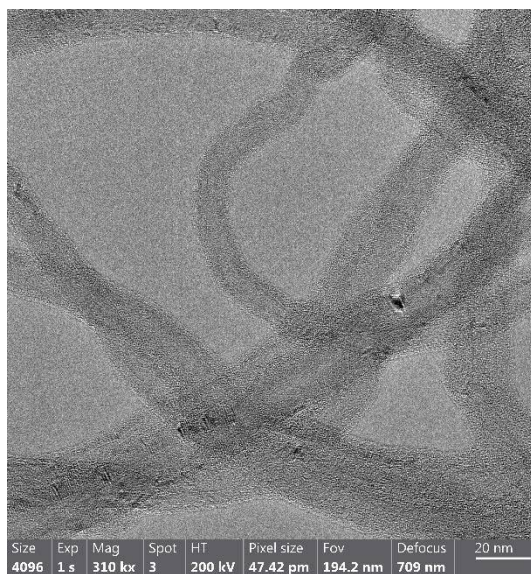
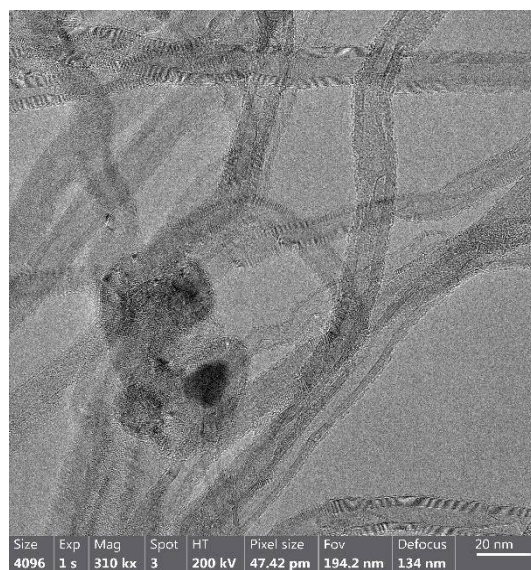
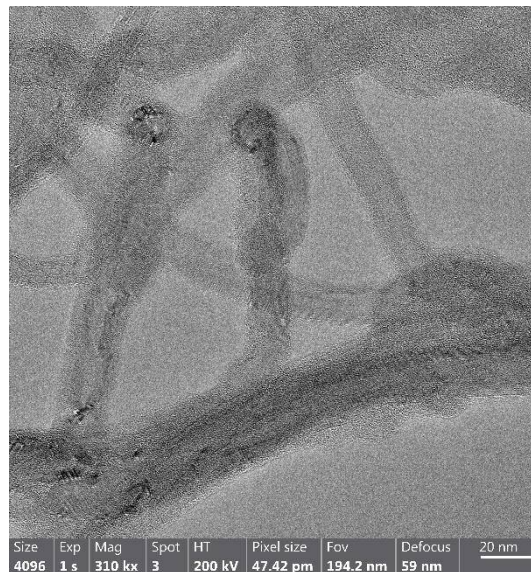
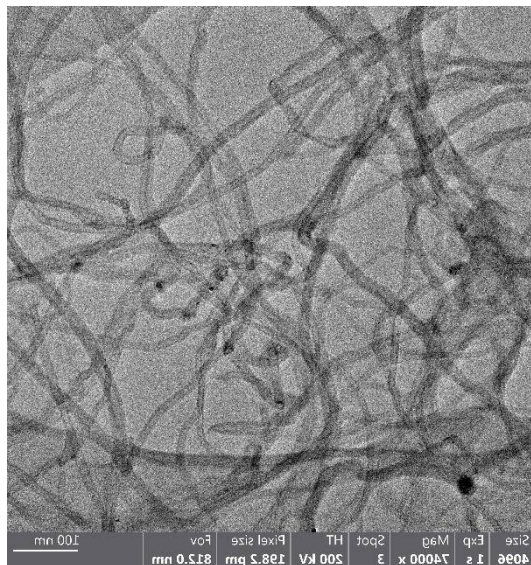


Figure S2: BF-TEM of pure CNT.

Cu/CNT:

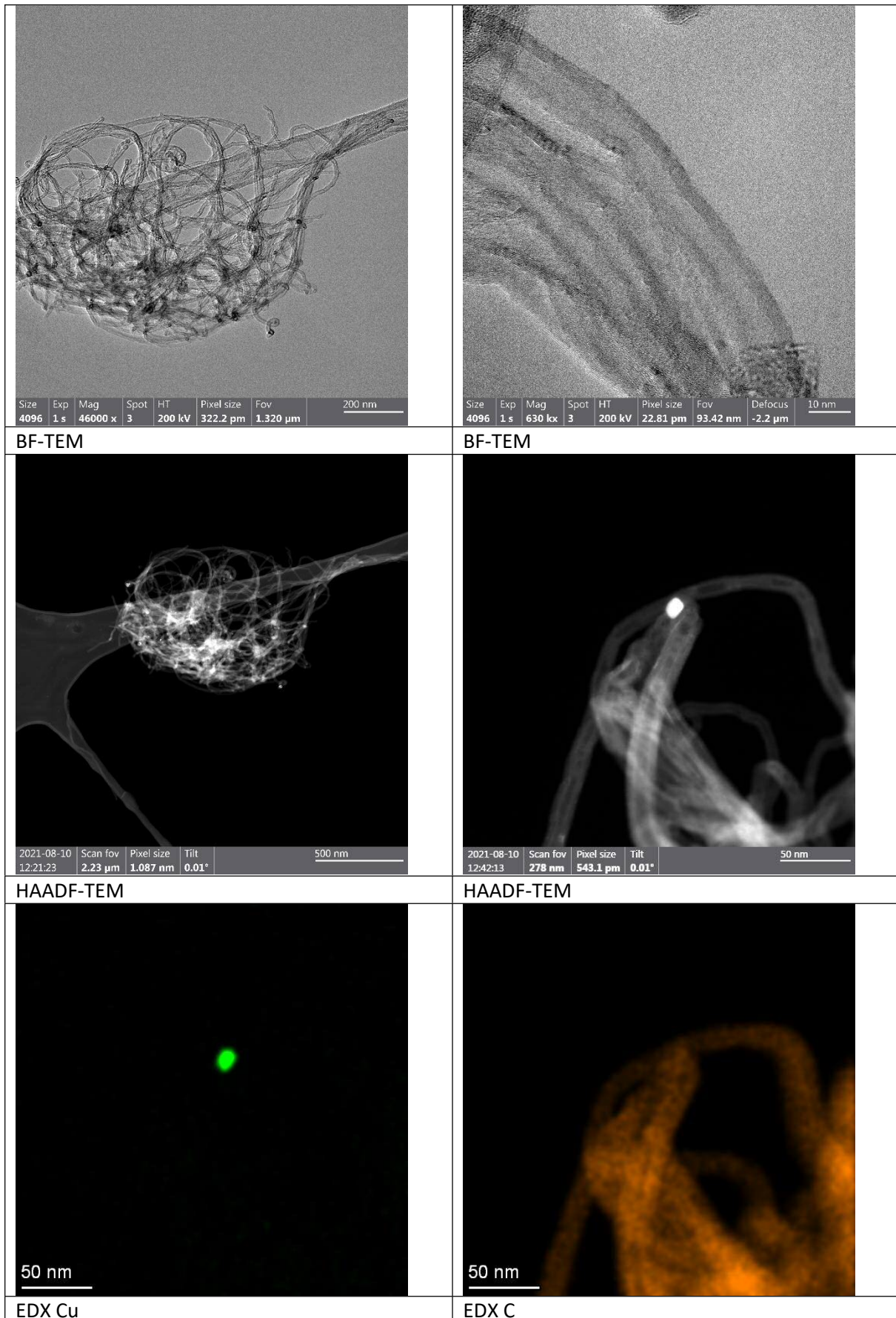


Figure S3: BF-TEM, HAADF-TEM and EDX of Cu/CNT.

Ru/CNT:

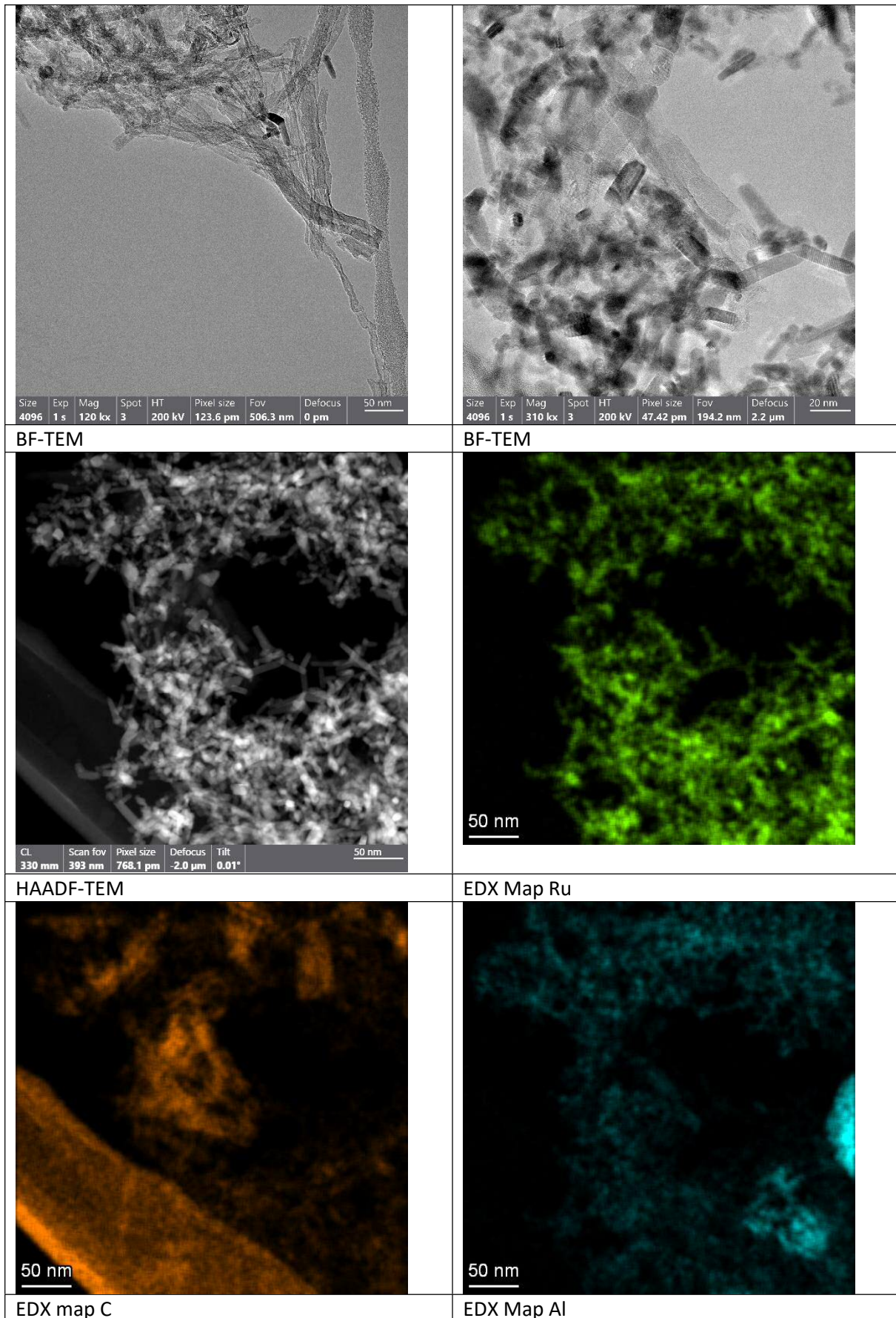


Figure S4: BF-TEM, HAADF-TEM and EDX of Ru/CNT.

Ru₁Fe₂/CNT:

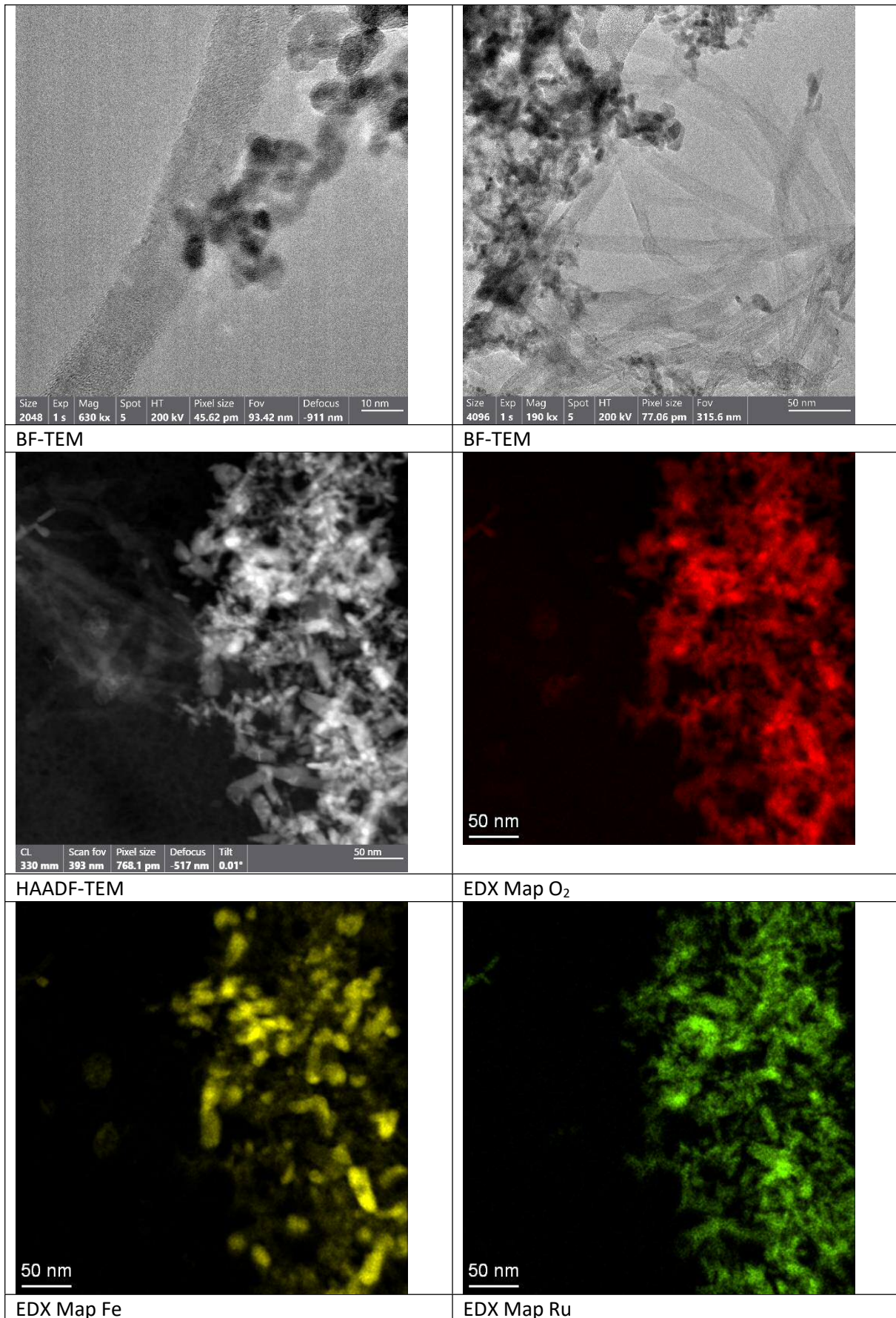


Figure S5: BF-TEM, HAADF-TEM and EDX of Ru₁Fe₂/CNT.

H₂-TPR profiles of several CNT supported catalysts

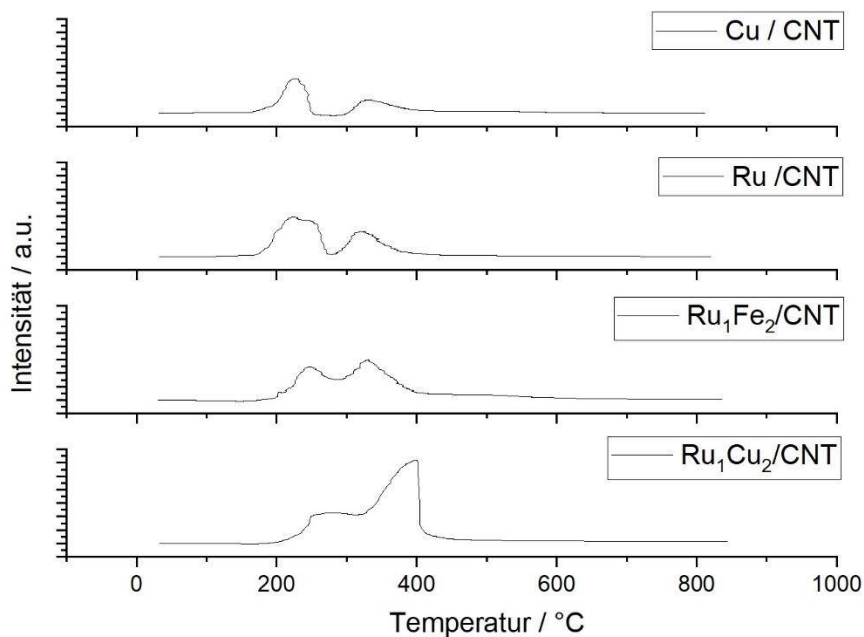


Figure S6: H₂-TPR profiles of several metal/CNT catalysts.

Details of ICP-OES elemental analysis

Table S1: Results of ICP-OES elemental analysis.

Analysenmethode	M 02.015	M 02.015	M 02.015	M 02.015	M 02.015
	Fe	Al	Si	Cu	Ru
Probe	g/Kg	g/Kg	g/Kg	g/Kg	g/Kg
CNT rein	3.99	53.4	--	< 1,20	< 1,20
Cu / CNT	13.2	173	--	162	< 1,20
Ru / CNT	13.2	230	--	< 1,20	13.6
Ru1Fe1 / CNT	96.4	246	--	< 1,20	56.2
Ru1Fe2 / CNT	131	245	--	< 1,20	53.3
Ru2Fe1 / CNT	58.6	233	--	< 1,20	44.0
Ru1Cu2 / CNT	18.0	248	--	133	20.4
Ru2Cu1 / CNT	15.8	251	--	44.4	14.8

References

- 1- B. Li, J. Wang, Y. Yuan, H. Ariga, S. Takakusagi and K. Asakura, ACS Catal., 2011, 1, 1521–1528.
- 2- H. Meeuw, J. Körbelin, V. Wisniewski, A. Nia, A. Vázquez, M. Lohe, X. Feng, B. Fiedler, Polymers, 2019, 11 (2), 231.

10.7. Supplementary information of chapter 6

Content

Supporting Notes:

- 1- Compositional analysis of biomasses
- 2- Catalyst screening with beech wood
- 3- Gas phase analysis
- 4- References

Compositional analysis of biomasses

The compositional analysis was performed at Hamburg University of Technology by Timo Steinbrechen in order to find the composition of beech wood and digestates, and can be described as follows:

The ash content of biomass samples was determined by ashing at 550 °C according to DIN EN ISO 18122 [1]. The CHNS elemental composition was determined via a CHNS elemental analyzer (Vario Macro Cube, Elementar, Langensfeld, Germany) by the central laboratory of the TU Hamburg [2]. Based on the nitrogen content thereby determined, the protein contents of the biomass samples were estimated by applying a protein-to-nitrogen conversion factor of 6.25. Extractives were removed and gravimetrically quantified by two consecutive Soxhlet extractions using first water and subsequently ethanol, following the protocol TP-510-42619 published by the NREL (National Renewable Energy Laboratory) [3]. Subsequently, the content of the structural carbohydrates and lignin was determined by a two-stage acid hydrolysis according to protocol TP-510-42618 [4]. The hydrolysate obtained from this two-stage acid hydrolysis was analyzed for dissolved sugars (D-cellobiose, D(+)glucose, D(+)xylose, L(+)arabinose), acetic acid, hydroxymethylfurfural and furfural using an HPLC system (Infinity II HPLC Series, Agilent, Santa Clara, CA, USA), equipped with a Hi-Plex H+ column (Agilent, Santa Clara, CA, USA) and a refraction index detector and 5 mM sulfuric acid in deionized water as mobile phase. Based on the amount of dissolved sugars and acetic acid, the corresponding cellulose and hemicellulose contents were then calculated according to the protocol TP-510-42618. The acid-soluble lignin content was determined using UV spectrometry at a wavelength of 320 nm and calculated with an absorptivity of 30 L/(g cm). The weight of the acid insoluble residue after the two-stage acid hydrolysis was corrected for ash and protein content in order to obtain the value for acid insoluble lignin.

Catalyst screening with beech wood

Table S1: Monomer yields obtained after RCF of beech wood without catalyst or using C and Al₂O₃ supports compared to NiSat catalyst.

Catalyst type	SPOH	SP	GPOH	GP	Gpe	Gpe (trans)	HP	Monomer yield (wt.%)
NiSat	19.86	1.46	9.11	0.368	0.0	0.0	0.0	30.8
No catalyst	0.07	0.01	0.033	0.002	0.009	0.126	0.0	0.25
C- support	0.057	0.043	0.15	0.031	0.19	1.48	0.0	1.95
Al ₂ O ₃ -support	0.063	0.009	0.042	0.002	0.014	0.179	0.0	0.31

*Reaction conditions of 10 mL methanol, 250 mg substrate, 50 mg catalyst, T= 200 °C, P=50 bars H₂, t= 24 h.

Gas phase analysis

Table S2: Gas phase analysis for RCF of different biomasses.

Biomass type	Catalyst type	CO	CO ₂	CH ₄	C ₂ H ₆	C ₃ H ₈	Sum
		in % C					in % C
Beech wood	Ru/C	2.3	0.1	7.3	0.2	0.2	10.1
	Pt/C	1.0	0.4	0.2	0.0	0.0	1.6
	Ni/C	0.2	0.2	0.3	0.0	0.0	0.7
	Ru/Al ₂ O ₃	1.7	0.6	7.9	0.7	0.5	11.4
	Pt/Al ₂ O ₃	1.4	0.7	0.2	0.0	0.0	2.3
	Ni/Al ₂ O ₃	0.3	0.5	0.9	0.0	0.0	1.7
	NiSat	0.9	0.4	32.6	2.1	1.1	37.1
	No catalyst	0.0	0.3	0.0	0.0	0.0	0.3
	C- support	0.0	0.2	0.0	0.0	0.0	0.2
	Al ₂ O ₃ -support	0.0	0.6	0.0	0.0	0.0	0.6
Rye straw	NiSat	2.3	1.0	15.9	1.2	0.7	21.0
Rye straw digestate	NiSat	1.0	0.6	9.8	0.3	0.1	12.0
Industrial straw digestate	NiSat	0.6	0.3	19.5	1.0	0.6	22.0

*Reaction conditions of 10 mL methanol, 250 mg substrate, 50 mg catalyst, T= 200 °C, P=50 bars H₂, t= 24 h.

References:

1- DIN EN ISO 18122:2016-03, Biogene Festbrennstoffe_ - Bestimmung des Aschegehaltes (ISO_18122:2015); Deutsche Fassung EN_ISO_18122:2015; Beuth Verlag GmbH: Berlin.

2- Diedrich, H.; Stahl, A.; Frerichs, H. NCHS-Elementaranalyse: M02.001. 02., Hamburg, 2019. Available online:

<https://www.tuhh.de/zentrallabor/methoden/ac-methoden/m02001.html> (accessed 21.04.22).

3- Sluiter, A.; Ruiz, R.; Scarlata, C.; Sluiter, J.; Templeton, D. Determination of Extractives in Biomass: Laboratory Analytical Procedure (LAP) NREL/TP-510-42620, 2005. Available online: <https://www.nrel.gov/docs/gen/fy08/42620.pdf> (accessed on 10 August 2021)

4- Sluiter, A.; Hames, B.; Ruiz, R.; Scarlata, C.; Sluiter, J.; Templeton, D.; Crocker, D. Determination of structural carbohydrates and lignin in biomass: Laboratory Analytical Procedure (LAP) NREL/TP-510-42618, 2012. Available online:

<https://www.nrel.gov/docs/gen/fy13/42618.pdf> (accessed 10 August 2021)

Acknowledgements

I stand at the end of a long, challenging, yet immensely rewarding journey, and as I reflect on the arduous path I have travelled, I am filled with immense gratitude to all those who have supported me along the way.

First and foremost, I would like to express my deepest appreciation to my wife (Rehab Hussein), my daughter (Aysel Sherbi) and both our families, who have stood by me through thick and thin, offering unwavering love and support in times of both joy and adversity. Their unwavering faith in my abilities and their steadfast encouragement have been a constant source of motivation for me, and without their support, I would not have been able to reach this milestone.

I am indebted to my supervisor, Prof. Dr. Ing Jakob Albert, for his invaluable guidance, encouragement, and expertise throughout the course of this research. His vast knowledge and experience in the field of chemical engineering have been instrumental in shaping my research project and in helping me navigate the complex challenges that come with pursuing my PhD. His unwavering commitment to excellence and his steadfast dedication to his students have been a constant source of inspiration to me, and I am honored to have had the privilege of working under his mentorship. I would also like to extend my heartfelt thanks to all members of Prof. Albert's research group, who have provided invaluable support and guidance throughout my PhD journey. I would like to extend a special thank you to Dr. Dorothea Voß and Dr. Maximilian Poller for their invaluable contributions to my research project. Their critical feedback, constructive criticism, and innovative ideas have been instrumental in shaping and refining my work. I am grateful for the opportunity to have worked alongside such talented and dedicated individuals.

I am also grateful to my previous supervisor, Prof. Peter Wasserscheid and all members of his research group, for their support and mentorship during my earlier research work in the institute of chemical reaction engineering at Erlangen-Nuremberg University.

I would like to extend my sincere thanks to our collaboration partners in TUHH for their support and for their invaluable contributions to our research projects. I am particularly grateful to my friend Timo Steinbrecher, whose assistance and support have been invaluable in helping me to overcome various challenges and in making this collaboration a success.

I would like to express my sincere gratitude to my former master supervisors, Prof. Dr. Abeer Shoaib and Prof. Dr. Rehab El-Maghraby at Suez University in Egypt. Their emotional support and guidance have been invaluable to me on this PhD journey.

Finally, I wish to express my gratitude to DAAD and MSHER in Egypt for their generous financial support, which has been invaluable in enabling me to pursue my academic goals.

As I conclude, I would like to express my gratitude to all those who have supported and contributed to my academic journey and have helped me reach this significant milestone, including those I may have unintentionally did not mention. Your support has been essential in helping me to achieve my goal. Thank you all, and I look forward to continuing working with you to make meaningful progress in the field of chemistry and chemical engineering.

Eidesstattliche Versicherung

„Hiermit versichere ich an Eides statt, die vorliegende Dissertation selbst verfasst und keine anderen als die angegebenen Hilfsmittel benutzt zu haben. Die eingereichte schriftliche Fassung entspricht der auf dem elektronischen Speichermedium. Ich versichere, dass diese Dissertation nicht in einem früheren Promotionsverfahren eingereicht wurde.“

Magdy Sherbi

Unterschrift: *Magdy Sherbi*

Datum: 28.08.2023

Declaration on oath

I hereby affirm on oath that this PhD dissertation was written by me, and I did not use any aids other than what was mentioned. The submitted written version corresponds to the one on the electronic storage medium. I declare that this dissertation was written maintaining the Rules of Good Scientific Practice of the German Research Foundation and it was not submitted in a previous promotion procedure.

Magdy Sherbi

Signature: *Magdy Sherbi*

Date: 28.08.2023

Curriculum Vitae

PERSONAL INFORMATION

Magdy Seoud Elsayed Sherbi



 Berliner Str. 8, 25746, Heide, Germany

 +491774215807

 magdy.sherbi@gmail.com

Sex Male | Date of birth 28/08/1992 | Nationality Egyptian

EDUCATIONAL BACKGROUND

PhD student in Technical Chemistry

Institute of Technical and Macromolecular Chemistry, University of Hamburg, Hamburg
09.2020 – 04.2023

PhD student in chemical engineering

Institute of Chemical Reaction Engineering, Friedrich-Alexander University, Erlangen-Nürnberg
04.2019 - 09.2020

Master of Science in chemical engineering and oil refining

Faculty of petroleum and mining engineering, Suez University, Egypt

Instructor

Department of refining engineering and petrochemicals, Suez University, Egypt
12.2015-12.2018

Bachelor of Science in refining engineering and petrochemicals

Faculty of petroleum and mining engineering, Suez University, Egypt
08.2009 -08.2014

Languages

Arabic	English	German
Native	C1	C1

Computer skills

- MS Office
- Design Expert Software
- MATLAB
- Aveva Unified Supply chain: Plan
- Aspen HYSYS & Aspen Plus
- AutoCAD & AutoCAD plant 3D
- Aveva Unified Supply chain: Feedstock management

Hobbys



Reading



Table Tennis